Bioresponsive delivery of anticatabolic and anabolic agents for muscle regeneration using bioinspired strategies

Dissertation zur Erlangung des naturwissenschaftlichen Doktorgrades der

Julius-Maximilians-Universität Würzburg

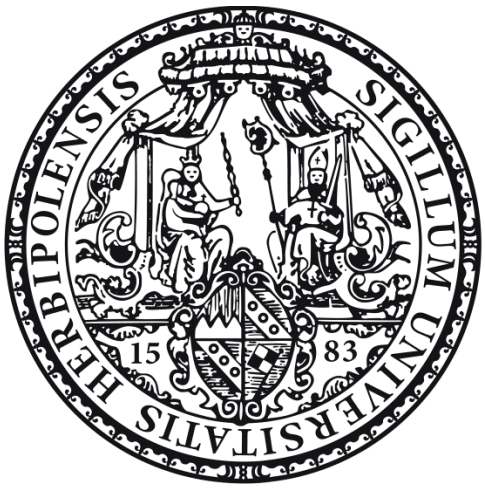

vorgelegt von

Alexandra Carolin Braun

aus Stuttgart

Würzburg 2018

Eingereicht bei der Fakultät für Chemie und Pharmazie am

Gutachter der schriftlichen Arbeit

1. Gutachter:

2. Gutachter:

Prüfer des öffentlichen Promotionskolloquiums

1. Prüfer:

2. Prüfer:

3. Prüfer:

Datum des öffentlichen Promotionskolloquiums

Doktorurkunde ausgehändigt am

Die vorliegende Arbeit wurde in der Zeit von Februar 2013 bis September 2017 am Institut für Pharmazie und Lebensmittelchemie der Bayerischen Julius-Maximilians-Universität Würzburg unter der Anleitung von Herrn Prof. Dr. Dr. Lorenz Meinel angefertigt.

To my parents

Table of contents

Summary **1**

Zusammenfassung **5**

Chapter 1: Bioorthogonal strategies for site-directed decoration of biomaterials with therapeutic proteins **11**

Chapter 2: Matrix metalloproteinase responsive delivery of myostatin inhibitors **55**

Chapter 3: Bioresponsive release of insulin-like growth factor-I from its PEGylated conjugate **91**

Chapter 4: Predicting critical micelle concentration and micelle molecular weight of polysorbate 80 using compendial methods **133**

Conclusion and outlook **165**

Abbreviations **174**

Curriculum vitae **177**

Acknowledgments **179**

Documentation of authorship **181**

Summary

Progressive loss of skeletal muscle mass, strength and function poses a major threat to independence and quality of life, particularly in the elderly. To date, sarcopenia therapy consists of resistance exercise training in combination with protein supplementation due to the limited efficacy of available pharmacological options in counteracting the effects of muscle wasting. Therapeutic intervention with growth factors including insulin-like growth factor I (IGF-I) or inhibitors of myostatin – a potent suppressor of myogenesis – hold potential to rebalance the altered activity of anabolic and catabolic cytokines. However, dosing limitations due to acute side effects and disruptions of the homeostasis have so far precluded clinical application.

Intending to provide a therapy with a superior safety and efficacy profile by directing drug release to inflamed tissue and minimizing off-target activity, we designed bioresponsive delivery systems for an anti-catabolic peptide and anabolic IGF-I responding to local flares of muscle wasting.

In **Chapter I,** current concepts for bioorthogonal conjugation methods are discussed and evaluated based on various drug delivery applications. With a focus on protein delivery, challenges and potential pitfalls of each chemical and enzymatic conjugation strategy are analyzed and opportunities regarding their use for coupling of biomolecules are given. Based on various studies conjugating proteins to polymers, particles and biomaterials using different site-directed approaches, the chapter summarizes available strategies and highlights certain aspects requiring particular consideration when applied to biomolecules. Finally, a decision process for selection of an optimum conjugation strategy is exemplarily presented.

Three of these bioorthogonal coupling reactions are applied in **Chapter II** detailing the potential of site-directed conjugation in the development of novel, homogenous drug delivery systems. The chapter describes the design of a delivery system of a myostatin inhibitor (MI) for controlled and local release counteracting myositis flares. MI release from the carrier is driven by increased matrix metalloproteinase (MMP) levels in compromised muscle tissues cleaving the interposed linker, thereby releasing the peptide inhibitor from the particulate carrier. Release experiments were performed to assess the response towards various MMP isoforms (MMP-1, -8, -9 and -13) – as upregulated during skeletal muscle

myopathies – and the release pattern of the MI in case of disease progression was analyzed. By selection of the protease-sensitive linker (PSL) showing variable susceptibilities to proteases, release rates of the MI can be controlled and adapted. Immobilized MI as well as released MI as response to MMP upregulation was able to antagonize the effects of myostatin on cell signalling and myoblast differentiation.

The approach of designing bioresponsive protein delivery systems was also applied to the anabolic growth factor IGF-I, as described in **Chapter III**. Numerous studies of PEGylated proteins or peptides reveal, that successful therapy is challenged by safety and efficacy issues, as polymer attachment considerably alters the properties of the biologic, thereby jeopardizing clinical efficacy. To this end, a novel promising approach is presented, intending to exploit beneficial effects of PEGylation on pharmacokinetics, but addressing the pharmacodynamic challenges by releasing the protein upon entering the target tissue. This was realized by integration of a PSL between the PEG moiety and the protein. The soluble polymer conjugate was produced by site-directed, enzymatic conjugation of IGF-I to the PSL, followed by attachment of a 30 kDa-PEG using Strain-promoted azide-alkyne cycloaddition (SPAAC). This strategy illustrates the potential of bioorthogonal conjugation (as described in Chapter I) for generation of homogenous protein-polymer conjugates with reproducible outcome, but also emphasizes the altered protein properties resulting from permanent polymer conjugation. As compared to wild type IGF-I, the PEGylated protein showed considerable changes in pharmacologic effects – such as impaired insulin-like growth factor binding protein (IGFBPs) interactions, submaximal proliferative activity and altered endocytosis patterns. In contrast, IGF-I characteristics were fully restored upon local disintegration of the conjugate triggered by MMP upregulation and release of the natural growth factor.

For successful formulation development for the proteins and conjugates, the careful selection of suitable excipients is crucial for a safe and reliable therapy. **Chapter IV** addresses one aspect by highlighting the chemical heterogeneity of excipients and associated differences in performance. Polysorbate 80 (PS80) is a surfactant frequently used in protein formulations to prevent aggregation and surface adsorption. Despite being widely deployed as a standard excipient, heterogeneous composition and performance entails the risk of eliciting degradation and adverse effects on protein stability. Based on a comprehensive study using different batches of various suppliers, the PS80 products were characterized regarding

chemical composition and physicochemical properties, facilitating the assessment of excipient performance in a formulation. Noticeable deviations were recorded between different suppliers as well as between batches of the same suppliers. Correlation of all parameters revealed, that functionality related characteristics (FRCs) could be reliably predicted based on chemical composition alone or by a combination of chemical and physicochemical properties, respectively.

In summary, this thesis describes and evaluates novel strategies for the targeted delivery and controlled release of biologics intended to counteract the imbalance of anabolic and catabolic proteins observed during aging and musculoskeletal diseases. Two delivery platforms were developed and characterized *in vitro* – (i) using anti-catabolic peptides immobilized on a carrier for local delivery and (ii) using soluble IGF-I polymer conjugates for systemic application. Both approaches were implemented by bioorthogonal coupling strategies, which were carefully selected in consideration of limitations, side reactions and efficiency aspects. Bioresponsive release of the active biomolecules following increased protease activity could be successfully realized. The therapeutic potential of these approaches was demonstrated using various cell-based potency assays. The systems allow targeted and controlled release of the growth factor IGF-I and anti-catabolic peptides thereby overcoming safety concerns of current growth factor therapy and thus positively impacting the benefit-risk profile of potent therapeutics. Taking potential heterogeneity and by-product concerns into account, comprehensive excipient characterization was performed and a predictive algorithm for FRCs developed, in order to facilitate formulation design and guarantee a safe and efficient therapy from start to finish.

Zusammenfassung

Der zunehmende Verlust an Skelettmuskelmasse, Kraft und Funktion stellt insbesondere bei Älteren eine wesentliche Gefährdung der Unabhängigkeit und Lebensqualität dar. Bislang besteht die Sarkopenie-Therapie infolge der eingeschränkten Wirksamkeit verfügbarer pharmakologischer Möglichkeiten, den Auswirkungen des Muskelschwunds entgegenzuwirken, aus einer Kombination von Krafttraining und erhöhter Proteinzufuhr. Therapeutische Intervention mit Wachstumsfaktoren wie Insulin-like growth factor (IGF-I) oder Inhibitoren von Myostatin – eines wirkungsvollen Hemmstoffes der Myogenese – bietet das Potenzial, die veränderte Aktivität der anabolen und katabolen Zytokine wieder ins Gleichgewicht zu bringen. Allerding haben Dosiseinschränkungen aufgrund akuter Nebenwirkungen und Beeinträchtigungen der Homöostase bislang eine klinische Anwendung ausgeschlossen.

Mit der Absicht, eine Therapie mit besserem Sicherheits- und Wirksamkeitsprofil zu bieten, indem die Freisetzung des Wirkstoffs auf entzündetes Gewebe gelenkt wird und Aktivitäten außerhalb des Zielgewebes minimiert werden, entwickelten wir bioresponsive Freisetzungssysteme für ein antikataboles Peptid und das anabole IGF-I, die auf lokalen Ausbruch von Muskelschwund reagieren.

In **Kapitel I** werden aktuelle Konzepte bioorthogonaler Konjugationsmethoden diskutiert und auf Basis einer Vielzahl von Drug Delivery Anwendungen beurteilt. Mit besonderem Fokus auf die Verabreichung von Proteinen werden Herausforderungen und Schwierigkeiten jeder chemischen und enzymatischen Konjugationsstrategie analysiert und Möglichkeiten im Hinblick auf ihre Verwendung für die Kopplung von Biomolekülen aufgezeigt. Auf Grundlage diverser Studien zur Verknüpfung von Proteinen mit Polymeren, Partikeln und Biomaterialien unter Verwendung verschiedener ortsspezifischer Ansätze, fasst das Kapitel vorhandene Strategien zusammen und hebt gewisse Aspekte hervor, die bei Anwendung auf Biomoleküle besondere Beachtung erfordern. Abschließend wird ein Entscheidungsprozess zur Auswahl einer optimalen Verknüpfungsstrategie exemplarisch dargestellt.

Drei dieser bioorthogonalen Kopplungsreaktionen werden in **Kapitel II** angewendet, wodurch das Potenzial der ortsgerichteten Konjugation für die Entwicklung neuer, homogener Drug Delivery Systeme detailliert aufgezeigt wird. Dieses Kapitel beschreibt die

Gestaltung eines Delivery Systems für einen Myostatin- Inhibitor (MI) für kontrollierte und lokale Freisetzung, um Myositis-Ausbrüchen entgegenzuwirken. Die Freisetzung des MI vom Träger wird durch erhöhte Konzentration an Matrix-Metalloproteinasen (MMPs) in betroffenem Muskelgewebe vorangetrieben, die durch Spaltung des dazwischen positionierten Linkers das Peptid vom Partikelträger freisetzen. Es wurden Freisetzungsexperimente durchgeführt, um die Reaktion gegenüber mehreren MMP-Isoformen (MMP-1, -8, -9 und -13), die im Verlauf von Skelettmuskelmyopathien hochreguliert sind, festzustellen, und es wurde das Freisetzungsmuster des MI im Falle einer Krankheitsprogression analysiert. Durch Auswahl der Protease-sensitiven Linker (PSL), die unterschiedliche Empfindlichkeit gegenüber Proteasen zeigen, können die Freisetzungsraten des MI kontrolliert und angepasst werden. Sowohl der immobilisierte MI, als auch der auf MMP-Hochregulation hin freigesetzte MI, waren dazu in der Lage, die Wirkungen von Myostatin auf Signaltransduktion von Zellen und Myoblastendifferenzierung aufzuheben.

Das Konzept, bioresponsive Delivery Systeme für Proteine zu designen, wurde auch auf den anabolen Wachstumsfaktor IGF-I angewendet, wie in **Kapitel III** beschrieben wird. Zahlreiche Studien zu PEGylierten Proteinen oder Peptiden offenbaren, dass eine erfolgreiche Therapie durch Sicherheits- und Wirksamkeitsprobleme herausgefordert wird, da der Polymeranhang die Eigenschaften des biologischen Wirkstoffs beachtlich verändern und dadurch die klinische Wirksamkeit gefährden kann. Zu diesem Zweck wird ein neuer, vielversprechender Ansatz vorgestellt, mit der Absicht, die vorteilhaften Auswirkungen der PEGylierung auf die Pharmakokinetik zu nutzen, aber auch die pharmakodynamischen Herausforderungen dadurch zu adressieren, dass das Protein bei Eintritt ins Zielgewebe freigesetzt wird. Das wurde durch Einfügen eines PSL zwischen den PEG-Teil und das Protein erreicht. Das lösliche Polymerkonjugat wurde durch ortsspezifische, enzymatische Konjugation von IGF-I an den PSL hergestellt, gefolgt von Verknüpfung mit einem 30k Da-PEG unter Verwendung von kupferfreier Azid-Alkin Cycloaddition (SPAAC). Diese Strategie veranschaulicht das Potenzial der bioorthogonalen Konjugation (wie in Kapitel I beschrieben) zur Erzeugung homogener Protein-Polymer-Konjugate mit reproduzierbarem Ergebnis, aber betont auch die veränderten Proteineigenschaften, die sich aus der dauerhaften Polymerkonjugation ergeben. Verglichen mit dem Wildtyp-IGF-I zeigte das PEGylierte Protein beachtliche Veränderungen der pharmakologischen Eigenschaften, wie verminderte Interaktionen mit Insulin-like growth factor Bindungsproteinen (IGFBPs), eine

submaximale proliferative Aktivität und ein verändertes Endozytosemuster. Im Gegensatz dazu wurden die Eigenschaften von IGF-I bei lokaler Spaltung des Konjugates durch MMP-Hochregulation und Freisetzung des natürlichen Wachstumsfaktors vollständig wiederhergestellt.

Für eine erfolgreiche Formulierungsentwicklung der Proteine und Konjugate ist eine sorgfältige Auswahl geeigneter Hilfsstoffe für eine sichere und zuverlässige Therapie essenziell. **Kapitel IV** befasst sich mit einem Aspekt davon, indem die chemische Heterogenität von Hilfsstoffen und damit verbundene Unterschiede in der Leistung hervorgehoben werden. Polysorbat 80 (PS80) ist ein in Proteinformulierungen häufig verwendeter Hilfsstoff, der Aggregation und Oberflächenadsorption verhindern soll. Trotz dieser breiten Anwendung als Standardhilfsstoff birgt die heterogene Zusammensetzung und Performance Risiken, wie eine begünstigte Zersetzung und nachteilige Auswirkungen auf die Proteinstabilität. Auf Basis einer umfassenden Studie mit verschiedenen Chargen diverser Anbieter wurden die PS80 Produkte hinsichtlich ihrer chemischen Zusammensetzung und ihrer physikochemischen Eigenschaften charakterisiert, um eine Beurteilung der Hilfsstoffperformance in einer Formulierung zu ermöglichen. Auffällige Abweichungen sowohl zwischen unterschiedlichen Anbietern, also auch zwischen Chargen des gleichen Anbieters konnten verzeichnet werden. Die Korrelation aller Parameter ergab, dass funktionalitätsbezogene Eigenschaften (FRCs) auf Basis der chemischen Zusammensetzung alleine bzw. durch eine Kombination aus chemischen und physikochemischen Eigenschaften zuverlässig prognostiziert werden konnten.

Zusammenfassend beschreibt und bewertet diese Dissertation neue Strategien für eine zielgerichtete und kontrollierte Freisetzung von biologischen Wirkstoffen mit der Absicht, dem Ungleichgewicht zwischen anabolen und katabolen Proteinen, welches im Laufe der Alterung und im Zuge muskuloskelettaler Erkrankungen beobachtet wird, entgegenzuwirken. Zwei Wirkstoff-Verabreichungsplattformen wurden entwickelt und *in vitro* charakterisiert: (i) unter Verwendung antikataboler Peptide, die für eine lokale Applikation auf einem Träger immobilisiert werden, und (ii) unter Verwendung löslicher IGF-I-Polymer Konjugate für die systemische Anwendung. Beide Ansätze wurden mittels bioorthogonaler Kopplungsstrategien, die unter Berücksichtigung von Einschränkungen, Nebenreaktionen und Effizienzaspekten sorgfältig ausgewählt wurden, durchgeführt. Die bioresponsive Freisetzung der aktiven Biomoleküle als Folge einer erhöhten

Proteaseaktivität konnte erfolgreich umgesetzt werden. Das therapeutische Potenzial dieser Ansätze wurde anhand mehrerer zellbasierter Wirksamkeitsassays gezeigt. Die Systeme ermöglichen eine zielgerichtete und kontrollierte Freisetzung des Wachstumsfaktors IGF-I und antikataboler Peptide, wobei sie die Sicherheitsbedenken aktueller Wachstumsfaktortherapie bewältigen und somit das Nutzen-Risiko-Profil hochwirksamer Therapeutika positiv beeinflussen. Unter Berücksichtigung der potenziellen Bedenken bezüglich Heterogenität und Nebenprodukten wurde eine umfassende Hilfsstoffcharakterisierung durchgeführt und ein prognostischer Algorithmus für FRCs entwickelt, um die Formulierungsentwicklung zu erleichtern und eine sichere und effiziente Therapie von Anfang bis zum Ende zu garantieren.

Chapter 1: Bioorthogonal strategies for site-directed decoration of biomaterials with therapeutic proteins

Alexandra C. Braun, Marcus Gutmann, Tessa Lühmann, Lorenz Meinel

Institute for Pharmacy and Food Chemistry, University of Wuerzburg, Am Hubland, DE-97074 Wuerzburg, Germany

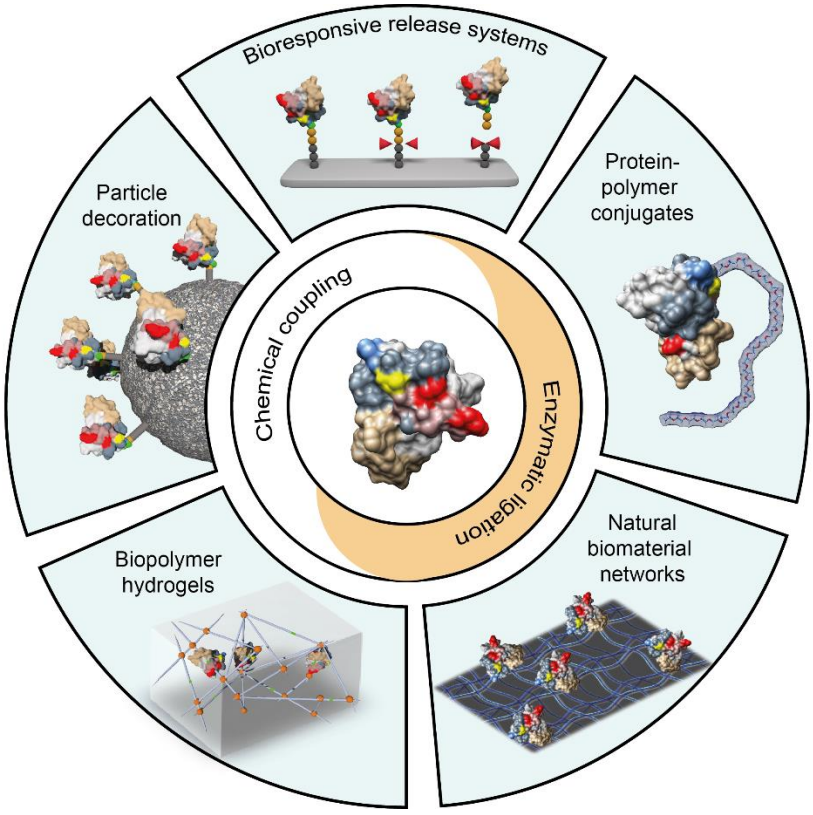

This chapter was originally published in Journal of Controlled Release, vol. 273, pp. 68-85, 2018; DOI: 10.1016/j.jconrel.2018.01.018. With permission of Elsevier, license number: 4347530894173.

Abstract

Emerging strategies targeting site-specific protein modifications allow for unprecedented selectivity, fast kinetics and mild reaction conditions with high yield. These advances open exciting novel possibilities for the effective bioorthogonal decoration of biomaterials with therapeutic proteins. Site-specificity is particularly important to the therapeutics' end and translated by targeting specific functional groups or introducing new functional groups into the therapeutic at predefined positions. Biomimetic strategies are designed for modification of therapeutics emulating enzymatic strategies found in Nature. These strategies are suitable for a diverse range of applications – not only for protein-polymer conjugation, particle decoration and surface immobilization, but also for the decoration of complex biomaterials and the synthesis of bioresponsive drug delivery systems. This article reviews latest chemical and enzymatic strategies for the biorthogonal decoration of biomaterials with therapeutic proteins and inter-positioned linker structures. Finally, the numerous reports at the interface of biomaterials, linkers, and therapeutic protein decoration are integrated into practical advice for design considerations, intended to support the selection of productive ligation strategies.

1. Introduction

Covalent conjugation of therapeutic peptides or proteins to biomaterials or polymers opens promising new interfaces for the design of functionalized implants with improved pharmaceutical properties [1]. Among these, attachment of targeting moieties to biologics as done with antibody-drug conjugates (ADCs) [2, 3], polymer conjugation (e.g. PEG conjugates) [4, 5], immobilization on biomaterials [6-8] and preparation of controlled release delivery systems [9] are preeminent examples improving efficacy, pharmacokinetics (PK), distribution and safety of therapeutics. Despite this great potential, current approaches have limitations, particularly resulting from the heterogeneity of formed conjugation products as of unspecific modification. It is this heterogeneity, giving rise to analytical as well as safety and efficacy concerns. For example, some ADCs with heterogeneously attached cancer drugs had reduced clinical efficacy compared to the free drugs which was at least in part linked to unspecific coupling chemistries [3]. Similarly, the development of Mylotarg® (Gemtuzumab ozogamicin) – the first ADC approved by the FDA in 2000 and unspecifically carrying the cancer drug at the antibody's amine groups – was withdrawn from the market in 2010 following a post marketing clinical trial for insufficient clinical benefit and toxic side effects associated with its heterogeneity [10]. It was further detailed that the drug-antibody ratio (DAR) strongly impacted Mylotarg's therapeutic efficacy with the large portion of the unlabeled antibody (of ~ 50%) serving as a competitive inhibitor to the ADC for cellular uptake which is a prerequisite for its activity [11]. Conversely, a high DAR commonly increases toxicity and hydrophobicity of the ADC, thereby inducing precipitation, reducing stability and accelerating plasma clearance [12, 13]. Especially in case of ADCs with cytotoxic payload, statistical conjugation of the highly potent drug affects the therapeutic window of the ADC jeopardizing safe and efficient therapy [3]. Moreover, multiple drug-loaded forms of ADCs (usually with DARs from 0 to 8 [14]) have distinct PK *in vivo* and differ in clinical performance, immunogenicity, clearance and stability [15, 16]. Despite narrowing the DAR by purification, the multitude of different conjugation sites – e.g. in case of Kadcyla® (Trastuzumab emtansine) 70 of the 88 lysines were shown to be conjugated – generates a mixture of ADC species with substantial differences in clinical performance and PK properties [17]. Consequently, 'second generation' ADCs were developed with the ultimate goal to reduce product heterogeneity providing a therapeutic tool with predictable properties and batch-to-batch consistency [2, 18-21]. Recent effort was placed on (i) identification of regions that are well suited for site-specific drug attachment [22, 23], (ii)

development of versatile chemical linker strategies to modulate drug release [24] and (iii) pharmacokinetic/pharmacodynamic modeling [25].

In analogy to this example, these considerations are also promoting the development of conjugates for other therapeutic proteins such as enzymes, growth factors or cytokines for which new synthetic approaches are sought leading to clearly defined physicochemical, biological and pharmaceutical properties. Batch-to-batch quality differences of such heterogeneous products causes concerns as illustrated by the recall of five batches of PEG-asparaginase between 2000 and 2003 due to deviations in activity associated with unspecific coupling [26]. The polydispersity of various species of multi-PEGylated variants and positional isomers involves difficult separation and mitigates biological activity for a significant fraction of the product species. For example, PEGylated Interferon α-2a retains only a fraction of its activity (7%) in comparison to the original protein [27], as it is PEGylated at 9 different lysines resulting in 9 positional isomers exhibiting significantly distinct specific bioactivities [28]. Essentially the same was observed for unspecifically surface-conjugated enzymes, such as glycosyltransferase, for which a loss of bioactivity by ¼ was reported whereas site-directed approaches had a loss of $^{1}/_{10}$ only [29]. Due to the convincing body of data demonstrating the advantages of site-directed coupling strategies, a change of direction becomes apparent with the first site-specifically conjugated ADCs entering clinical trials [30, 31]. Furthermore, among the recently FDA-approved PEGylated proteins and those in phase I-III clinical trials a growing number is produced by bioorthogonal methods (e.g. Cimzia®, a PEG-anti-TNFα antibody fragment or Neulasta®, PEGfilgrastim). However, site-directed conjugation chemistries are yet to find broad entry into bioengineering of functionalized biomaterials [6, 32-39].

In this review, we summarize novel, bioorthogonal chemical and enzymatic coupling strategies and discuss them with a focus on the site-directed decoration of biologics and the functionalization of biomaterials. Pros and cons of each strategy are critically discussed. We are addressing novel approaches integrating the complexity of site-directed coupling of (i) therapeutic proteins, (ii) linkers, and (iii) biomaterials. Ultimately, we try emulating these various strategies into one blueprint / flow chart in an effort to facilitate future selection processes for those who aim for the site-directed conjugation of therapeutics to a biomaterial or polymer with or without inter-positioned linkers.

2. General considerations for protein based bioconjugates

Covalent conjugation of biologics to biomaterials allows for implant materials with lasting bioactivity [40]. The challenges for biologic-decorated biomaterial manufacture are manifold, more importantly the preservation of the therapeutics' stability during the coupling reaction and during storage [41] and – with arguably increasing importance - site-directed decoration for the aforementioned advantages [42]. This is why the focus is on mild reaction conditions to preserve the integrity, and biological function of the biologics to the maximal possible extent [43]. 'Biologics' in our context are a diverse set of molecules (e.g. peptides, polypeptide hormones, large proteins, high molecular weight antibodies, but also nucleic acids, blood products and vaccines) and it is this diversity requiring a suite of chemical/enzymatic strategies for synthesis and a guided rationale for selecting the most promising one for conjugate development.

The consequences of unspecific versus specific labeling are illustrated for insulin-like growth factor I (IGF-1) (**Figure 1**). IGF-1 has 4 amino groups, three from its 3 lysine residues and one from the N-terminal amino group [45]. Therefore, conventional amine-targeting strategies - including N-hydroxysuccinimide (NHS)-chemistry – end up in unspecific conjugation to one, two, three, or all of the 4 different amines. Assuming identical probability of labeling among all 4 amines (which is a theoretical consideration for illustration purposes), the relatively small growth factor IGF-I with 7.4 kDa already allows for $[4^{(n+1)} - 1]$ or 15 species following conjugation through its amines (**Figure 1A**). Challenges associated with this random protein orientation include partial or full blockade of a protein's active site and an associated loss of bioactivity [46, 47] along with potential unfolding increasing the immunological risk. In case of IGF-I, conjugation through the surface-exposed K27 (Variant #1) and partially also through K65, K68 or the N-terminus (Variants #2 – #4), respectively, masks important binding sites to receptors and binding proteins (IGFBPs), thereby impacting efficacy of immobilized growth factor [48, 49]. These concerns can be met by introducing non-natural amino acids such as azido-homoalanine at an ideal position into the therapeutics' primary structure resulting in optimum protein conformation for ligand interaction [50]. This chemo- and region-selective ligation method (**Figure 1B**), is only one yet quite promising approach selected from the choices outlined in the next section.

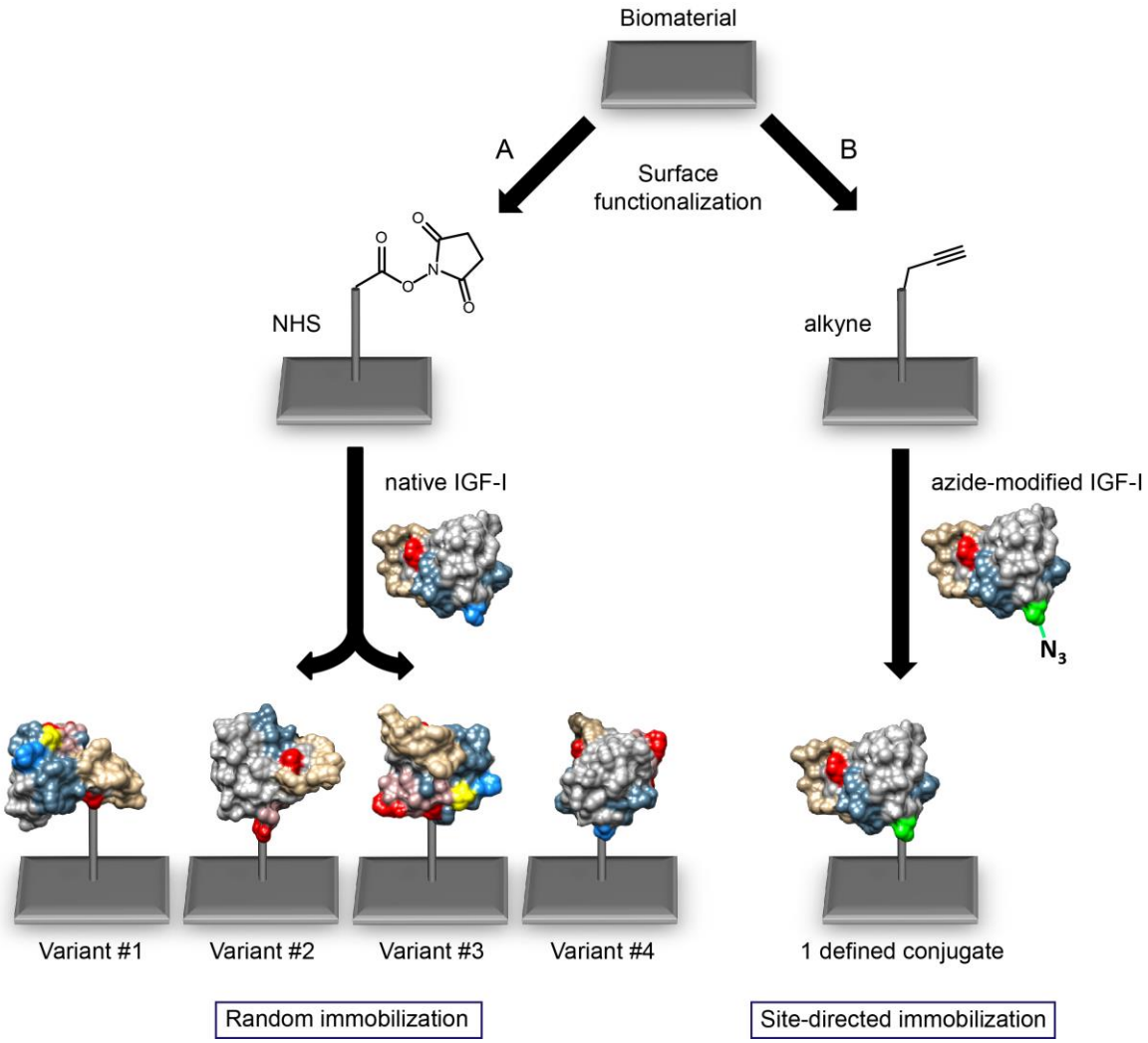

Figure 1: Schematic illustration of IGF-1 immobilization onto a solid surface by (A) random and (B) site-directed coupling strategies [44]. (A) The carrier surface is chemically functionalized with NHS activated carboxylic acids, followed by IGF-1 coupling via amino groups entailing 4 different protein orientations. (B) Surface functionalization with alkyne groups facilitates covalent IGF-1 conjugation through one azide functionality introduced into the sequence at a selected position, thereby resulting in homogenous protein orientation.

3. Chemical conjugation strategies for site-specific protein immobilization

Site-specific covalent coupling of a protein to a carrier requires a distinguishing functional group within the protein. This distinguishing functional group can be an unique proteinogenic amino acid (e.g. a free cysteine) or an introduced unnatural amino acid [50]. The introduction of novel functional groups (e.g. a thiol group) – referred to as site-directed mutagenesis – offers

an elegant method for site-specific conjugation, but is restricted to proteins with no [51] naturally occurring free cysteine [52, 53]. Cysteine's nucleophilicity at pH 7 features rapid reaction with chemical functionalities such as α-haloacetyl- and maleimide-modified surfaces leading to covalent thioether bonds. Studies describe fusion protein synthesis of therapeutic peptides with serum albumin using this method, as albumin possesses exactly one free thiol group [54]. One common challenge of this approach, however, is the formation of intermolecular disulfide isomers jeopardizing the yield and pharmaceutical properties of the product. Additionally, free cysteines are frequently required within enzymes' active sites. Furthermore, introduced cysteine residues can cause changes in the disulfide bond pattern thereby jeopardizing proper protein folding [55]. Lack of selectivity of cysteine-involving syntheses was also reported. Many of the electrophiles traditionally used with thiols including iodoacetamides, maleimides or vinyl sulfones, are subject to competing reactions with other nucleophilic amino acids aside of cysteines, typically lysine and histidine [53]. In any case, the formed maleimide bonds suffer from instability due to hydrolysis or retro-addition reactions with free thiols after administration of the therapeutic, e.g. to serum albumin [53] causing some concerns for *in vivo* application of these conjugates [43].

The challenge of disulfide isomers and unspecific reaction with lysines/histidines and instability of the maleimide bonds is met by introducing novel functionalities into the protein sequence by 'genetic code expansion' **(Figure 2)** [56, 57]. Thereby, artificial or unnatural amino acids (uAA) are incorporated into proteins and it is these uAA that are site-specifically conjugated for homogenous product outcome (e.g. as outlined for IGF-I in **Figure 1B**) [58, 59]. Alternatively, several uAA can be introduced using 'post-translational mutagenesis' into a suitable cysteine mutant of recombinant target proteins [60]. The biorthogonal chemistries available for l modification are now discussed.

In general, chemical conjugation strategies can be divided into three main categories: (i) metal-catalyzed bioorthogonal reactions, (ii) photocatalytic reactions and (iii) bioorthogonal reactions proceeding without need for catalysts.

The most relevant metal-catalyzed bioorthogonal reaction is the Huisgen 1,3-dipolar cycloaddition linking an azide with an alkyne to form a 1,2,3-triazole, typically catalyzed by copper(I) [33, 34] (**Figure 2A**). This copper(I)-catalyzed azide-alkyne cycloaddition (CuAAC) proceeds pH-independently at considerably rapid rates [61, 62]. As azide and alkyne groups are essentially absent from biological systems, they are truly orthogonal in their reactivity. A

number of Cu(I) sources are available but the catalyst is preferentially prepared *in situ* by reducing Cu(II) salts, such as $CuSO_4$, with TCEP or sodium L-ascorbate while THPTA or TBTA are added as Cu(I)-stabilizing agent [63]. The presence of copper causes concerns related to toxicity of traces in the final product or protein precipitation [64]. For example, oxidative stress and biological damage have been associated with CuAAC due to Cu(I)-promoted generation of reactive oxygen species (ROS) as side products [63-67]. Furthermore, the ascorbate – used to reduce Cu(II) to Cu(I) – can cause protein crosslinking - by virtue of the electrophilic properties of its oxidized form dehydroascorbate - reacting with lysine, arginine [68] and cysteine [69] side chains and possibly triggering crosslinks. Due to the widespread use of this synthesis we decided to further detail it for its side reactions (**Figure 2B**). For that, agarose particles were decorated with either alkyne-, hydroxyl- or thiol groups. In parallel, short peptides were synthesized containing azide and/or thiol, lysine or arginine residues. The modified particles and the synthesized particles were now reacted under CuAAC conditions (50 µM $CuSO_4$, 250 µM tris(3-hydroxypropyltriazolylmethyl)amine (THPTA), and 2.5 mM sodium L-ascorbate, '+ Cu') at ambient conditions. Identical reaction conditions but in absence of copper ('– Cu') were used as negative controls. In summary, reaction was observed for cysteines' thiol groups but –contrasting previous reports [68] – not through lysine and arginine residues even at higher copper concentrations in the milli-molar range (**Figure 2B**, panel B1–B3). The thiol-yne reaction [70] was also less pronounced at standard CuAAC conditions (**Figure 2B**, panel B3 first row), corresponding to previous reports describing the requirement of catalysts or radical initiating species (such as UV irradiation) for efficient conversion [70].

Interestingly, the cross-links formed in absence of the copper catalyst were easily reduced by dithiothreitol (DTT), however, when formed in presence of copper, cross-links were by far more resistant including stressed conductions at temperatures of 95 °C and at 1 molar DTT concentration (**Figure 2C**). In conclusion, CuAAC is a particularly feasible coupling method for proteins without free cysteines, but should be used cautiously for proteins with free cysteines. Similarly, bioorthogonal sulfonylazides and terminal alkynes can react under the catalysis of Cu(I) to form stable N-acylsulfonamides in aqueous solution (**Figure 2D**; [36, 71]).

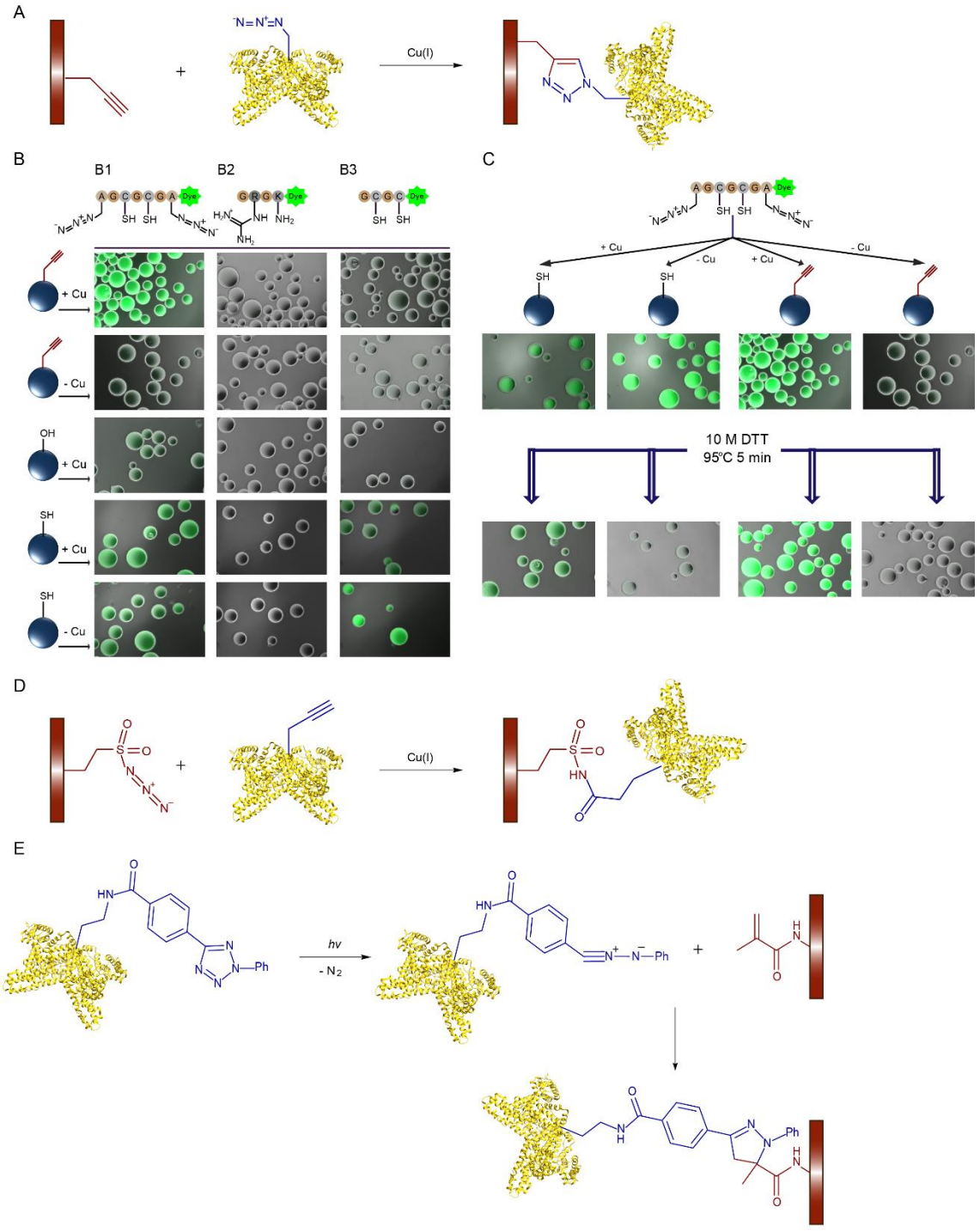

Figure 2: Metal-catalyzed and photo-induced bioorthogonal conjugation reactions for biomolecules. (A) Copper-catalyzed azide−alkyne 1,3-dipolar cycloaddition (CuACC); (B, C) Unspecific side reactions observed during the performance of CuAAC. Short peptide sequences with reactive functionalities and fluorescence label were coupled to alkyne-/ hydroxyl-/ and thiol-functionalized agarose particles under standard conditions deployed for CuAAC, and absence of Cu(I), respectively. (B) Particle fluorescence after 30 minutes incubation with 50 µM $CuSO_4$, 250 µM THPTA and 2.5 mM sodium L-ascorbate (+ Cu) and the same conditions in absence of $CuSO_4$ (– Cu). (C) Change in fluorescence intensity after washing with 1 M DTT and heating to 95 °C for 5 minutes to remove non-covalently bound peptide; (D) Click sulfonamide reaction (CSR); (E) Photoinducible 1,3-dipolar cycloaddition of 2,5-diaryltetrazoles and alkenes.

This ‘click sulfonamide reaction’ (CSR) proceeds regioselectively at room temperature in water. The versatility of this method was shown by surface immobilization of different types of biomolecules including biotin, carbohydrates, phosphopeptides and proteins [72]. The major drawback of CSR is the requirement of the copper(I) catalyst and associated stability and toxicity issues (*vide supra*) [71]. Besides copper, palladium is used as catalyst for aqueous Suzuki−Miyaura cross-coupling with the option of protein or peptide conjugation [59, 73].

Similar to metal catalysts, light can be used to activate bioorthogonal functional groups and thus control reagent availability. Among several photochemically triggered bioorthogonal reactions available, the light-induced 1,3-dipolar cyclodaddition is most frequently used for biologics (**Figure 2E**) [74]. In this reaction, the diaryl-tetrazole incorporated into the protein undergoes a cycloreversion reaction upon irradiation with UV light to form *in situ* a nitrile imine. This 1,3-dipole reacts with an alkene to form a stable pyrazoline cycloadduct [75]. The formation of the nitrile imine proceeds fast in buffer systems at room temperature avoiding exposure of sensitive proteins to UV light for more than 1–4 minutes [76]. Besides the advantage of the fluorogenic pyrazoline product allowing easy reaction monitoring [77], the inducibility by light is an attractive feature for spatiotemporal control over initiation and termination of the coupling reaction, e.g. for imaging or biosensor applications [78-80]. However, the bioorthogonal coupling for *in vivo* applications is limited, as the incorporation of the tetrazole moiety into the biologic is challenging and often results in low yields [74, 76]. Similar to the tetrazole-based photoclick reaction, azirines can be activated as nitrile ylides as shown for PEGylation of lysozyme [81]. Recently, several other photolabile protecting groups were described providing strategies with spatiotemporal control through the application of light with defined wavelength, intensity and exposure time [82]. To this end, various reactive groups can be protected with light-responsive groups, enabling controlled activation of the respective conjugation reaction, e.g. thiol-michael addition [83] or SPAAC [84]. Similarly, novel concepts of light-controlled enzymatic biomolecule patterning to PEG hydrogels were developed. By masking the enzymatic peptide substrate for transglutaminase with a photolabile cage, controlled photoactivation enables localized biomolecule tethering [85]. This approach circumvents difficult biomolecule modification with photosensitive moieties and light-induced damage of fragile proteins. Limitations of photo-triggered bioorthogonal reactions are the restricted biological applicability and side reactions of the photo-protected precursors with endogenous functionalities such as thiols [86].

A variety of catalyst-free reactions were described, proceeding site-specifically with fast kinetics, despite absence of metal ions or photoirradiation (**Figure 3**). Some time ago, ketones and aldehydes were explored for biorthogonal modification of biologics, as they react with amine nucleophiles enhanced by the α-effect, such as alkoxyamines and hydrazines [87-89] (**Figure 3A**). Under acidic conditions (pH 4–5.5) the amines along the peptide chain, which may also react with aldehydes and ketones, are protonated, while the aminooxy group serves as a nucleophile to attack the electron-deficient carbon in the aldehyde/ketone with high reactivity, leading to formation of oxime and hydrazone linkages, respectively. The use of carbonyl compounds is limited due to the slow rate constants, lability of the hydrazone- and oxime bond and competition with endogenous aldehydes and ketones of biomolecules inside cells [61, 90, 91]. As the reaction rate is pH-dependent, aniline or *m*-phenylenediamine (mPDA) are used as catalysts to accelerate the reaction under neutral conditions [91, 92]. Oxime formation conjugation strategies have been applied in site-specific polymer attachment [93, 94], protein immobilization on polymer films [95] and antibody labeling for targeted drug delivery [96, 97].

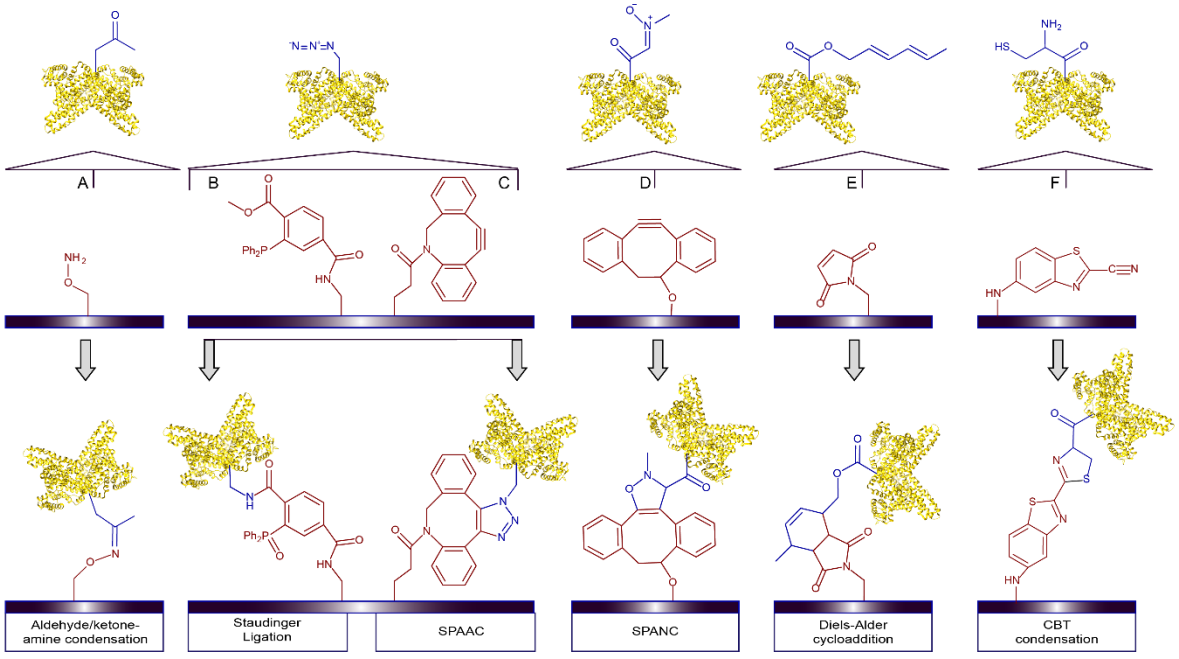

Figure 3: Representative examples of chemical bioorthogonal reactions without catalysts deployed for protein conjugation to biomaterials. (A) Aldehyde-/ketone condensation with amine nucleophiles leading to oxime or hydrazone linkages, respectively. (B) Staudinger ligation of azides and triarylphosphines; (C) Strain-promoted azide−alkyne 1,3-dipolar cycloaddition (SPAAC); (D) Strain-promoted alkyne−nitrone 1,3-dipolar cycloaddition (SPANC); (E) Diels-Alder cycloaddition and (F) 1,2-aminothiol cyanobenzothiazole (CBT) condensation.

The Staudinger ligation is a bioorthogonal coupling strategy linking an azide group with a phosphine-containing ester or thioester creating an amide bond (**Figure 3B**) [37, 98].

The reaction provides high yield and proceeds under physiological conditions. Depending on the strategy, the byproduct phosphine oxide can either remain attached to ('classical' Staudinger ligation [37]), or released from the final product ('traceless' Staudinger ligation [99]). The Staudinger ligation has limitations. The phosphine reagents easily oxidize in air and in general the reaction proceeds relatively slowly. In case of the 'classical' Staudinger ligation, the attached diphenylphospine oxide adversely affects water solubility of the conjugate [35, 43].

Due to the toxicological concerns of copper species, a copper-free variant of CuAAC was developed, using the ring strain energy of a cyclooctyne group and referred to as strain-promoted azide-alkyne cycloaddition (SPAAC). SPAAC proceeds rapidly and removes the need of catalysts (**Figure 3C)** [35]. Different cyclooctyne reagents were developed differing in stability, rate, biocompatibility, and PK properties, including difluorinated cyclooctynes (DIFO) or dibenzocyclooctynes (DBCO) [62]. SPAAC has also been effectively deployed in cell surface decoration or *in vivo* experiments in zebrafish [64, 100]. SPAAC has limitations. Cyclooctynes undergo nucleophilic addition with cellular nucleophiles such as glutathione and homotrimerization [42] as well as reaction with oxidized cysteines/sulfenic acids [101]. Another arguably alarming limitation of SPAAC for pharmaceutical development is due to the bulky, hydrophobic structure of the cyclooctyne component, which may alter the integrity and safety of the protein conjugates. Improved kinetics and biocompatibility of reactions with strained alkynes can be realized by choosing alternative 1,3-dipoles such as nitrones as reaction partners generating N-alkylated isoxazolines (**Figure 3D**). The strain-promoted alkyne-nitrone cycloaddition (SPANC) demonstrated high rate constants [102] and has been used for N-terminal peptide modification [103]. Recently, SPANC was used for the development of nitrone complexes as phosphorogenic bioorthogonal labels and imaging reagents for cyclooctyne-modified proteins [104]. More recently introduced methods such as SPANC or tetrazine ligation were linked to stability challenges from hydrolysis [42].

The Diels–Alder cycloaddition usually takes place between a dienophile and a diene to form an unsaturated six-membered ring (**Figure 3E**) [32]. This reaction proceeds in water with high selectivity and yield, offering a potential ligation method for peptides and functional proteins [105, 106] and proceeds site-specifically [106, 107]. Limitations are the reversibility of the reaction, hydrolysis susceptibility of the dienophiles and slow reaction kinetics [108].

The 2-cyanobenzothiazole (CBT) condensation reaction with 1,2-aminothiols (CBT-AT) is also called the split luciferin reaction, as the reaction constitutes the final step in the synthesis of luciferin (**Figure 3F**) [109]. Apart from proteins bearing N-terminal cysteines, 1,2-aminothiols are not found in proteins rendering it bioorthogonal for most biomolecules [110]. The condensation reaction proceeds under biologically compatible conditions and is used for labeling N-terminal cysteines of proteins [111, 112] or for biomolecule imaging [113].

Along these arguably more prevalent examples, several other bioorthogonal techniques were applied for protein immobilization. These include the Pictet-Spengler reaction linking aldehydes and tryptamine nucleophiles [114], tetrazine ligations [115], isocyanide-based click reactions [116] or quadricyclane ligations [117].

4. Enzymatic conjugation strategies for site-specific protein immobilization

Enzymes typically operate under ambient, mostly physiological conditions – in aqueous solution, at physiological pH and benign temperatures ranging from 4 to 37°C. Additionally, their high substrate-specificity and selectivity and fast reaction kinetics render them interesting tools for protein conjugation, typically occurring site-specifically (**Figure 4, Table 1**).

The translation of enzyme-catalyzed ligation strategies found in Nature to the conjugation of biologics typically requires the introduction of a recognition tag into the biologic or at its termini. By means of its tag, the biologic becomes a substrate for enzymatic ligation reactions, e.g. catalyzed by sortase A, transglutaminase, biotin ligase, lipoic acid ligase or tyrosinase.

These crosslinking enzymes offer a diverse array of site-specific conjugation approaches, that can be categorized according to different conjugation reactions and applications (**Figure 4**).

Transglutaminases (TGases) and sortases are physiologically relevant enzymes catalyzing crosslinking of antiparallel fibrin chains to mechanically stable clots [133] or anchoring of surface proteins to the cell wall of gram positive bacteria [134, 135], respectively. Owing to this natural cross-linking capability, these enzymes are well-suited for direct covalent conjugation of proteins to peptides, generation of protein-protein crosslinks [136, 137], synthesis of ADCs [2, 21, 138, 139], immobilization of proteins to the extracellular matrix (ECM) [6, 8], liposome modification [135] or covalent assembly into macromolecular networks [140] (**Figure 4A1**).

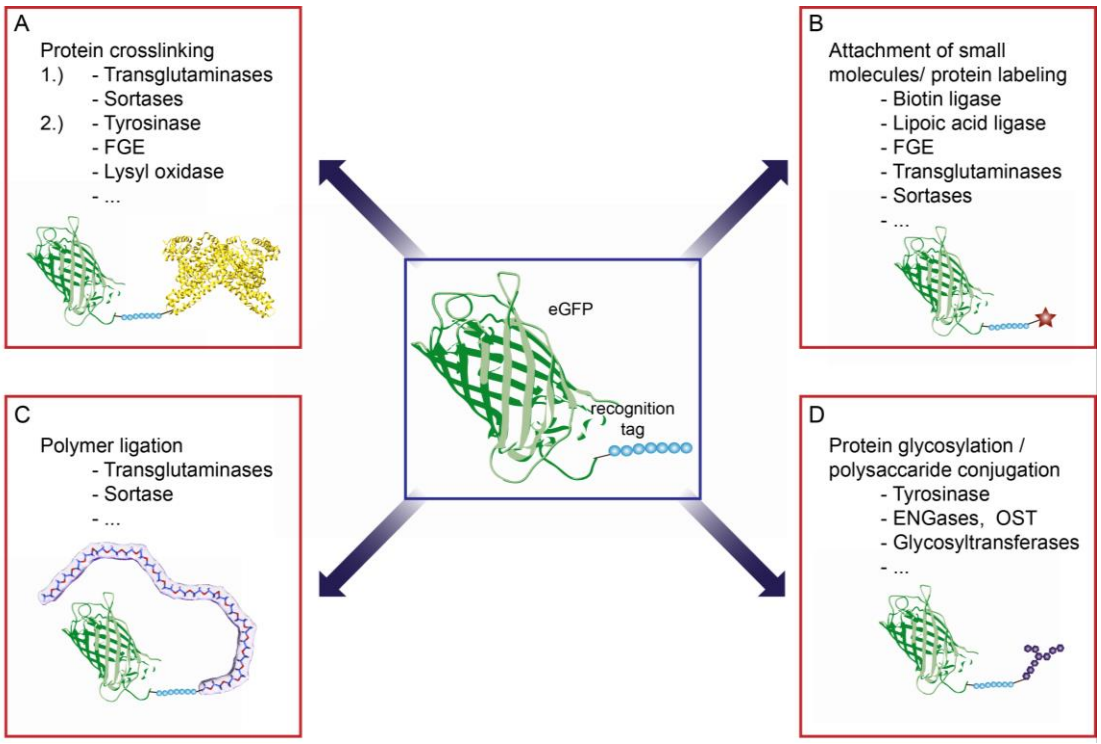

Figure 4: Overview of common applications catalyzed by cross-linking enzymes. (A) Intermolecular transpeptidation reactions to connect proteins with peptides, larger proteins or formation of networks, (1) directly catalyzed by e.g. transglutaminases (TGases) [8] or sortases [118] or (2) via formation of reactive intermediates catalyzed by tyrosinase [119, 120] or formylglycine-converting enzyme (FGE) [121]; (B) Conjugation of small molecules for labelling or drug delivery purposes is mediated by various enzymes, such as biotin ligase [122, 123], lipoic acid ligase [124, 125], FGE [121], TGase [126] or sortase [127, 128]; (C) Attachment of polymers, as mainly described for TGase [4] and rarely also for sortase A [129] (D) Conjugation of oligo- and polysaccharides, either directly by glycosylating enzymes such as Endo-β-N-acetylglucosaminidases (ENGases), glycosyltransferases or oligosaccharyltransferases (OST) [130], or via reactive species generated by tyrosinases [131, 132].

Besides this direct protein crosslinking by formation of new peptide bonds, various other enzymes mediate covalent protein crosslinking reactions via generation of reactive species, which spontaneously react with protein side chains. For example, tyrosinases convert surface-exposed tyrosyl side chains into *o*-quinones, followed by spontaneous reaction with side chains of proteins to form covalent cross-links [120](*vide infra*, **Figure 4A2**). Enzymes such as biotin ligase and lipoic acid ligase are preferably deployed to attach small molecules – such as cytotoxic drugs, fluorescent dyes or certain cofactors or tags [123, 124, 128] – to proteins (*vide infra*, **Figure 4B**). In addition, some of these enzymes also proved suitable for improving the PK properties of target proteins by effective polymer ligation [4] or protein glycosylation [130](**Figure 4C,D**). Combinations of enzymatic glycosylation followed by transferase-catalyzed PEGylation (termed 'Glycopegylation') were also proposed [141].

TGases catalyze acyl-transfer reactions between a carboxamide group of a glutamine residue and an unbranched primary amine, commonly the ε-amino group of a lysine side chain (**Figure 5A**) [142]. Site-specificity is obtained by confining the reaction to groups presented within defined amino acid sequences [143]. The most commonly used TGases – microbial TGase and (less frequently) tissue TGase and Factor XIIIa – are efficient mediators of amino acid conjugation due to their ability to form extremely stable covalent bonds and to function under a wide range of pH, salt, and temperature conditions [144]. The use of Factor XIII (Fibrogammin®P/ Corifact™) is particularly attractive for pharmaceutical application, as Factor XIII is FDA approved for treatment of congenital FXIII deficiency. Besides bridging fibrin monomers during wound healing, Factor XIIIa catalyzes covalent linkage of other ECM molecules or growth factors to fibrin fibrils [8, 133]. Intending to emulate this natural process, a recognition tag derived from α2 plasmin inhibitor (α_2PI, sequence NQEQVSPL) was previously introduced into recombinantly expressed proteins to enable site-specific immobilization into fibrin hydrogels [6, 145]. A variety of applications arose from this strategy, including site-specific protein PEGylation [4], preparation of ADCs [2, 139], generation of protein – enzyme conjugates [137] or immobilization of therapeutic proteins on biomaterials [146, 147], mainly by using the less specific microbial TGase.

Sortase A (derived from *S. aureus*) and its engineered variants are frequently used to attach oligoglycine derivatives to proteins expressed with a LPxTG tag. The transpeptidase cleaves the bond between threonine and glycine and a new peptide bond is created between the N-terminus of the oligoglycine and the threonine (**Figure 5B**) [127]. 'Sortagging' has been used extensively for bioconjugation *in vitro* and in living cells – especially for cell surface proteins expressing the LPxTG motif [128], for site-specific PEGylation [148], protein immobilization on glass slides [149] or antigen coupling to virus-like particles [150]. Disadvantages of sortase-mediated conjugation are mainly the high K_M of 5500 µM compared to 17 µM of transglutaminase (**Table 1**) and the reversibility of the reaction, as the glycine residue released in the first step can act as a nucleophile to reform the original species. For this reason, high excess of the oligoglycine nucleophile is required, along with continuous removal of the released glycine-peptide [138]. Depending on protein stability, a short tag (consisting of ≤ 5 amino acids) is sufficient for recognition by TGase or sortase A. An additional asset of TGase- or sortase-catalyzed reaction is their tolerance regarding the location of the modification site within the therapeutic, which can be within the target protein sequence or at its termini. Many other enzymatic methods are limited in this sense, restricting conjugation to the biologics' N-

or C-terminal tags or highly flexible loops. This feature can be particularly useful if the biologics' termini are essential for bioactivity.

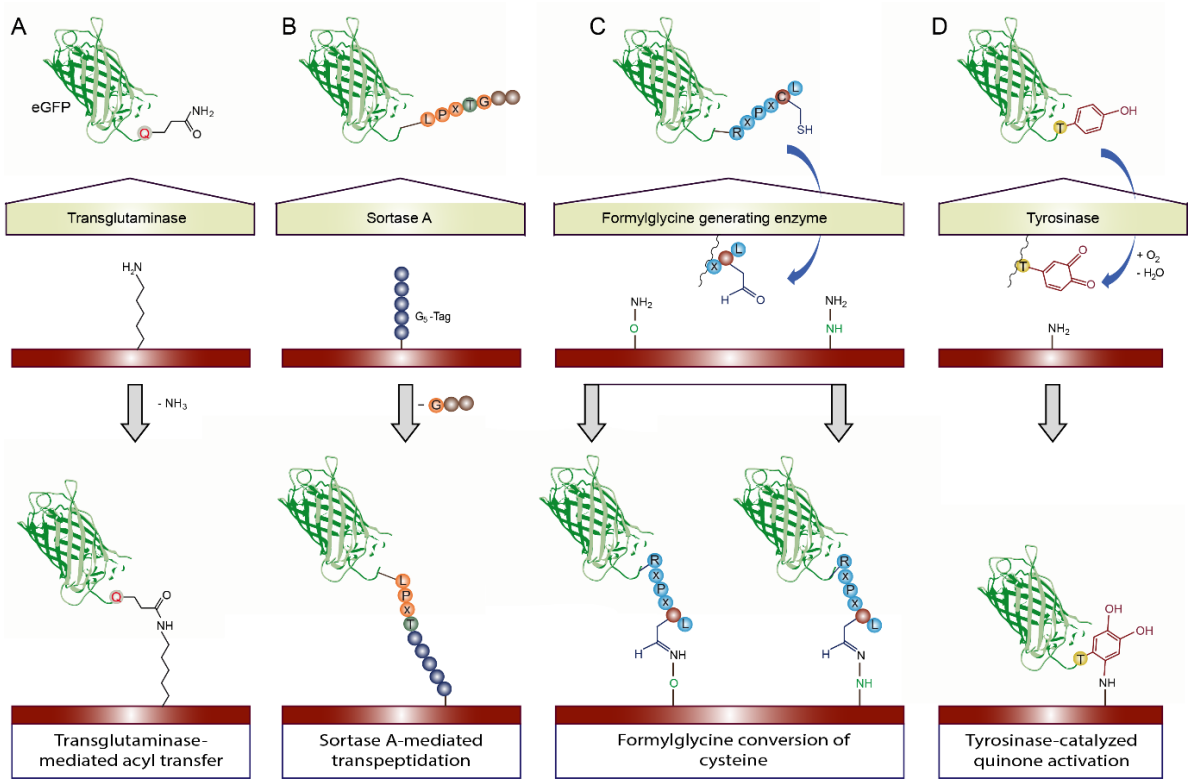

Figure 5: Representative examples of enzymatic bioorthogonal reactions deployed for protein coupling to biomaterials. (A) Transglutaminase-catalyzed acyl-transfer reaction; (B) Sortase A-mediated transpeptidation; (C) Formylglycine conversion and (D) Tyrosinase-catalyzed quinone activation.

Formylglycine generating enzyme (FGE) post-translationally modifies by converting a cysteine within the CxPxR motif to formylglycine. Thereby, an aldehyde group is site-specifically introduced into the protein and available for modification through bioorthogonal oxime or hydrazone ligation (**Figure 5C**). Also different synthetic peptides were found to be recognized by FGE [121]. In spite of 6 residues of the aldehyde tag being sufficient for FGE recognition, an extension of the tag to 13 residues (LCTPSRGSLFTTGR) provides higher levels of conversion, potentially due to better accessibility to the enzyme's active site. The introduction of these large recognition tags can alter the protein structure with potential reduction in bioactivity [122, 158].

Table 1: Kinetic parameters of relevant enzymes used for protein conjugation.

Enzyme	Tag sequence	Substrate	K_M [µM]	Reference
Tissue transglutaminase	Ac-GQQQLG	Ac-FKG-NH_2 Dopa-FKG-NH_2	46.9 17	[143]
Factor XIIIa	- (colorimetric assay) Abz-NE(Cad-Dnp)EQVSPLTLLK	– Glycine-methylester	25 19.8	[151] [152]
Sortase A Triple mutant Sortase A	LPXTG LPETG LPRTG	GGG-R GGGGG GGG	5500 7300 560	[153] [134] [154]
Formylglycine generating enzyme	MTDFYVPVSLCTPSRA ALLTGRS	– (FG conversion)	0.013	[155]
Tyrosinase	L-DOPA	– (conversion)	933	[156]
Lipoic acid ligase	GFEIDKVWYDLDA GFEIDKVWYDLDA	Lipoic acid Azide lipoic acid	13.32 127	[157] [125]
Biotin ligase	GLNDIFEAQKIEWHE	Biotin	25	[122]

Tyrosinase is a copper-containing enzyme modifying tyrosine residues. The enzyme catalyzes the oxidation into reactive *o*-quinones, which in return become substrates to non-enzymatic reactions with nucleophilic amine and sulfhydryl groups of amino acid residues (**Figure 5D**). This strategy has been demonstrated for the decoration of chitosan [131], is widely used in the food industry [159], was applied to immobilize proteins on pH-responsive chitosan gels [120] or for the modification of silk fibroin or sericin peptides [119]. The major drawback of tyrosinases are the high reactivity of *o*-quinones, leading to condensation with each other and reaction with nucleophiles, such as the amino and sulfhydryl groups of amino acid residues [159].

5. Combining enzymatic and chemical conjugation strategies

The strategy is to firstly introduce a reactive functional group into the biologic, followed by a second conjugation reaction to this introduced functional group (**Figure 6**). A well-known example is the use of lipoic acid ligase, a natural enzyme catalyzing the acylation of a sequence-specific lysine residue with lipoic acid (**Figure 6A**). Replacing lipoic acid by chemically modified lipoic acid analogues expanded the enzyme's use to selective protein modification, in that firstly the lipoic acid derivative containing a certain functionality is enzymatically introduced into the biologic, which in return is chemically conjugated using e.g. CuAAC, SPAAC, Staudinger ligation or inverse Diels-Alder reaction [124, 125].

Site-specific attachment of biotin groups onto biomolecules was performed using biotin ligase, catalyzing the transfer of biotin to the ε-amino group of a lysine residue within a special recognition tag (**Figure 6B**) [122]. This biotinylated biologic becomes a substrate for avidin and its derivatives complexing biotin in a covalent manner ($K_{diss} \sim 10^{-15}$ M). Alternatively, ketone derivatives of biotin were used followed by hydrazone ligation or Staudinger ligation [123, 158]. Biotin ligase is frequently used to modify proteins for live imaging applications [160]. All these ligases are particularly suitable for the two-step approach outlined in this section as the ligases' restriction in the size of the processed substrate are elegantly addressed – a small substrate is attached through the ligase and in a second reaction this substrate is linked to e.g. large biomolecules or polymers which would not be processed by ligase. The two-step strategy can be also extended to TGase or sortase proving beneficial in cases in which the coupling should proceed fast (e.g. due to stability issues of the biologic or enzyme; **Figure 6C**). In these cases, biotin ligase or TGase are superior compared to sortase (with $K_M < 30$ µM compared to 5.5 mM), ensuring remarkably short reaction times with sufficiently good conjugation yield [161].

6. Comparison of advantages and drawbacks of enzymatic and chemical conjugation strategies

Sensitive proteins frequently benefit from enzymatic crosslinking owing to the remarkably fast reaction rates (with exception of sortase A; **Table 1;** [61]) and highly specific activity under mild aqueous conditions, retaining the native conformation and bioactivity of most target proteins [29]. These properties contrast toxicity concerns of chemical compounds or their harmful byproducts, which could perturb the activity or conformation of the protein and/or jeopardize its solubility [63-66]. In addition, the exceptional substrate specificity of the majority of crosslinking enzymes generates homogenous products absent from side products, that are difficult to purify [2, 29]. A supplementary advantage is the catalytic function of enzymes, entailing their complete restoration after each catalytic cycle [139]. On the other hand, chemical compounds are distinguished by their high versatility, commercial availability and small size, avoiding interference with the native protein structure [1, 162]. In contrast, the sequence specificity of most enzymes – except tyrosinases and to a certain degree TGases [2, 4, 120] – implies the requirement of longer recognition motifs, potentially altering protein structure [157, 163].

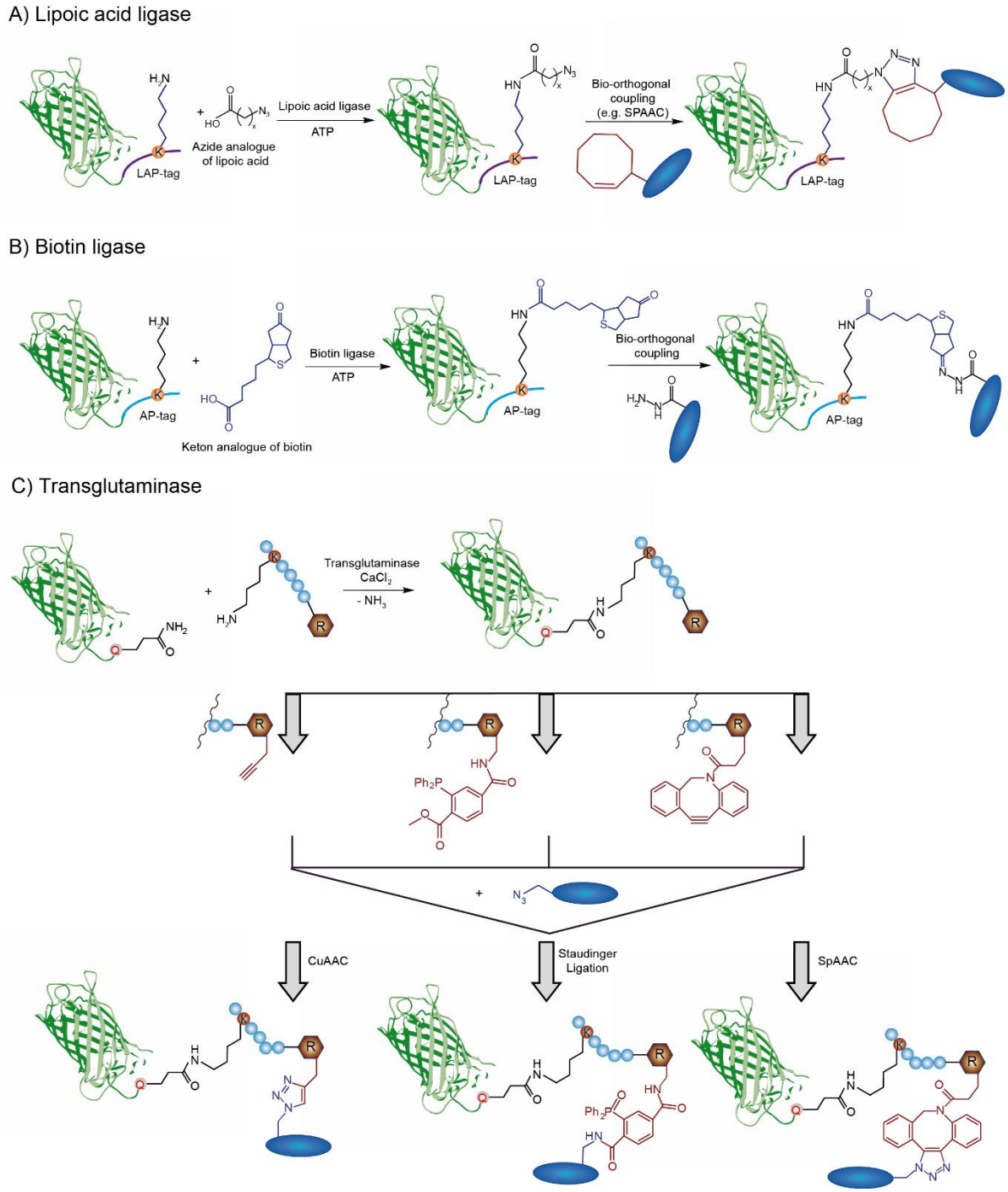

Figure 6: Combinations of enzymatic and chemical site-directed coupling strategies. In these examples, the first enzymatic conjugation step is used to attach a reactive functional group into the protein, which can be subsequently used to perform a secondary chemical coupling reaction in a site-specific manner. (A) Lipoic acid ligase-catalyzed introduction of an azide-modified lipoic acid derivative, followed by SPAAC using a cyclooctyne-functionalized biomaterial. (B) Biotinylation of a protein at a specific lysine residue catalyzed by biotin ligase and subsequent oxime formation. (C) Integration of a chemically functionalized linker into the protein mediated by transglutaminase, enabling a variety of different chemical site-specific reactions, such as CuAAC, Staudinger ligation or SPAAC.

The broad range of chemical reagents available for targeting different functional groups provide space for individual modification with structurally diverse target molecules at different locations within the protein sequence [50]. In contrast, several enzymes are more restricted regarding the position of the introduced tag (e.g. biotin ligase and FGE require N-or C-terminal regions, TGases and sortases at least flexible loops for accessibility [127, 133]). Highly effective enzymatic conjugation is achieved using substrates showing similarity in size and shape to the natural substrate of the respective enzyme for reaching the active site [125, 134], thus limiting several modifications. Among the different enzymes available, the pronounced substrate specificity and absence of side products applies best to mammalian TGases and sortase A, while tyrosinase- and FGE-catalyzed crosslinking can be difficult to control, as only the initial activation of amino acid residues is enzyme-mediated and the formed reactive species can undergo spontaneous consecutive reactions [43, 119, 121].

7. Application

A selection of relevant applications is exemplarily depicted in **Figure 7** and **Table 2**.

7.1 Biologic-polymer conjugates

Many therapeutic proteins have been conjugated with polyethylene glycol (PEG), e.g. PEG-Intron® for Hepatitis C [164], PEGASYS® (PEG-IFN-alpha 2a) and PEG-Neupogen® (PEG-G-CSF) [26]. The physical and pharmacological properties of PEGylated proteins are affected by the number and the size of PEG chains attached to the polypeptide (degree of heterogeneity), the location at which the PEGs are attached to the biologic, and the conjugation chemistry used for PEGylation [5]. Typically, the ε-amino groups of a biologic are randomly PEGylated, yielding the aforementioned positional isomers and heterogeneous outcome [26]. For instance, PEGASYS® is a product within which up to 9 different lysines of Interferon α-2a are PEGylated resulting in isomers with substantially distinct bioactivities [28]. PEGylation of Intron® A generated a broad variety of PEGylated products of which 48% were reported to be derivatized at the His34 residue but also at various lysines, the N-terminal cysteine, as well as serine, tyrosine, and further histidine residues [164].

Enzymatic conjugation strategies and chemical conjugation strategies have been shown to effectively overcome the challenges of conjugation heterogeneity (**Table 2**). Guinea-pig liver transglutaminase was shown to catalyze the site-specific incorporation of PEG-alkylamine into

proteins at natural or genetically introduced glutamine residues [4]. For example, the cytokine interleukin-2 was site-specifically PEGylated using TGase with preserved bioactivity [165]. Furthermore, azide-modified superoxide dismutase-1 (SOD) was site-specifically PEGylated using CuAAC [5]. By using 5 kDa and 20 kDa PEG-alkyne, respectively, 70-85% conjugation rates were reported at 37 °C yielding PEG-modified SOD derivatives with wild type bioactivity.

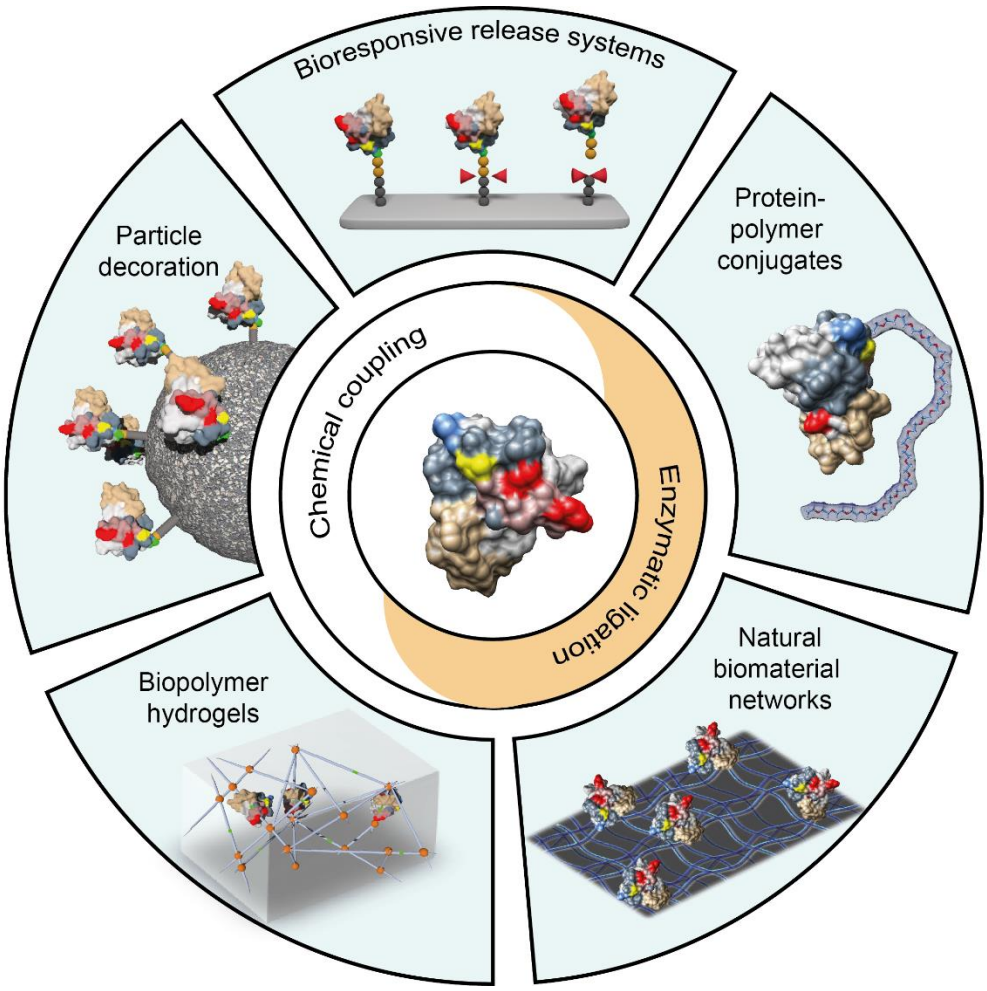

Figure 7: Applications of bioorthogonal strategies for protein delivery, shown by the example of insulin-like growth factor-1.

Besides the general shortcomings of CuAAC for protein modification, such as (i) Cu(I) toxicity, and (ii) poor solubility of Cu(I)-stabilizing chelating ligands, the (iii) complexation of copper ions by polyethylene glycol is a particularly important aspect when using CuAAC for PEGylation [26, 166]. Therefore, copper-free 1,3-dipolar cycloadditions are suitable alternatives for the conjugation of polyethylene glycol to proteins and enzymes. Following that approach, one study reported the attachment of the aza-dibenzocyclooctyne analogue DIBAC-PEG_{2000} to *Candida antarctica* Lipase B with higher conversion compared CuAAC [167, 168].

A second study used SPAAC for PEGylation of therapeutic proteins [169]. In spite of PEGs dominating importance, other polymers such as poly(2-oxazoline) (POx) were site-specifically conjugated to interleukin-4 (IL-4) analogues by CuAAC [170]. Similar approaches were reported for azide-polystyrene [171], polystyrene-*b*-polyethylene glycol (PS_m-*b*-PEG_{113}) diblock copolymers [172] and propargyl-containing P(LA90–co–MPC10) polymers [173]. Typically, high coupling yields were reported when reacting the polymer at a 1.5 to 2 fold excess with the therapeutic.

Aside of these linear polymers, dendrimers were effectively decorated by CuAAC, thereby increasing the interaction of otherwise weakly interacting ligands through avidity [174]. For example, decoration of the dendrimer end groups with epidermal growth factor (EGF) [175] induced effective targeting of EGF receptor expressing cells. Furthermore, $\alpha_v\beta_3$ integrin dependent uptake was reported for CuAAC decorated dendrimers carrying RGD [176].

7.2 Decorated surfaces

Site-directed protein and enzyme immobilization on planar surfaces - such as biochips and microarrays presenting biologics - propelled the reproducibility and catalytic activity of assays through homogeneous orientation (**Figure 1**; **Table 2**) [38, 41, 46, 177-179]. This advantage was illustrated with alkyne- and azide-functionalized proteins, proving an increased binding activity compared to random immobilization and the absence of nonspecific side reactions [180] and other studies proved the storage stability of the decorated surfaces [38, 177]. Similar to these cycloadditions, Cu(I) dependent CSR and (copper free) Diels-Alder reaction were reported for site-specific immobilization of functional proteins on modified surfaces [72, 106]. Other studies modifying glass inter-positioned a bifunctional PEG linker between the biomolecule and the surface combining Huisgen 1,3-dipolar cycloaddition with a Diels–Alder reaction and as demonstrated for biotin, lactose and thrombomodulin [107]. Along these studies on planar surfaces, many studies outline the decoration of e.g. agarose-, magnetic-, or luminescent particles, respectively [181-186]. For delivery of therapeutic proteins, such as growth factors or cytokines, immobilization on agarose particles using bioorthogonal methods represents a reliable method to provide constitutively active surfaces [181, 187].

The advantage of site-specific immobilization through CuAAC contrasting conventional amide bond formation methods was demonstrated for Maltose binding protein (MBP) bound to PEGylated magnetic nanoparticles and yielding two fold increased bioactivity [188]. Similar

to the inter-positioned PEG, bioresponsively cleaved linkers were inter-positioned between the biologic and the surfaces responding to pH or enzymes [189, 190]. The specificity of the bioorthogonal coupling reaction opens an additional interesting feature, the conjugation of functionalized proteins present at exceptionally low concentrations in complex mixtures including cell lysates [182, 183].

7.3 Biomaterial conjugation

Favorable biomaterials for drug delivery of biologics are components of the extracellular matrix (ECM) due to their excellent biocompatibility and natural environment, positively impacting cell attachment, migration, proliferation and differentiation [204]. Biomaterials including collagen, fibrin, hyaluronic acid or silk fibroin (SF) were also decorated site-specifically, e.g. for tissue regeneration [40, 162] and / or drug delivery purposes [46, 205, 206]. Quite frequently, the biologics were loaded non-covalently to the biomaterial, but this typically triggered high burst release and short activity [207, 208], which is why novel site-specific syntheses were featured for decoration. ‘Site-directed adsorption’ was achieved by fusing a collagen-binding domain (CBD) to growth factors, which in return bind through their CBD to collagen materials [209]. Similarly, other strategies exploit affinity interactions of growth factors with heparin binding domains of fibronectin [210].

Enhanced stability and matricrine effects of immobilized proteins were reported following covalent anchoring to biomaterials [7, 211]. As fibrin fibrils are covalently crosslinked by the plasma transglutaminase Factor XIIIa to form a dense network during wound healing, the enzymatic mechanism has been exploited to covalently incorporate biologics within the fibrin network. Several proteins were recombinantly expressed with a transglutaminase substrate site from the N-terminus of α2-plasmin inhibitor for covalent immobilization within fibrin networks [145, 201, 202]. Besides fibrin, natural transglutaminase substrate sequences are present in other ECM proteins, such as fibronectin and collagen II, thereby allowing site-specific anchoring of modified biologics using enzymatic crosslinking without the need for biomaterial modification [8]. In these cases of covalent protein immobilization on the biomaterial, release depends on the matrix degradation rate. For example, drugs covalently bound to fibrin or collagen are released by the action of cell-secreted or cell-activated proteases such as matrix metalloproteinases and plasmin, which degrade the matrix.

Table 2: Representative examples of bioorthogonal protein conjugation for therapeutic use

	Material	**Strategy**	**Protein**	**Ref**
Synthetic polymers	Linear synthetic polymers	CuAAC	Protein transduction domain	[171]
	Polymer fibers	CuAAC	Testis specific protease (TSP50)	[173]
	Polyethylene glycol (PEG)	CuAAC	Superoxid dismutase 1	[5]
		SPAAC	Candida Antarctica lipase B	[167]
		SPAAC	Designed Ankyrin Repeat Proteins	[169]
		Transglutaminase	Interleukin-2, hGH, calcitonin	[165]
		Photoinduced azirine ligation	Lyoszyme	[81]
	PEG hydrogels	Transglutaminase	Vascular endothelial growth factor	[192]
	Block copolymers	CuAAC	Myoglobin, Horse radish peroxidase	[172]
	Amphiphiles	CuAAC	Bovine serum albumin	[193]
	Polyacrylamide hydrogels	Oxime ligation	ECM proteins	[93]
Dendrimers	Azide/Alkyne dendrimers	CuAAC	RGD peptide	[176]
		CuAAC	Polyethylene glycol	[194]
		CuAAC	Epidermal growth factor	[175]
		CuAAC	Antimicrobial peptide	[195]
Planar surfaces	Glass slides	CuAAC, Diels Alder	Thrombomodulin	[107]
		Staudinger	Rab7 protein	[178]
		CuAAC + Staudinger	Green fluorescent protein/GST	[177]
		Click Sulfonamide	Cherry-Ypt7, RBD	[72]
		Diels Alder	Streptavidin	[106]
	Gold surface	CuAAC	Myoglobin	[179]
	Microarray	CuAAC	Enhanced green fluorescent protein	[180]
		Staudinger	Ribonuclease A	[38]
Particles	Agarose particles	CuAAC	Fibroblast growth factor (FGF)	[181]
		CuAAC	Farnesyl-transferase	[182]
		CuAAC	Peptides	[183]
	Magnetic nanoparticle	CuAAC	Maltose binding protein	[188]
		CuAAC	Human serum albumin	[184]
	Luminescent nanoparticles	CuAAC	Protein receptor interaction site	[185]
	Gold nanoparticle	CuAAC	Lipase	[39]
	Silica nanoparticles	Thiol-maleimide	Insulin-like growth factor-I	[196]
	Polymer beads	Sortase	Fluorescent proteins	[197]
Self-assembled structures	Micelles / SCKs	CuAAC	Peptides	[198]
	Liposomes	CuAAC	Peptides	[199]
Natural or semi-synthetic materials	Chitosan	Tyrosinase	Sericin peptides	[119]
		Tyrosinase	Enhanced green fluorescent protein	[120]
	Hyaluronic acid	N-terminal functionalization	Human growth hormone	[200]
	Fibrin	Transglutaminase	Bone-morphogenetic protein-2	[6]
		Transglutaminase	Vascular endothelial growth factor	[201]
		Transglutaminase	L1Ig6	[202]
	Collagen	SPAAC	Epidermal growth factor	[7]
	Fibronectin	Transglutaminase	Azide-modified peptide	[8]
	Elastin-like polypeptides	Genetic fusion	Interferon alpha	[203]
	Silk fibroin	CuAAC	Fibroblast growth factor (FGF)	[162]

7.4 Bioresponsive release systems

For all above mentioned applications, linkers can be integrated conferring benefits to the protein and biomaterial, mainly reducing adsorption to hydrophobic surfaces or increasing the distance for improved accessibility to binding sites [39, 107, 188]. Additionally, these inter-positioned linkers can be stimuli-responsive, e.g. susceptible to pH, light, redox potential or index proteases to provide better control over drug action [52, 212]. For example, intracellular drug release can be achieved using linkers, that are hydrolyzed by the acidic pH of endosomes (i.e. N-cis-aconityl acid spacer and hydrazon linkages [213]) or by lysosomal enzymes [190]. Especially for cancer therapeutics, drug targeting to tumors and controlled activation of the cytotoxic drug is highly desirable [214]. This aim of specifically releasing potent drugs in the intracellular environment of tumors can be accomplished based on the increased glutathione content and higher concentration of reductases in cancer cells, which is able to break disulfide bonds of integrated linkers [215, 216]. Controlled drug release in a specific target tissue is realized using linkers responding to elevated protease activity, releasing the active drug at the target side during disease progression [189, 217]. The purpose of such prodrug strategies is to limit off-target toxicity and to enhance PK properties such as biodistribution. The preparation of inactive conjugates can be performed by site-specific modification of the therapeutic protein with a stimuli-responsive linker attached close to the ligand binding site. Thus, activation at the target site reveals the protein's therapeutic function [189]. For instance, as local inflammation preludes the onset of myositis flares, localized matrix metalloproteinase (MMP) upregulation can serve as a surrogate marker driving release of therapeutics from a carrier within tissues of need [9]. Similar approaches were also applied to biomaterials for tissue engineering [218]. A study describes the immobilization of vascular endothelial growth factor (VEGF) immobilized on fibrin matrices via a plasmin-sensitive sequence for accelerated, cell-demanded release [201]. As the PK improvements of PEGylation are often opposed by bioactivity impairments due to attachment of the large polymer, the concept of reversible PEGylation is gaining increasing attention [219]. Apart from cleavable linkers, novel concepts describe the use of degradable polymers for development of stimuli-responsive conjugates. For example, integration of an acid-cleavable unit into functional PEG chains enables protein release at low pH [220] or photosensitive groups can provide control over removal of a PEG photocage [221]. Furthermore, progress in the area of bioorthogonal cleavage reactions was made aiming for special applications such as intracellular prodrug activation [222, 223].

Besides drug delivery purposes, site-specific protein conjugation found application in many other fields. A main area is labelling of biomolecules to study interaction and distribution phenomena [224] and to image biological processes in living cells [64, 123, 124]. Typically, fluorophores or small molecules are attached to the biologic in a site-specific fashion to study protein interactions at molecular level *in vivo* [158]. Modification of cell surface proteins is possible using chemical [64, 225] or enzymatic methods [123]. Bioorthogonal approaches are also perfectly suited for attachment of cytotoxic drugs [226] or targeting molecules – such as antibody fragments, folate [227, 228] or antigens for vaccine delivery [150]. As mentioned before, the presented coupling reactions are suitable for diagnostic applications as well [229]. Several protein-based biosensors have been developed by applying 'Sortagging' technology [149] or by chemical bioorthogonal strategies [46, 230]. As an aside, crosslinking enzymes – most frequently microbial TGases – are used in food industry applications for modification of texture and appearance of food products [144, 159] or for development of biomimetic tissues scaffolds or for strengthening protein-based fibers for textile fabrication [231].

8. Defining the conjugation strategy

For maximum benefit of the biologic's potential, all features of the biomaterial and biologic have to be optimally adapted and interconnected. The biomaterial selection should be based on biocompatibility and degradation aspects, as well as mechanical and physicochemical parameters due to the strong impact on cell adhesion, drug release and therapeutic efficacy of the entire bioconjugate. The material characteristics were studied in detail and reviewed elsewhere [205]. In case a soluble conjugate is advantageous for desired application, hyaluronic acid or elastin-like polymers (ELPs) can be used as a substitute for PEG prolonging the circulating half-life of biologics [200, 203, 232, 233]. Important design parameters featuring biologics on surfaces include the therapeutics' release rate - occurring either passively or bioresponsively - and stability considerations. Both aspects are essentially driving the need for and nature of a linker between the therapeutic and the surface (**Figure 8**) [188, 189]. For passive release, biodegradable biomaterials – particularly elastin, collagen and fibrin – enable sustained release of covalently bound biologics due to the natural susceptibility to proteolytic enzymes, such as collagenases and elastase [6, 201]. For stimuli-responsive release, cleavage of an inter-positioned linker releases bioactive molecules in case of disease flares [189, 222]. This strategy is particularly advantageous, if the therapeutic does not target extracellular or soluble epitopes

but binds to an intracellular target. Therefore, efficacy depends on the efficient cellular uptake and release into the cytosol [52].

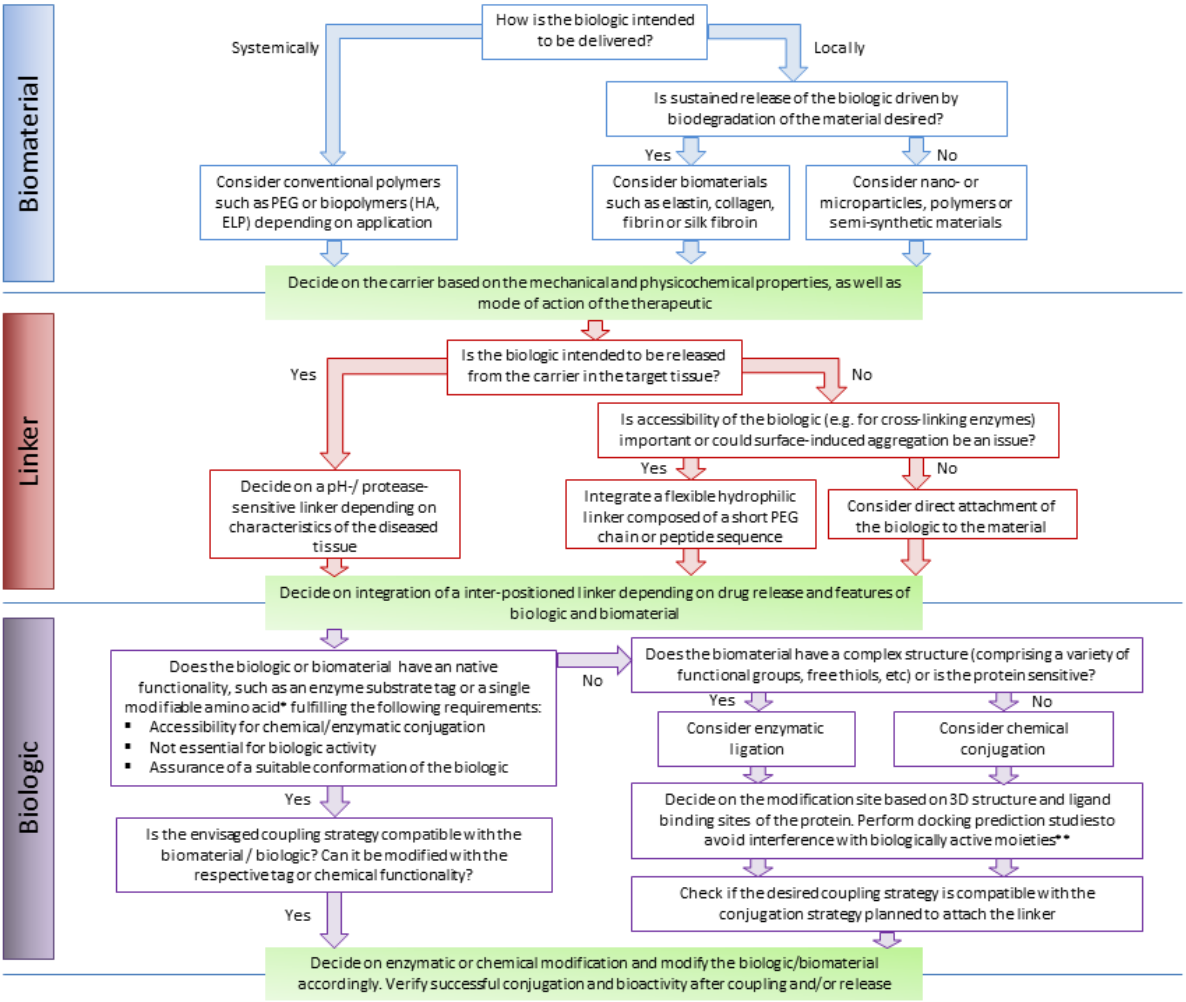

Figure 8: Outline of a decision process for choosing an appropriate site-directed bioconjugation strategy. [* site-directed modification with one lysine is only possible when the N-terminus is acetylated or not accessible for conjugation; **Protein structure prediction can be performed e.g. by Robetta beta and docking studies of the protein to a target e.g. using ZDOCK [236]. The impact of a certain modification on the bioactivity can be estimated e.g. by RosettaBackrub, [237]].

Controlled biologic release can be realized by integration of a pH- or enzyme-cleavable linker between the therapeutic and the biomaterial or by using smart polymers that undergo reversible changes in size and hydrophobicity in response to external stimuli such as temperature, light and/or pH [190, 213, 234]. Alternatively, linkers can be used to address stability challenges of sensitive biologics, as direct attachment to biomaterials frequently introduces steric constraint potentially impacting bioactivity of the therapeutic protein or jeopardizing safety through partial unfolding and associated immune responses [107, 188]. In this case, site-directed

attachment of CPPs also proves advantageous to achieve efficient intracellular delivery bypassing the endocytotic pathway [235].

The selection of the conjugation strategy is typically dictated by the therapeutics' characteristics [55]. In cases in which one distinguishing amino acid is available in the primary sequence (such as lysine, cysteine, tryptophan or tyrosine [52, 238, 239]) and in case these sites are promising anchor sites for the intended purpose, standard chemical ligation methods can be used for immobilization [59, 110]. Similarly, therapeutics with an inherent substrate sequence for e.g. transglutaminase or sortase A [158] are effectively immobilized enzymatically [240]. Biologics rarely provide these advantageous features readily, but these can be rationally engineered into the proteins [56, 58]. For example, site-specific incorporation of a substrate tag for an enzymatic ligation reaction, e.g. catalyzed by sortase A or transglutaminase [145, 197] or artificial amino acids for chemical ligation [50, 57, 187] allows unique functionalities to be introduced into the protein sequence. Due to the exceptionally high specificity of enzymes, faster kinetics and milder coupling conditions compared to chemical conjugation, enzymatic ligation provides advantages, especially for sensitive biologics and complex biomaterials [61, 161]. In cases in which artificial amino acids are sought for chemical ligation, the decision whether CuAAC or SPAAC is more suitable, is typically based on the therapeutics' propensity to copper or the intended application restricting the use of trace metals [64]. For example, free thiols in the therapeutic or the biomaterial may limit the success of CuAAC due to copper induced aggregation [168, 241, 242]. To identify a suitable position for modification with the unnatural amino acid or tag, structural information of the biologic helps to avoid interference with ligand binding sites and to estimate accessibility of the conjugation site. Several structure and docking prediction tools are available [236] and the impact of the modification on bioactivity can also be estimated [237]. The functional importance of the conjugation site was also demonstrated for ADCs, having a pronounced effect on PK properties, plasma stability, rate of drug release and efficacy of ADC species *in vivo* [13, 23].

For those cases in which integration of a flexible or stimuli-responsive linker is intended, a second site-specific conjugation strategy is required (*vide supra*). In case of a peptide linker, expression of the fusion protein consisting of biologic and linker sequence is an attractive option, thereby circumventing the second purification step. After successful conjugation, a variety of analytical tools and bioactivity assays is available to assess bioconjugation success and potency of the conjugate [55, 181]. Finally, the evolution from native (or slightly modified)

biomolecule to therapeutic conjugates through attachment of complex structures such as polymers, large proteins or biomaterials introduces new challenges related to stability, immunogenicity and elimination of the protein therapeutic. These altered characteristics can substantially affect the pharmacology and PK of the conjugates. Therefore, they have to be considered and ADME properties should be assessed [243].

9. Conclusion

The nature of the biomaterial/polymer, the need and type of linker structure, and the features of the biologic impact the selection of chemical or enzymatic ligation strategies for conjugation synthesis. This inter-disciplinary effort is essential for the rational and successful design of conjugates. This review aimed at facilitating that selection process by discussing these strategies in detail and then emulating published examples into one flow chart overarching and integrating the aspects of conjugate synthesis. One focus was on heterogeneous product outcome, translating the need for well characterized conjugates for diagnostic or clinical application [244]. To summarize, the countless opportunities arising from well-defined, homogenous conjugates enable development of effective protein delivery systems with potential to overcome current challenges associated with protein therapeutics, such as their pharmacokinetic weakness, instability and the limited membrane permeability to reach intracellular targets [245].

Acknowledgment

The financial support of the Bundesministerium für Bildung und Forschung (German Federal Ministry of Education and Research; #13N13454) is gratefully acknowledged.

References

[1] B. Tabisz, W. Schmitz, M. Schmitz, T. Luehmann, E. Heusler, J.-C. Rybak, L. Meinel, J.E. Fiebig, T.D. Mueller, J. Nickel, Site-Directed Immobilization of BMP-2: Two Approaches for the Production of Innovative Osteoinductive Scaffolds, Biomacromolecules, 18 (2017) 695-708.

[2] J. Spidel, B. Vaessen, E. Albone, X. Cheng, A. Verdi, J.B. Kline, Site-Specific Conjugation to Native and Engineered Lysines in Human Immunoglobulins by Microbial Transglutaminase, Bioconjugate Chemistry, (2017).

[3] D. Schumacher, C.P.R. Hackenberger, H. Leonhardt, J. Helma, Current Status: Site-Specific Antibody Drug Conjugates, Journal of Clinical Immunology, 36 (2016) 100-107.

[4] H. Sato, Enzymatic Procedure for Site-Specific Pegylation of Proteins, Advanced Drug Delivery Reviews, 54 (2002) 487-504.

[5] A. Deiters, T.A. Cropp, D. Summerer, M. Mukherji, P.G. Schultz, Site-Specific PEGylation of Proteins Containing Unnatural Amino Acids, Bioorganic & Medicinal Chemistry Letters, 14 (2004) 5743-5745.

[6] H.G. Schmoekel, F.E. Weber, J.C. Schense, K.W. Grätz, P. Schawalder, J.A. Hubbell, Bone Repair with a Form of BMP-2 Engineered for Incorporation into Fibrin Cell Ingrowth Matrices, Biotechnology and Bioengineering, 89 (2005) 253-262.

[7] H.J. Lee, G.M. Fernandes-Cunha, I. Putra, W.-G. Koh, D. Myung, Tethering Growth Factors to Collagen Surfaces Using Copper-Free Click Chemistry: Surface Characterization and *in Vitro* Biological Response, ACS Applied Materials & Interfaces, 9 (2017) 23389-23399.

[8] S.M. Früh, P.R. Spycher, M. Mitsi, M.A. Burkhardt, V. Vogel, I. Schoen, Functional Modification of Fibronectin by N-Terminal FXIIIa-Mediated Transamidation, ChemBioChem, 15 (2014) 1481-1486.

[9] A.C. Braun, M. Gutmann, R. Ebert, F. Jakob, H. Gieseler, T. Luhmann, L. Meinel, Matrix Metalloproteinase Responsive Delivery of Myostatin Inhibitors, Pharmaceutical Research, 34 (2017) 58-72.

[10] A.D. Ricart, Antibody-Drug Conjugates of Calicheamicin Derivative: Gemtuzumab Ozogamicin and Inotuzumab Ozogamicin, Clinical Cancer Research, 17 (2011) 6417-6427.

[11] L. Wang, G. Amphlett, W.A. Blättler, J.M. Lambert, W. Zhang, Structural Characterization of the Maytansinoid–Monoclonal Antibody Immunoconjugate, huN901–DM1, by Mass Spectrometry, Protein Science, 14 (2005) 2436-2446.

[12] R.P. Lyon, T.D. Bovee, S.O. Doronina, P.J. Burke, J.H. Hunter, H.D. Neff-LaFord, M. Jonas, M.E. Anderson, J.R. Setter, P.D. Senter, Reducing Hydrophobicity of Homogeneous Antibody-Drug Conjugates Improves Pharmacokinetics and Therapeutic Index, Nature Biotechnology, 33 (2015) 733.

[13] Y.T. Adem, K.A. Schwarz, E. Duenas, T.W. Patapoff, W.J. Galush, O. Esue, Auristatin Antibody Drug Conjugate Physical Instability and the Role of Drug Payload, Bioconjugate Chemistry, 25 (2014) 656-664.

[14] Q. Luo, H.H. Chung, C. Borths, M. Janson, J. Wen, M.K. Joubert, J. Wypych, Structural Characterization of a Monoclonal Antibody–Maytansinoid Immunoconjugate, Analytical Chemistry, 88 (2016) 695-702.

[15] K.J. Hamblett, P.D. Senter, D.F. Chace, M.M.C. Sun, J. Lenox, C.G. Cerveny, K.M. Kissler, S.X. Bernhardt, A.K. Kopcha, R.F. Zabinski, D.L. Meyer, J.A. Francisco, Effects of Drug Loading on the Antitumor Activity of a Monoclonal Antibody Drug Conjugate, Clinical Cancer Research, 10 (2004) 7063-7070.

[16] K. Lin, J. Tibbitts, Pharmacokinetic Considerations for Antibody Drug Conjugates, Pharmaceutical Research, 29 (2012) 2354-2366.

[17] M.T. Kim, Y. Chen, J. Marhoul, F. Jacobson, Statistical Modeling of the Drug Load Distribution on Trastuzumab Emtansine (Kadcyla), a Lysine-Linked Antibody Drug Conjugate, Bioconjugate Chemistry, 25 (2014) 1223-1232.

[18] S. Dickgiesser, N. Rasche, D. Nasu, S. Middel, S. Hörner, O. Avrutina, U. Diederichsen, H. Kolmar, Self-Assembled Hybrid Aptamer-Fc Conjugates for Targeted Delivery: A Modular Chemoenzymatic Approach, ACS Chemical Biology, 10 (2015) 2158-2165.
[19] J.Y. Axup, K.M. Bajjuri, M. Ritland, B.M. Hutchins, C.H. Kim, S.A. Kazane, R. Halder, J.S. Forsyth, A.F. Santidrian, K. Stafin, Y. Lu, H. Tran, A.J. Seller, S.L. Biroc, A. Szydlik, J.K. Pinkstaff, F. Tian, S.C. Sinha, B. Felding-Habermann, V.V. Smider, P.G. Schultz, Synthesis of Site-Specific Antibody-Drug Conjugates using Unnatural Amino Acids, Proceedings of the National Academy of Sciences, 109 (2012) 16101-16106.
[20] V. Chudasama, A. Maruani, S. Caddick, Recent Advances in the Construction of Antibody-Drug Conjugates, Nature chemistry, 8 (2016) 114-119.
[21] P. Agarwal, C.R. Bertozzi, Site-Specific Antibody–Drug Conjugates: The Nexus of Bioorthogonal Chemistry, Protein Engineering, and Drug Development, Bioconjugate Chemistry, 26 (2015) 176-192.
[22] J.R. Junutula, H. Raab, S. Clark, S. Bhakta, D.D. Leipold, S. Weir, Y. Chen, M. Simpson, S.P. Tsai, M.S. Dennis, Y. Lu, Y.G. Meng, C. Ng, J. Yang, C.C. Lee, E. Duenas, J. Gorrell, V. Katta, A. Kim, K. McDorman, K. Flagella, R. Venook, S. Ross, S.D. Spencer, W. Lee Wong, H.B. Lowman, R. Vandlen, M.X. Sliwkowski, R.H. Scheller, P. Polakis, W. Mallet, Site-Specific Conjugation of a Cytotoxic Drug to an Antibody Improves the Therapeutic Index, Nature Biotechnology, 26 (2008) 925.
[23] B.-Q. Shen, K. Xu, L. Liu, H. Raab, S. Bhakta, M. Kenrick, K.L. Parsons-Reponte, J. Tien, S.-F. Yu, E. Mai, D. Li, J. Tibbitts, J. Baudys, O.M. Saad, S.J. Scales, P.J. McDonald, P.E. Hass, C. Eigenbrot, T. Nguyen, W.A. Solis, R.N. Fuji, K.M. Flagella, D. Patel, S.D. Spencer, L.A. Khawli, A. Ebens, W.L. Wong, R. Vandlen, S. Kaur, M.X. Sliwkowski, R.H. Scheller, P. Polakis, J.R. Junutula, Conjugation Site Modulates the *in vivo* Stability and Therapeutic Activity of Antibody-Drug Conjugates, Nature Biotechnology, 30 (2012) 184.
[24] K. Tsuchikama, Z. An, Antibody-Drug Conjugates: Recent Advances in Conjugation and Linker Chemistries, Protein & Cell, (2016).
[25] N.L. Jumbe, Y. Xin, D.D. Leipold, L. Crocker, D. Dugger, E. Mai, M.X. Sliwkowski, P.J. Fielder, J. Tibbitts, Modeling the Efficacy of Trastuzumab-DM1, an Antibody Drug Conjugate, in Mice, Journal of pharmacokinetics and pharmacodynamics, 37 (2010) 221-242.
[26] V. Gaberc-Porekar, I. Zore, B. Podobnik, V. Menart, Obstacles and Pitfalls in the PEGylation of Therapeutic Proteins, Current opinion in drug discovery & development, 11 (2008) 242-250.
[27] P. Bailon, A. Palleroni, C.A. Schaffer, C.L. Spence, W.-J. Fung, J.E. Porter, G.K. Ehrlich, W. Pan, Z.-X. Xu, M.W. Modi, A. Farid, W. Berthold, M. Graves, Rational Design of a Potent, Long-Lasting Form of Interferon: A 40 kDa Branched Polyethylene Glycol-Conjugated Interferon α-2a for the Treatment of Hepatitis C, Bioconjugate Chemistry, 12 (2001) 195-202.
[28] S. Foser, A. Schacher, K.A. Weyer, D. Brugger, E. Dietel, S. Marti, T. Schreitmüller, Isolation, Structural Characterization, and Antiviral Activity of Positional Isomers of Monopegylated Interferon α-2a (PEGASYS), Protein Expression and Purification, 30 (2003) 78-87.
[29] T. Ito, R. Sadamoto, K. Naruchi, H. Togame, H. Takemoto, H. Kondo, S.-I. Nishimura, Highly Oriented Recombinant Glycosyltransferases: Site-Specific Immobilization of Unstable Membrane Proteins by Using Staphylococcus aureus Sortase A, Biochemistry, 49 (2010) 2604-2614.
[30] P. Strop, T.-T. Tran, M. Dorywalska, K. Delaria, R. Dushin, O.K. Wong, W.-H. Ho, D. Zhou, A. Wu, E. Kraynov, L. Aschenbrenner, B. Han, C.J. O'Donnell, J. Pons, A. Rajpal, D.L. Shelton, S.-H. Liu, RN927C, a Site-Specific Trop-2 Antibody–Drug Conjugate (ADC) with Enhanced Stability, Is Highly Efficacious in Preclinical Solid Tumor Models, Molecular Cancer Therapeutics, 15 (2016) 2698-2708.
[31] A.M. Sochaj, K.W. Świderska, J. Otlewski, Current methods for the synthesis of homogeneous antibody–drug conjugates, Biotechnology Advances, 33 (2015) 775-784.
[32] O. Diels, K. Alder, Synthesen in der Hydroaromatischen Reihe, Justus Liebigs Annalen der Chemie, 460 (1928) 98-122.
[33] R. Huisgen, Centenary Lecture - 1,3-Dipolar Cycloadditions, Proceedings of the Chemical Society, (1961) 357-396.

[34] H.C. Kolb, M.G. Finn, K.B. Sharpless, Click Chemistry: Diverse Chemical Function from a Few Good Reactions, Angewandte Chemie International Edition, 40 (2001) 2004-2021.
[35] N.J. Agard, J.A. Prescher, C.R. Bertozzi, A Strain-Promoted [3 + 2] Azide−Alkyne Cycloaddition for Covalent Modification of Biomolecules in Living Systems, Journal of the American Chemical Society, 126 (2004) 15046-15047.
[36] S.H. Cho, E.J. Yoo, I. Bae, S. Chang, Copper-Catalyzed Hydrative Amide Synthesis with Terminal Alkyne, Sulfonyl Azide, and Water, Journal of the American Chemical Society, 127 (2005) 16046-16047.
[37] E. Saxon, C.R. Bertozzi, Cell Surface Engineering by a Modified Staudinger Reaction, Science, 287 (2000) 2007-2010.
[38] J. Kalia, N.L. Abbott, R.T. Raines, General Method for Site-Specific Protein Immobilization by Staudinger Ligation, Bioconjugate Chemistry, 18 (2007) 1064-1069.
[39] J.L. Brennan, N.S. Hatzakis, T.R. Tshikhudo, V. Razumas, S. Patkar, J. Vind, A. Svendsen, R.J.M. Nolte, A.E. Rowan, M. Brust, Bionanoconjugation via Click Chemistry: The Creation of Functional Hybrids of Lipases and Gold Nanoparticles, Bioconjugate Chemistry, 17 (2006) 1373-1375.
[40] L. Uebersax, H.P. Merkle, L. Meinel, Biopolymer-Based Growth Factor Delivery for Tissue Repair: From Natural Concepts to Engineered Systems, Tissue engineering Part B, Reviews, 15 (2009) 263-289.
[41] F. Rusmini, Z. Zhong, J. Feijen, Protein Immobilization Strategies for Protein Biochips, Biomacromolecules, 8 (2007) 1775-1789.
[42] C.S. McKay, M.G. Finn, Click Chemistry in Complex Mixtures: Bioorthogonal Bioconjugation, Chemistry & Biology, 21 (2014) 1075-1101.
[43] E.M. Sletten, C.R. Bertozzi, Bioorthogonal Chemistry: Fishing for Selectivity in a Sea of Functionality, Angewandte Chemie International Edition, 48 (2009) 6974-6998.
[44] E.F. Pettersen, T.D. Goddard, C.C. Huang, G.S. Couch, D.M. Greenblatt, E.C. Meng, T.E. Ferrin, UCSF Chimera - A Visualization System for Exploratory Research and Analysis, Journal of Computational Chemistry, 25 (2004) 1605-1612.
[45] I. Schultz, J. Wurzel, L. Meinel, Drug Delivery of Insulin-Like Growth Factor I, European Journal of Pharmaceutics and Biopharmaceutics, 97, Part B (2015) 329-337.
[46] W. Huang, J. Wang, D. Bhattacharyya, L.G. Bachas, Improving the Activity of Immobilized Subtilisin by Site-Specific Attachment to Surfaces, Analytical Chemistry, 69 (1997) 4601-4607.
[47] D. Wasserberg, C. Nicosia, E.E. Tromp, V. Subramaniam, J. Huskens, P. Jonkheijm, Oriented Protein Immobilization using Covalent and Noncovalent Chemistry on a Thiol-Reactive Self-Reporting Surface, Journal of the American Chemical Society, 135 (2013) 3104-3111.
[48] M.L. Bayne, J. Applebaum, D. Underwood, G.G. Chicchi, B.G. Green, N.S. Hayes, M.A. Cascieri, The C Region of Human Insulin-like Growth factor (IGF) I is Required for High Affinity Binding to the Type 1 IGF Receptor, Journal of Biological Chemistry, 264 (1989) 11004-11008.
[49] M.A. Cascieri, G.G. Chicchi, J. Applebaum, N.S. Hayes, B.G. Green, M.L. Bayne, Mutants of Human Insulin-like Growth Factor I with Reduced Affinity for the Type 1 Insulin-like Growth Factor Receptor, Biochemistry, 27 (1988) 3229-3233.
[50] A.J. de Graaf, M. Kooijman, W.E. Hennink, E. Mastrobattista, Nonnatural Amino Acids for Site-Specific Protein Conjugation, Bioconjugate chemistry, 20 (2009) 1281-1295.
[51] R.J. Goodson, N.V. Katre, Site-Directed Pegylation of Recombinant Interleukin-2 at its Glycosylation Site, Nature Biotechnology, 8 (1990) 343-346.
[52] L. Ducry, B. Stump, Antibody-Drug Conjugates: Linking Cytotoxic Payloads to Monoclonal Antibodies, Bioconjugate Chemistry, 21 (2010) 5-13.
[53] A.D. Baldwin, K.L. Kiick, Tunable Degradation of Maleimide–Thiol Adducts in Reducing Environments, Bioconjugate Chemistry, 22 (2011) 1946-1953.
[54] D. Xie, C. Yao, L. Wang, W. Min, J. Xu, J. Xiao, M. Huang, B. Chen, B. Liu, X. Li, H. Jiang, An Albumin-Conjugated Peptide Exhibits Potent anti-HIV Activity and Long *In Vivo* Half-life, Antimicrobial agents and chemotherapy, 54 (2010) 191-196.
[55] N. Stephanopoulos, M.B. Francis, Choosing an Effective Protein Bioconjugation Strategy, Nature Chemical Biology, 7 (2011) 876-884.

[56] C. Noren, S. Anthony-Cahill, M. Griffith, P. Schultz, A General Method for Site-Specific Incorporation of Unnatural Amino Acids into Proteins, Science, 244 (1989) 182-188.
[57] S. Eger, M. Scheffner, A. Marx, M. Rubini, Synthesis of Defined Ubiquitin Dimers, Journal of the American Chemical Society, 132 (2010) 16337-16339.
[58] K. Lang, J.W. Chin, Cellular Incorporation of Unnatural Amino Acids and Bioorthogonal Labeling of Proteins, Chemical Reviews, 114 (2014) 4764-4806.
[59] C.P. Hackenberger, D. Schwarzer, Chemoselective Ligation and Modification Strategies for Peptides and Proteins, Angewandte Chemie International Edition, 47 (2008) 10030-10074.
[60] T.H. Wright, B.G. Davis, Post-Translational Mutagenesis for Installation of Natural and Unnatural Amino Acid Side Chains into Recombinant Proteins, Nature Protocols, 12 (2017) 2243.
[61] K. Lang, J.W. Chin, Bioorthogonal Reactions for Labeling Proteins, ACS Chemical Biology, 9 (2014) 16-20.
[62] J.C. Jewett, E.M. Sletten, C.R. Bertozzi, Rapid Cu-Free Click Chemistry with Readily Synthesized Biarylazacyclooctynones, Journal of the American Chemical Society, 132 (2010) 3688-3690.
[63] V. Hong, S.I. Presolski, C. Ma, M.G. Finn, Analysis and Optimization of Copper-Catalyzed Azide–Alkyne Cycloaddition for Bioconjugation, Angewandte Chemie International Edition, 48 (2009) 9879-9883.
[64] M. Gutmann, E. Memmel, A.C. Braun, J. Seibel, L. Meinel, T. Lühmann, Biocompatible Azide–Alkyne "Click" Reactions for Surface Decoration of Glyco-Engineered Cells, ChemBioChem, 17 (2016) 866-875.
[65] G.J. Brewer, Risks of Copper and Iron Toxicity during Aging in Humans, Chemical Research in Toxicology, 23 (2010) 319-326.
[66] G. Tabbì, S.C. Fry, R.P. Bonomo, ESR Study of the Non-Enzymic Scission of Xyloglucan by an Ascorbate–H2O2–Copper System: The Involvement of the Hydroxyl Radical and the Degradation of Ascorbate, Journal of Inorganic Biochemistry, 84 (2001) 179-187.
[67] E.R. Stadtman, Protein Oxidation and Aging, Free Radical Research, 40 (2006) 1250-1258.
[68] O. Reihl, M.O. Lederer, W. Schwack, Characterization and Detection of Lysine–Arginine Cross-Links Derived from Dehydroascorbic Acid, Carbohydrate Research, 339 (2004) 483-491.
[69] P. Kay, J.R. Wagner, H. Gagnon, R. Day, K. Klarskov, Modification of Peptide and Protein Cysteine Thiol Groups by Conjugation with a Degradation Product of Ascorbate, Chemical Research in Toxicology, 26 (2013) 1333-1339.
[70] A.B. Lowe, C.E. Hoyle, C.N. Bowman, Thiol-yne Click Chemistry: A Powerful and Versatile Methodology for Materials Synthesis, Journal of Materials Chemistry, 20 (2010) 4745-4750.
[71] M.P. Cassidy, J. Raushel, V.V. Fokin, Practical Synthesis of Amides from In Situ Generated Copper(I) Acetylides and Sulfonyl Azides, Angewandte Chemie, 118 (2006) 3226-3229.
[72] T. Govindaraju, P. Jonkheijm, L. Gogolin, H. Schroeder, C.F.W. Becker, C.M. Niemeyer, H. Waldmann, Surface Immobilization of Biomolecules by Click Sulfonamide Reaction, Chemical Communications, (2008) 3723-3725.
[73] J.M. Chalker, C.S.C. Wood, B.G. Davis, A Convenient Catalyst for Aqueous and Protein Suzuki−Miyaura Cross-Coupling, Journal of the American Chemical Society, 131 (2009) 16346-16347.
[74] W. Song, Y. Wang, J. Qu, M.M. Madden, Q. Lin, A Photoinducible 1,3-Dipolar Cycloaddition Reaction for Rapid, Selective Modification of Tetrazole-Containing Proteins, Angewandte Chemie, 120 (2008) 2874-2877.
[75] C.P. Ramil, Q. Lin, Photoclick Chemistry: A Fluorogenic Light-Triggered *In Vivo* Ligation Reaction, Current Opinion in Chemical Biology, 21 (2014) 89-95.
[76] A. Herner, Q. Lin, Photo-Triggered Click Chemistry for Biological Applications, Topics in Current Chemistry 374 (2016) 1.
[77] Z. Yu, L.Y. Ho, Z. Wang, Q. Lin, Discovery of New Photoactivatable Diaryltetrazoles for Photoclick Chemistry via 'Scaffold Hopping', Bioorganic & Medicinal Chemistry Letters, 21 (2011) 5033-5036.
[78] W. Song, Z. Yu, M.M. Madden, Q. Lin, A Bioorthogonal Chemistry Strategy for Probing Protein Lipidation in Live Cells, Molecular BioSystems, 6 (2010) 1576-1578.

[79] R.K.V. Lim, Q. Lin, Photoinducible Bioorthogonal Chemistry: A Spatiotemporally Controllable Tool to Visualize and Perturb Proteins in Live Cells, Accounts of Chemical Research, 44 (2011) 828-839.
[80] Z. Li, L. Qian, L. Li, J.C. Bernhammer, H.V. Huynh, J.-S. Lee, S.Q. Yao, Tetrazole Photoclick Chemistry: Reinvestigating Its Suitability as a Bioorthogonal Reaction and Potential Applications, Angewandte Chemie International Edition, 55 (2016) 2002-2006.
[81] R.K.V. Lim, Q. Lin, Azirine Ligation: Fast and Selective Protein Conjugation via Photoinduced Azirine-Alkene Cycloaddition, Chemical Communications, 46 (2010) 7993-7995.
[82] W. Xi, M. Krieger, C.J. Kloxin, C.N. Bowman, A new Photoclick Reaction Strategy: Photo-induced Catalysis of the Thiol-Michael Addition via a Caged Primary Amine, Chemical Communications, 49 (2013) 4504-4506.
[83] X. Zhang, W. Xi, C. Wang, M. Podgórski, C.N. Bowman, Visible-Light-Initiated Thiol-Michael Addition Polymerizations with Coumarin-Based Photobase Generators: Another Photoclick Reaction Strategy, ACS Macro Letters, 5 (2016) 229-233.
[84] D.M. Patterson, J.A. Prescher, Orthogonal Bioorthogonal Chemistries, Current Opinion in Chemical Biology, 28 (2015) 141-149.
[85] K.A. Mosiewicz, L. Kolb, A.J. van der Vlies, M.M. Martino, P.S. Lienemann, J.A. Hubbell, M. Ehrbar, M.P. Lutolf, In situ Cell Manipulation through Enzymatic Hydrogel Photopatterning, Nature Materials, 12 (2013) 1072-1078.
[86] A. Poloukhtine, V.V. Popik, Highly Efficient Photochemical Generation of a Triple Bond: Synthesis, Properties, and Photodecarbonylation of Cyclopropenones, The Journal of Organic Chemistry, 68 (2003) 7833-7840.
[87] W.P. Jencks, Studies on the Mechanism of Oxime and Semicarbazone Formation, Journal of the American Chemical Society, 81 (1959) 475-481.
[88] D. Rideout, Self-Assembling Cytotoxins, Science, 233 (1986) 561-563.
[89] S. Ulrich, D. Boturyn, A. Marra, O. Renaudet, P. Dumy, Oxime Ligation: A Chemoselective Click-Type Reaction for Accessing Multifunctional Biomolecular Constructs, Chemistry – A European Journal, 20 (2014) 34-41.
[90] J. Kalia, R.T. Raines, Hydrolytic Stability of Hydrazones and Oximes, Angewandte Chemie, 120 (2008) 7633-7636.
[91] A. Dirksen, S. Dirksen, T.M. Hackeng, P.E. Dawson, Nucleophilic Catalysis of Hydrazone Formation and Transimination: Implications for Dynamic Covalent Chemistry, Journal of the American Chemical Society, 128 (2006) 15602-15603.
[92] M. Rashidian, M.M. Mahmoodi, R. Shah, J.K. Dozier, C.R. Wagner, M.D. Distefano, A Highly Efficient Catalyst for Oxime Ligation and Hydrazone–Oxime Exchange Suitable for Bioconjugation, Bioconjugate Chemistry, 24 (2013) 333-342.
[93] J.P. Lee, E. Kassianidou, J.I. MacDonald, M.B. Francis, S. Kumar, N-terminal Specific Conjugation of Extracellular Matrix Proteins to 2-Pyridinecarboxaldehyde Functionalized Polyacrylamide Hydrogels, Biomaterials, 102 (2016) 268-276.
[94] A.P. Esser-Kahn, M.B. Francis, Protein-Cross-Linked Polymeric Materials through Site-Selective Bioconjugation, Angewandte Chemie, 120 (2008) 3811-3814.
[95] K.L. Christman, R.M. Broyer, Z.P. Tolstyka, H.D. Maynard, Site-specific Protein Immobilization through N-terminal Oxime Linkages, Journal of Materials Chemistry, 17 (2007) 2021-2027.
[96] C. Netirojjanakul, L.S. Witus, C.R. Behrens, C.-H. Weng, A.T. Iavarone, M.B. Francis, Synthetically Modified Fc Domains as Building Blocks for Immunotherapy Applications, Chemical Science, 4 (2013) 266-272.
[97] L.S. Witus, C. Netirojjanakul, K.S. Palla, E.M. Muehl, C.-H. Weng, A.T. Iavarone, M.B. Francis, Site-Specific Protein Transamination Using N-Methylpyridinium-4-carboxaldehyde, Journal of the American Chemical Society, 135 (2013) 17223-17229.
[98] K.L. Kiick, E. Saxon, D.A. Tirrell, C.R. Bertozzi, Incorporation of Azides into Recombinant Proteins for Chemoselective Modification by the Staudinger Ligation, Proceedings of the National Academy of Sciences, 99 (2002) 19-24.
[99] E. Saxon, J.I. Armstrong, C.R. Bertozzi, A "Traceless" Staudinger Ligation for the Chemoselective Synthesis of Amide Bonds, Organic Letters, 2 (2000) 2141-2143.

[100] K.W. Dehnert, J.M. Baskin, S.T. Laughlin, B.J. Beahm, N.N. Naidu, S.L. Amacher, C.R. Bertozzi, Imaging the Sialome during Zebrafish Development with Copper-Free Click Chemistry, ChemBioChem, 13 (2012) 353-357.
[101] T.H. Poole, J.A. Reisz, W. Zhao, L.B. Poole, C.M. Furdui, S.B. King, Strained Cycloalkynes as New Protein Sulfenic Acid Traps, Journal of the American Chemical Society, 136 (2014) 6167-6170.
[102] C.S. McKay, M. Chigrinova, J.A. Blake, J.P. Pezacki, Kinetics studies of Rapid Strain-Promoted [3 + 2]-Cycloadditions of Nitrones with Biaryl-Aza-Cyclooctynone, Organic & Biomolecular Chemistry, 10 (2012) 3066-3070.
[103] X. Ning, R.P. Temming, J. Dommerholt, J. Guo, D.B. Ania, M.F. Debets, M.A. Wolfert, G.-J. Boons, F.L. van Delft, Protein Modification by Strain-Promoted Alkyne–Nitrone Cycloaddition, Angewandte Chemie International Edition, 49 (2010) 3065-3068.
[104] L.C.-C. Lee, J.C.-W. Lau, H.-W. Liu, K.K.-W. Lo, Conferring Phosphorogenic Properties on Iridium(III)-Based Bioorthogonal Probes through Modification with a Nitrone Unit, Angewandte Chemie, 128 (2016) 1058-1061.
[105] W. Blokzijl, M.J. Blandamer, J.B.F.N. Engberts, Diels-Alder Reactions in Aqueous Solutions. Enforced Hydrophobic Interactions Between Diene and Dienophile, Journal of the American Chemical Society, 113 (1991) 4241-4246.
[106] A.D. de Araújo, J.M. Palomo, J. Cramer, M. Köhn, H. Schröder, R. Wacker, C. Niemeyer, K. Alexandrov, H. Waldmann, Diels–Alder Ligation and Surface Immobilization of Proteins, Angewandte Chemie International Edition, 45 (2006) 296-301.
[107] X.-L. Sun, C.L. Stabler, C.S. Cazalis, E.L. Chaikof, Carbohydrate and Protein Immobilization onto Solid Surfaces by Sequential Diels−Alder and Azide−Alkyne Cycloadditions, Bioconjugate Chemistry, 17 (2006) 52-57.
[108] S.A. Fisher, A.E.G. Baker, M.S. Shoichet, Designing Peptide and Protein Modified Hydrogels: Selecting the Optimal Conjugation Strategy, Journal of the American Chemical Society, 139 (2017) 7416-7427.
[109] Z. Zheng, P. Chen, G. Li, Y. Zhu, Z. Shi, Y. Luo, C. Zhao, Z. Fu, X. Cui, C. Ji, F. Wang, G. Huang, G. Liang, Mechanistic Study of CBT-Cys Click Reaction and its Application for Identifying Bioactive N-terminal Cysteine Peptides in Amniotic Fluid, Chemical Science, 8 (2017) 214-222.
[110] C.B. Rosen, M.B. Francis, Targeting the N Terminus for Site-Selective Protein Modification, Nature Chemical Biology, 13 (2017) 697-705.
[111] H. Ren, F. Xiao, K. Zhan, Y.-P. Kim, H. Xie, Z. Xia, J. Rao, A Biocompatible Condensation Reaction for the Labeling of Terminal Cysteine Residues on Proteins, Angewandte Chemie International Edition, 48 (2009) 9658-9662.
[112] D.P. Nguyen, T. Elliott, M. Holt, T.W. Muir, J.W. Chin, Genetically Encoded 1,2-Aminothiols Facilitate Rapid and Site-Specific Protein Labeling via a Bio-orthogonal Cyanobenzothiazole Condensation, Journal of the American Chemical Society, 133 (2011) 11418-11421.
[113] Y. Yuan, G. Liang, A Biocompatible, Highly Efficient Click Reaction and its Applications, Organic & biomolecular chemistry, 12 (2014) 865-871.
[114] J. Stöckigt, A.P. Antonchick, F. Wu, H. Waldmann, The Pictet–Spengler Reaction in Nature and in Organic Chemistry, Angewandte Chemie International Edition, 50 (2011) 8538-8564.
[115] M.L. Blackman, M. Royzen, J.M. Fox, Tetrazine Ligation: Fast Bioconjugation Based on Inverse-Electron-Demand Diels−Alder Reactivity, Journal of the American Chemical Society, 130 (2008) 13518-13519.
[116] H. Stockmann, A.A. Neves, S. Stairs, K.M. Brindle, F.J. Leeper, Exploring Isonitrile-Based Click Chemistry for Ligation with Biomolecules, Organic & Biomolecular Chemistry, 9 (2011) 7303-7305.
[117] E.M. Sletten, C.R. Bertozzi, A Bioorthogonal Quadricyclane Ligation, Journal of the American Chemical Society, 133 (2011) 17570-17573.
[118] E. Gau, D.M. Mate, Z. Zou, A. Oppermann, A. Töpel, F. Jakob, D. Wöll, U. Schwaneberg, A. Pich, Sortase-Mediated Surface Functionalization of Stimuli-Responsive Microgels, Biomacromolecules, (2017).

[119] A. Anghileri, R. Lantto, K. Kruus, C. Arosio, G. Freddi, Tyrosinase-Catalyzed Grafting of Sericin Peptides onto Chitosan and Production of Protein–Polysaccharide Bioconjugates, Journal of Biotechnology, 127 (2007) 508-519.
[120] A.T. Lewandowski, D.A. Small, T. Chen, G.F. Payne, W.E. Bentley, Tyrosine-Based "Activatable Pro-Tag": Enzyme-Catalyzed Protein Capture and Release, Biotechnology and Bioengineering, 93 (2006) 1207-1215.
[121] J.S. Rush, C.R. Bertozzi, New Aldehyde Tag Sequences Identified by Screening Formylglycine Generating Enzymes *In Vitro* and *In Vivo*, Journal of the American Chemical Society, 130 (2008) 12240-12241.
[122] D. Beckett, E. Kovaleva, P.J. Schatz, A Minimal Peptide Substrate in Biotin Holoenzyme Synthetase-Catalyzed Biotinylation, Protein Science, 8 (1999) 921-929.
[123] I. Chen, M. Howarth, W. Lin, A.Y. Ting, Site-Specific Labeling of Cell Surface Proteins with Biophysical Probes using Biotin Ligase, Nature methods, 2 (2005) 99-104.
[124] M. Best, A. Degen, M. Baalmann, T.T. Schmidt, R. Wombacher, Two-step Protein Labeling by using Lipoic Acid Ligase with Norbornene Substrates and Subsequent Inverse-Electron Demand Diels-Alder Reaction, Chembiochem, 16 (2015) 1158-1162.
[125] M. Fernandez-Suarez, H. Baruah, L. Martinez-Hernandez, K.T. Xie, J.M. Baskin, C.R. Bertozzi, A.Y. Ting, Redirecting Lipoic Acid Ligase for Cell Surface Protein Labeling with Small-Molecule Probes, Nature Biotechnology, 25 (2007) 1483-1487.
[126] N.M. Rachel, J.L. Toulouse, J.N. Pelletier, Transglutaminase-Catalyzed Bioconjugation Using One-Pot Metal-Free Bioorthogonal Chemistry, Bioconjugate Chemistry, 28 (2017) 2518-2523.
[127] C.P. Guimaraes, M.D. Witte, C.S. Theile, G. Bozkurt, L. Kundrat, A.E.M. Blom, H.L. Ploegh, Site-Specific C-Terminal and Internal Loop Labeling of Proteins using Sortase-Mediated Reactions, Nature Protocols, 8 (2013) 1787-1799.
[128] M.W. Popp, J.M. Antos, G.M. Grotenbreg, E. Spooner, H.L. Ploegh, Sortagging: A Versatile Method for Protein Labeling, Nature Chemical Biology, 3 (2007) 707-708.
[129] M.W. Popp, S.K. Dougan, T.-Y. Chuang, E. Spooner, H.L. Ploegh, Sortase-Catalyzed Transformations that Improve the Properties of Cytokines, Proceedings of the National Academy of Sciences, 108 (2011) 3169-3174.
[130] S.V. Moradi, W.M. Hussein, P. Varamini, P. Simerska, I. Toth, Glycosylation, an Effective Synthetic Strategy to Improve the Bioavailability of Therapeutic Peptides, Chemical Science, 7 (2016) 2492-2500.
[131] T. Chen, D.A. Small, L.-Q. Wu, G.W. Rubloff, R. Ghodssi, R. Vazquez-Duhalt, W.E. Bentley, G.F. Payne, Nature-Inspired Creation of Protein−Polysaccharide Conjugate and Its Subsequent Assembly onto a Patterned Surface, Langmuir, 19 (2003) 9382-9386.
[132] L.-Q. Wu, G.F. Payne, Biofabrication: Using Biological Materials and Biocatalysts to Construct Nanostructured Assemblies, Trends in Biotechnology, 22 (2004) 593-599.
[133] C.L. Nikolajsen, T.F. Dyrlund, E.T. Poulsen, J.J. Enghild, C. Scavenius, Coagulation Factor XIIIa Substrates in Human Plasma: Identification and Incorporation into the Clot, The Journal of Biological Chemistry, 289 (2014) 6526-6534.
[134] M.L. Bentley, H. Gaweska, J.M. Kielec, D.G. McCafferty, Engineering the Substrate Specificity of Staphylococcus aureus Sortase A: The β6/β7 Loop from SrtB Confers NPQTN Recognition to SrtA, Journal of Biological Chemistry, 282 (2007) 6571-6581.
[135] J.R. Silvius, R. Leventis, A Novel "Prebinding" Strategy Dramatically Enhances Sortase-Mediated Coupling of Proteins to Liposomes, Bioconjugate Chemistry, 28 (2017) 1271-1282.
[136] C. Albayrak, J.R. Swartz, Direct Polymerization of Proteins, Acs Synthetic Biology, 3 (2014) 353-362.
[137] T. Tanaka, N. Kamiya, T. Nagamune, N-Terminal Glycine-Specific Protein Conjugation Catalyzed by Microbial Transglutaminase, FEBS Letters, 579 (2005) 2092-2096.
[138] S. Möhlmann, C. Mahlert, S. Greven, P. Scholz, A. Harrenga, *In vitro* Sortagging of an Antibody Fab Fragment: Overcoming Unproductive Reactions of Sortase with Water and Lysine Side Chains, ChemBioChem, 12 (2011) 1774-1780.

[139] P. Spycher, C.A. Amann, J. Wehrmuller, D.R. Hurwitz, O. Kreis, A. Ritler, D. Messmer, A. Kuchler, A. Blanc, P. Walde, M. Behe, R. Schibli, Dual Site-Specifically Modified Antibodies with Solid-Phase Immobilized Microbial Transglutaminase, Chembiochem, (2017).
[140] T. Chen, D.A. Small, M.K. McDermott, W.E. Bentley, G.F. Payne, Enzymatic Methods for in situ Cell Entrapment and Cell Release, Biomacromolecules, 4 (2003) 1558-1563.
[141] F.S. De, D. Zopf, R. Bayer, C. Bowe, D. Hakes, X. Chen, Glycopegylation Methods and Proteins/Peptides Produced by the Methods, in, Google Patents, 2011.
[142] M. Griffin, R. Casadio, C.M. Bergamini, Transglutaminases: Nature's Biological Glues, The Biochemical Journal, 368 (2002) 377-396.
[143] B.-H. Hu, P.B. Messersmith, Rational Design of Transglutaminase Substrate Peptides for Rapid Enzymatic Formation of Hydrogels, Journal of the American Chemical Society, 125 (2003) 14298-14299.
[144] P. Strop, Versatility of Microbial Transglutaminase, Bioconjugate Chemistry, 25 (2014) 855-862.
[145] J.C. Schense, J.A. Hubbell, Cross-Linking Exogenous Bifunctional Peptides into Fibrin Gels with Factor XIIIa, Bioconjugate Chemistry, 10 (1999) 75-81.
[146] M.E.R. Jones, P.B. Messersmith, Facile Coupling of Synthetic Peptides and Peptide–Polymer Conjugates to Cartilage via Transglutaminase Enzyme, Biomaterials, 28 (2007) 5215-5224.
[147] P.S. Lienemann, M. Karlsson, A. Sala, H.M. Wischhusen, F.E. Weber, R. Zimmermann, W. Weber, M.P. Lutolf, M. Ehrbar, A Versatile Approach to Engineering Biomolecule-Presenting Cellular Microenvironments, Advanced Healthcare Materials, 2 (2013) 292-296.
[148] M.W.-L. Popp, H.L. Ploegh, Making and Breaking Peptide Bonds: Protein Engineering Using Sortase, Angewandte Chemie International Edition, 50 (2011) 5024-5032.
[149] A. Sinisi, M.W.-L. Popp, J.M. Antos, W. Pansegrau, S. Savino, M. Nissum, R. Rappuoli, H.L. Ploegh, L. Buti, Development of an Influenza virus Protein Array Using Sortagging Technology, Bioconjugate Chemistry, 23 (2012) 1119-1126.
[150] S. Tang, B. Xuan, X. Ye, Z. Huang, Z. Qian, A Modular Vaccine Development Platform Based on Sortase-Mediated Site-Specific Tagging of Antigens onto Virus-Like Particles, Scientific Reports, 6 (2016) 25741.
[151] I.H. Lee, S.I. Chung, S.Y. Lee, Effects of Val34Leu and Val35Leu Polymorphism on the Enzyme Activity of the Coagulation Factor XIII-A, Experimental & molecular medicine, 34 (2002) 385-390.
[152] K. Oertel, A. Hunfeld, E. Specker, C. Reiff, R. Seitz, R. Pasternack, J. Dodt, A Highly Sensitive Fluorometric Assay for Determination of Human Coagulation Factor XIII in Plasma, Analytical Biochemistry, 367 (2007) 152-158.
[153] R.G. Kruger, P. Dostal, D.G. McCafferty, Development of a High-Performance Liquid Chromatography Assay and Revision of Kinetic Parameters for the Staphylococcus aureus Sortase Transpeptidase SrtA, Analytical Biochemistry, 326 (2004) 42-48.
[154] E. Cambria, K. Renggli, C.C. Ahrens, C.D. Cook, C. Kroll, A.T. Krueger, B. Imperiali, L.G. Griffith, Covalent Modification of Synthetic Hydrogels with Bioactive Proteins via Sortase-Mediated Ligation, Biomacromolecules, 16 (2015) 2316-2326.
[155] T. Dierks, B. Schmidt, L.V. Borissenko, J. Peng, A. Preusser, M. Mariappan, K. von Figura, Multiple Sulfatase Deficiency Is Caused by Mutations in the Gene Encoding the Human Cα-Formylglycine Generating Enzyme, Cell, 113 (2003) 435-444.
[156] K.U. Zaidi, A.S. Ali, S.A. Ali, Purification and Characterization of Melanogenic Enzyme Tyrosinase from Button Mushroom, Enzyme Research, 2014 (2014) 120739.
[157] S. Puthenveetil, D.S. Liu, K.A. White, S. Thompson, A.Y. Ting, Yeast Display Evolution of a Kinetically Efficient 13-Amino Acid Substrate for Lipoic Acid Ligase, Journal of the American Chemical Society, 131 (2009) 16430-16438.
[158] J. Lotze, U. Reinhardt, O. Seitz, A.G. Beck-Sickinger, Peptide-Tags for Site-Specific Protein Labelling *In Vitro* and *In Vivo*, Molecular BioSystems, 12 (2016) 1731-1745.
[159] G. Matheis, J.R. Whitaker, A review: Enzymatic Cross-linking of Proteins Applicable to Foods, Journal of Food Biochemistry, 11 (1987) 309-327.

[160] M. Howarth, W. Liu, S. Puthenveetil, Y. Zheng, L.F. Marshall, M.M. Schmidt, K.D. Wittrup, M.G. Bawendi, A.Y. Ting, Monovalent, Reduced-Size Quantum Dots for Imaging Receptors on Living Cells, Nature methods, 5 (2008) 397-399.
[161] M. Rashidian, J.K. Dozier, M.D. Distefano, Enzymatic Labeling of Proteins: Techniques and Approaches, Bioconjugate Chemistry, 24 (2013) 1277-1294.
[162] H. Zhao, E. Heusler, G. Jones, L. Li, V. Werner, O. Germershaus, J. Ritzer, T. Luehmann, L. Meinel, Decoration of Silk Fibroin by Click Chemistry for Biomedical Application, Journal of Structural Biology, 186 (2014) 420-430.
[163] R. Parthasarathy, S. Subramanian, E.T. Boder, Sortase A as a Novel Molecular "Stapler" for Sequence-Specific Protein Conjugation, Bioconjugate Chemistry, 18 (2007) 469-476.
[164] Y.-S. Wang, S. Youngster, M. Grace, J. Bausch, R. Bordens, D.F. Wyss, Structural and Biological Characterization of Pegylated Recombinant Interferon alpha-2b and its Therapeutic Implications, Advanced Drug Delivery Reviews, 54 (2002) 547-570.
[165] H. Sato, M. Ikeda, K. Suzuki, K. Hirayama, Site-Specific Modification of Interleukin-2 by the Combined Use of Genetic Engineering Techniques and Transglutaminase, Biochemistry, 35 (1996) 13072-13080.
[166] S. Zhen Pan, L. Xin Song, J. Chen, F. Yun Du, J. Yang, J. Xia, Noncovalent Interaction of Polyethylene glycol with Copper Complex of Ethylenediaminetetraacetic acid and its Application in Constructing Inorganic Nanomaterials, Dalton Transactions, 40 (2011) 10117-10124.
[167] M.F. Debets, S.S. van Berkel, S. Schoffelen, F.P.J.T. Rutjes, J.C.M. van Hest, F.L. van Delft, Aza-dibenzocyclooctynes for Fast and Efficient Enzyme PEGylation via Copper-Free (3+2) Cycloaddition, Chemical Communications, 46 (2010) 97-99.
[168] S. Schoffelen, M.H.L. Lambermon, M.B.v. Eldijk, J.C.M.v. Hest, Site-Specific Modification of Candida antarctica Lipase B via Residue-Specific Incorporation of a Non-Canonical Amino Acid, Bioconjugate Chemistry, 19 (2008) 1127-1131.
[169] M. Simon, U. Zangemeister-Wittke, A. Plueckthun, Facile Double-Functionalization of Designed Ankyrin Repeat Proteins using Click and Thiol Chemistries, Bioconjugate Chemistry, 23 (2012) 279-286.
[170] T. Lühmann, M. Schmidt, M.N. Leiske, V. Spieler, T.C. Majdanski, M. Grube, M. Hartlieb, I. Nischang, S. Schubert, U.S. Schubert, L. Meinel, Site-Specific POxylation of Interleukin-4, ACS Biomaterials Science & Engineering, (2016).
[171] J. Lutz, H.G. Börner, K. Weichenhan, 'Click' Bioconjugation of a Well-Defined Synthetic Polymer and a Protein Transduction Domain, Australian Journal of Chemistry, 60 (2007) 410-413.
[172] I.C. Reynhout, J.J.L.M. Cornelissen, R.J.M. Nolte, Self-Assembled Architectures from Biohybrid Triblock Copolymers, Journal of the American Chemical Society, 129 (2007) 2327-2332.
[173] Q. Shi, X. Chen, T. Lu, X. Jing, The Immobilization of Proteins on Biodegradable Polymer Fibers via Click Chemistry, Biomaterials, 29 (2008) 1118-1126.
[174] E. Lallana, F. Fernandez-Trillo, A. Sousa-Herves, R. Riguera, E. Fernandez-Megia, Click Chemistry with Polymers, Dendrimers, and Hydrogels for Drug Delivery, Pharmaceutical Research, 29 (2012) 902-921.
[175] H. Yu, Y. Nie, C. Dohmen, Y. Li, E. Wagner, Epidermal Growth Factor–PEG Functionalized PAMAM-Pentaethylenehexamine Dendron for Targeted Gene Delivery Produced by Click Chemistry, Biomacromolecules, 12 (2011) 2039-2047.
[176] I. Dijkgraaf, A.Y. Rijnders, A. Soede, A.C. Dechesne, G.W. van Esse, A.J. Brouwer, F.H.M. Corstens, O.C. Boerman, D.T.S. Rijkers, R.M.J. Liskamp, Synthesis of DOTA-Conjugated Multivalent Cyclic-RGD Peptide Dendrimers via 1,3-dipolar Cycloaddition and their Biological Evaluation: Implications for Tumor Targeting and Tumor Imaging Purposes, Organic & Biomolecular Chemistry, 5 (2007) 935-944.
[177] C. Gauchet, G.R. Labadie, C.D. Poulter, Regio- and Chemoselective Covalent Immobilization of Proteins through Unnatural Amino Acids, Journal of the American Chemical Society, 128 (2006) 9274-9275.

[178] A. Watzke, M. Köhn, M. Gutierrez-Rodriguez, R. Wacker, H. Schröder, R. Breinbauer, J. Kuhlmann, K. Alexandrov, C.M. Niemeyer, R.S. Goody, H. Waldmann, Site-Selective Protein Immobilization by Staudinger Ligation, Angewandte Chemie, 118 (2006) 1436-1440.
[179] Z.P. Tolstyka, W. Richardson, E. Bat, C.J. Stevens, D.P. Parra, J.K. Dozier, M.D. Distefano, B. Dunn, H.D. Maynard, Chemoselective Immobilization of Proteins by Microcontact Printing and Bio-orthogonal Click Reactions, ChemBioChem, 14 (2013) 2464-2471.
[180] P.-C. Lin, S.-H. Ueng, M.-C. Tseng, J.-L. Ko, K.-T. Huang, S.-C. Yu, A.K. Adak, Y.-J. Chen, C.-C. Lin, Site-Specific Protein Modification through CuI-Catalyzed 1,2,3-Triazole Formation and Its Implementation in Protein Microarray Fabrication, Angewandte Chemie, 118 (2006) 4392-4396.
[181] T. Luehmann, G. Jones, M. Gutmann, J.-C. Rybak, J. Nickel, M. Rubini, L. Meinel, Bio-orthogonal Immobilization of Fibroblast Growth Factor 2 for Spatial Controlled Cell Proliferation, Acs Biomaterials-Science & Engineering, 1 (2015) 740-746.
[182] B.P. Duckworth, J. Xu, T.A. Taton, A. Guo, M.D. Distefano, Site-Specific, Covalent Attachment of Proteins to a Solid Surface, Bioconjugate Chemistry, 17 (2006) 967-974.
[183] S. Punna, E. Kaltgrad, M.G. Finn, "Clickable" Agarose for Affinity Chromatography, Bioconjugate Chemistry, 16 (2005) 1536-1541.
[184] L. Polito, D. Monti, E. Caneva, E. Delnevo, G. Russo, D. Prosperi, One-Step Bioengineering of Magnetic Nanoparticles via a Surface Diazo Transfer/Azide-Alkyne Click Reaction Sequence, Chemical Communications, (2008) 621-623.
[185] W.H. Binder, R. Sachsenhofer, C.J. Straif, R. Zirbs, Surface-Modified Nanoparticles via Thermal and Cu(I)-Mediated "Click" Chemistry: Generation of Luminescent CdSe Nanoparticles with Polar Ligands Guiding Supramolecular Recognition, Journal of Materials Chemistry, 17 (2007) 2125-2132.
[186] S. Avvakumova, M. Colombo, P. Tortora, D. Prosperi, Biotechnological Approaches Toward Nanoparticle Biofunctionalization, Trends in Biotechnology, 32 (2014) 11-20.
[187] T. Lühmann, V. Spieler, V. Werner, M.-G. Ludwig, J. Fiebig, T. Müller, L. Meinel, Interleukin-4 Clicked Surfaces Drive M2 Macrophage Polarization, ChemBioChem, (2016) n/a-n/a.
[188] A. Mero, M. Schiavon, F.M. Veronese, G. Pasut, A New Method to Increase Selectivity of Transglutaminase Mediated PEGylation of Salmon Calcitonin and Human Growth Hormone, Journal of Controlled Release, 154 (2011) 27-34.
[189] A. Sala, M. Ehrbar, D. Trentin, R.G. Schoenmakers, J. Voros, F.E. Weber, Enzyme Mediated Site-Specific Surface Modification, Langmuir, 26 (2010) 11127-11134.
[190] A.J. Dirks, S.S. van Berkel, N.S. Hatzakis, J.A. Opsteen, F.L. van Delft, J.J.L.M. Cornelissen, A.E. Rowan, J.C.M. van Hest, F.P.J.T. Rutjes, R.J.M. Nolte, Preparation of Biohybrid Amphiphiles via the Copper Catalysed Huisgen [3 + 2] Dipolar Cycloaddition Reaction, Chemical Communications, (2005) 4172-4174.
[191] A. Gopin, S. Ebner, B. Attali, D. Shabat, Enzymatic Activation of Second-Generation Dendritic Prodrugs: Conjugation of Self-Immolative Dendrimers with Poly(ethylene glycol) via Click Chemistry, Bioconjugate Chemistry, 17 (2006) 1432-1440.
[192] C.J. Arnusch, H. Branderhorst, B. de Kruijff, R.M.J. Liskamp, E. Breukink, R.J. Pieters, Enhanced Membrane Pore Formation by Multimeric/Oligomeric Antimicrobial Peptides, Biochemistry, 46 (2007) 13437-13442.
[193] P.-C. Lin, S.-H. Ueng, S.-C. Yu, M.-D. Jan, A.K. Adak, C.-C. Yu, C.-C. Lin, Surface Modification of Magnetic Nanoparticle via Cu(I)-Catalyzed Alkyne-azide [2 + 3] Cycloaddition, Organic Letters, 9 (2007) 2131-2134.
[194] J. Pasold, K. Zander, B. Heskamp, C. Grüttner, F. Lüthen, T. Tischer, A. Jonitz-Heincke, R. Bader, Positive Impact of IGF-1-Coupled Nanoparticles on the Differentiation Potential of Human Chondrocytes Cultured on Collagen Scaffolds, International Journal of Nanomedicine, 10 (2015) 1131-1143.
[195] L. Chan, H.F. Cross, J.K. She, G. Cavalli, H.F.P. Martins, C. Neylon, Covalent Attachment of Proteins to Solid Supports and Surfaces via Sortase-Mediated Ligation, PLoS ONE, 2 (2007) e1164.

[196] R.K. O'Reilly, M.J. Joralemon, K.L. Wooley, C.J. Hawker, Functionalization of Micelles and Shell Cross-linked Nanoparticles Using Click Chemistry, Chemistry of Materials, 17 (2005) 5976-5988.
[197] F. Said Hassane, B. Frisch, F. Schuber, Targeted Liposomes: Convenient Coupling of Ligands to Preformed Vesicles Using "Click Chemistry", Bioconjugate Chemistry, 17 (2006) 849-854.
[198] J.A. Yang, E.S. Kim, J.H. Kwon, H. Kim, J.H. Shin, S.H. Yun, K.Y. Choi, S.K. Hahn, Transdermal Delivery of Hyaluronic acid - Human Growth Hormone Conjugate, Biomaterials, 33 (2012) 5947-5954.
[199] M. Ehrbar, A. Metters, P. Zammaretti, J.A. Hubbell, A.H. Zisch, Endothelial Cell Proliferation and Progenitor Maturation by Fibrin-Bound VEGF Variants with Differential Susceptibilities to Local Cellular Activity, Journal of Controlled Release, 101 (2005) 93-109.
[200] T. Lühmann, P. Hänseler, B. Grant, H. Hall, The Induction of Cell Alignment by Covalently Immobilized Gradients of the 6th Ig-Like Domain of Cell Adhesion Molecule L1 in 3D-Fibrin Matrices, Biomaterials, 30 (2009) 4503-4512.
[201] J. Hu, G. Wang, X. Liu, W. Gao, Enhancing Pharmacokinetics, Tumor Accumulation, and Antitumor Efficacy by Elastin-Like Polypeptide Fusion of Interferon Alpha, Advanced Materials, 27 (2015) 7320-7324.
[202] T. Lühmann, L. Meinel, Nanotransporters For Drug Delivery, Current Opinion in Biotechnology, 39 (2016) 35-40.
[203] R. Duncan, H.C. Cable, J.B. Lloyd, P. Rejmanová, J. Kopeček, Polymers Containing Enzymatically Degradable Bonds, 7. Design of Oligopeptide Side-Chains in Poly[N-(2-hydroxypropyl)methacrylamide] Copolymers to Promote Efficient Degradation by Lysosomal Enzymes, Die Makromolekulare Chemie, 184 (1983) 1997-2008.
[204] T.J. Levingstone, A. Matsiko, G.R. Dickson, F.J. O'Brien, J.P. Gleeson, A Biomimetic Multi-Layered Collagen-Based Scaffold for Osteochondral Repair, Acta Biomaterialia, 10 (2014) 1996-2004.
[205] O. Germershaus, T. Lühmann, J.C. Rybak, J. Ritzer, L. Meinel, Application of Natural and Semi-Synthetic Polymers for the Delivery of Sensitive Drugs, International Materials Reviews, 60 (2015) 101-131.
[206] Y. Jiang, J. Chen, C. Deng, E.J. Suuronen, Z. Zhong, Click Hydrogels, Microgels and Nanogels: Emerging Platforms for Drug Delivery and Tissue Engineering, Biomaterials, 35 (2014) 4969-4985.
[207] G. Bhakta, Z.X.H. Lim, B. Rai, T. Lin, J.H. Hui, G.D. Prestwich, A.J. van Wijnen, V. Nurcombe, S.M. Cool, The Influence of Collagen and Hyaluronan Matrices on the Delivery and Bioactivity of Bone Morphogenetic Protein-2 and Ectopic Bone Formation, Acta Biomaterialia, 9 (2013) 9098-9106.
[208] L.M. Mullen, S.M. Best, R.A. Brooks, S. Ghose, J.H. Gwynne, J. Wardale, N. Rushton, R.E. Cameron, Binding and Release Characteristics of Insulin-Like Growth Factor-1 from a Collagen–Glycosaminoglycan Scaffold, Tissue Engineering. Part C, Methods, 16 (2010) 1439-1448.
[209] S. Tada, T. Kitajima, Y. Ito, Design and Synthesis of Binding Growth Factors, International Journal of Molecular Sciences, 13 (2012) 6053.
[210] M.M. Martino, P.S. Briquez, E. Güç, F. Tortelli, W.W. Kilarski, S. Metzger, J.J. Rice, G.A. Kuhn, R. Müller, M.A. Swartz, J.A. Hubbell, Growth Factors Engineered for Super-Affinity to the Extracellular Matrix Enhance Tissue Healing, Science, 343 (2014) 885-888.
[211] Y. Miyagi, L.L.Y. Chiu, M. Cimini, R.D. Weisel, M. Radisic, R.-K. Li, Biodegradable Collagen Patch with Covalently Immobilized VEGF for Myocardial Repair, Biomaterials, 32 (2011) 1280-1290.
[212] G. Salzano, D.F. Costa, V.P. Torchilin, siRNA Delivery by Stimuli-Sensitive Nanocarriers, Current pharmaceutical design, 21 (2015) 4566-4573.
[213] F. Kratz, U. Beyer, M.T. Schutte, Drug-Polymer Conjugates Containing Acid-Cleavable Bonds, Critical Reviews in Therapeutic Drug Carrier Systems, 16 (1999) 245-288.
[214] T. Lammers, F. Kiessling, W.E. Hennink, G. Storm, Drug Targeting to Tumors: Principles, Pitfalls and (Pre-)Clinical Progress, Journal of Controlled Release, 161 (2012) 175-187.

[215] R. Riehle, B. Pattni, A. Jhaveri, A. Kulkarni, G. Thakur, A. Degterev, V. Torchilin, Combination Nanopreparations of a Novel Proapoptotic Drug - NCL-240, TRAIL and siRNA, Pharmaceutical research, 33 (2016) 1587-1601.
[216] G. Salzano, R. Riehle, G. Navarro, F. Perche, G. De Rosa, V.P. Torchilin, Polymeric Micelles containing Reversibly Phospholipid-modified Anti-Survivin siRNA: a Promising Strategy to Overcome Drug Resistance in Cancer, Cancer letters, 343 (2014) 224-231.
[217] K.Y. Choi, M. Swierczewska, S. Lee, X. Chen, Protease-Activated Drug Development, Theranostics, 2 (2012) 156-178.
[218] P.S. Briquez, J.A. Hubbell, M.M. Martino, Extracellular Matrix-Inspired Growth Factor Delivery Systems for Skin Wound Healing, Advances in Wound Care, 4 (2015) 479-489.
[219] D. Filpula, H. Zhao, Releasable PEGylation of Proteins with Customized Linkers, Advanced Drug Delivery Reviews, 60 (2008) 29-49.
[220] C. Dingels, S.S. Müller, T. Steinbach, C. Tonhauser, H. Frey, Universal Concept for the Implementation of a Single Cleavable Unit at Tunable Position in Functional Poly(ethylene glycol)s, Biomacromolecules, 14 (2013) 448-459.
[221] W.E. Georgianna, H. Lusic, A.L. McIver, A. Deiters, Photocleavable Polyethylene Glycol for the Light-Regulation of Protein Function, Bioconjugate Chemistry, 21 (2010) 1404-1407.
[222] J. Li, P.R. Chen, Development and Application of Bond Cleavage Reactions in Bioorthogonal Chemistry, Nature Chemical Biology, 12 (2016) 129-137.
[223] K.L. Diehl, I.V. Kolesnichenko, S.A. Robotham, J.L. Bachman, Y. Zhong, J.S. Brodbelt, E.V. Anslyn, Click and Chemically Triggered Declick Reactions through Reversible Amine and Thiol Coupling via a Conjugate Acceptor, Nature chemistry, 8 (2016) 968-973.
[224] A.P. Crochet, M.M. Kabir, M.B. Francis, C.D. Paavola, Site-selective Dual Modification of Periplasmic Binding Proteins for Sensing Applications, Biosensors & bioelectronics, 26 (2010) 55-61.
[225] S.T. Laughlin, C.R. Bertozzi, Metabolic Labeling of Glycans with Azido Sugars and subsequent Glycan-profiling and Visualization via Staudinger Ligation, Nature Protocols, 2 (2007) 2930-2944.
[226] D.J. Lee, E. Kessel, D. Edinger, D. He, P.M. Klein, L. Voith von Voithenberg, D.C. Lamb, U. Lachelt, T. Lehto, E. Wagner, Dual Antitumoral Potency of EG5 siRNA Nanoplexes Armed with Cytotoxic Bifunctional Glutamyl-Methotrexate Targeting Ligand, Biomaterials, 77 (2016) 98-110.
[227] D.J. Lee, E. Kessel, T. Lehto, X. Liu, N. Yoshinaga, K. Padari, Y.C. Chen, S. Kempter, S. Uchida, J.O. Radler, M. Pooga, M.T. Sheu, K. Kataoka, E. Wagner, Systemic Delivery of Folate-PEG siRNA Lipopolyplexes with Enhanced Intracellular Stability for *In Vivo* Gene Silencing in Leukemia, Bioconjugate Chemistry, 28 (2017) 2393-2409.
[228] D.J. Lee, D. He, E. Kessel, K. Padari, S. Kempter, U. Lachelt, J.O. Radler, M. Pooga, E. Wagner, Tumoral Gene Silencing by Receptor-Targeted Combinatorial siRNA Polyplexes, Journal of Controlled Release, 244 (2016) 280-291.
[229] L.S. Wong, F. Khan, J. Micklefield, Selective Covalent Protein Immobilization: Strategies and Applications, Chemical Reviews, 109 (2009) 4025-4053.
[230] A.K. Trilling, J. Beekwilder, H. Zuilhof, Antibody Orientation on Biosensor Surfaces: a Minireview, Analyst, 138 (2013) 1619-1627.
[231] T. Heck, G. Faccio, M. Richter, L. Thöny-Meyer, Enzyme-Catalyzed Protein Crosslinking, Applied Microbiology and Biotechnology, 97 (2013) 461-475.
[232] E.L. Ferguson, A.M.J. Alshame, D.W. Thomas, Evaluation of Hyaluronic Acid–Protein Conjugates for Polymer Masked–Unmasked Protein Therapy, International Journal of Pharmaceutics, 402 (2010) 95-102.
[233] J.I. MacDonald, H.K. Munch, T. Moore, M.B. Francis, One-Step Site-Specific Modification of Native Proteins with 2-Pyridinecarboxyaldehydes, Nature Chemical Biology, 11 (2015) 326-331.
[234] A.S. Hoffman, Bioconjugates of Intelligent Polymers and Recognition Proteins for Use in Diagnostics and Affinity Separations, Clinical Chemistry, 46 (2000) 1478-1486.
[235] V.P. Torchilin, R. Rammohan, V. Weissig, T.S. Levchenko, TAT Peptide on the Surface of Liposomes Affords their Efficient Intracellular Delivery even at Low Temperature and in the

Presence of Metabolic Inhibitors, Proceedings of the National Academy of Sciences, 98 (2001) 8786-8791.
[236] B.G. Pierce, K. Wiehe, H. Hwang, B.-H. Kim, T. Vreven, Z. Weng, ZDOCK Server: Interactive Docking Prediction of Protein–Protein Complexes and Symmetric Multimers, Bioinformatics, 30 (2014) 1771-1773.
[237] F. Lauck, C.A. Smith, G.F. Friedland, E.L. Humphris, T. Kortemme, RosettaBackrub—a Web Server for Flexible Backbone Protein Structure Modeling and Design, Nucleic Acids Research, 38 (2010) W569-W575.
[238] A.O.-Y. Chan, C.-M. Ho, H.-C. Chong, Y.-C. Leung, J.-S. Huang, M.-K. Wong, C.-M. Che, Modification of N-Terminal α-Amino Groups of Peptides and Proteins Using Ketenes, Journal of the American Chemical Society, 134 (2012) 2589-2598.
[239] L.H. Jones, A. Narayanan, E.C. Hett, Understanding and Applying Tyrosine Biochemical Diversity, Molecular BioSystems, 10 (2014) 952-969.
[240] M. Sivaramakrishnan, T.I. Croll, R. Gupta, D. Stupar, D.R. Van Lonkhuyzen, Z. Upton, G.K. Shooter, Lysine residues of IGF-I are substrates for transglutaminases and modulate downstream IGF-I signalling, Biochimica et Biophysica Acta (BBA) - Molecular Cell Research, 1833 (2013) 3176-3185.
[241] Y. Hou, J. Hu, H. Park, M. Lee, Chitosan Based Nanoparticles as a Sustained Protein Release Carrier for Tissue Engineering Applications, Journal of Biomedical Materials Research. Part A, 100 (2012) 939-947.
[242] Y. Bin, X. Li, Y. He, S. Chen, J. Xiang, Amyloid-β Peptide (1–42) Aggregation Induced by Copper Ions under Acidic Conditions, Acta Biochimica et Biophysica Sinica, 45 (2013) 570-577.
[243] J. Tibbitts, D. Canter, R. Graff, A. Smith, L.A. Khawli, Key Factors influencing ADME Properties of Therapeutic Proteins: A need for ADME Characterization in Drug Discovery and Development, mAbs, 8 (2016) 229-245.
[244] N. Krall, F.P. da Cruz, O. Boutureira, G.J. Bernardes, Site-Selective Protein-Modification Chemistry for Basic Biology and Drug Development, Nature chemistry, 8 (2016) 103-113.
[245] M. Yu, J. Wu, J. Shi, O.C. Farokhzad, Nanotechnology for Protein Delivery: Overview and Perspectives, Journal of Controlled Release, 240 (2016) 24-37.

Chapter 2: Matrix metalloproteinase responsive delivery of myostatin inhibitors

Alexandra C. Braun[1], Marcus Gutmann[1], Regina Ebert[2], Franz Jakob[2], Henning Gieseler[3], Tessa Lühmann[1], Lorenz Meinel[1]

[1] Institute for Pharmacy and Food Chemistry, University of Wuerzburg, Am Hubland, DE-97074 Wuerzburg, Germany

[2] Orthopedic Center for Musculoskeletal Research, University of Würzburg, Friedrich-Bergius-Ring 15, 97076 Würzburg, Germany

[3] GILYOS GmbH, Friedrich-Bergius-Ring 15, 97076 Würzburg, Germany

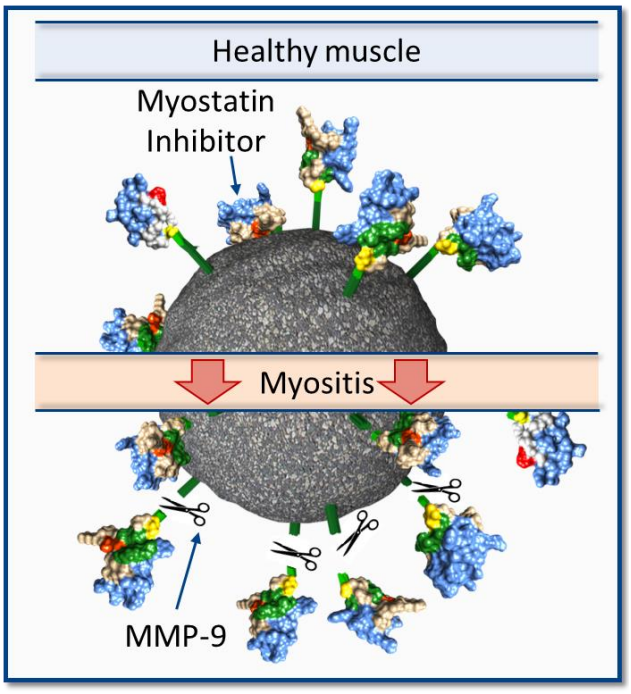

This chapter was originally published in Pharmaceutical Research, vol. 34(1), pp. 58-72, 2017. DOI: 10.1007/s11095-016-2038-6. With permission of Springer Nature, license number: 4347531320903.

Abstract

Purpose: The inhibition of myostatin - a member of the transforming growth factor (TGF–β) family - drives regeneration of functional skeletal muscle tissue. We developed a bioresponsive drug delivery system (DDS) linking release of a myostatin inhibitor (MI) to inflammatory flares of myositis to provide self-regulated MI concentration gradients within tissues of need.

Methods: A protease cleavable linker (PCL) – responding to MMP upregulation – is attached to the MI and site-specifically immobilized on microparticle surfaces.

Results: The PCL disintegrated in a matrix metalloproteinase (MMP) 1, 8, and particularly MMP-9 concentration dependent manner, with MMP-9 being an effective surrogate biomarker correlating with the activity of myositis. The bioactivity of particle-surface bound as well as released MI was confirmed by luciferase suppression in stably transfected HEK293 cells responding to myostatin induced SMAD phosphorylation.

Conclusions: We developed a MMP-responsive DDS for MI delivery responding to inflammatory flare of a diseased muscle matching the kinetics of MMP-9 upregulation, with MMP-9 kinetics matching (patho-) physiological myostatin levels.

Introduction

Sarcopenia is an age-related decrease in both mass and function of skeletal muscle fueling frailty and placing patients at higher risk for a loss of independence, impaired quality of life, and increased mortality [1]. It is associated with lower plasma and tissue concentrations of anabolic growth factors including insulin-like growth factor I (IGF-I) [2], and/or upregulated inhibitory factors including myostatin (growth differentiation factor 8, GDF-8) - a strong inhibitor of muscle differentiation and inductor of skeletal muscle atrophy [3, 4]. Myostatin binds to the activin receptor IIB (ActRIIB) leading to phosphorylation and activation of the transcription factors SMAD2 and 3, which in return translocate to the nucleus and induce gene expression [5]. Skeletal myopathies – whether occurring in specific muscles or systemically – are typically driven by NF-κB regulated inflammatory responses, with NF-κB being a strong inducer of myostatin [4, 6, 7]. However, in spite of the causal, inflammatory nexus, blockade of specific inflammatory cytokines has limited effect in preventing muscle wasting [8]. Therefore, many of the current therapeutic approaches target the ActRIIB receptor, use myostatin and activin A inhibiting follistatin, or scavenger antibodies against myostatin [9-11]. The myostatin inhibitors (MI) used in this study have a molecular mass of 2.6 kDa and selectively bind to myostatin thereby inhibiting receptor interaction with an affinity in the lower μM range [12]. However, this approximately 2 μM affinity of this low molecular weight peptide goes along with its small size, thereby presumably providing advantages in terms of tissue penetration or optimized payload for future drug delivery systems to which these MI are bound. It is for this relatively low affinity that prompted us to develop a drug delivery system (DDS) precisely clocking MI release to disease flare. Flaring myopathy is closely linked to inflammation (*vide supra*) which is why we hypothesized that "clocking" drug release to the onset of inflammatory markers in the index muscle(s) is constructive to catch the diseases in its very early phases. Translating this hypothesis into a practical, pharmaceutical design scheme, we linked bioresponsive MI release to the onset of the activity of matrix metalloproteinases (MMPs), which are upregulated in episodes of flaring myopathy [13]. These inflammatory MMPs - and particularly the gelatinase MMP-9 - drive the degradation of the basal lamina in necrotic fibers followed by inflammatory cell invasion [14]. In turn, TNFα and IL-1β secreted by activated macrophages upregulate MMP-9 during this acute inflammation [15]. MMP-9 expression and processing into the active form was reported to be strongly induced within 24 hours following muscle injury [16], coinciding with the profile of myostatin regulation following muscle trauma in mice [17]. Furthermore, MMP-9 expression is a biomarker for

monitoring disease progression in Duchenne muscular dystrophy (DMD) [18], and – within the purpose of this study – its use as a surrogate marker for the onset of myositis drives MI release from the DDS in flaring disease (and not in remission).

Bioresponsive hydrogels [19] and drug delivery systems responding to upregulated proteases have been used to optimally drive tissue responses e.g. as reported for stromal cell-derived factor 1α [20] or chemotherapeutics [21]. However, the assembly of these complex systems is quite frequently challenged by the use of (pharmaceutically questionable) non-specific chemistries including the use of EDC (1-Ethyl-3-(3dimethylaminopropyl)carbodiimide) / NHS (N-hydroxysuccinimide) chemistry or maleimide conjugation of cysteines [22, 23]. These non-specific conjugation strategies result in heterogeneous outcome, in that the presence of multiple functional groups on a protein drug results in unclear stoichiometry risking reproducible pharmacokinetic and pharmacodynamic performance [24, 25]. Therefore, next generation chemistries aim at selective decoration providing tight stoichiometric and spatial control e.g. by introducing unnatural functional groups into the therapeutic proteins followed by bioorthogonal assembly of the constructs [25-27].

This MMP responsive DDS presented here acts by a two-gated mechanism on myostatin misbalance in that a flaring inflammation drives bioresponsive release of MI (gate #1; as present in myositis) into the surrounding muscle(s) while restricting action to myopathy characterized by myostatin upregulation (gate #2; myostatin inhibition).

Materials and Methods

Materials

Dulbecco's Modified Eagle Medium (DMEM) high glucose, L-glutamine, 4’,6-diamidino-2-phenylindole (DAPI), copper (II) sulphate, sodium L-ascorbate, tris(3-hydroxypropyltriazolylmethyl)amine (THPTA), 1-hydroxybenzotriazole hydrate (HOBt), N,N′-Diisopropylcarbodiimide (DIC) and N,N-Diisopropylethylamine (DIPEA) were purchased from Sigma Aldrich (Schnelldorf, Germany). N-α-(9-Fluorenylmethyloxycarbonyl)-protected natural L-amino acids were purchased from VWR (Ismaning, Germany), Fmoc-NH-PEG(3)-COOH, Fmoc-Rink-Amid PEG AM Resin (loading 0.52 mmol/g) and modified amino acids for SPAAC and CuAAC (Fmoc-L-Pra-OH and Fmoc-L-Aha-OH) were from Iris Biotech GmbH (Marktredwitz, Germany). Acetonitrile (HPLC grade) and trifluoroacetic acid (HPLC grade) were from VWR. Human neutrophil matrix metalloproteinases (MMPs) were from EMD

Millipore Corporation (Billerica, MA). Penicillin G and streptomycin solution (Pen/Strep) were purchased from Biochrom AG (Berlin, Germany). Fetal bovine serum (FBS) was from GIBCO life technologies (Carlsbad, CA) and horse serum and secondary antibody goat anti-mouse IgG horseradish peroxidase (HRP) conjugate was from Sigma Aldrich. α-tubulin rabbit monoclonal antibody (#2125) and goat anti-rabbit IgG horseradish peroxidase (HRP) conjugate was from Cell signaling (Danvers, MA). Recombinant human/mouse myostatin (GDF-8; 788-G8-010) and monoclonal primary antibody for immunostaining and Western Blot against myosin heavy chain (MyHC; MAB4470) were from R&D Systems (Minneapolis, MN) and goat anti-mouse IgG secondary antibody Alexa Fluor® 488 conjugate (A11001), Bradford Protein Assay Kit, Pierce BCA Protein Assay Kit, Pierce Luciferase (2X) Cell lysis buffer, M-PER mammalian protein extraction reagent and Alexa Fluor 488 succimidyl ester were from Thermo Fisher Scientific (Schwerte, Germany). Mowiol 4-88 was from Carl Roth (Karlsruhe, Germany). TaqMan Gene Expression Master Mix, High Capacity cDNA Reverse Transcription Kit, GAPDH- and myogenin probe sets, TaqMan Gene Expression Assay were purchased from Applied Biosystems (Foster City, CA) and RNEasy Mini Kit was from Qiagen (Hilden, Germany). NHS activated sepharose TM4 Fast flow (crosslinked 4% agarose beads; mean particle size 90 µm, particle range 45µm – 186 µm) was from GE Healthcare (Freiburg, Germany). 3D Carboxy-poly(methylmethacrylate) particles (5% solid content, mean particle size 4.6 µm) was from PolyAn (Berlin, Germany). All other reagents were obtained from Sigma Aldrich and were at least of pharmaceutical grade unless otherwise stated.

Synthesis, chemical modification, and molecular weight of the myostatin inhibitors

The myostatin inhibitor (MI) variants and protease cleavable linkers (PCL) were synthesized manually by solid phase peptide synthesis (SPPS) using Fmoc strategy as described before [28]. In brief, Fmoc-Rink-Amid PEG AM Resin as solid support was loaded into in a polypropylene-reactor with polyethylene frit and plastic fit (MultiSynTech GmbH, Witten, Germany). After Fmoc-deprotection using 40 % (V/V) piperidine in DMF for 3 minutes followed by 20 % (V/V) piperidine for 15 minutes in DMF and 6 washing steps using DMF, a 5 molar excess as compared to the functional groups on the resin of Fmoc-protected amino-acid dissolved in 0.5 M HOBt in DMF with 80 µL DIC and 88 µL DIPEA was loaded on the resin and incubated for at least 3 hours. The sequence of the first variant manufactured for EDC (1-Ethyl-3-(3dimethylaminopropyl)carbodiimide)/ NHS (N-hydroxysuccinimide) chemistry was Ac-K-PEG(3)-SQGHCTRWPWMCPPQGWG-K, of the second variant manufactured for factor XIII

linkage [29] was Ac-GNQEQVSPLGG-PEG(3)-SQGHCTRWPWMCPPQGWG-K, and the third variant manufactured for copper(I) catalyzed azide-alkyne cycloaddition was Ac-Pra-GGG-PEG(3)-VATQGQCTRWPWMCPPQGWG-G(5)-Pra. The PCL sequence used was Ac-FKG-PEG(3)-GPQGIAGQ-PEG(6)-A(N_3) [30] and of the assembled MI-protease-sensitive linker (MI-PCL) Ac-FKG-PEG(3)-G-VATQGQCTRWPWMCPPQGWG-PEG(6)-GPQGIAGQ-PEG(3)-A(N_3). Structure prediction was done by PEP-FOLD 3.0 [31] and molecular graphics created by Chimera [32].

After cleavage from the resin, the peptides were purified by reversed phase chromatography using an FPLC system (GE Healthcare Äkta Purifier, Life sciences, Freiburg, Germany) with a Jupiter 15u C18 300A column (21.2 mm x 250 mm, Phenomenex Inc., Torrance, CA). A sample of each fraction was taken and desalted using Zip Tip pipette tips (C18 resin, Millipore) following the manufacturer's instructions. One µL of the eluate was embedded in a matrix, consisting of equal parts of 4-Bromo-α-cyanocinnamic acid and ACN/0.1 % TFA in water (1:4). Matrix-assisted laser desorption ionization (MALDI)-MS spectra were acquired in the linear positive mode by using an Autoflex II LRF instrument from Bruker Daltonics Inc. (Billerica, USA) fitted with a λ = 337 nm nitrogen laser. After purification, fractions were filled in 10 mL vials, semi-stoppered and lyophilization was performed using a VirTis AdVantage Plus (SP Scientific, Gardiner, NY) laboratory-scale freeze-dryer. First, the vials were transferred into a −80°C deep freezer to ensure fast solidification and maintained at this temperature for at least 2 hours before loading onto the precooled shelves (-40°C) of the freeze drier. Primary drying was performed by controlling the shelf temperature at 5 °C over a period of 24 h and the chamber pressure at 80 mTorr. Secondary drying was carried out at the same chamber pressure applied during primary drying but increasing the shelf temperature to 25°C and maintaining this temperature for 6 h. Thin wire thermocouples (Omega Engineering, Newport, CT) were applied to monitor product temperature throughout the course of the freeze-drying process. Lyophilisates were stored at -80 °C until use.

Bioconjugation of the different MI variants

The first MI variant with N- and C-terminal lysines was either directly coupled to the NHS-activated fluorescent dye Alexa Fluor 488 succimidyl ester (NHS-dye) or reacted with dibenzocyclooctyne-PEG4-N-hydroxysuccinimidyl ester (DBCO-PEG(4)-NHS ester) followed by labelling with Azide Fluor 488 (azide-dye). For the first set, the lyophilized lysine-containing MI was dissolved in PBS and reacted with the NHS-dye at a 1:1 molar ratio with

respect to the two amino groups present in the MI. The coupling was performed in a total volume of 100 µL in PBS buffer at pH 7.4 for 2 hours at room temperature in the dark with a MI variant devoid of free amino groups (alkyne-MI) as a negative control. The reaction was stopped by freezing the samples at -80°C. For the second set, the lysine containing MI variant was first reacted with NHS-PEG(4)-DBCO under the same conditions as described above followed by dialysis to remove unreacted NHS-reagent. In the next step, the concentration of the DBCO-MI conjugate was measured using the BCA assay and incubated with Azide Fluor 488 at a 1:1 molar ratio at room temperature for 1 hour in PBS. As negative control, the unreacted lysine-containing MI variant was incubated with the azide-dye under the same conditions to verify the specificity of this two-step conjugation reaction.

For factor XIIIa mediated acyl transfer reaction, a linker containing a N-terminally acetylated FKG-sequence and a C-terminal azide group was synthesized by SPPS. The MI variant containing the NQEQVSPLG-sequence – generated from the TGase substrate sequence of alpha-2 plasmin inhibitor [29] – was incubated with 2-fold molar excess of the FKG-containing linker peptide in the presence of 0.18 units of thrombin-activated fXIII, 5 mM $CaCl_2$ and 50 mM tris–HCl buffer containing 150 mM sodium chloride (pH adjusted to 8.0 at room temperature) in 50 µL reaction volumes at 37 °C for 2 hours with slight agitation. The reaction mixture was stopped by separation of factor XIIIa and additives using Vivaspin 500 ultrafiltration spin columns (30 000 MWCO PES membranes, Sartorius Stedium, Goettingen, Germany) followed by performance of the SPAAC reaction to label the azide group of the linker and the coupling product with DBCO-5,6-carboxyrhodamine 110 in PBS for 1 h at room temperature. For the copper(I)-catalyzed azide-alkyne cycloaddition a solution containing $CuSO_4$, THPTA and sodium L-ascorbate was prepared and incubated in the dark for 10 minutes before use to reduce generated reactive oxygen species and thereby, limit the oxidative effects. The lyophilized alkyne-modified MI was dissolved in PBS and the Cu(I) solution added to reach final concentrations of 50 µM $CuSO_4$, 250 µM THPTA, and 2.5 mM sodium L-ascorbate. The fluorescent dye azide Fluor 488 was added in a molar ration of 1:1 with respect to the two alkyne groups present in the MI and the mixture was incubated for 1 h at room temperature in the dark. After coupling, all reaction mixtures were directly transferred to a 16 % tricine-SDS-PAGE gel [33] and analyzed for fluorescence on a Gene flash doku system (Syngene, Cambridge, UK) for detection of the peptide-dye conjugate. Subsequent peptide staining was done by Coomassie brilliant blue.

Luciferase-based reporter gene assay

HEK-293 cells (ATCC-Number CRL-1573, ATCC, Manassas, VA) stably transfected with a pGl3ti vector, linearized with the restriction enzyme BsaI (New England BioLabs GmbH, Frankfurt, Germany), containing a SMAD binding element (SBE) – responding to phosphorylation of SMAD 2, 3 an 4 – at the promotor of the firefly luciferase gene and a hygromycin resistance to select for transfected cells were used for the reporter assay [34]. Briefly, 1.8 x 10^4 cells/24-well were transfected at 50-70% confluence. Liposome-mediated transfection was performed using Lipofectamine® 2000 Transfection Reagent (Thermo Fisher Scientific, Langenselbold, Germany). 2 µL of Lipofectamine® 2000 and 0.9 µg of linearized constructs were diluted in 100 µL serum-free medium (DMEM containing 4.5 g/L D-glucose, 2 mM L-glutamine, 100 U/mL penicillin G and 100 µg/µL streptomycin) and incubated for 30 min. 124 µL serum-free medium was added, and the solution was then carefully dripped onto the cells. HEK293 cells were incubated for 5 h in transfection solution at 37°C and 5 % CO_2. After removal of the medium cells were cultivated with medium containing 10% heat-inactivated FCS. After 24 h 50 µg/mL hygromycin was added as selection antibiotic. The cells were maintained in 75 cm^2 culture flasks in growth medium at 37°C and 5 % CO_2. Before use, the cells were harvested from exponentially growing sub-confluent monolayers in growth medium and seeded at a final cell density of 3 x 10^4 cells/well (using 100 µL per well) in 96-well clear tissue culture plates (Thermo Fisher Scientific) in growth medium and grown for 24 hours at 37°C and 5 % CO_2. After two washing steps with PBS, the cells were exposed to the ligands (in the first set of experiments with 4 nM myostatin alone or in combination with MI or MI-PCL, in the second set of experiments with MI-PCL-functionalized particles or cleaved fragments present in the supernatant after exposure to MMPs or incubated in buffer, respectively) in assay medium (DMEM high glucose with 2 mM L-glutamine, 0.5% heat inactivated FCS, 100 U/mL penicillin G and 100 µg/µL streptomycin and 50µg/mL hygromycin). In case of the MI-PCL functionalized particles, the dilution series of MMP-exposed and -unexposed particles (*vide infra*) was pre-incubated with myostatin for 15 minutes before addition to the reporter cells. Following stimulation with the ligands for 48 hours at 37 °C and 5 % CO_2, the cells were washed once with PBS and lysed using 80 µL of luciferase assay buffer and 50 µL of the lysate was transferred to a white bottom 96-well plate (Thermo Fisher Scientific) and frozen at -80°C. Luciferase activity was monitored following the addition of 100 µL Luciferase Assay Reagent (Promega GmbH, Mannheim, Germany) to each well and the chemiluminescence was read on an Orion II Microplate Luminometer (Titertek-Berthold,

Pforzheim, Germany) after 1 second as described previously [35]. For normalization to cell number a Bradford Assay with the cell lysates was conducted (using Quick Start 1x dye reagent, Biorad, Germany). Protein content was determined by a BSA calibration (50–1000 µg/mL BSA standard curve) and luciferase activity was specified as RLU (relative light units) per µg protein.

C2C12 differentiation and immunostaining

C2C12 myoblasts (ATCC CRL-1772) were cultured in growth medium (DMEM containing 4.5 g/L D-glucose, 2 mM L-glutamine, 10 % heat inactivated FCS, 100 U/mL penicillin G and 100 µg/µL streptomycin). 50,000 cells/well were seeded in 4-well plates (Greiner Bio One, Frickenhausen, Germany) in growth medium. Following 24 hours of incubation myoblast differentiation was initiated by changing to differentiation medium (DMEM supplemented with 2 % horse serum) at which point the compounds were added (myostatin alone or in combination with MI or MI-PCL, respectively). Cell differentiation into myotubes was followed for 5 days. Due to the high metabolic activity of the cells during differentiation the medium had to be renewed every 24 hours. To maintain the effect of the MI or MI-PCL on the cells, they were premixed with myostatin and diluted with fresh medium before addition to the cells.

After 5 days of differentiation, the medium was gently aspirated and the cells were washed twice with PBS and fixed and permeabilized with ice-cold methanol for 10 minutes at 4°C. Following 4 washing steps with PBS, non-specific binding was blocked with 5% bovine serum albumin (BSA) in PBS prior to incubation with anti-myosin heavy chain antibody at 4°C over night and Alexa Fluor 488 secondary antibody (diluted in PBS + 5% BSA) for 60 minutes at room temperature. Cell nuclei were counterstained with DAPI. The cells on the cover slides were mounted on microscope slides with Mowiol 4-88 and visualized at 10 fold magnification using a Zeiss Axio Observer Z1 epifluorescence microscope equipped with a A-Plan 10x/0.25 Ph1 objective (Zeiss, Oberkochen, Germany). Fluorescence excitation was measured at $\lambda = 495$ nm with an exposure time of 1.7 seconds.

Western Blot of differentiated C2C12 cells

After 5 days of differentiation cells were lysed using M-PER mammalian protein extraction reagent and cell extracts centrifuged at 14,000 ×g for 15 min at 4 °C. The total protein concentration of cell extracts was determined using the BCA protein assay kit. Equivalent amounts of total proteins were mixed with 6× SDS reducing sample buffer, denatured for 5 minutes at 95°C and then subjected to 5% SDS-polyacrylamide gel electrophoresis. The protein bands of the polyacrylamide gel were then transferred onto a nitrocellulose membrane, blocked

in TBS containing 0.1% Tween 20 and 5% BSA followed by incubation with primary antibodies (anti-myosin heavy chain antibody for the upper part of the membrane and anti-α-tubulin as loading control for the lower part of the membrane) at 4°C over night. After three washing steps for 10 min each with TBS/T, the membranes were incubated with horseradish peroxidase-conjugated IgG antibody diluted 1:5000 in TBS/T for 90 min at room temperature followed by three 10-min washing steps with TBS/T. The signals were visualized by using SuperSignal West Pico Chemiluminescent Substrate according to the manufacturer's instructions.

RT-PCR (Quantitative real-time PCR of differentiation markers)

Total RNA was isolated from the 5 days differentiated C2C12 myoblasts using RNEasy Mini Kit according to the manufacturer's instructions. The concentrations of total RNA were determined spectrophotometrically using a NanoDrop ND-1000 (NanoDrop Technologies, Wilmington, DE) and adjusted to the same concentration. Samples were prepared for reverse transcription PCR by using oligo(dT) primers (High Capacity cDNA Reverse Transcriptase Kit) and 100 ng cDNA amplified by PCR. A TaqMan probe set for myogenin was used (Myog: Mm00446194_m1; GAPDH: Mm99999915_g1; Applied Biosystems) with TaqMan Gene Expression Master Mix and analyzed by qPCR in a ABI prism7900 HT Real-Time PCR System (Applied Biosystems). cDNA levels were normalized to the expression of the housekeeping gene GAPDH; relative values were calculated by the comparative CT Method [36].

Cleavage experiments of the protease cleavable linkers

Pro-MMPs (MMP-1, MMP-8 and MMP-9) were activated with 4-aminophenylmercuric acetate (APMA) as described before [37]. Lyophilized protease cleavable linkers (PCL) were diluted in MMP-buffer (50 mM Tris, 150 mM NaCl, 1 µM $ZnCL_2$, 10 mM $CaCl_2$, pH 7.4) to a final concentration of 1 mM. For the experiments targeting the time-dependent release profile, 100 µL of these solutions were mixed either with one of the matrix metalloproteinases (MMP)-1, -8 or -9 alone or with a combination of all MMPs to reach a final protease concentration of 16 nM and incubated at 37 °C with gentle agitation for defined periods of time (ranging from 30 min to 24 hours). The protease activity was stopped by addition of 1 mM EDTA and heating to 95 °C for 5 minutes. For the experiments targeting the MMP concentration-dependent cleavage of the PCL, a combination of all three MMPs was used. 100 µL of the PCL solution was incubated at 37 °C for 24 hours with equimolar amounts of MMP-1, -8 and -9 to reach total concentrations of 0.16 to 16 nM protease. Following 24 hours incubation, protease activity was

stopped with 1 mM EDTA and heating to 95°C for 5 minutes. Cleavage efficiency was assessed on a LaChromUltra UPLC system equipped with a Hitachi L-2455U diode array detector and two L-2160U pumps (VWR Hitachi, Tokyo, Japan). 30 µL PCL sample was applied on a ZORBAX Eclipse XDB-C18 column (4.6 mm x 150 mm, Agilent, Santa Clara, CA) equilibrated with a solution of 95 % water containing 0.1 % TFA and 5 % acetonitrile (ACN) containing 0.1 % TFA. PCL and cleaved fragments were eluted by a linear gradient of 5 – 60 % ACN containing 0.1 % TFA with a flow rate of 1 mL/min. Column temperature was kept at 40°C by a L-2300 column oven and absorbance was monitored at λ = 215 nm.

Decoration of 3D Carboxy-poly(methyl methacrylate) particles and exposure to MMPs

Transparent 3D-carboxy-PMMA beads (100 µL solution corresponded to approximately 0.7 µmol carboxyl groups according to the manufacturer's information) was activated with EDC (1-Ethyl-3-(3dimethylaminopropyl)carbodiimide)/NHS (N-hydroxysuccinimide) in MES buffer pH 6.5, followed by modification with equimolar amounts of dibenzocyclooctyne-amine (DBCO-amine), or ethanolamine for the control particles in PBS buffer at pH 7.4 for 2 hours with gentle shaking. The particle solution was subsequently blocked with 500 mM ethanolamine in 100 mM Tris-HCl buffer (pH 8.4), containing 0.5 M NaCl, for 1 hour. The DBCO particles and the ethanolamine (control) particles were washed several times with PBS and each allocated in two groups, one group was incubated with 0.2 µmol PCL and the other group with 0.2 µmol MI-PCL in PBS for 2 hours at RT with gentle shaking. Following several washing steps, the immobilized PCL or MI-PCL was labelled with Alexa Fluor 488 succimidyl ester for 30 minutes at room temperature followed by two washing steps with PBS containing 0.02 % polysorbate 20, one step with 1 % sodium dodecyl sulfate in MQ water and two steps with PBS. The particles were incubated overnight in MMP 9 buffer (50 mM Tris, 150 mM NaCl, 1 µM $ZnCl_2$, 10 mM $CaCl_2$, pH 7.4) to remove non-specifically bound peptide and dye. Half of these functionalized particles were incubated at 37°C in protease buffer for 24 hours with equimolar amounts of MMP-1, -8 and -9 to reach a total protease concentration of 8 nM and the other half incubated in MMP buffer alone without MMP. Following 24 hours incubation, the particles were washed five times with PBS containing 0.02 % polysorbate 20 and analyzed using flow cytometry and on a LaChromUltra UPLC system equipped with a L-2485U fluorescence detector (Hitachi, VWR).

Flow cytometry

5,000 beads each (n = 3) were analyzed by recording forward scatter, sideward scatter and fluorescence signals at λ = 488 nm and detection at λ = 530 nm using a FACS Calibur system (Becton Dickinson, NY, USA). Analysis was performed with the 'Flowing Software' 2.5.0. (Perttu Terho, Turku Centre for Biotechnology, Turku, Finland).

Decoration of NHS activated agarose particles and exposure to MMPs

NHS activated agarose bead slurry solution (100 µL solution corresponds to 2 µmol NHS) was washed once with PBS, followed by 1 mM hydrochloric acid and again two times with PBS followed by modification with equimolar amounts of DBCO-amine, or ethanolamine for control particles in PBS buffer at pH 7.4 for 2 hours with gentle shaking. The particle solution was subsequently blocked with 500 mM ethanolamine in 100 mM Tris-HCl buffer (pH 8.4) containing 0.5 M NaCl for 1 hour. 60 mg particles decorated with DBCO-amine or ethanolamine, respectively, were weighted and incubated each with 1 µmol PCL or MI-PCL in PBS (to make a total reaction volume of 500 µL) for 3 hours at RT with gentle shaking. After 15, 30, 60, 120 and 180 minutes during the reaction, 5 µL samples of the supernatant were taken and the peptide content of the supernatant was measured by a Bicinchoninic acid (BCA) assay to assess the progress of the SPAAC reaction. Hence, coupling efficiency was calculated by the reduction of the peptide concentration in the supernatant compared to the initial concentration (t = 0). Subsequently, five washing steps with PBS were performed and the particles incubated over a period of 3 days in MMP buffer (50 mM Tris, 150 mM NaCl, 1 µM $ZnCl_2$, 10 mM $CaCl_2$, pH 7.4) to remove non-specifically bound peptides. The particle solution was split and one half was incubated at 37°C in protease buffer for 24 hours with equimolar amounts of MMP-1, -8 and -9 to reach a total protease concentration of 8 nM and the other half incubated in MMP buffer alone (without MMPs). After 0.5, 1, 3, 6 and 24 hours during MMP exposition and buffer incubation of the control particles, respectively, samples of 5 µL were taken and the peptide content of the supernatant was assessed by a BCA assay.. Cleavage kinetics was calculated by the increase in peptide concentration in the supernatant following MMP digestion with regard to particle amount and peptide loading). Following 24 hours incubation, protease activity was stopped with 0.1 mM EDTA, the particles were centrifuged for 5 minutes with 2000 x g using a Micro 2416 centrifuge (VWR) and the supernatant was separated from the particles and lyophilized using a VirTis AdVantage Plus freeze-dryer (SP Scientific, *vide supra*). After reconstitution of the lyophilized supernatants in 100 µL PBS, peptide concentration was

determined by a BCA assay and subsequently diluted with 500 µL DMEM. The solution was sterile-filtered and added to the cells for bioactivity testing. The collected particles after MMP digest and buffer incubation, respectively, were washed twice with PBS containing 0.02 % polysorbate 20, then the supernatant was aspirated and the particles weighed and 30 mg were taken and washed three times with sterile PBS before addition to the cells (10 mg/well).

Statistical analysis

Data were analyzed using Student's t-test or one-way ANOVA followed by pair-wise comparisons using Tukey Kramer *post-hoc* test. SigmaPlot (Systat Software Inc., CA) or Minitab 16 (Minitab, Coventry, UK) was used. Results were considered statistically significant at $p \leq 0.05$ (*; $p \leq 0.01$ (**)) and results are displayed as mean with standard deviation (SD).

Results

Preparation of the myostatin inhibitor variants for bioorthogonal coupling

We developed three analogues of the myostatin inhibitors (MIs) with the ultimate goal to retain bioactivity and gain flexibility in terms of orthogonal coupling chemistries used for DDS assembly (**Figure 1**). The design of the MIs preserved the core sequence of 20 amino acids - required for binding to myostatin [12] - and featured different functional groups as coupling sites which were connected via a PEG(3) spacer. A first variant carrying two terminal lysines/primary ε-amino groups was developed for compatibility with EDC/NHS chemistry [38]. The otherwise non-specific EDC/NHS chemistry - randomly coupling primary amino with carboxyl groups (*vide supra*) - was nevertheless specific in our specific setting, as the MI itself did not contain any primary amino groups (**Figure 1A**). A second variant carrying one N-terminal transglutaminase / factor XIII sequence - derived from the natural substrate of α2-plasmin inhibitor (α2PI) - and a C-terminal lysine/primary ε-amino group was developed for heterobifunctional synthesis through enzymatic and EDC/NHS coupling, respectively (**Figure 1B**) [29, 39, 40]. This variant allows the coupling of different molecules to the MI as one end is decorated through enzymatic ligation and the other end chemically. The third MI variant carried two terminal alkyne groups for compatibility with 1,3-cycloaddition reactions (**Figure 1C**) [26, 41]. After purification, the resulting variants were analyzed by MALDI-MS, resulting in an obs. average mass of 2623 Da (calc. average mass = 2622 Da), 3573 Da (cal. average mass = 3572 Da), and 3307 Da (calc. average mass = 3307 Da) for the first, second, and third variant, respectively (**Figure S1A-C**). Myostatin inhibition of the three MI variants was tested with a reporter gene luciferase assay in HEK293T cells, monitoring SMAD phosphorylation in response to MI concentration. All three MI variants had a dose-dependent inhibitory effect on myostatin-induced SMAD phosphorylation, displaying IC_{50} values in the µ-molar range with 2.0 ± 0.5 µM, 2.0 ± 0.5 µM, and 48.5 ± 7.6 µM for the first (two terminal lysines), second (N-terminal factor XIII sequence, C-terminal lysine), and third variant (two terminal alkynes), respectively (**Figure 1A-C,** panels B). The higher IC_{50} value observed for the alkyne-modified variant could be attributed to an increased tendency to form aggregates (data not shown).

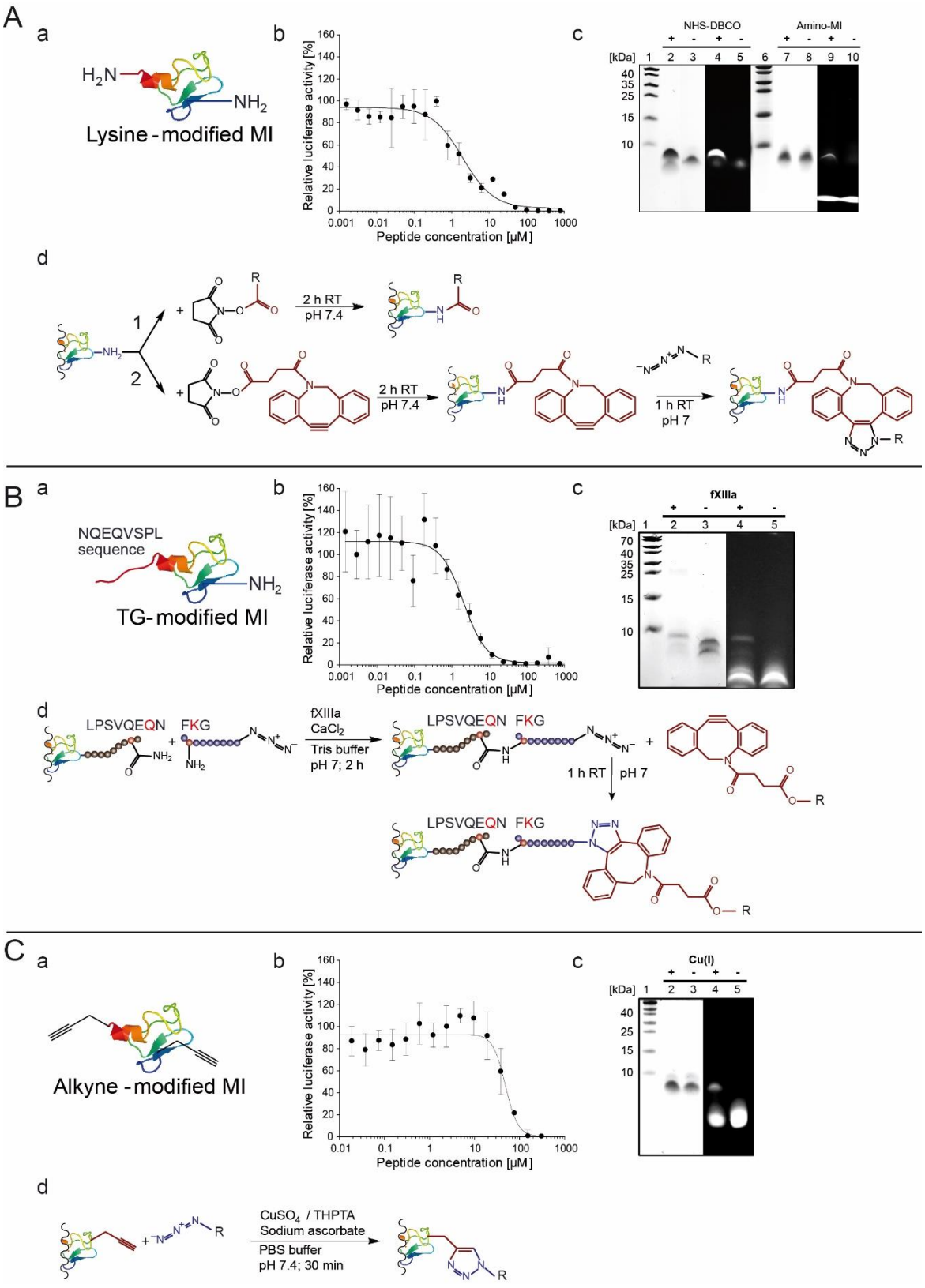

Figure 1: Characterization of the myostatin inhibitors with modifications for bioorthogonal conjugation: (A) Lysine-modifications for EDC/NHS chemistry (Ac-K-PEG(3)-SQGHCTRWPWMCPPQGWG-K), (B) Transglutaminase-modifications for enzymatic coupling (Ac-GNQEQVSPLGG-PEG(3)-SQGHCTRWPWMCPPQGWG-K), and (C) alkyne- modification for copper-catalyzed azide-alkyne click reaction (CuAAC; Ac-Pra-GGG-PEG(3)-VATQGQCTRWPWMCPPQGWG-G(5)-Pra).

(A-C, panels b) Bioactivity was assessed by a luciferase-based reporter gene assay with 100 % activity corresponding to 4 nM myostatin. Data are shown as mean ± STDEV (n = 3). (A – C, panels c) Conjugation reactions assessed by tricine-SDS-PAGE, each following the scheme depicted in d. Peptide staining by Coomassie brilliant blue is on the left, fluorescence of the gel for detection of dye-peptide conjugates is on the right. Lane 1 was loaded with protein standard. (A, panel c, d) NHS reaction of DBCO-PEG(4)-NHS with lysine-modified MI, followed by SPAAC reaction with azide Fluor 488 (lanes #2 and #4) compared to reaction of lysine-modified MI with azide Fluor 488 (lanes #3 and #5, negative control). NHS coupling of lysine-modified MI (lanes #7 and #9) and alkyne-modified MI (lanes #8 and #10, negative control), respectively, with Alexa Fluor 488 succimidyl ester. (B, panel c, d) FXIIIa mediated acyl transfer reaction between TG-modified MI and an azide-containing linker peptide in presence (lanes #2 and #4) and absence (lanes #3 and #5) of fXIIIa, followed by reaction with DBCO-5,6-carboxyrhodamine. (C, panel c, d) CuAAC between alkyne-modified MI and azide Fluor 488 in the presence (lanes #2 and #4) or absence of copper(I) (lanes #3 and #5).

To study the functionality of the introduced groups for site-specific chemical or enzymatic conjugation, the coupling reactions were performed with fluorophores as conjugation partners. The covalent dye attachment was visualized by tricine-SDS-gel electrophoresis and fluorescence imaging (**Figure 1A-C**, panels C) following the reaction schemes depicted below (**Figure 1A-C**, panels D). For the first variant, two possible conjugation strategies are presented, the direct decoration of the amino groups with NHS-activated carboxyl groups (**Figure 1A**, panel D1) and the reaction with DBCO-PEG(4)-NHS followed by SPAAC reaction with an azide-containing molecule (**Figure 1A**, panel D2). Both strategies resulted in high coupling efficiencies after 2 hours incubation, with low background fluorescence for the negative controls (**Figure 1A**, panel C). As negative control in case of the NHS-coupling, the alkyne-modified variant described in **Figure 1C** with no primary amino groups was used (**Figure 1A**, panel C, lanes #8 and #10) and compared to the positive control with N-and C terminal lysines (lanes #7 and #9). For the alternative strategy using a combination of NHS-and SPAAC chemistries, the azide-dye was conjugated to DBCO-MI (lanes #2 and #4) and to the lysine-MI as a negative control (lanes #3 and #5). The fluorescent labelling of the peptides in the positive controls indicated that under applied conditions the functional groups are accessible and react specifically with the dyes. In case of the MI variant for enzymatic ligation, the factor XIIIa-mediated acyl transfer reaction was performed with a linker containing the complementary TG recognition sequence and a C-terminal azide group (**Figure 1B**, panel C,D). Subsequent performance of the SPAAC reaction showed an additional fluorescent band in the tricine-SDS-PAGE of about 7 kDa size in the positive control (**Figure 1B**, panel C, lane #4), whereas in absence of fXIIIa in the first coupling step, only the linker reacted with the dye (lane #5). The functionality of the alkyne groups in the third variant was also assessed by performance of the CuAAC (**Figure 1C** panel C, following the scheme of panel D) with an azide fluorophore

using copper(II) sulfate in the presence of sodium L-ascorbate as mild reducing agent and the water-soluble base THPTA as previously described [27]. After click reaction, fluorescence labelling of the MI was detected (lane #4), whereas in absence of copper(II) sulfate only excess fluorescent dye appeared in the gel (lane #5). As bioactivity and conjugation of all three MI variants was verified, we decided to proceed using SPAAC as favored coupling strategy for the DDS due to (i) negative side effects and toxicity of copper species required for CuAAC, (ii) specificity issues in complex systems by using EDC/NHS chemistry and (iii) sensitivity to external influences when applying enzymatic conjugation.

Characterization of protease cleavable linker

A matrix-metalloproteinase (MMP) sensitive protease cleavable linker (PCL) was used (GPQGIAGQ; derived from the human type I collagen sequence [30]) to feature bioresponsive release of the MI in inflammatory/MMP enriched cellular environment. The PCL was modified with an azide group with an intermediate PEG(6) spacer and a lysine for attachment of a NHS activated fluorescent dye (for ESI-MS spectrum see **Figure S2C)**.

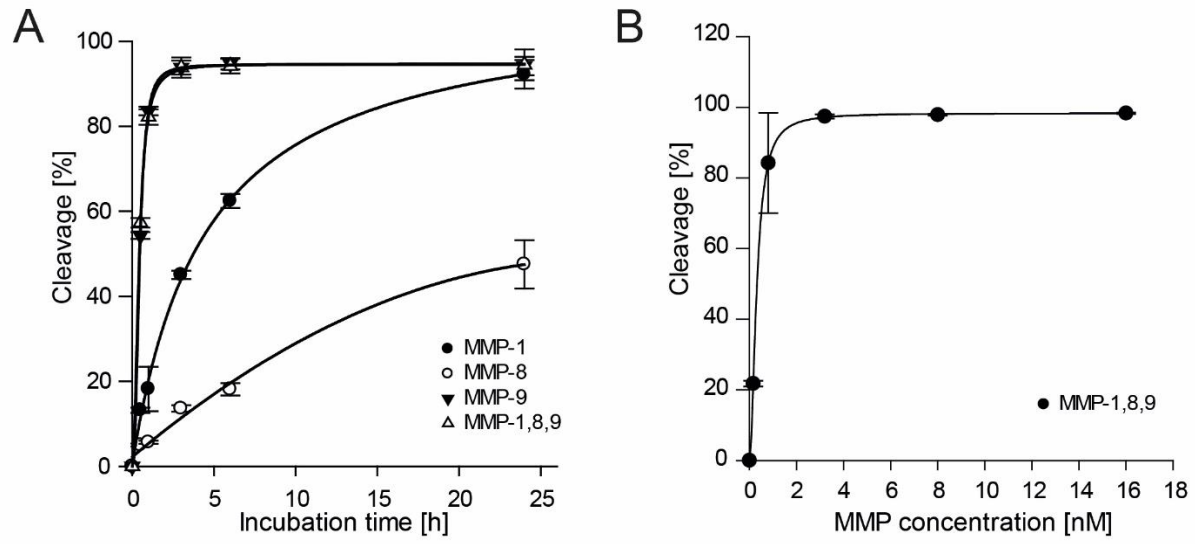

Figure 2: Characterization of the protease cleavable linker. (A) Comparison of cleavage efficiency of MMP-1,-8 and -9 alone and a combination of all 3 proteases at 37°C as a function of incubation time. (B) Cleavage efficiency as a function of MMP concentration using a mixture of MMP-1,-8 and -9 exposed for 24 hours. Data are shown as mean ± STDEV (n = 3)

The cleavage rate of the protease cleavable linker (PCL) was analyzed in response to MMP-1, MMP-8, and MMP-9 (**Figure 2**). RP-HPLC analysis revealed effective cleavage, with MMP-9 (approximated by $95 * (1 - e^{-2x})$; $r^2 = 0.99$) > MMP-1 (approximated by $\frac{109x}{4+x}$; $r^2 = 0.99$) >

MMP-8 (approximated by $\frac{83x}{18+x}$; $r^2 = 0.99$) , respectively ($p < 0.05$; **Figure S2A,B** for selected HPLC chromatograms, **Figure S2D-F** for ESI-MS spectra of cleaved fragments). For example, after 3 hours PCL cleavage was significantly different with 93.8 ± 2.4 %, 45.0 ± 1.0 %, and 13. 6 ± 0.8 % for MMP-9, MMP-1, and MMP-8, respectively ($p < 0.05$). Following 24 hours of incubation, PCL cleavage was 94.2 ± 2.2 %, 92.2 ± 3.3 %, and 47.5 ± 5.7 % for MMP-9, MMP-1, and MMP-8, respectively. Using an equimolar combination of the three MMPs - each at concentrations used for the assessment of its individual cleavage potential – resulted in identical performance as observed for MMP-9 alone (**Figure 2A**). A mixture of equimolar concentrations of MMPs (MMP-1, MMP-8, MMP-9) were tested at three total concentrations of 0.16 nM, 0.8 nM, or 3.2 nM and resulted in 21.8 ± 0.8 %, 84.2 ± 14.1 %, and 97.4 ± 0.6 % cleavage after 24 hours incubation, respectively (following $98.57 * (1 - e^{-2.07x})$; r^2=0.994; **Figure 2B**).

Bioactivity of selected myostatin inhibitor (MI) and assembled MI-protease-sensitive linker

The MMP-sensitive sequence was directly attached to the myostatin inhibitor generating the assembled MI-PCL (**Figure 3A**, for MALDI-MS spectra see **Figure S3A, S3B**) and bioactivity of the combination was compared to the MI alone. The MI-PCL construct had a C-terminal azide group to allow for conjugation via copper(I)-catalyzed azide-alkyne cycloaddition (CuAAC [42, 43]) or strain promoted azide-alkyne cycloaddition (SPAAC [44]). We started off by designing the MI-PCL based on an *in silico* peptide structure PEP-FOLD prediction of the resulting construct (**Figure 3B;** and for prediction of myostatin interaction **Figure S3C, S3D**) [31]. The prediction suggested, that the PCL (attached to the C-terminus of the MI) was distant to the pharmacologically active MI moiety and that both (the PCL and the MI part of the molecule) will be surface exposed. Therefore, we speculated that the resulting MI-PCL will provide spatial conditions allowing effective MMP access to the PCL and effective MI binding to myostatin.

MI and MI-PCL were characterized with the SMAD luciferase reporter assay in HEK293 cells resulting in IC_{50} values of 2.0 ± 0.5 µM and 7.7 ± 3.0 µM for MI and the MI-PCL, respectively (**Figure 3C**). We then assessed the performances of the MI and MI-PCL on myogenic differentiation of C2C12 myoblasts (**Figure 3D**) [3]. Cells exposed to differentiation medium alone (differentiation medium, DM, **Figure 3D1**) myostatin supplemented DM (**Figure 3D2**) or myostatin supplemented DM with MI or MI-PCL (**Figure 3D3** and **3D4**) were grown for 6 days and then stained with DAPI and an antibody against myosin heavy chain to visualize the

cell nuclei and differentiated myotubes, respectively. Myostatin exposure resulted in a decrease in size and number of myotubes as qualitatively observed (**Figure 3D** insert **2A**). Co-treatment of myostatin with MI or MI-PCL inhibited the myostatin-mediated effects, and restored myotube differentiation and hypertrophy (**Figure 3D** insert **3A, 4A**).

Proliferation of the myoblasts was less impacted by myostatin treatment and inhibition of myostatin as assessed qualitatively (**Figure 3D** inserts **1B, 2B, 3B, 4B**). The degree of myotube formation in C2C12 myoblasts treated with two different concentrations of myostatin alone or with the high myostatin concentration in combination with MI or MI-PCL, respectively, was quantified by immunoblotting with a MyHC antibody using α-tubulin as loading control (**Figure 3E, S3E**). Myostatin treatment resulted in a concentration-dependent decrease in the number of differentiated myotubes to 58.6 ± 3.7 % and 33.1 ± 14.7 % for concentrations of 4 nM and 20 nM myostatin, respectively. Co-treatment of 20 nM myostatin with 6 µM MI or MI-PCL significantly reversed myostatin-induced inhibition of myoblast differentiation and increased MyHC expression to levels comparable to control (92.9 ± 9.2 % for the MI, and 99.2 ± 23.8 % for the MI-PCL, respectively). Additionally, mRNA expression of the myogenic differentiation marker myogenin was determined after 5 days stimulation of C2C12 myoblasts under the same conditions as described above and normalized to GAPDH expression using quantitative RT-PCR (**Figure 3F**). Myogenin was found to induce terminal differentiation of myoblasts into myocytes and subsequent fusion to multinucleated myotubes [45]. Myostatin treatment at a higher concentration for 5 days led to a 4.7 fold reduction of myogenin mRNA expression compared to untreated control. This reduction of myogenin mRNA levels was mostly compensated by co-treatment with MI or MI-PCL, reaching 89.8 ± 6.4 % and 106.8 ± 12.1 % compared to control for the MI and MI-PCL, respectively. Analysis of the fusion index (determined as the ratio of the number of nuclei inside myotubes to the number of total nuclei) supported this finding, as myostatin treatment decreased the fusion index by 31.62 %, but co-treatment with MI or MI-PCL partially rescued the differentiation of myostatin-treated myoblasts and increased the fusion index to levels similar to control (**Figure S3F**).

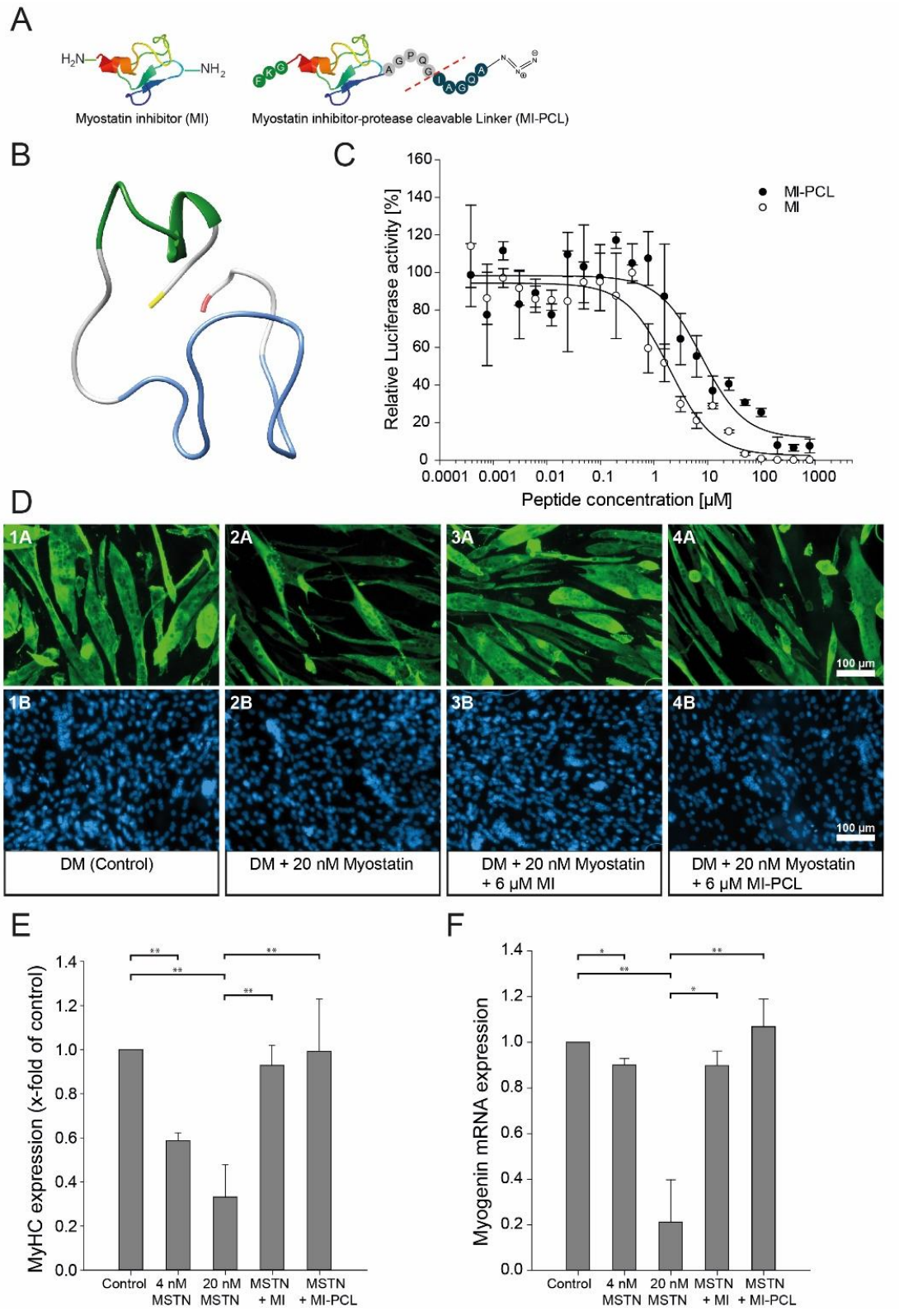

Figure 3: Bioactivity of myostatin inhibitor (MI) and assembled MI-protease cleavable linker (MI-PCL) before bound to particle surfaces. (A) Schematic illustration of the synthesized MI sequences highlighting functional groups for site-specific labelling (Lys) and immobilization (N_3). (B) Predicted structure of the MI-PCL conjugate according to PEP-FOLD 3.0 [31]. The MI moiety is highlighted in blue, the PCL region in dark green and the N-terminus and C-terminus in red and yellow, respectively. (C) Luciferase reporter gene activity in myostatin exposed HEK293 cells following the MI and MI-PCL supplementation, respectively.

(D) C2C12 myoblast differentiation after treatment with myostatin and in combination of MI and MI-PCL, respectively. The differentiated myotubes were stained with anti-myosin heavy chain (MyHC, 1A – 4A) and DAPI (1B – 4B). (E) Immunoblotting of C2C12 cell lysates after 5 days differentiation in presence of 4 nM or 20 nM myostatin or co-treated with 20 nM myostatin and 6 µM MI or MI-PCL, respectively. The lysates were immunoblotted with anti-MyHC antibody and equal loading was monitored with anti-α-tubulin antibody. Densitometry data are shown as mean ± STDEV (n = 3; *p < 0.05, ** p < 0.01). (F) Expression of the myogenic marker myogenin in C2C12 myoblasts after 5 days differentiation treated as described in (E). Data are normalized to GAPDH expression and depicted relative to expression in untreated cells by the comparative CT method (n = 3; *p < 0.05, ** p < 0.01).

MMP-responsive on poly(methyl methacrylate) microparticle surfaces

The protease-cleavable linker (PCL) was immobilized on DBCO-functionalized poly(methylmethycrylate) (PMMA) particle surfaces using strain promoted azide-alkyne cycloaddition and the PCL's N-terminal lysine subsequently reacted with a fluorescent dye for monitoring of coupling and cleavage efficacy by flow cytometry (SPAAC; **Figure 4A, S4A**). OH-functionalized PMMA particle surfaces (negative control; no covalent coupling was possible as of the missing DBCO) were treated under otherwise identical experimental conditions to assess non-specific binding of the PCL or dye. Both groups (DBCO- and OH-functionalized PMMA particle surfaces) were (i) evaluated for the impact of PCL concentrations used in the reaction/adsorption (using 0.1 µmol and 1 µmol referred to as PCL_{low} and PCL_{high}) and (ii) for bioresponsive cleavage when exposed to 8 nM MMP-1,-8 and -9 or buffer for 24 hours, respectively (**Figure 4A, S4A**). OH-functionalized PMMA particle surfaces (negative control) incubated with the PCL and the fluorescent dye had low background fluorescence (5.2 ± 0.2 arbitrary units (au), and 8.3 ± 0.4 au for PCL_{low} and PCL_{high}). In contrast, the DBCO-functionalized PMMA particle surfaces reacted efficiently with the PCL-dye and significant differences were detected between the PCL_{low} and PCL_{high} reaction conditions yielding 89.56 ± 4.4 au and 198.5 ± 29.9 au fluorescence ($p < 0.05$). The fluorescence of these PCL-dye decorated DBCO-functionalized PMMA particle surfaces was significantly reduced when exposed to MMP-1,-8 and -9 for a period of 24 hours by 77.6 ± 3.6 %, and 76.3 ± 4.0 % for the PCL_{low} and PCL_{high} reaction conditions, respectively. Identically treated particles but incubated without MMP (control) did not alter the level of fluorescence (data not shown).

Starting off these studies with the PCL-dye decorated surfaces (*vide supra*), the DBCO/OH-functionalized PMMA particle surfaces were now reacted/adsorbed with bioactive MI-PCL (**Figure 4B, S4B)** again assessing the impact of $MI\text{-}PCL_{low}$ and $MI\text{-}PCL_{high}$ reaction conditions on outcome. In contrast to the experiments using PCL-dye alone (**Figure 4A**), the use of MI-

PCL-dye (**Figure 4B**) with OH-decorated particle surfaces resulted in strong adsorption with 39.2 ± 0.3 au, and 25.4 ± 0.2 au fluorescence for MI-PCL$_{low}$ and MI-PCL$_{high}$, adsorption conditions, respectively ($p < 0.05$).

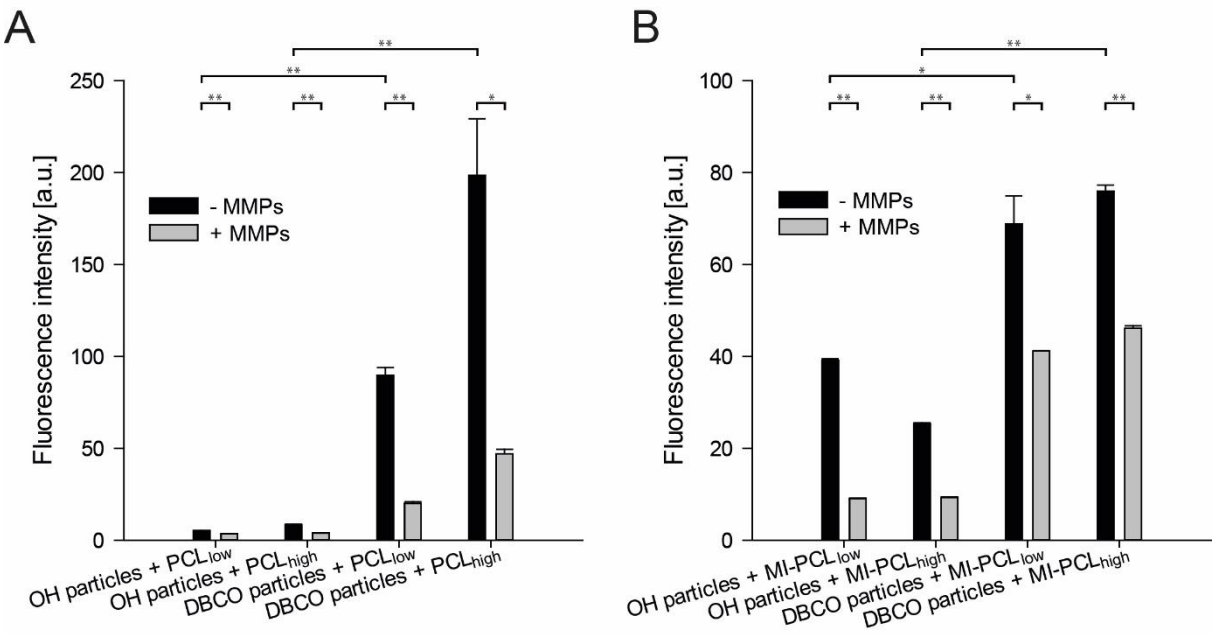

Figure 4: Poly(methyl methacrylate) (PMMA) particle functionalization with (A) protease cleavable linker (PCL) and (B) MI-protease cleavable linker (MI-PCL). Flow cytometry analysis of the PMMA constructs incubated with MMP-1,-8 and -9 for 24 hours (+ MMPs) and incubated in buffer for the same time (- MMP). PCL and MI-PCL were coupled to DBCO- modified particles on one end and a fluorescent dye at the other. OH- modified particles were used as negative control. Data are shown as mean ± STDEV (n = 3; *p < 0.05, ** p < 0.01)

Interestingly (and in spite of the MI-PCL being only adsorbed on the OH-functionalized PMMA particle surfaces and not covalently bound), exposure to MMP-1,-8 and -9 demonstrated significant bioresponsiveness resulting in 9.1 ± 0.0 au, and 9.3 ± 0.1 au fluorescence upon cleavage for the MI-PCL$_{low}$ and MI-PCL$_{high}$ group, respectively ($p < 0.05$). In spite of the non-covalent nature of the interaction of the OH-functionalized PMMA particle surfaces, the reduced fluorescence was not a result of non-specific wash out but a result of bioresponsive MMP cleavage (**Figure S4C**). The reaction of the DBCO-functionalized particle surfaces with MI-PCL-dye resulted in significantly higher particle fluorescence compared to the adsorbed OH-functionalized particle surface control group and the difference among groups when using MI-PCL$_{low}$ or MI-PCL$_{high}$ for the reaction was less pronounced resulting in 68.8 ± 6.1 au, and 75.9 ± 1.4 au, respectively. These covalently decorated surfaces showed bioresponsive properties when exposed to MMP-1,-8 and -9 for a period of 24 hours, significantly reducing

the fluorescence intensity by 40.2 ± 0.1 %, and 39.3 ± 0.5 % for the MI-PCL$_{low}$ and MI-PCL$_{high}$ reaction conditions, respectively.

Switching from PMMA particles to agarose particles to decrease non-specific adsorption to the particle surface

These studies were conducted in an effort to decrease the impact of non-specific adsorption and/or aggregation of MI-PCL as observed for the PMMA particle surfaces (*vide supra*) by changing from relatively hydrophobic PMMA to relatively hydrophilic agarose and modifying the surface texture. In analogy to the PMMA particle surfaces, agarose particle surfaces were modified with DBCO and OH (control) groups, respectively. Whereas negligible or no non-specific adsorption was observed for the OH-agarose particle surface control group (e.g. 4.1 ± 4.3 % was measured on the particle surface after 15 minutes of incubation as compared to the overall quantity deployed for the coupling - mean values of 5 % were never exceeded independent of the incubation time), rapid reaction of the DBCO-functionalized surfaces with MI-PCL were recorded by SPAAC (approximated by $\frac{70*x}{12+x}$; $r^2 = 0.99$, **Figure 5A**). For example, 42.3 ± 9.7 % of the MI-PCL was bound after 15 minutes and 65.8 ± 4.9 % after 120 minutes and plateauing, thereafter. The resulting particles were washed for 3 days and exposed to MMP-1,-8 and -9 or buffer for 24 hours (**Figure 5B**). The cleavage profile in response to MMPs followed a sigmoidal pattern (approximated by $\frac{74}{1+e^{-(\frac{x-5}{1.4})}}$; $r^2 = 0.99$) with an initially slower increase of 1.0 ± 1.9 %, and 4.6 ± 4.6 % after 30 and 60 minutes, respectively, followed by a steep rise to 50.4 ± 13.9 % and 74.1 ± 4.7 % after 6 and 24 hours, respectively. The OH-agarose particle surfaces did not show a relevant decrease reflecting the very low (if any) surface adsorption of the pre-exposure state.

These MMP exposed particles were collected after 24 hours, washed and their residual bioactivity was characterized in comparison to non-MMP exposed particles (**Figure 5C**). The data confirmed the loss of particle-surface bound MI as a result of MMP exposure (*vide supra*) in that the MMP exposed MI-PCL agarose particles had a substantially reduced ability to decrease myostatin-reporting luciferase expression in HEK293 cells as compared to non-MMP exposed particles (with IC_{50} values of 4.2 mg/well in case of the MMP-exposed particles in comparison to 0.37 mg/well for the non- MMP exposed particles).

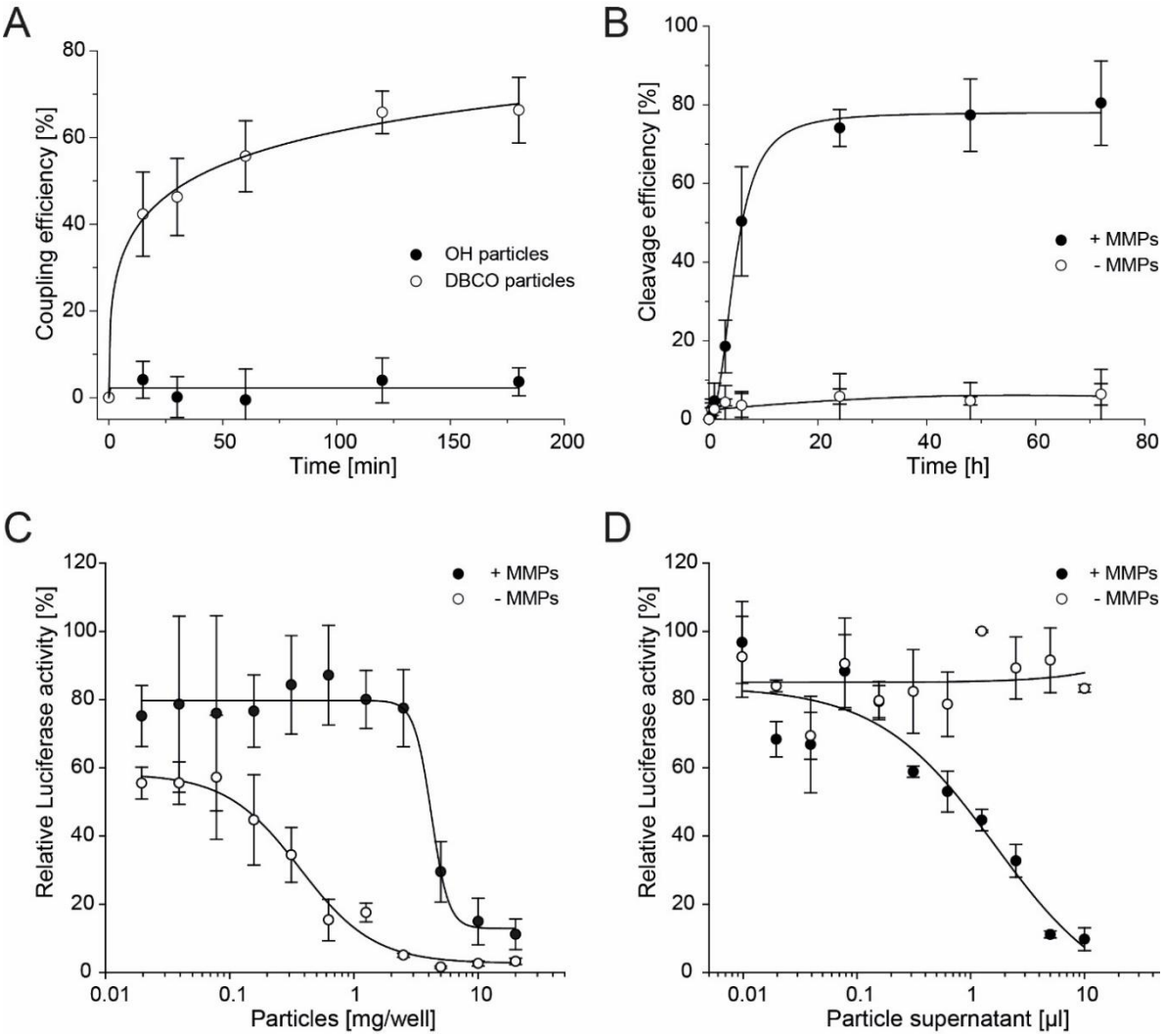

Figure 5: Agarose particles decorated with MI-protease cleavable linker (MI-PCL). (A) Time-course of the strain-promoted azide-alkyne cycloaddition (SPAAC). Coupling efficacy was compared between the MI-PCL coupled to DBCO-functionalized agarose particles versus OH-functionalized control particles using a bicinchoninic acid assay (normalized to the initial concentration of the solution before addition to the particles). (B) Time-dependent cleavage of the MI-PCL loaded particles exposed to MMP-1,-8 and -9 in comparison to non-MMP exposed particles. (C) Residual particle activity of the MI-PCL-functionalized agarose particles following exposure to MMP-1,-8 and -9 for 24 hours (+ MMPs) in comparison to unexposed particles (- MMPs) measured by a SMAD luciferase reporter gene assay. (D) Bioactivity of the supernatant of MI-PCL-functionalized agarose particles after exposure to MMP-1,-8 and -9 (+ MMPs) compared to the supernatant of unexposed particles (- MMPs). Data are shown as mean ± STDEV (n = 3)

This was further confirmed by assessing the supernatant of MMP exposed versus non-MMP exposed particles (**Figure 5D**), with no anti-myostatin activity in supernatants collected from non-MMP exposed particles and a decrease of myostatin signaling as a function of the used amount of supernatant collected from the MMP exposed particles. The highest quantity of supernatant from MMP exposed particles used (10 µL supernatant) corresponds to a

concentration of about 105 µM MI-PCL fragment as calculated by a BCA assay. An arguably rough assessment would, thereby, link the observed IC_{50} value for the supernatant collected from the MMP exposed particles as of 1.6 ± 2.0 µL to an IC_{50} value of 17 µM for the MI-PCL fragment.

Discussion

Aiming for clocking myostatin inhibitor (MI) delivery to a state of inflammatory flare of a diseased muscle or following injury, we developed a MMP-responsive drug delivery system. The drug delivery system (DDS) was designed to respond to inflammatory challenge by massive release of MI in an effort to build up clinically relevant MI concentration gradients within tissues of need. As inflammation typically preludes the onset of myositis flares, we used localized MMP upregulation as a surrogate marker driving release from the DDS. The protease cleavable linkers (PCL; selected from an in-house library of > 180 sequences (unpublished results) with the chosen one being described before [30]) were selected to match the MMP-9 profile and the myostatin expression profile based on previous reports. These studies reported matching profiles for MMP-9 and myostatin following muscle trauma, with both being upregulated in the acute inflammatory stage within the first days with peaking mRNA levels after approximately 24 hours [16, 17]. This initial phase of muscle regeneration correlates with activation of muscle satellite cells (SCs) and the maturation of the myotubes into multinucleated myofibers [4]. At the site of tissue repair MMPs are responsible for the comprehensive remodeling of extracellular matrix (ECM) during myoblast fusion whereas myostatin functions as an inhibitor of SC activation and proliferation [17]. Our DDS for the MI was developed accordingly to comply with these kinetics of MMP-9 and myostatin upregulation. The *in vitro* data correlate with these profiles demonstrating a sustained release of bioactive MI from agarose particles for 24 hours (**Figure 5B**).

Deploying agarose particles as carriers was instrumental for the efficient, bioorthogonal site-directed surface modification with MI-PCL with negligible non-specific adsorption. The delivery device effectively released MI within 24 hours in response to MMPs and bioactivity of the cleaved fragments in the supernatant. The MI-PCL was designed for constitutive activity when surface bound (**Figure 3B**), which was experimentally corroborated by the inhibitory effect of the decorated (non-cleaved) particle surfaces on myostatin-induced SMAD phosphorylation in the luciferase reporter assay (**Figure 5**). Therefore, the design parameters translated into constitutively active particle surfaces, providing a DDS binding myostatin to the

decorated particle surface, while effectively showering the broader muscle(s) area following MMP-triggered release of MI in flare (**Figure 5**). It is for this dual feature – (i) constitutive silencing of myostatin within the immediate (paracrine) environment of the particles and (ii) cascade-like release of the MI in presence of index proteases for silencing more distant myostatin (e.g. in adjacent muscles) – that this system optimally translates local requirements into drug delivery kinetics. The encouraging *in vitro* data profiling MMP-responsive delivery of MI requires corroboration by future *in vivo* studies in relevant animal systems, particularly with a focus on the assessment of a possible benefit resulting from bioresponsive release *versus* constitutively particle-surface bound MI (not bioresponsively releasing).

Another interesting finding was the MMP-responsive release of MI from OH-modified (control) PMMA particle surfaces and in spite of the fact that covalent binding was impossible in this setting (**Figure 4**). We speculate that the MI-PCL aggregated on the PMMA control surfaces with the MMP driving events leading to release of these aggregates. MI-PCL aggregation may be a result of the 3D structure of the PMMA particles composed of long-chain polymers and the general hydrophobicity of the material. Without deciphering the precise mechanisms behind, we consider these particles insufficient in serving as reliable bioresponsive release system for *in vivo* use. Changing from the PMMA to agarose particles with different surface texture removed the challenge of non-specific adsorption (**Figure 5**).

We developed a versatile system for the delivery of therapeutics in response to myositis. Bioresponsive release profiles can be easily adapted by exchanging the PCL (aiming e.g. at more sustained delivery profiles or sensitivity to other proteases) or the therapeutic may be replaced by another drug. Current studies aim at combining the anti-catabolic stimulus through the MI (to remove the inhibiting effect of myostatin on myogenesis) with the anabolic activity of insulin-like growth factor I (IGF-I) [46, 47]. The intended setup features [MI – PCL – IGF-I – PCL]$_n$ designs leading to simultaneous bioresponsive delivery of both factors. Other approaches feature block designs with different PCL for the MI and IGF-I, respectively, in an effort to bioresponsively release first the MI, followed by IGF-I, etc..

Conclusion

We developed a bioresponsive delivery system responding to injured muscle, flaring myositis. This platform approach - shown for myostatin inhibitors in combination with a release profile matching MMP-9 regulation in early inflammation - provides the necessary building blocks to adapt the DDS to future needs providing the flexibility to tune the (i) number of drugs released,

(ii) amount of drug(s) released, (iii) time-profile of drug(s) released, and (iv) fine-tuning of the dynamic ratio of surface-bound, active drug *versus* released drug.

Acknowledgment

We thank Petra Knaus (Freie Universität Berlin, Germany) for providing us with the pGl3ti-SBE constructs and Melanie Krug for excellent technical assistance. We thank Dr. Joachim Nickel for providing C2C12 myoblast cells. The financial support of the Bavarian research foundation (grant # AZ-1044-12 'FORMOsA') and the Deutsche Forschungsgemeinschaft (DFG; ME 3820/3-1) is gratefully acknowledged. H.G. is full time associate of GILYOS GmbH.

Supplementary information

Supplementary figures:

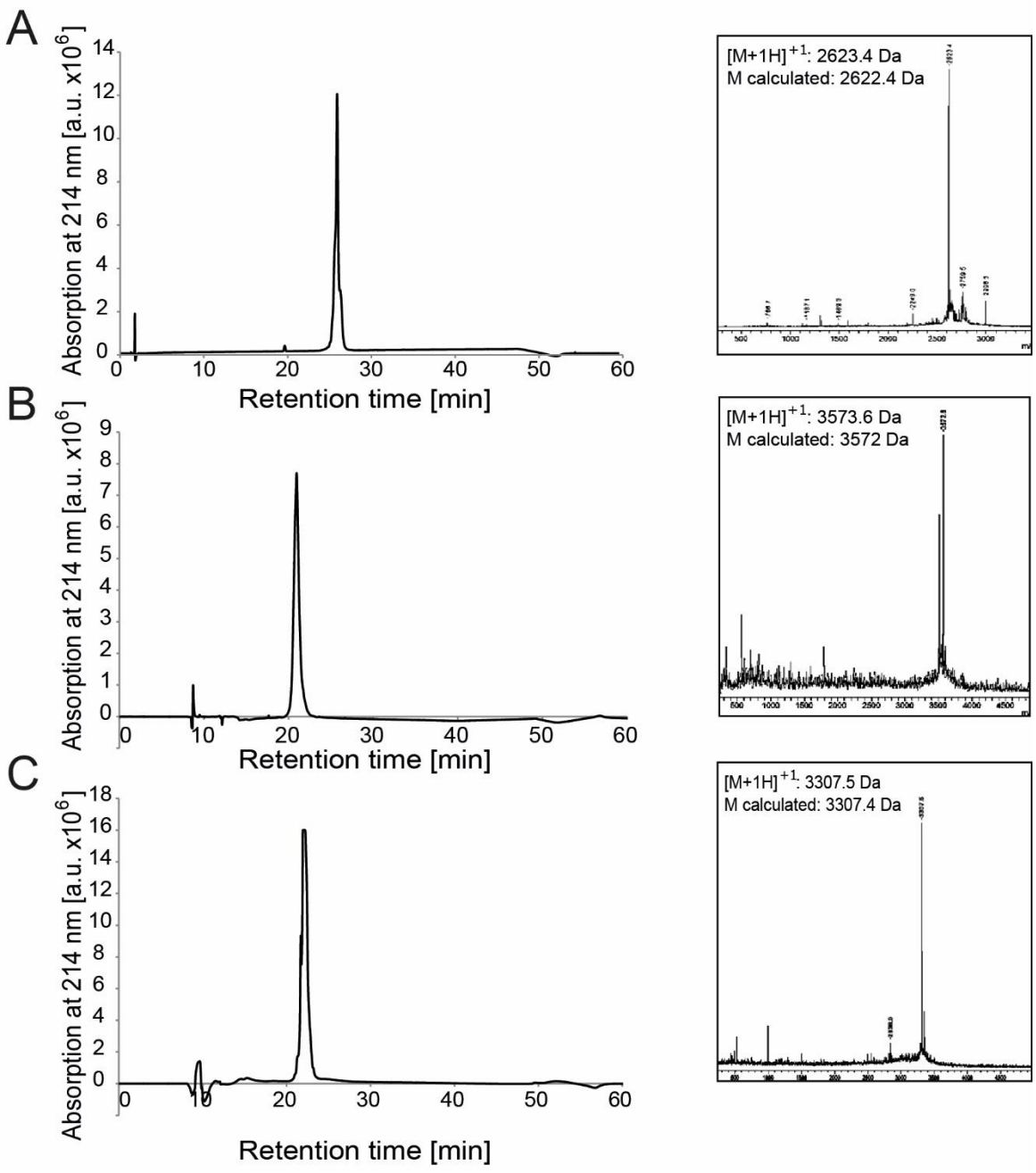

Supplementary figure 1: RP-HPLC analytics and MALDI-MS spectra of the synthesized myostatin Inhibitors (MI) to assess functionality and purity: (A) Lysine-modificated variant for EDC/NHS chemistry, (B) Transglutaminase-modificated variant for enzymatic coupling, and (C) alkyne-modificated variant for copper-catalyzed azide-alkyne click reaction (CuAAC).

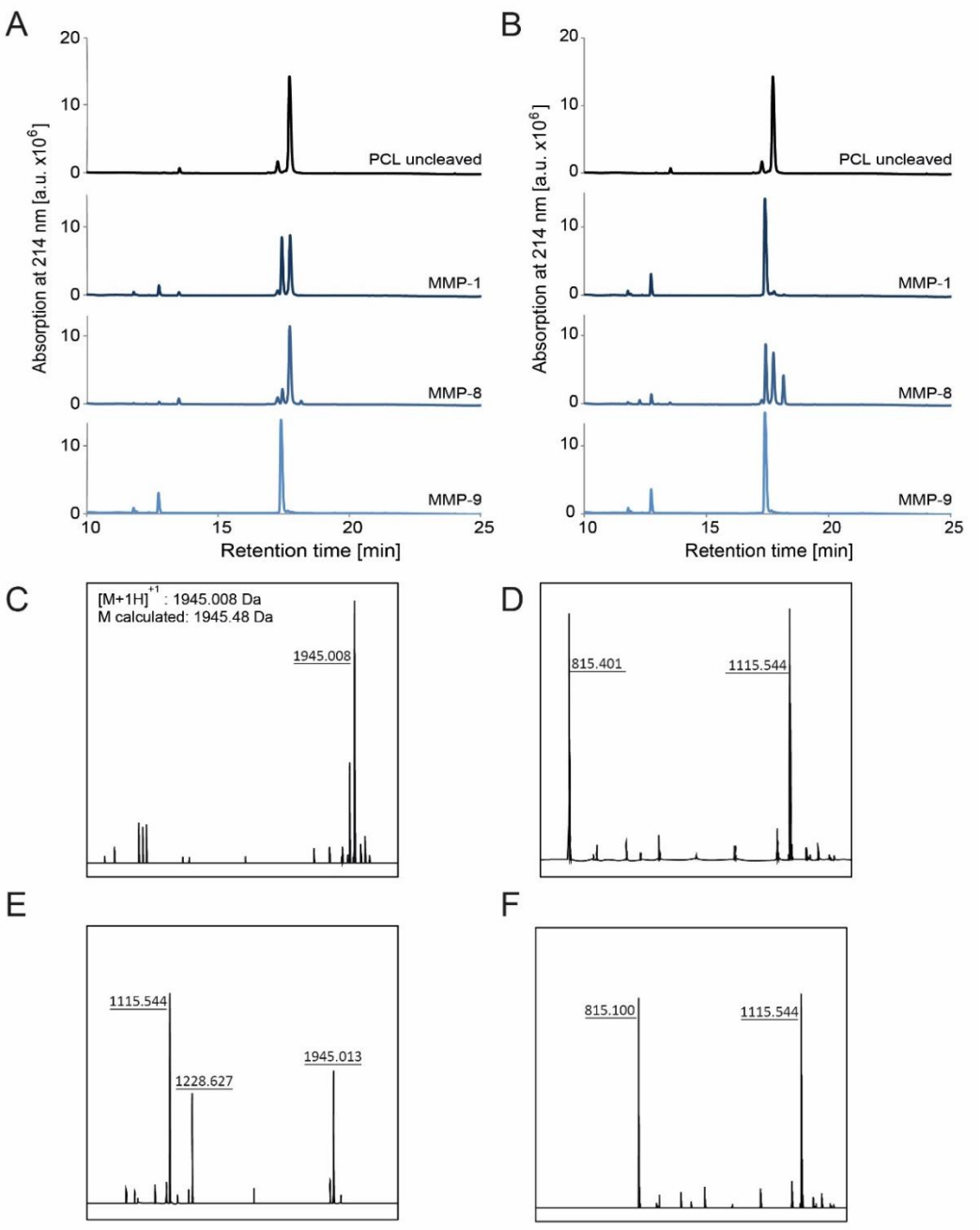

Supplementary figure 2: HPLC analytics of the cleavage products after incubation of the azide-modified protease cleavable linker (PCL) with 16 nM matrix metalloproteinase (MMP)-1, -8 and -9 for (A) 3 hours and (B) 24 hours, respectively. The peak areas were used to calculate the amount of cleaved fragments compared to non-cleaved linker. MALDI-MS spectra of PCL (C) in buffer, (D) exposed to MMP-1, (E) MMP-8, and (F) MMP-9 for 24 hours, respectively. The signal with a mass of $[M+1H]^{+1}$ = 1945.0 Da corresponded to the non-cleaved PCL with a calculated mass of 1945.5 Da, the cleaved fragment with the mass of $[M+1H]^{+1}$ = 815.4 corresponded to the C-terminal fragment [IAGQ-PEG(6)-A(N3), calculated mass of 849.9] and the fragment with the mass of $[M+1H]^{+1}$ = 815.4 corresponded to the N-terminal fragment [Fmoc-FKG-PEG(3)-GPGQ, calculated mass of 1115.6]. The additional signal seen after exposure to MMP-8 with $[M+1H]^{+1}$ = 1228.8 (e) suggested an additional cleavage site within the sequence for this protease, resulting in a Fmoc-FKG-PEG(3)-GPGQI fragment (calculated mass: 1228.9 Da).

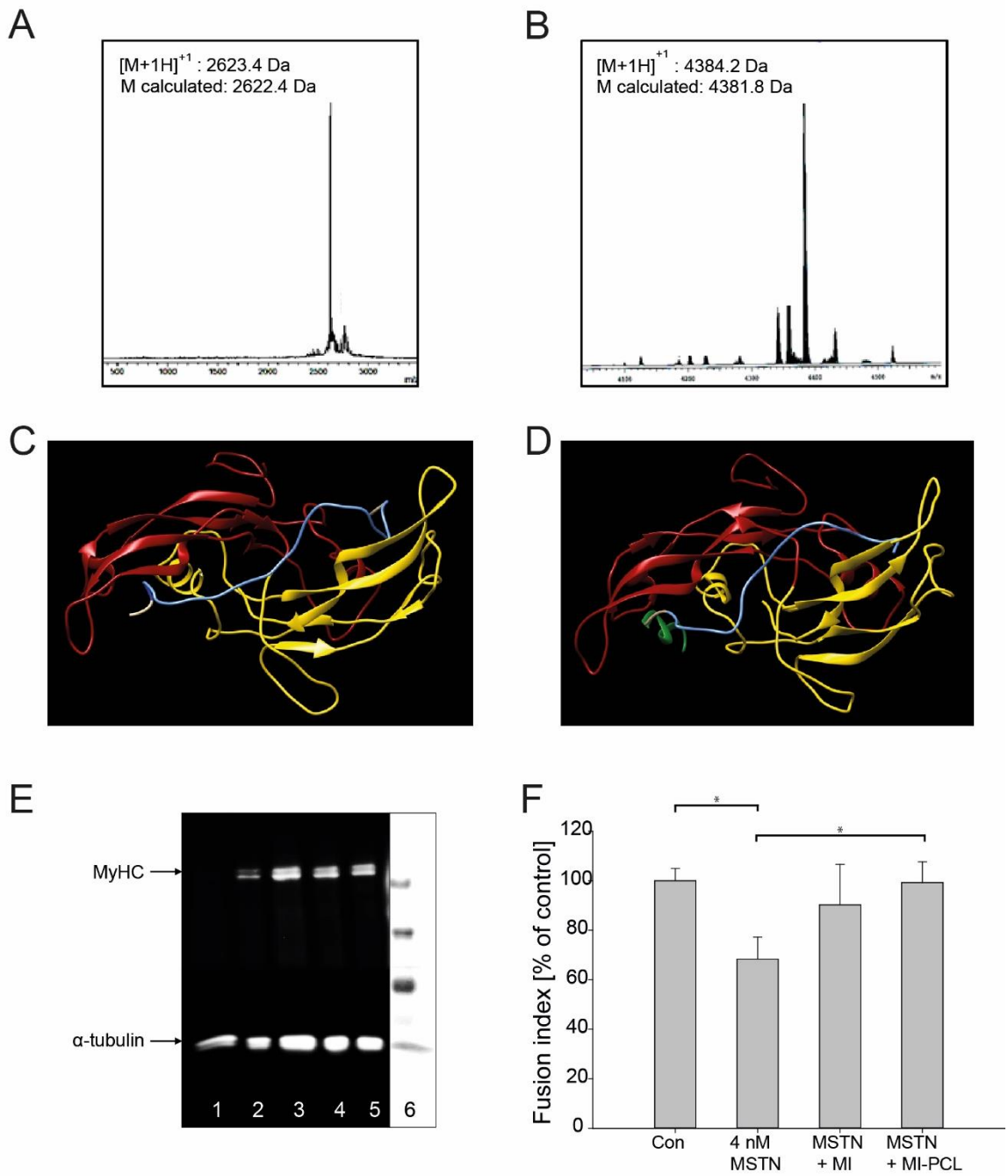

Supplementary figure 3: MALDI-MS spectra of (A) myostatin inhibitor (MI), and (B) MI-protease cleavable linker (MI-PCL)-conjugate. Predicted interaction of the (C) MI and (D) MI-PCL with the myostatin dimer according to CABS-dock. The MI moiety is shown in blue, the PCL region in dark green and the two myostatin monomers in dark red and yellow, respectively. The docking prediction suggested that the MI (or MI-PCL, respectively) influenced the dimerization of myostatin by interacting with the interface of the monomers in a linear conformation. (E) Western Blot of anti-MyHC of cell lysates derived from 5 days differentiated C2C12 myoblasts. Cells were incubated in differentiation medium (DM) containing 20 nM myostatin (lane #1), 4 nM myostatin (lane #2), 20 nM myostatin combined with 6 µM MI-PCL (lane #3), 20 nM myostatin combined with 6 µM MI (lane #4) and in DM alone (lane 5, control). Lane 6 was loaded with protein size marker. MyHC expression was normalized to the loading control α-tubulin. (F) Fusion index of myotubes differentiated for 5 days. Data are expressed as percentage of control (first bar, no myostatin and myostatin inhibitor, *$p < 0.05$).

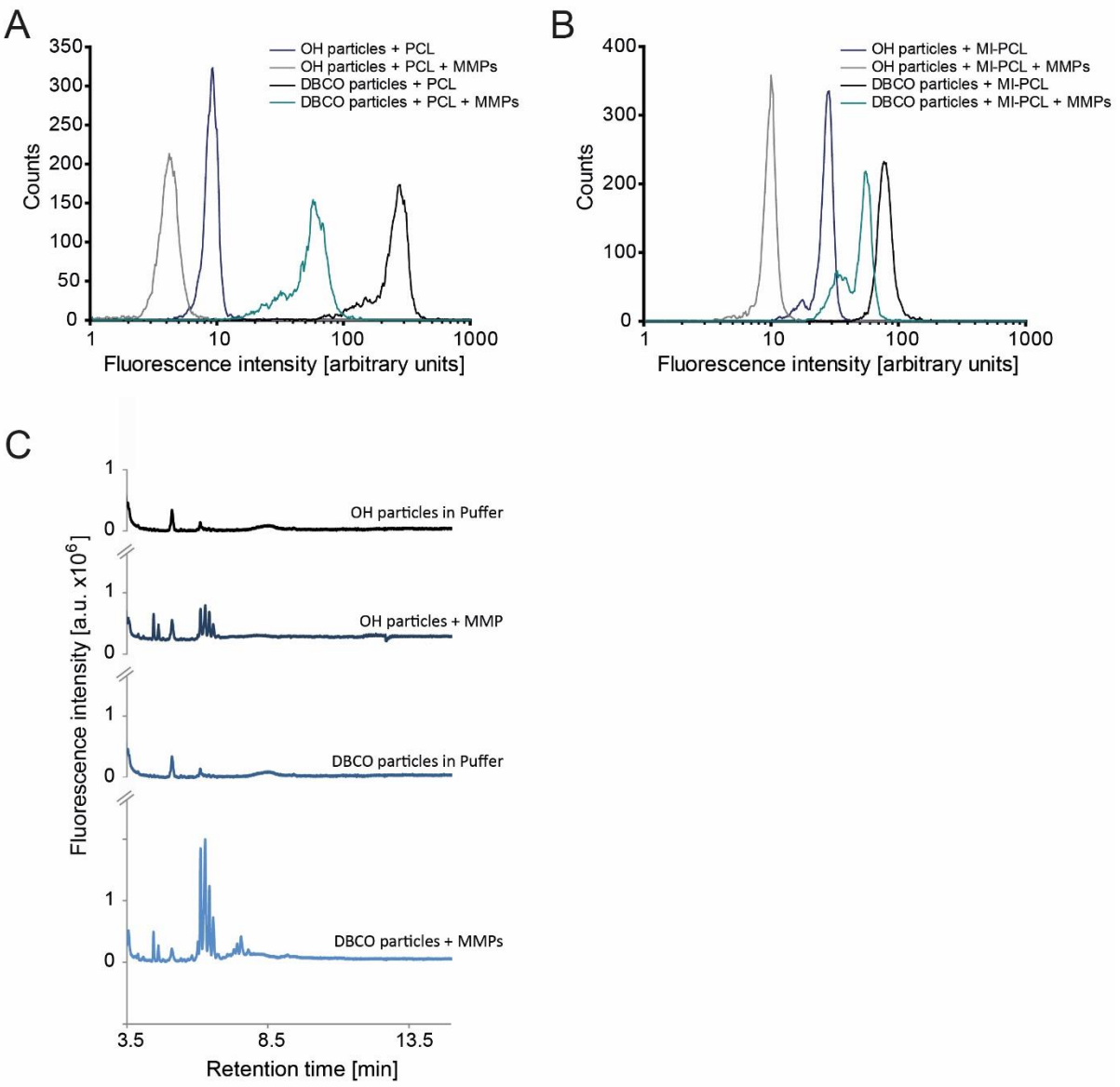

Supplementary figure 4: (A, B) Representative fluorescence intensity histograms of the PMMA constructs with (A) protease cleavable linker (PCL) and (B) MI-protease cleavable linker (MI-PCL) incubated with 8 nM MMP-1,-8 and -9 (+ MMPs) or buffer (- MMP) for 24 hours, respectively. (C) HPLC chromatogram of the supernatant collected from OH control particle surfaces with MI-PCL and the DBCO-MI-PCL construct exposed to MMP-1,-8 and -9 for 24 hours. No cleavage fragments were found in the supernatant for both, the OH-functionalized PMMA particle surfaces (control) and the covalently decorated surfaces (DBCO-functionalized PMMA particle surfaces). Exposure to MMP-1,-8 and -9 under otherwise identical experimental conditions resulted in increased supernatant fluorescence, demonstrating bioresponsiveness to both, the adsorbed and the covalently bound PCL-MI-dye constructs.

References

[1] Roubenoff R, Hughes VA. Sarcopenia: Current concepts. Journals of Gerontology Series a-Biological Sciences and Medical Sciences. 2000;55(12):M716-M24.
[2] Egerman MA, Glass DJ. Signaling pathways controlling skeletal muscle mass. Critical Reviews in Biochemistry and Molecular Biology. 2014;49(1):59-68.
[3] Trendelenburg AU, Meyer A, Rohner D, Boyle J, Hatakeyama S, Glass DJ. Myostatin reduces Akt/TORC1/p70S6K signaling, inhibiting myoblast differentiation and myotube size. American Journal of Physiology-Cell Physiology. 2009;296(6):C1258-C70.
[4] Cohen S, Nathan JA, Goldberg AL. Muscle wasting in disease: molecular mechanisms and promising therapies. Nature Reviews Drug Discovery. 2015;14(1):58-74.
[5] Tsuchida K, Nakatani M, Ueztjmi A, Murakami T, Cui XL. Signal transduction pathway through activin receptors as a therapeutic target of musculoskeletal diseases and cancer. Endocrine Journal. 2008;55(1):11-21.
[6] Sriram S, Subramanian S, Juvvuna PK, Ge X, Lokireddy S, McFarlane CD, et al. Myostatin Augments Muscle-Specific Ring Finger Protein-1 Expression Through an NF-kB Independent Mechanism in SMAD3 Null Muscle. Molecular Endocrinology. 2014;28(3):317-30.
[7] Yamaki T, Wu C-L, Gustin M, Lim J, Jackman RW, Kandarian SC. Rel A/p65 is required for cytokine-induced myotube atrophy. American Journal of Physiology-Cell Physiology. 2012;303(2):C135-C42.
[8] Reid MB, Li YP. Tumor necrosis factor-alpha and muscle wasting: a cellular perspective. Respiratory Research. 2001;2(5):269-72.
[9] Lach-Trifilieff E, Minetti GC, Sheppard K, Ibebunjo C, Feige JN, Hartmann S, et al. An Antibody Blocking Activin Type II Receptors Induces Strong Skeletal Muscle Hypertrophy and Protects from Atrophy. Molecular and Cellular Biology. 2014;34(4):606-18.
[10] Gilson H, Schakman O, Kalista S, Lause P, Tsuchida K, Thissen J-P. Follistatin induces muscle hypertrophy through satellite cell proliferation and inhibition of both myostatin and activin. American Journal of Physiology-Endocrinology and Metabolism. 2009;297(1):E157-E64.
[11] Latres E, Pangilinan J, Miloscio L, Bauerlein R, Na E, Potocky TB, et al. Myostatin blockade with a fully human monoclonal antibody induces muscle hypertrophy and reverses muscle atrophy in young and aged mice. Skeletal Muscle. 2015;5.
[12] Han H, Min H, Boone TC, inventors; Amgen Inc, assignee. Binding agents which inhibit myostatin patent #1581649, Priority claimed as of 20.12.02/USP435923. 2011 Apr 19 2011.
[13] Schoser BGH, Blottner D, Stuerenburg HJ. Matrix metalloproteinases in inflammatory myopathies: enhanced immunoreactivity near atrophic myofibers. Acta Neurologica Scandinavica. 2002;105(4):309-13.
[14] Fukushima K, Nakamura A, Ueda H, Yuasa K, Yoshida K, Takeda Si, et al. Activation and localization of matrix metalloproteinase-2 and-9 in the skeletal muscle of the muscular dystrophy dog (CXMDJ). Bmc Musculoskeletal Disorders. 2007;8.
[15] Brenner DA, Ohara M, Angel P, Chojkier M, Karin M. Prolonged Activation of jun and collagenase genes by tumor-necrosis factor-alpha. Nature. 1989;337(6208):661-3.
[16] Kherif S, Lafuma C, Dehaupas M, Lachkar S, Fournier JG, Verdiere-Sahuque M, et al. Expression of matrix metalloproteinases 2 and 9 in regenerating skeletal muscle: A study in experimentally injured and mdx muscles. Developmental Biology. 1999;205(1):158-70.
[17] McCroskery S, Thomas M, Platt L, Hennebry A, Nishimura T, McLeay L, et al. Improved muscle healing through enhanced regeneration and reduced fibrosis in myostatin-null mice. Journal of Cell Science. 2005;118(15):3531-41.
[18] Nadarajah VD, van Putten M, Chaouch A, Garrood P, Straub V, Lochmueller H, et al. Serum matrix metalloproteinase-9 (MMP-9) as a biomarker for monitoring disease progression in Duchenne muscular dystrophy (DMD). Neuromuscular Disorders. 2011;21(8):569-78.
[19] Lutolf MP, Lauer-Fields JL, Schmoekel HG, Metters AT, Weber FE, Fields GB, et al. Synthetic matrix metalloproteinase-sensitive hydrogels for the conduction of tissue regeneration: Engineering cell-invasion characteristics. Proceedings of the National Academy of Sciences of the United States of America. 2003;100(9):5413-8.

[20] Steinhagen M, Hoffmeister P-G, Nordsieck K, Hoetzel R, Baumann L, Hacker MC, et al. Matrix Metalloproteinase 9 (MMP-9) Mediated Release of MMP-9 Resistant Stromal Cell-Derived Factor 1 alpha (SDF-1 alpha) from Surface Modified Polymer Films. Acs Applied Materials & Interfaces. 2014;6(8):5891-9.
[21] van Rijt SH, Boeluekbas DA, Argyo C, Datz S, Lindner M, Eickelberg O, et al. Protease-Mediated Release of Chemotherapeutics from Mesoporous Silica Nanoparticles to ex Vivo Human and Mouse Lung Tumors. Acs Nano. 2015;9(3):2377-89.
[22] Pompe T, Salchert K, Alberti K, Zandstra P, Werner C. Immobilization of growth factors on solid supports for the modulation of stem cell fate. Nature Protocols. 2010;5(6):1042-50.
[23] Ducry L, Stump B. Antibody-Drug Conjugates: Linking Cytotoxic Payloads to Monoclonal Antibodies. Bioconjugate Chemistry. 2010;21(1):5-13.
[24] Zhao H, Heusler E, Jones G, Li L, Werner V, Germershaus O, et al. Decoration of silk fibroin by click chemistry for biomedical application. Journal of Structural Biology. 2014;186(3):420-30.
[25] Luehmann T, Jones G, Gutmann M, Rybak J-C, Nickel J, Rubini M, et al. Bio-orthogonal Immobilization of Fibroblast Growth Factor 2 for Spatial Controlled Cell Proliferation. Acs Biomaterials-Science & Engineering. 2015;1(9):740-6.
[26] Eger S, Scheffner M, Marx A, Rubini M. Synthesis of Defined Ubiquitin Dimers. Journal of the American Chemical Society. 2010;132(46):16337-9.
[27] Gutmann M, Memmel E, Braun AC, Seibel J, Meinel L, Lühmann T. Biocompatible Azide–Alkyne "Click" Reactions for Surface Decoration of Glyco-Engineered Cells. ChemBioChem. 2016;17(9):866-75.
[28] Coin I, Beyermann M, Bienert M. Solid-phase peptide synthesis: from standard procedures to the synthesis of difficult sequences. Nature Protocols. 2007;2(12):3247-56.
[29] Schense JC, Hubbell JA. Cross-linking exogenous bifunctional peptides into fibrin gels with factor XIIIa. Bioconjugate Chemistry. 1999;10(1):75-81.
[30] Nagase H, Fields GB. Human matrix metalloproteinase specificity studies using collagen sequence-based synthetic peptides. Biopolymers. 1996;40(4):399-416.
[31] Alland C, Moreews F, Boens D, Carpentier M, Chiusa S, Lonquety M, et al. RPBS: a web resource for structural bioinformatics. Nucleic Acids Research. 2005;33:W44-W9.
[32] Pettersen EF, Goddard TD, Huang CC, Couch GS, Greenblatt DM, Meng EC, et al. UCSF chimera - A visualization system for exploratory research and analysis. Journal of Computational Chemistry. 2004;25(13):1605-12.
[33] Schagger H. Tricine-SDS-PAGE. Nat Protocols. 2006;1(1):16-22.
[34] Jonk LJC, Itoh S, Heldin CH, ten Dijke P, Kruijer W. Identification and functional characterization of a Smad binding element (SBE) in the JunB promoter that acts as a transforming growth factor-beta, activin, and bone morphogenetic protein-inducible enhancer. Journal of Biological Chemistry. 1998;273(33):21145-52.
[35] Ebert R, Jovanovic M, Ulmer M, Schneider D, Meissner-Weigl J, Adamski J, et al. Down-regulation by nuclear factor kappa B of human 25-hydroxyvitamin D-3 1 alpha-hydroxylase promoter. Molecular Endocrinology. 2004;18(10):2440-50.
[36] Schmittgen TD, Livak KJ. Analyzing real-time PCR data by the comparative CT method. Nat Protocols. 2008;3(6):1101-8.
[37] O'Connell JP, Willenbrock F, Docherty AJP, Eaton D, Murphy G. Analysis of the role of the COOH-terminal domain in the activation, proteolytic activity, and tissue inhibitor of metalloproteinase interactions of gelatinase B. Journal of Biological Chemistry. 1994;269(21):14967-73.
[38] Staros JV, Wright RW, Swingle DM. Enhancement by N-Hydroxysulfosuccinimide of Water-Soluble Carbodiimide-Mediated Coupling Reactions. Analytical Biochemistry. 1986;156(1):220-2.
[39] Lienemann PS, Karlsson M, Sala A, Wischhusen HM, Weber FE, Zimmermann R, et al. A Versatile Approach to Engineering Biomolecule-Presenting Cellular Microenvironments. Advanced Healthcare Materials. 2013;2(2):292-6.

[40] Luehmann T, Haenseler P, Grant B, Hall H. The induction of cell alignment by covalently immobilized gradients of the 6th Ig-like domain of cell adhesion molecule L1 in 3D-fibrin matrices. Biomaterials. 2009;30(27):4503-12.
[41] Huisgen R. Kinetics and Mechanism of 1,3-Dipolar Cycloadditions. Angewandte Chemie International Edition in English. 1963;2(11):633-45.
[42] Agard NJ, Prescher JA, Bertozzi CR. A strain-promoted 3+2 azide-alkyne cycloaddition for covalent modification of blomolecules in living systems. Journal of the American Chemical Society. 2004;126(46):15046-7.
[43] Lutz J-F, Zarafshani Z. Efficient construction of therapeutics, bioconjugates, biomaterials and bioactive surfaces using azide-alkyne "click" chemistry. Advanced Drug Delivery Reviews. 2008;60(9):958-70.
[44] Debets MF, van Berkel SS, Schoffelen S, Rutjes FPJT, van Hest JCM, van Delft FL. Aza-dibenzocyclooctynes for fast and efficient enzyme PEGylation via copper-free (3+2) cycloaddition. Chemical Communications. 2010;46(1):97-9.
[45] Chargé SBP, Rudnicki MA. Cellular and Molecular Regulation of Muscle Regeneration. Physiological Reviews. 2004;84(1):209-38.
[46] Bikle DD, Tahimic C, Chang W, Wang Y, Philippou A, Barton ER. Role of IGF-I signaling in muscle bone interactions. Bone. 2015;80:79-88.
[47] Bursac N, Juhas M, Rando TA. Synergizing Engineering and Biology to Treat and Model Skeletal Muscle Injury and Disease. In: Yarmush ML, editor. Annual Review of Biomedical Engineering, Vol 17. Annual Review of Biomedical Engineering. 172015. p. 217-42.

Chapter 3: Bioresponsive release of insulin-like growth factor-I from its PEGylated conjugate

Alexandra C. Braun[1], Marcus Gutmann[1], Thomas D. Mueller[2], Tessa Lühmann[1] and Lorenz Meinel[1,§]

[1] Institute for Pharmacy and Food Chemistry, University of Würzburg, Am Hubland, 97074 Würzburg, Germany

[2] Julius-von-Sachs Institute, Department for Molecular Plant Physiology and Biophysics, University of Würzburg, Julius-von-Sachs Platz 2, 97082 Würzburg, Germany

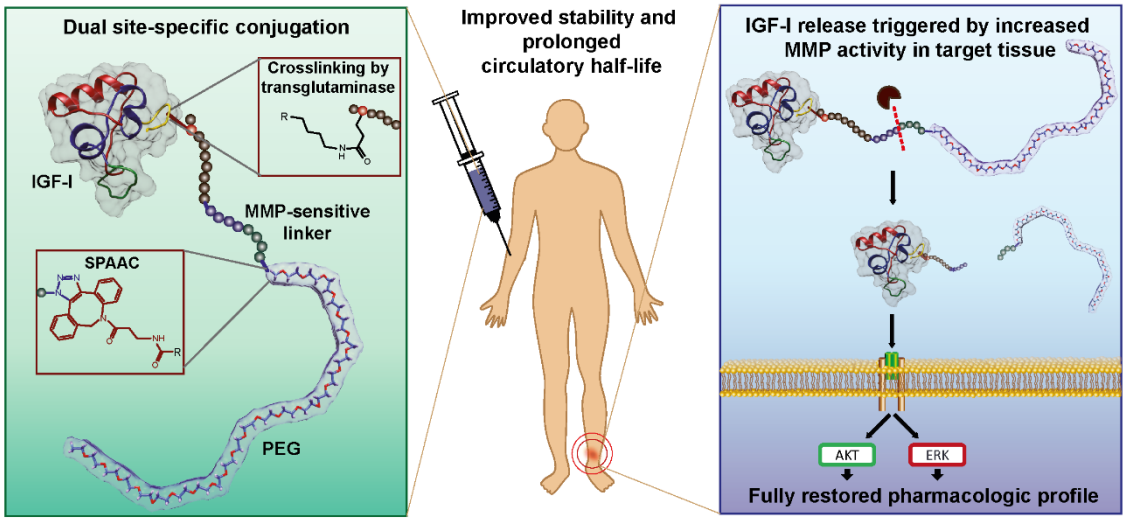

This chapter was originally published in Journal of Controlled Release, vol. 279, pp. 17-28, 2018; DOI: 10.1016/j.jconrel.2018.04.009. With permission of Elsevier, license number: 4347540115037.

Abstract

PEGylation of protein ligands, the attachment of polyethylene glycol (PEG) polymers to a therapeutic protein, increases therapeutics' half-life but frequently comes at the cost of reduced bioactivity. We are now presenting a bioinspired strategy leading out of this dilemma. To this end, we selected a position within insulin-like growth factor-I (IGF-I) for decoration with a $PEG_{30\ kDa}$-modified protease-sensitive peptide linker (PSL) using a combination of enzymatic and chemical bioorthogonal coupling strategies. The PSL sequence responded to matrix metalloproteinases (MMP) to provide a targeted release in diseased tissue. The IGF-PSL-PEG conjugate had different binding protein affinity, cell proliferation, and endocytosis patterns as compared to the wild type. Exposure of the conjugate to elevated levels of activated MMPs, as present in inflamed tissues, fully reestablished the wild type properties through effective PSL cleavage. In conclusion, this bioinspired approach provided a blueprint for PEGylated therapeutics combining the pharmacokinetic advantages of PEGylation, while locally restoring the full suite of biological potential of therapeutics.

Introduction

PEGylation is a common method to improve the retention of therapeutic proteins in the circulation by increasing their hydrodynamic size and by reducing immunogenicity by masking surface epitopes from recognition by the immune system [1-3]. Numerous PEGylated proteins are in therapeutic use, e.g. interferon α2a, interferon α2b, granulocyte colony stimulating factor, erythropoietin or a fragment antigen-binding for tumor necrosis factor [1, 4]. However, this pharmacokinetic (PK) improvements frequently come at the price of reduced bioactivity (pharmacodynamics – PD) [5, 6]. For example, a marketed product of PEGylated interferon α2a has approximately 7% bioactivity of the wild type protein [7]. However, these losses in PD are offset by the improved PK profiles. Impaired efficacy of PEGylated therapeutics compared to the non-PEGylated wild type is typically assigned to unspecific coupling of the polymer to the therapeutic and recent studies highlight the importance of the PEGylation process and point out, that the number, shape and location of PEG chains conjugated to a protein affect the stability and limit efficacy of the drug conjugate [5, 8]. Using conventional conjugation approaches based on lysines or cysteines in the protein sequence, reproducible PK and PD performance is jeopardized [1, 9]. PEGylation near an active site can be critical to protein activity by causing a conformational change, sterically interfering or altering electrostatic binding properties [8]. Consequently, a lot of recent effort was placed on strategies, that result in the site-specific conjugation in order to avoid heterogeneous mixtures resulting from multi-PEGylated proteins and positional isomers of mono-PEGylated variants with potential reduction in protein bioactivity [10]. Selective conjugation can be achieved by introduction of artificial functional groups into the therapeutic proteins followed by bioorthogonal assembly with the polymer [11-13] or by enzymatic linkage of the polymer to the protein [14, 15].

A favorable method to site-specifically PEGylate therapeutic peptides or proteins is the transglutaminase-catalyzed cross-linking [10]. Transglutaminases (TGs) catalyze acyl-transfer reactions resulting in formation of ε-(γ-glutamyl)lysine cross-links [16]. In the absence of reactive amino groups, the enzymatic reaction with water leads to deamidation of glutamine side chains. Due to their high selectivity and mild reaction conditions, TG-catalyzed PEGylation provides a beneficial strategy of bioorthogonal polymer attachment for proteins without multiple TG-reactive glutamines or lysines [14, 17-19]. Most frequently, microbial transglutaminases (mTGs) are used for this purpose, as they are more flexible in terms of amine

donor substrates, recognizing different molecules containing primary amino groups in addition to lysine, e.g. PEG-amine [14, 18]. However, the low substrate specificity of mTGs impede their biotechnological use as enzymes owing to cross-reactions with nontarget substrates [20]. Factor XIIIa – a human TG activated from Factor XIII by thrombin proteolysis during wound healing – is responsible for cross-linking fibrin monomers and plays an important role in ECM stabilization and promotion of cell adhesion and survival [16, 21]. Conjugation by FXIIIa found application in the incorporation of exogenous peptides into fibrin gels [22], the controllable cross-linking in biological or synthetic hydrogels, surface functionalization [23] and can also be deployed for efficient bioorthogonal protein PEGylation.

In spite of these site-specific decoration strategies, a principal challenge remains. PEG – as a hydrophilic polymer – has a large hydrodynamic diameter, contrasting the small size of its protein cargo, e.g. in cases of growth factors or cytokines. Therefore, the bulky PEG shields at least in part protein cargo access to cellular surfaces, receptors, and other binding partners even in cases of optimized decoration sites. This balance illustrates the knife's edge for successful PEGylated therapeutics buying PK improvements through PD costs. An avenue leading out of this dilemma is the removal of the polymer from the therapeutic at target sites to locally unfold the full spectrum of wild type characteristics including fully retained bioactivity or reestablished trafficking patterns of the cargo (**Figure 1**).

Current approaches of reversible PEGylation mainly refer to spontaneously hydrolysable prodrugs, releasing the API by chemical hydrolysis in the circulation [27]. This strategy is frequently applied to peptides and small proteins showing reduced biological potency due to steric entanglement of polymer chains during ligand recognition [28]. Protein-polymer conjugates prepared by such approaches – mainly using bicine linkers [29, 30], substituted maleic anhydride or succinate linkers [31, 32] or thiol-reactive linkers [33, 34] – undergo slow, spontaneous chemical hydrolysis at physiological conditions, releasing the active peptide or protein from the inactive conjugates over prolonged periods. Due to the drawbacks in terms of protein release during purification and shelf-storage [35] and toxicity of the chemical linkers [27], current approaches use peptide linkers susceptible to blood proteases for sustained release of the drug from the conjugate during residence in serum [36-38].

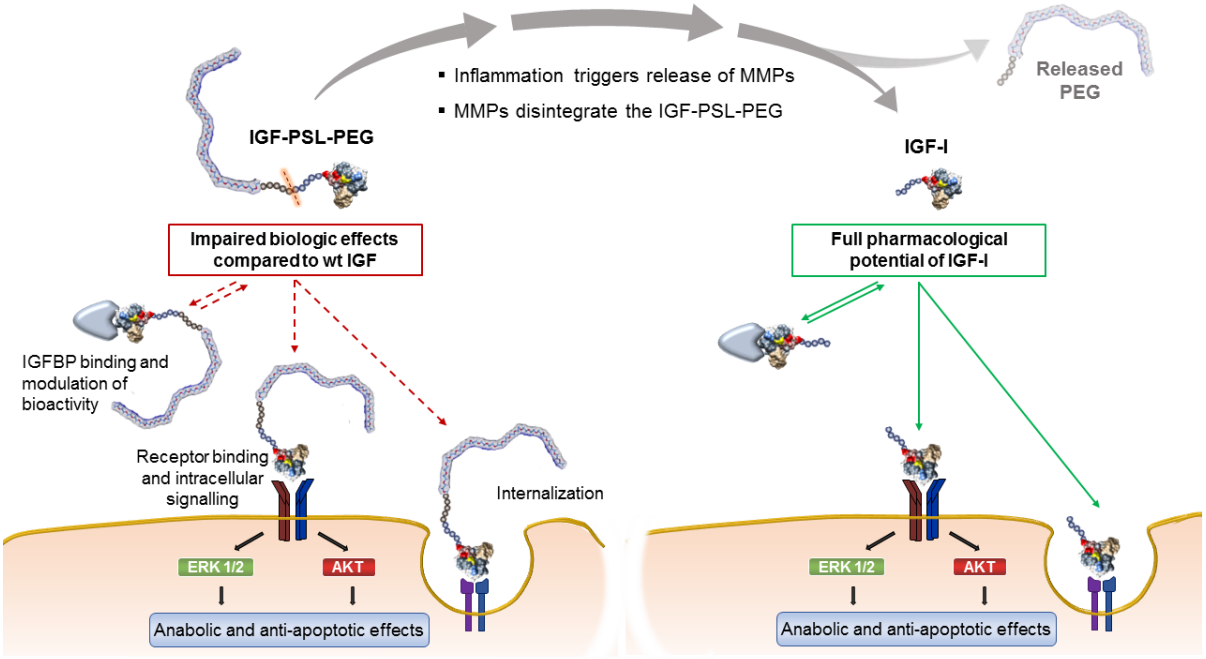

Figure 2: Pharmacologic effects of the IGF-PSL-PEG and the IGF-I fragment after proteolytic disintegration in diseased tissue. The IGF-PSL-PEG interacts with IGFBPs – thereby controlling its bioavailability – induces intracellular effects via IGF-I receptor signaling and is internalized via the IGF-IIR/Mannose-6-phosphate-receptor. Upon entry into the inflamed tissue characterized by increased MMP activity [24-26], the inter-positioned PSL is cleaved, releasing IGF from the polymer. The pharmacologic profile of the released growth factor is compared to the features of the PEGylated IGF-I, regarding IGFBP affinity, IGF-I receptor-mediated effects and internalization rate.

We are now providing a novel, generally applicable strategy for controlled release of the small size (7.5 kDa) insulin-like growth factor-I (IGF-I) from a (30 kDa) PEG triggered by disease-associated proteases. IGF-I is a mitogenic growth factor controlling essential functions including growth, tissue repair and regeneration by stimulating anabolic processes within the tissue and is used for the treatment of dwarfism and acromegaly while having been profiled for various other applications including musculoskeletal diseases [39-41] or dexamethasone- and denervation-induced atrophy [42](**Supplementary scheme 1**). IGF's short half-life has sparked interest in locally implanted IGF-I depot systems providing sustained localized activity e.g. for bone regeneration after implantation [43-49] or localized administration [50, 51]. Alternatives for locally implanted depots are systemically used IGF-PEG conjugates, however, leading to the aforementioned reduced PD characteristics [52, 53]. We designed a bioresponsive method of transient PEGylation of IGF-I striving to avoid the pitfalls associated with permanent growth factor PEGylation and making it possible to tune release kinetics to fit the medical needs. By incorporation of a proteolytically degradable linkage between polymer and biomolecule, the growth factor can be specifically released at the target site at the onset of musculoskeletal

diseases [54]. As skeletal myopathies are typically driven by NF-κB-regulated inflammatory responses, we linked bioresponsive IGF-I release to the increased activity of matrix metalloproteinases (MMPs). These inflammatory MMPs - and particularly the gelatinase MMP-9 – were reported to be strongly induced within 24 hours following muscle injury [25], in muscular dystrophies [24] and in various forms of arthritis [55-57], thereby enabling targeted IGF-I release in diseased tissues.

Materials and methods

Materials

Recombinant human IGF-I was kindly provided by Genentech (San Francisco, CA) and Factor XIII (1250 I.U. Fibrogammin) was kindly provided by CSL Behring (Bern, Switzerland). Dibenzocyclooctyl-PEG_{30kDa} (DBCO-PEG) was purchased from Dundee Cell Products, Dundee, UK. Monoclonal anti-insulin-like growth factor-I antibody (produced in mouse), Dulbecco's Modified Eagle Medium (DMEM) high glucose, Minimal Essential Medium Eagle (MEM), L-glutamine, 4',6-diamidino-2-phenylindole (DAPI), 1-hydroxybenzotriazole hydrate (HOBt), N,N′-Diisopropylcarbodiimide (DIC) and N,N-Diisopropylethylamine (DIPEA) were purchased from Sigma Aldrich (Schnelldorf, Germany). N-α-(9-Fluorenylmethyloxycarbonyl)-protected natural L-amino acids were purchased from VWR (Ismaning, Germany), Fmoc-NH-PEG(3)-COOH, Fmoc-Rink-Amid PEG AM Resin (loading 0.52 mmol/g) were from Iris Biotech GmbH (Marktredwitz, Germany). Acetonitrile (HPLC grade) and trifluoroacetic acid (HPLC grade) were from VWR. Human neutrophil matrix metalloproteinases (MMPs) were from EMD Millipore Corporation (Billerica, MA). Penicillin G and streptomycin solution (Pen/Strep) were purchased from Biochrom AG (Berlin, Germany). Fetal bovine serum (FBS) was from GIBCO life technologies (Carlsbad, CA). Goat anti-mouse IgG secondary antibody Alexa Fluor® 488 conjugate (A11001), Coomassie Brilliant Blue G250, Mammalian Cell Lysis Buffer, BCA Protein Assay Kit and SuperSignal West Pico Chemiluminescent Substrate were from Thermo Fisher Scientific (Schwerte, Germany). Anti-phospho p-$44/42^{MAPK}$($Thr^{183/202}$/$Tyr^{187/204}$), anti p-$44/42^{MAPK}$, anti phospho-AKT (Ser473) and anti-AKT antibodies were from Cell signaling (Hitchin, UK). Water soluble tetrazolium (WST-1) was from Roche (Basel, Switzerland). Mowiol 4-88 and Roti-Block were from Carl Roth (Karlsruhe, Germany). Centrifugal ultrafiltration devices Vivaspin 500 were from Satorius (Goettingen, Germany). All other reagents were obtained from Sigma Aldrich and were at least of pharmaceutical grade unless otherwise stated.

Synthesis and purification of the α_2PI_{1-8}-PSL

A protease-sensitive linker (PSL) with the sequence Ac-GNQEQVSPL-PEG(3)-GPQGIAGQ-PEG(6)-A(N_3) [58] was used, composed of (i) a substrate for Factor XIII (NQEQVSPL – derived from the N-terminus of α-2 plasmin inhibitor (α_2PI_{1-8}) [22]) and (ii) a MMP-responsive cleavable linker with the sequence GPQGIAGQ (derived from collagen type I [58]) separated by a triethylen glycol and a hexaethylen glycol spacer, respectively. The α_2PI_{1-8}-PSL was manually synthesized by solid phase peptide synthesis (SPPS) using Fmoc strategy as described [59]. In brief, Fmoc-Rink-Amid PEG AM Resin was used as solid support and following Fmoc-deprotection using piperidine in DMF, amino acids were added, activated with HOBt/DIC in DMF and allowed to react for at least 3 hours.

After cleavage from the resin, the peptides were purified by reversed phase chromatography using an FPLC system (GE Healthcare Äkta Purifier, Life sciences, Freiburg, Germany) using a Jupiter 15u C18 300A column (21.2 mm x 250 mm, Phenomenex Inc., Torrance, CA).

Conjugation of IGF-I to the PSL in presence of activated transglutaminase

FXIII (200 U/mL, Fibrogammin®, CSL Behring) was activated in the presence of 2.5 mM $CaCl_2$ with 20 U/ml thrombin in TBS (20 mM Tris HCl, 150 mM NaCl, pH 7.6) for 30 min at 37°C. Small aliquots (182 U/mL) of activated Factor XIII were stored at -80°C until further use.

Lyophilized recombinant IGF-I (Genentech) was dissolved in TBS and incubated with fivefold molar excess of α_2PI_{1-8}-PSL in the presence of 10 U/mL Factor XIIIa at 37 °C for 30 min in 100 µL reaction volumes in the presence of 2.5 mM $CaCl_2$ and 20 mM Tris-HCl (pH adjusted to 7.6 at room temperature). The reaction products were analyzed using SDS-PAGE (under reducing conditions) and Western immunoblotting with a monoclonal mouse anti-IGF-I antibody. The course of the reaction was followed by HPLC using a Zorbax® 300SB-CN column (4.6 × 150 mm). For each time point, 3 samples were incubated at 37°C with gentle agitation and after incubation periods of 2, 5, 10, 30 and 60 min, respectively; the reaction was stopped by adding EDTA to a final concentration of 10 mM together with 0.01% TFA.

MALDI-MS

Samples containing IGF-I and α_2PI_{1-8}-PSL coupled in presence or absence of FXIIIa for 30 minutes were desalted using ZipTipC18-tips (EMD Millipore corporation, Billerica, MA) following the manufacturer's instructions. Matrix-assisted laser desorption ionization (MALDI-MS) spectra were acquired in the linear positive mode by using an Autoflex II LRF instrument

(Billerica, USA). Mass spectra were calibrated externally with a protein standard I from Bruker Daltonics Inc. (Billerica, USA), containing insulin, ubiquitin, myoglobin, and cytochrome C.

Site-specific PEGylation with DBCO-PEG$_{30kDA}$

The IGF-I conjugates were purified by reversed phase chromatography using an FPLC system (GE Healthcare Äkta Purifier, Life sciences, Freiburg, Germany) using a Source™ 15 RPC ST 4.6/100 column (GE Healthcare, Freiburg, Germany) equilibrated with water containing 0.1% TFA and acetonitrile (ACN) containing 0.1% TFA (95:5 v/v). The IGF-I conjugate was eluted by a linear gradient of 5−60% ACN containing 0.1% TFA with a gradient of 1.5 % ACN/min and a flow rate of 1 mL/min. UV-absorbance was monitored at λ = 214 nm. Following solvent evaporation and lyophilization, the purified conjugate was reconstituted in PBS buffer and modified with equimolar amounts of Dibenzocyclooctyl-PEG$_{30kDa}$ (DBCO-PEG) at pH 7.4 for 24 hours with gentle shaking. The PEGylated conjugates were purified by cation exchange chromatography using an FPLC system with a HiTrap SP-HP column (GE Healthcare, Life sciences, Freiburg, Germany). IGF-PSL-PEG was eluted with 50 mM sodium acetate buffer pH 4.3 containing 1 M NaCl. After purification, fractions containing IGF-PSL-PEG were dialyzed against PBS, lyophilized and stored at -80°C. IGF-PSL and IGF-PSL-PEG concentrations were determined by BCA protein assay following the manufacturer's instructions.

High performance liquid chromatography

IGF-I was assayed using a LaChromUltra UPLC system (VWR Hitachi, Tokyo, Japan) consisting of an autosampler (L-2200U), a column oven (L-2300), two pumps (L-2160U), and a diode array (L-2455U) detector. Separation was performed on a Zorbax® 300SB CN column (150×4.6 mm) at 40°C under gradient conditions at a flow rate of 1.0 mL/min. Two eluents were used, (A) consisting of 0.1 % TFA in water and (B) 0.1% TFA in acetonitrile. The solvent was initially composed of 95% (v/v) eluent A and changed over 30 min to 60% eluent B. Then, initial conditions were set to wash the column. IGF-I was detected at λ = 215 nm and quantified by measuring the peak area.

To analyze the cleavage efficiency of the PSL or IGF-PSL-PEG with respect to different MMP concentrations or time points, the samples were diluted with eluent A (0.1 % TFA in water) and analyzed on a Synergi™ 4 μm Hydro-RP 80 Å, 100 x 3 mm column. Peptide fragments and polymer conjugates were eluted by a linear gradient of 5−60% ACN containing 0.1% TFA with a gradient of 2 % ACN/min and a flow rate of 1 mL/min. Column temperature was kept at 40

°C and UV-absorbance was monitored at λ = 214 nm and λ = 280 nm. The same method was applied for the serum samples of IGF-I and IGF-PSL-PEG.

SDS-PAGE and Western Blot for IGF-I variants

The IGF-I conjugates after transglutaminase coupling and click reaction with DBCO-PEG were analyzed by tris-glycine SDS-PAGE under reducing conditions using a 12% polyacrylamide separating gel as outlined before [60]. Bands were visualized by both PEG-specific iodine staining based on Kurfürst's method [61, 62], followed by Coomassie Brilliant Blue G250. Briefly, after fixation using a 5% glutaraldehyde solution for 15 min at room temperature, the gel was soaked in 25 mL perchloric acid (0.1 M) for 30 min, and then immersed in 5 mL of a 5% barium chloride solution for 10 minutes. Then, iodine solution (1.3% I_2 + 4% KI) was added and incubated for 5 min. The stained PEG bands appeared within a few minutes. Finally, the gel was left to destain in 0.05 M HCl for 30 min. The destained gel was put into a Coomassie Brilliant Blue G250 solution for protein visualization and documented using a FluorChem FC2 imaging system (Protein Simple, Santa Clara, CA).

For Western blotting, proteins were transferred to a nitrocellulose membrane using 80 V for 90 minutes. The membrane was blocked with Roti-Block in PBS for 1 hour at room temperature, prior to incubation with monoclonal anti-IGF-I antibody in tris-buffered saline containing 0.1 % (w/w) Tween 20 (TBST) at 4 °C overnight under agitation. The membrane was then washed with TBST and incubated with an anti-mouse HRP-conjugated secondary antibody for 1 hour at room temperature. Protein detection was performed using SuperSignal West Pico chemiluminescent substrate by a FluorChem FC2 imaging system (Protein Simple, Santa Clara, CA).

Mass spectrometric characterization after trypsin digestion

After coupling of IGF-I with a synthetic peptide (Ac-NQEQVSPL) for 10 minutes in presence of 10 U/mL Factor XIIIa, the conjugate was applied to SDS-PAGE and visualized by Coomassie Blue staining. The excised gel bands were destained with 30 % acetonitrile in 0.1 M NH_4HCO_3 (pH 8), shrunk with 100 % acetonitrile, and dried in a vacuum concentrator (Concentrator 5301, Eppendorf, Germany). Digests were performed with 0.1 µg trypsin per gel band overnight at 37 °C in 0.1 M NH_4HCO_3 (pH 8). After removing the supernatant, peptides were extracted from the gel slices with 5 % formic acid, and extracted peptides were pooled with the supernatant. NanoLC-MS/MS analyses were performed on a LTQ-Orbitrap Velos Pro (Thermo Scientific) equipped with a PicoView Ion Source (New Objective) and coupled to an

EASY-nLC 1000 (Thermo Scientific). Peptides were loaded on capillary columns (PicoFrit, 30 cm x 150 µm ID, New Objective) self-packed with ReproSil-Pur 120 C18-AQ, 1.9 µm (Dr. Maisch) and separated with a 30-minute linear gradient from 3% to 30% acetonitrile and 0.1% formic acid and a flow rate of 500 nL/min. MS scans were acquired in the Orbitrap analyzer with a resolution of 30000 at m/z 400, MS/MS scans were acquired in the Orbitrap analyzer with a resolution of 7500 at m/z 400 using HCD fragmentation with 30% normalized collision energy. A TOP5 data-dependent MS/MS method was used; dynamic exclusion was applied with a repeat count of 1 and an exclusion duration of 30 seconds; singly charged precursors were excluded from selection. Minimum signal threshold for precursor selection was set to 50000. Predictive AGC was used with a AGC target value of $1e^6$ for MS scans and $5e^4$ for MS/MS scans. Lock mass option was applied for internal calibration in all runs using background ions from protonated decamethylcyclopentasiloxane (m/z 371.10124).

Exposure of PSL and IGF-PSL-PEG to MMPs

Pro-MMPs (MMP-1, MMP-8 and MMP-9) were activated with 4-aminophenylmercuric acetate (APMA) as described before [63]. Lyophilized PSL and IGF-PSL-PEG were dissolved in MMP buffer (50 mM Tris, 150 mM NaCl, 1 µM $ZnCl_2$, 10 mM $CaCl_2$, pH 7.4) to a final concentration of 1 µM. For the experiments targeting the time-dependent release profile, the solution was split and one half was incubated at 37°C in protease buffer with gentle agitation for different time points with one subtype of MMP (MMP-1, -8, -9 or -13, respectively) to reach a total protease concentration of 8 nM and the other half incubated in MMP buffer alone (without MMPs). After 0.5, 1, 3, 6 and 24 hours during MMP exposition and buffer incubation of the control samples, respectively, protease activity was stopped by addition of 50 mM EDTA and heating to 95 °C for 5 minutes. The solution was injected into the UPLC to measure cleavage kinetics (*vide supra*). For the concentration-dependent cleavage, a dilution series of a mixture of MMP-8, -9 and-13 was prepared and each dilution incubated for a period of 6 hours with IGF-PSL-PEG. Subsequently, protease activity was stopped by addition of 50 mM EDTA and the samples were analyzed by UPLC.

For testing of the internalization rate of MMP-exposed compared to unexposed IGF-PSL-PEG conjugate, protease activity was inhibited afterwards by addition of 50 mM EDTA, which was subsequently removed by ultrafiltration, exchanging the buffer with at least two volumes of PBS, and using centrifugal ultrafiltration devices with 5 kDa cutoff. Following sterile filtration, the protein concentration was determined and the cleaved conjugate was added to the cells.

Cell culture

MG63 cells (human osteosarcoma cells, ATCC CRL-1427, Manassas, VA) were cultured in growth medium (MEM containing 10% FBS, 2 mM L-glutamine, 100 U/mL penicillin G and 100 µg/mL streptomycin, 1% non-essential amino acids (NEA)) in 25 cm^2 culture flasks. C2C12 myoblasts (ATCC CRL-1772) were maintained in growth medium (DMEM containing 4.5 g/L D-glucose, 2 mM L-glutamine, 10 % heat-inactivated FCS, 100 U/mL penicillin G and 100 µg/mL streptomycin) at 37°C and 5 % CO_2.

Cell proliferation assay (WST-1)

For the measurement of biological activity of IGF-I variants in comparison to unmodified IGF-I, a mitogenic bioassay with MG63 cells was performed. Briefly, $2*10^4$ MG63 cells/well were seeded in 96-well plates (Greiner Bio One, Frickenhausen, Germany) in assay medium (MEM containing 0.5% BSA, 2 mM L-glutamine, 100 U/mL penicillin G and 100 µg/mL streptomycin, 1% NEA) and incubated for 24 h at 37 °C and 5% CO_2. A dilution series of each IGF-I variant (IGF-I, IGF-PSL and IGF-PSL-PEG) from 0.01 nM to 100 nM in assay medium was prepared, added to the cells and incubated for 48 h at 37 °C and 5% CO_2. For measurement of the potency of the variants in presence of IGFBPs, a combination of a fixed concentration of 6.5 nM IGF-I, IGF-PSL or IGF-PSL-PEG, respectively, together with a dilution series of IGFBP-3 or IGFBP-5 from 0.16 nM to 160 nM was prepared, pre-incubated at 37 °C for 30 minutes and subsequently transferred to the cells. After 48 hours growth factor exposure, the cells were treated with WST-1 reagent for 4 h at 37 °C. The absorbance of the soluble formazan product was determined at 450 nm using a Spectramax 250 microplate reader (Molecular Devices, Sunnyvale, CA).

Cell signaling and Western immunoblotting

For measurement of AKT and ERK phosphorylation of MG63 and C2C12 cells treated with IGF-PSL-PEG in comparison to *wt* IGF-I, $5*10^4$ cells were seeded in assay medium in 96-well plates. After 16 hours in culture and around 70% confluence, the cells were serum-starved for 6 hours and incubated with different concentrations of *wt* IGF-I (ranging from 0.01 nM to 100 nM) in assay medium for 30 minutes at 37°C. After washing with ice-cold PBS, cells were lysed with M-PER Mammalian Cell Lysis Buffer and cell extracts were processed using standard SDS-PAGE and Western blotting procedures. Membranes were stained in Ponceau S reversible stain to verify protein transfer and then blocked for 1 hour in Roti-Block, followed by three washing steps using tris-buffered saline (TBS), containing 0.1 % (w/w) Tween 20

(TBST). For detection of phosphorylated proteins, the blot was cut and the upper half incubated overnight at 4°C with an anti-phospho p-44/42 ^{MAPK} ($Thr^{183/202}$/$Tyr^{187/204}$) antibody and the lower half with anti-phospho AKT (Ser473) antibody, both diluted 1:1000 in TBST. After incubation of the blot with a peroxidase-conjugated secondary antibody for 90 minutes at room temperature, signals were detected by chemoluminescence using a Super Signal West Pico Chemiluminescent Substrate and visualized by a FluorChem FC2 imaging system (Protein Simple, Santa Clara, USA). Subsequently, blots were stripped with 50 mM Tris-HCl, containing 2 % (w/w) SDS and 0.8 % 2-mercaptoethanol at pH 6.8 for 1 hour at room temperature before detection of total MAPK using an anti p-44/42^{MAPK} antibody and detection of total AKT using anti-AKT antibody (1:1000 diluted in TBST). Spot intensity was quantified and the values of phospho-AKT and phospho-MAPK normalized to the values of AKT and MAPK, respectively.

Serum stability

IGF and IGF-PSL-PEG conjugate, respectively, were diluted with 10% (v/v) human serum (taken from a pool of healthy donors; Sigma Aldrich, Schnelldorf, Germany) to a final concentration of 5 µM and incubated at 37 °C with gentle shaking (350 rpm; Thermomixer, Eppendorf AG, Hamburg, Germany). Aliquots were analyzed after 0, 3, 8 and 18 h. Peptides were quantified using RP-HPLC by recording the absorbance at λ = 214 nm and referred to standard curves of IGF-I or IGF-PSL-PEG, respectively. Standards were prepared in inactivated serum and analyzed immediately.

Surface Plasmon Resonance

The binding kinetics of each IGF-I analogue to IGFBP-3 and IGFBP-5 was determined by SPR using a ProteOn^{TM} XPR36 system (BioRad, Hercules, CA). HBS buffer (10 mM HEPES, 150 mM NaCl, 3.4 mM EDTA, 0.005% (v/v) polysorbate 20, pH 7.4) was used as running buffer for measurements while immobilization of the ligands was performed with HBS buffer supplemented with 500 mM NaCl. For immobilization onto the chip surface, a ProteOn GLC sensor chip (BioRad) was activated by perfusing the sensor chip with a solution containing 20 mM EDAC and 5 mM Sulfo-NHS (BioRad) for 360s at a flow rate of 30 µL min^{-1}. Then IGFBPs were immobilized at a concentration of 10 µg/mL in 10 mM sodium acetate pH 4.0 until densities of about 2000 resonance units (RU) were achieved. Free activated sites were quenched by perfusing the sensor chip with 1M ethanolamine pH 8.5 for 300s at a flow rate of 30 µL min^{-1}. To remove non-covalently attached proteins, the flow channels were washed for

300s with HBS_{500} buffer and subsequently for 60s with 100mM glycine pH 2.5. For all measurements of SPR data, the one-shot kinetic setup of the ProteOn XPR36 system was used. Here the flow cell unit is rotated by 90° compared to its orientation during immobilization, thereby providing six equivalent interaction spots allowing for simultaneous interaction data acquisition of up to six analyte concentrations. Bulk face effects and non-specific binding were removed from SPR data by subtracting the interaction of the analytes with the chip matrix either at the so-called interspots (non-coated spots within the flow channel resulting from the 90° rotation of the flow cell unit) or at a non-coated reference flow channel from the raw interaction data. Flow rate for SPR data acquisition was set to 100 µL min^{-1}. IGF-PSL-PEG or IGF-I were perfused over the biosensor in six different concentrations (1.56, 3.13, 6.25, 12.5, 25, and 50 nM), association was monitored for 120 seconds, dissociation was initiated by perfusing HBS_{150} running buffer and was monitored for 100s. The sensor surface was regenerated by injecting first 0.3 M sodium citrate, 0.4 M NaCl pH 5.0 and subsequently perfusing 100 mM glycine pH 2.5 for 60s. Binding affinities were calculated from the rate constants for association and dissociation using the ProteOn™ Manager 3.1 software (Bio-Rad) and applying a simple 1:1 Langmuir type interaction model. Binding affinities and rate constants are provided as mean with standard deviation derived from at least three independent SPR measurements.

IGF-II receptor-mediated internalization of IGF-I and IGF-PSL-PEG

C2C12 cells were seeded at 5×10^4 cells/well and onto 12 mm glass cover slides (Menzel Gläser, Braunschweig, Germany) in 4-well plates coated with 2% gelatin and grown for 24 hours. After starvation for 5 hours, cells were stimulated with 100 nM IGF-I, IGF-PSL-PEG or MMP-exposed IGF-PSL-PEG for different periods of time (5, 20 or 45 minutes) at 37 °C. Subsequently, the cells were washed with ice-cold PBS, followed by one washing step with acidic buffer (0.3 M sodium citrate, 0.4 M sodium chloride, pH 4.5) to remove non-internalized ligand, then immediately fixed with 4% paraformaldehyde for 10 minutes at 4°C and permeabilized using 0.1% Triton X in PBS for 15 minutes. Following 3 washing steps with PBS, non-specific binding was blocked with 5% BSA in PBS prior to incubation with mouse anti-IGF-I antibody and rabbit anti-IGF-IIR antibody at 4°C over night. The following day the samples were incubated with secondary antibodies conjugated with Alexa fluor 633 (anti-rabbit) and Alexa Fluor 488 (anti-mouse) in PBS for 60 minutes at room temperature. Cell nuclei were counterstained with DAPI. In the second set of experiments, the same procedure was used, but cells were fixed using ice-cold methanol for 10 min at 4 °C, followed by incubation with mouse anti-IGF-I antibody overnight and Alexa-Fluor 633 (anti-mouse)

antibody conjugate in PBS for 60 min. Actin was visualized using Phalloidin staining (Alexa Fluor 488 Phalloidin, Thermo Fisher Scientific) prior to cell nuclei counterstaining using DAPI. The cells on the cover slides were mounted on microscope slides with Mowiol 4-88 before analysis on a high resolution AOBS SP2 confocal laser scanning microscope (Leica microsystem, Wetzlar, Germany) with a 63x N.A. 1.4-0.60 Oil I BL HCX PL APO I objective. To avoid cross-talk the emission signals were collected independently. Image processing was performed in ImageJ (http://imagej.nih.gov/ij/).

For quantification of internalized ligands, C2C12 cells were seeded at 1×10^5 cells/well in gelatin-coated 6-well plates and grown for 24 hours. After starvation for 5 hours, cells were stimulated with 100 nM IGF-I, IGF-PSL-PEG or MMP-exposed IGF-PSL-PEG for 45 minutes at 37 °C. Internalization was stopped by washing with ice-cold PBS, followed by a washing step with acidic buffer (0.3 M sodium citrate, 0.4 M sodium chloride, pH 4.5) to remove non-internalized ligand, and 2 additional washing steps with PBS. Subsequently, cells were lysed with Tris-based lysis buffer (100 mM Tris, 150 mM NaCl, 1 mM EDTA, 1%Triton X-100) and frozen at -80°C. Internalized IGF-I and IGF conjugates, respectively, were quantified using a human IGF-I ELISA Kit (R&D Systems, Minneapolis, MN) according to manufacturer's instructions. For calculation of results, standard curves for IGF-I and IGF-PSL-PEG were created and sample amounts were calculated based on the curve fits.

Statistical analysis

Data were analyzed using Student's t-test or one-way ANOVA followed by pair-wise comparisons using Tukey Kramer *post-hoc* test. SigmaPlot (Systat Software Inc., CA) or Minitab 16 (Minitab, Coventry, UK) was used. Results were considered statistically significant at $p \leq 0.05$ (*; $p \leq 0.01$ (**)) and results are displayed as mean with standard deviation (SD).

Results and Discussion

Previous studies described the transglutaminase-mediated covalent binding of IGF-I through its lysine (K) in position 68 to components of the extracellular matrix (ECM) [53]. Taking advantage of this natural mechanism, we enzymatically decorated wild type IGF-I with full control of the decoration site contrasting unspecific chemistries or the need for genetically modifying the primary sequence [64]. The Lys-68 within the D domain of IGF-I is favored for conjugation, as it is not involved in binding to IGFBPs [65, 66] and its removal does not reduce receptor activation [67]. For that, IGF-I's transglutaminase substrate domain served as attachment site for the protease-sensitive linker (PSL) modified with an alpha-2 plasmin inhibitor (α_2PI)-derived donor peptide NQEQVSPL [68]. (**Scheme 1A**) We selected a MMP-sensitive linker from type I collagen with a C-terminal azide group for attachment of the PEG by Strain-promoted azide-alkyne cycloaddition (SPAAC) [54, 58, 69, 70] (**Scheme 1B**, **Figure S1**). The combination of these naturally occurring sequences is intended to reduce immunogenicity concerns and emulate mechanisms found in nature for regulation of protein activity [22, 71].

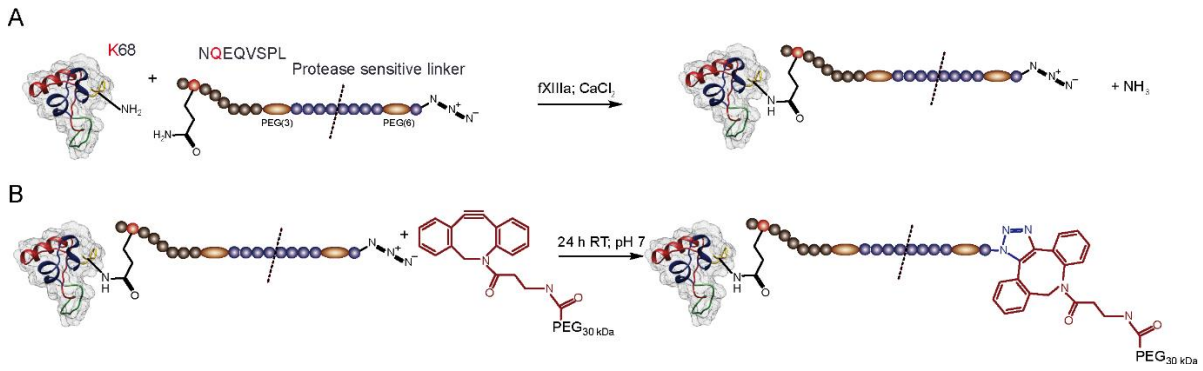

Scheme 1*:* Schematic representation of the site-directed synthesis of the IGF-PSL-PEG conjugate. (A) Enzymatic conjugation of a protease-sensitive linker (PSL) to IGF-I by human FXIIIa. The linker is modified with a TG recognition sequence at the N-terminus (NQEQVSPL) and contains a PSL sequence enabling fast release in response to matrix metalloproteinase upregulation in inflamed tissues. (B) Strain-promoted azide-alkyne cycloaddition (SPAAC) of the IGF-PSL conjugate (from A) to DBCO-PEG$_{30kDa}$ leading to IGF-PSL-PEG with full control of decoration sites. Molecular graphics were created with Chimera [72].

The enzymatic transamidation reaction between wild type IGF-I and the PSL was qualitatively assessed by gel electrophoresis followed by Coomassie staining and by Western blot indicating conjugation success (**Figure S2A**) and confirmed by RP-HPLC and MALDI-MS analysis detailing a 1:1 stoichiometry (**Figure S2B, C**). The enzymatic coupling of PSL to IGF-I was rapid, leading to complete turnover within 5 minutes (**Figure 2A**). LC-MS/MS analysis after trypsin digest confirmed, that conjugation was confined to K68 (i.e. K27 and/or K65 of IGF-I were not modified; **Figure 2B**). Following RP-HPLC purification of the IGF-PSL, $PEG_{30\ kDa}$ was now conjugated to the C-terminal azide group of the PSL using SPAAC (**Scheme 1B**) [11, 13, 73], resulting in complete conjugation within 24 h and a 1:1 stoichiometry (**Figure 2C**). Remaining unconjugated PEG and IGF-PSL were removed by purification using cation exchange chromatography resulting in at least 95 % purity (**Figure 2D, S2D**). This TG-catalyzed crosslinking approach also worked for the decoration of agarose particle surfaces (**Figure S2E**). Using K68 – the natural attachment site of IGF-I to substrates – offered a bioinspired template for designing conjugates with ultimate control over decoration sites, high yield, and very rapid synthesis. Previous studies have introduced and detailed TG based enzymatic crosslinking for immobilization of therapeutic proteins [74-77] and for site-specific PEGylation [14, 19]. These approaches use an amino-derivative of PEG ($PEG\text{-}NH_2$) as substrate for the enzymatic reaction to modify Gln residues of proteins. Depending on flexibility and accessibility of the Gln-containing regions, only one Gln is modified, resulting in site-specific PEGylation, as demonstrated for interleukin-2 [14]. However, this cross-linking results from two competing processes. The favorable reaction links the amino group of the PEG (acceptor) to the protein's Gln donor. In parallel, a competing hydrolytic reaction deamidates Gln thereby abolishing donor function. Consequently, the hydrolyzed Gln is no longer available for conjugation resulting in moderate coupling yields and loss of valuable protein [18]. Most frequently, high excess of the PEG-amine is deployed to achieve satisfactory yields [19]. In contrast, we take advantage of the high natural reactivity of the K acceptor within IGF-I and use a Q donor PSL peptide, resulting in more than 90 % yield within 5 min (**Figure 2A**). These considerations can be of help for future enzymatic coupling strategies to maximize the yields, as protein conversion is not limited due to hydrolysis of the glutamine to glutamic acid [78].

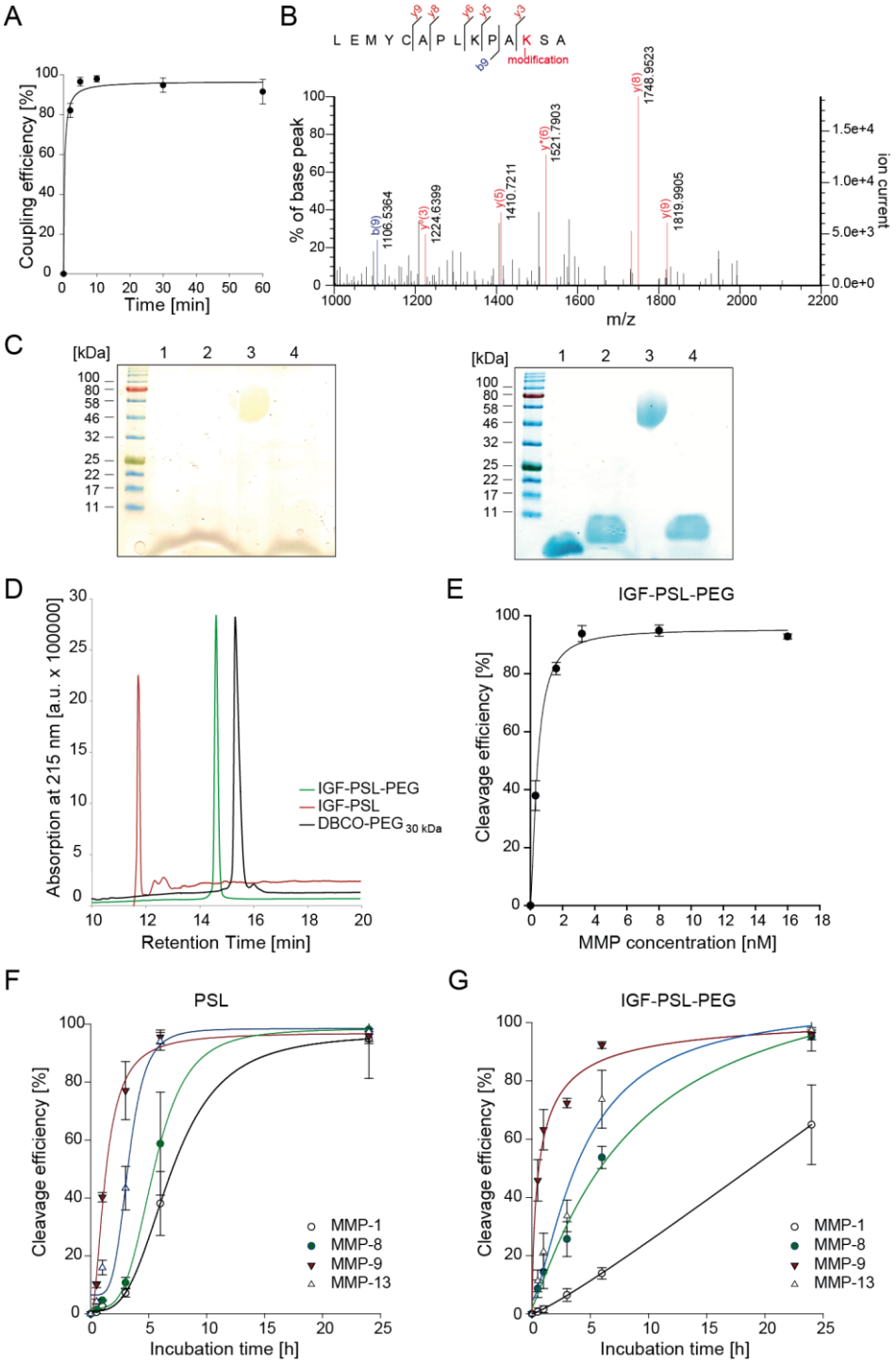

Figure 2: Characterization of the IGF-PSL and IGF-PSL-PEG conjugate following synthesis and cleavage kinetics after MMP exposure. (A) Coupling efficiency of the FXIIIa-catalyzed transamidation reaction between IGF-I and PSL over time analyzed by RP-HPLC. (B) Trypsin digest of IGF-I modified with the $\alpha 2PI_{1-8}$-derived peptide sequence confirmed K68 as the attachment site. (C) SDS-PAGE of IGF-I (lane #1), IGF-PSL (lane #2), IGF-PSL-PEG conjugate (lane #3) and IGF-PSL-PEG exposed to MMPs for a period of 24 hours (lane #4). The gel was stained with PEG-specific iodine (left) and Coomassie Brilliant Blue G250 (right). (D) RP-HPLC analysis of the IGF-PSL-PEG conjugate in comparison to IGF-PSL and unconjugated DBCO-PEG_{30kDa}. (E) Concentration-dependent cleavage of IGF-PSL-PEG after 6 hours exposition to MMP-8, -9 and -13. (F) Comparison of cleavage efficiency of the PSL regarding MMP-1, -8, -9 and -13 at 37°C as a function of incubation time. (G) Time-dependent cleavage of IGF-PSL-PEG exposed to MMP-1, -8, -9 and -13 and analyzed by RP-HPLC.

Thus, after having optimized the decoration site and synthesis of the construct, we analyzed PSL performances in detail [54, 79]. To assess the MMP concentration required for efficient cleavage of the conjugate, a dose escalation study with a combination of different activated MMP isoforms (MMP-8, -9 and -13) was performed (**Figure 2E, S3A**). Total concentrations of 4 nM resulted in almost complete cleavage of the IGF-PSL-PEG conjugate within 6 hours. The calculated EC_{50} for the 6 hour incubation period was found to be 0.423 nM. Next, we evaluated the response of different MMP isoforms towards the PSL and IGF-PSL-PEG (**Figure 2F, G**). For the PSL alone, cleavage was highest for MMP-9, followed by MMP-13, MMP-8 and MMP-1 (**Figure 2F, Table S1**). The IGF-PSL-PEG conjugate performed similarly despite the presence of the bulky PEG when exposed to identical protease concentrations other than MMP-1 (**Figure 2G, S3B-C**). Following 24 hours incubation, cleavage was complete for MMP-8, -9 and -13 but – in contrast to the PSL alone – only 65 ± 14 % for MMP-1. In conclusion, the PEG impaired MMP-1 performance, but did not impact the other MMPs similarly to observations made before for PSLs on solid substrates [79]. The concentration range (**Figure 2E**) fits closely to levels of proteolytically active MMP-9 in synovial fluid of rheumatoid arthritis patients [55], activated MMP-1 in knee synovial fluid after joint injury [56], and increased MMP-9 activity in dystrophic or injured muscles, respectively [25]. For these diseases, MMP profiles allow reliable and reproducible discrimination of diseased from healthy tissues [57].

Activities of MMPs are precisely controlled, not only by their gene expression in various cell types, but also by activation of their precursors (proMMPs) [80-83] and inhibition by endogenous inhibitors, such as α_2-macroglobulin (α_2M) and tissue inhibitors of metalloproteinases (TIMPs) [84]. The local increase in proteolytic activity of MMPs was associated with the pathogenesis of various musculoskeletal diseases [85]. For example, a positive correlation of MMP levels and extent of cartilage destruction was found in rheumatoid arthritis [55, 86, 87] and enhanced MMP-9 immunoreactivity contributes to the progression of inflammatory myopathies [24]. According to several studies, the temporal pattern of MMP-3 – a powerful activator of other MMPs including MMP-9 [63] – and TIMP-1 in synovial fluid of diseased joints displays a change from an excess of free TIMP-1 in the healthy joint to increased free MMP-3 in the injured joint [88]. It is assumed, that this imbalance in the expression of MMPs and endogenous TIMPs also contributes to the pathogenesis of musculoskeletal diseases [86, 89].

As the disease-associated increase in MMP activity frequently results in elevated serum levels of proMMPs, various MMP isoforms are discussed as biomarkers for monitoring disease progression in Duchenne muscular dystrophy (DMD) or several kinds of arthritis [87, 90, 91].

Next, we tested the bioactivity, long-term exposure (2 days incubation and proliferative response of MG63 cells; **Figure 3A**) and short-term exposure (AKT and ERK phosphorylation following 30 minute incubation in MG63 and C2C12 cells; **Figure 3B-C, S4A-C**). Cell proliferation after 2 days was comparable among groups with EC_{50} values of 1.4 ± 0.3 nM, 2.2 ± 0.9 nM and 1.9 ± 0.4 nM for IGF-I, IGF-PSL and IGF-PSL-PEG, respectively (**Figure 3A**) and in line with previous reports [52]. However, the maximum growth promoting efficiency (E_{max}) was reduced for the conjugate as compared to IGF-PSL and IGF-I reaching 1.6 ± 0.04, 1.7 ± 0.07, and 1.4 ± 0.03 -fold increases for IGF-I, IGF-PSL and IGF-PSL-PEG, respectively. Short term exposure after 30 minutes was assessed by AKT and ERK phosphorylation, respectively (**Figure 3B, C, S4A-C**). AKT phosphorylation was comparable for the conjugate and IGF-I in MG63 cells (**Figure 3B**), and C2C12 myoblasts showed similar AKT and ERK phosphorylation as response to stimulation with the different variants (**Figure 3C, S4A**). We further analyzed the functionality of the conjugate compared to IGF-I using the two most prevalent IGF-I binding proteins – IGFBP-3 and IGFBP-5 – for competitive binding in C2C12 myoblasts (**Figure 3D, E**). IGFBPs are modulators of IGF-I action playing important physiological roles in regulating IGF-I bioavailability and activity in various tissues [92]. Typically, IGF-I has a 2- to 50-fold higher affinity for IGFBPs than for the IGF-IR, but proteolytic modification of IGFBPs (e.g. by MMPs) strongly reduces their affinity for IGF-I and therefore increases the amount available to bind to receptors resulting in enhancement of IGF-I activity [26]. Proliferative responses to IGF-I were abolished at IGFBP-3 concentrations exceeding 100 nM. IC_{50} values of 15.0 ± 0.4 nM, 14.0 ± 0.8 nM, and 12.0 ± 1.2 nM were recorded for IGFBP-3 in presence of IGF-I, IGF-PSL, and IGF-PSL-PEG, respectively, corroborating comparable results reported by others (**Figure 3D**) [93]. However, the maximum growth promoting efficiency was significantly reduced for the conjugate (1.4 ± 0.03–fold) as compared to the IGF-PSL (1.8 ± 0.04) and IGF-I (1.9 ± 0.07). Essentially the same results were found for IGFBP-5 (**Figure 3E**). The similar biologic activity of the IGF-PSL compared to the native protein confirm the suitability of IGF-I's D domain as conjugation site.

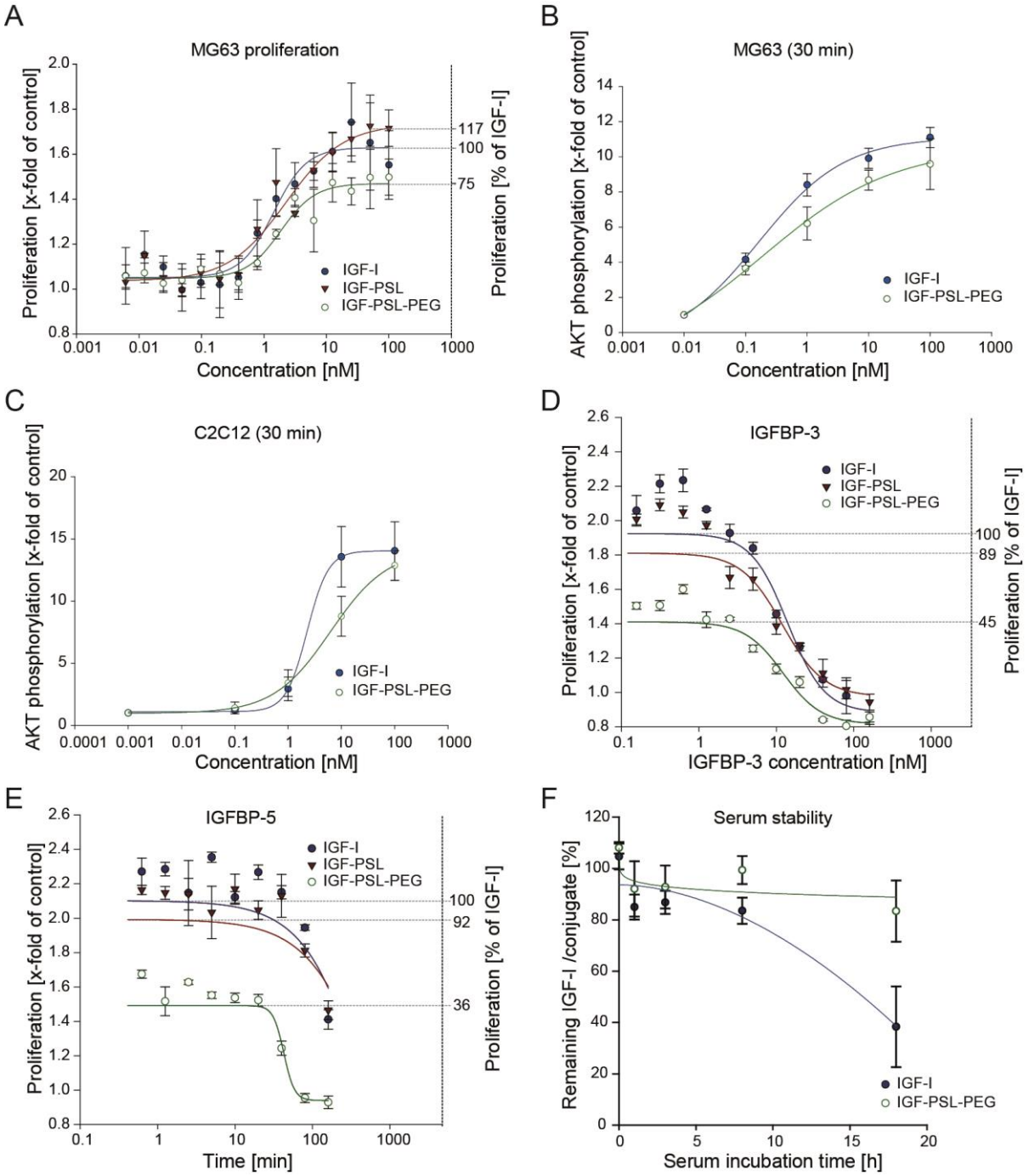

Figure 3: (A) MG63 cell proliferation assay of wild-type IGF-I, IGF-PSL and IGF-PSL-PEG (mean ± standard deviation, n = 3). (B) AKT phosphorylation in comparison to total AKT expression of MG63 cells after treatment with different concentrations of IGF-PSL-PEG and IGF-I for 30 min in serum-depleted medium as analyzed by Western blot analysis. (C) AKT phosphorylation of C2C12 cells normalized to total AKT expression. Cells were treated with different concentrations (ranging from 0.001 to 100 nM) of IGF-PSL-PEG or IGF-I for 30 min and analyzed by Western blot analysis. (D, E) C2C12 cell proliferation assay of 6.5 nM wild type IGF-I, IGF-PSL and IGF-PSL-PEG, respectively, in combination with a dilution series of (D) IGFBP-3 and (E) IGFBP-5, respectively (mean ± standard deviation, n = 3). (F) Stability of IGF-PSL-PEG in comparison to IGF-I in 10 % human serum at 37°C.

.

Due to its high flexibility and the preservation of all high affinity receptor binding domains, C-terminal modifications of IGF-I are well tolerated [65, 67]. This finding is supported by the presence of a natural variant with an E-peptide at the C-terminus displaying retained biological activity and increased stability [94]. For this reason, the short peptide tag remaining after MMP cleavage is not expected to reduce the biologic activity of the growth factor (**Figure 3A, E**).

Intending to prove the enhanced stability and favorable pharmacokinetic properties of the IGF-PSL-PEG, serum stability of the conjugate was analyzed in comparison to native IGF-I (**Figure 3F, S4D-H**). IGF-I and IGF-PSL-PEG remained stable for up to 8 hours when exposed to 10% human serum of healthy persons. Following 18 hours incubation, 63 ± 16 % degradation was observed for IGF-I, while the IGF-PSL-PEG conjugate showed increased stability with only 17 ± 12 % degradation (**Figure 3F**; $p < 0.05$; t-test).

These data provided evidence, that the PEG conjugation may increase circulatory half-life of IGF-I by increasing resistance to proteolytic enzymes, while mediating known advantages of PEGylation including improved solubility, decreased endocytosis and reduced renal filtration as shown for permanently PEGylated IGF-I [52, 95]. The increased stability provides the basis for a targeted growth factor release upon entering the diseased tissue.

We also analyzed the binding affinities to IGFBP-3 and -5 by surface plasmon resonance (SPR) with the BPs being amine-coupled onto the sensor chip as previously described [96]. IGF-I binding resulted in affinities of K_d = 11 ± 7 nM and 11 ± 1 nM for IGFBP-3 and IGFBP-5, respectively (**Figure S5A, B**). The dissociation of IGF-I from IGFBP-5 was almost 2-times faster than from IGFBP-3 (**Figure S5A, B**). These differences in dissociation (k_{off}) correlated with similar differences in the association rate constant (k_{on}), which is why similar dissociation constant / affinity (K_d) were calculated for IGF-I to its BPs. Similarly, the IGF-PSL-PEG conjugate bound to IGFBP-3 and IGFBP-5 with affinities of K_d =10 ± 2 nM and 20 ± 3 nM, respectively. However, signal amplitudes (RU) were lower for the conjugate than for IGF-I when perfused at the same concentration over the same flow cells, possibly reflecting partial binding and/or reduced association due to the larger size of the conjugate (**Figure S5C, D**).

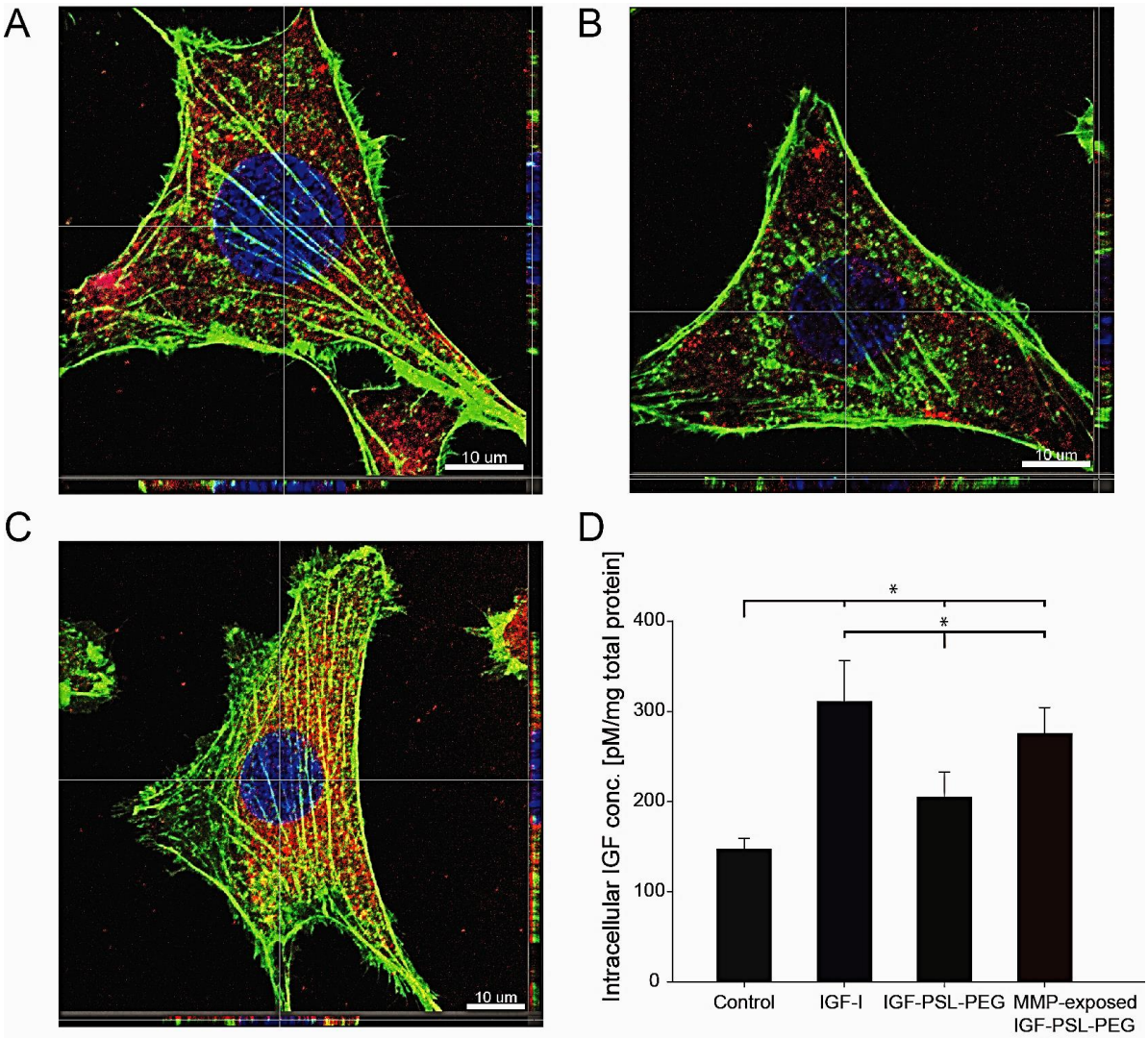

Figure 4: Internalization of (A) *wt*-IGF-I, (B) IGF-PSL-PEG and (C) MMP-exposed IGF-PSL-PEG into NIH3T3 cells with IGF-I in red, actin in green, and cell nuclei in blue. (D) Quantification of internalized ligand in C2C12 cells after 45 minutes ($n = 3$, $p < 0.05$; ANOVA, Tukey test for post hoc comparison).

We now studied the effect of PEGylation on endocytosis and cellular trafficking (**Figure 4**). Avalanches of data have demonstrated continued signaling of endocytosed receptor-ligand complexes and detailed its importance for IGF-I [97]. For example, receptor-mediated internalization of IGF-I is able to prolong the circulation, to control expression of IGFBPs, protein synthesis and to activate mitogenic responses through endosomes [98, 99].

The diverse roles of endocytosis in signal transduction are known for many growth factors [100]. IGF-I is internalized in a complex with the IGF-II/Mannose-6-phosphate receptor, what we confirmed for the conjugate as well (**Figure S6**) [98, 99]. Endocytosis of the conjugate was impaired, but reestablished upon MMP exposure (**Figure 4A-C**). We corroborated these qualitative observations quantitatively by ELISA. The conjugate had

significantly lower intracellular concentrations (205 ± 28 pM) as compared to IGF-I (311 ± 46 pM) and MMP incubated conjugate (275 ± 29 pM; **Figure 4D**).

Future studies are required to detail these findings in *in vivo* studies, including efficacy of MMP cleavage in inflamed tissues, off-target effects and overall stability during circulation. Ultimately, this approach represents a novel concept of personalized medicine by enabling tailored treatment to individual patients. Based on expression patterns of enzymes associated with pathogenesis of a particular musculoskeletal disease, patients can be stratified according to enzyme activities driving the release of IGF-I for optimum therapeutic benefit. Along with improved diagnosis for prediction of the person's response, this strategy has potential to allow treatment with precision and calculable risk-benefit ratio. The approach includes various options for individual adaptation. On the one hand, the release rate can be modified by exchanging amino acids in the sequence of the PSL, thereby increasing or reducing the sensitivity towards MMPs [58]. Additionally, the circulatory half-life can be changed by using PEGs with different molar weights or other polymers. Finally, this approach detailed for IGF-I can be extended to other proteins, peptides or small molecules.

Conclusion

By following bioinspired, enzymatic strategies, we developed an IGF-PSL-PEG construct with strict control of decoration sites and responding to MMPs by IGF-I discharge. The conjugate bound to IGFBP-3 and -5 with similar affinity as observed for IGF-I, but lower association rates. Furthermore, submaximal proliferative cellular responses were recorded and endocytosis was reduced. PEGylation impaired IGF-I bioactivities and endocytosis, which was reverted through bioinspired separation of IGF-I from the PEG in response to upregulated proteases as found in inflamed tissues. This approach shown for IGF-I is paving the way for future growth factor and cytokine constructs leveraging the pharmacokinetic advantages of PEGylation with fully regained, local performances.

Acknowledgment

The financial support of the Sino-German center for the promotion of sciences (grant # GZ1094) and the German Research Foundation (grant # ME 3820/3-1) is gratefully acknowledged. We thank Stephanie Lamer (Rudolf-Virchow-Center for experimental biomedicine, Würzburg) for Nano-LC-MS/MS measurements.

Supplementary information

Supplementary tables:

Supplementary table 1: Cleavage kinetics of the PSL and IGF-PSL-PEG conjugate

	Protease	Equation	r^2
PSL	MMP-1	$0.9+\frac{(96.8-0.9)}{1+(\frac{x}{6.9})^{-3.1}}$	1.00
	MMP-8	$1.9+\frac{(98.5-1.9)}{1+(\frac{x}{5.5})^{-3.8}}$	1.00
	MMP-9	$-1.2+\frac{(97.1+1.2)}{1+(\frac{x}{1.3})^{-1.9}}$	0.99
	MMP-13	$6.5+\frac{(98.5-6.5)}{1+(\frac{x}{3.3})^{-4.5}}$	0.99
IGF-PSL-PEG	MMP-1	$-1.6+11774*x;$	0.99
	MMP-8	$101.1*(1-e^{(-0.1*x)})$	0.99
	MMP-9	$\frac{(103.5)}{1+(\frac{x}{0.6})^{-0.7}}$	0.99
	MMP-13	$\frac{(107-4.4)}{1+(\frac{x}{4.3})^{-1.4}}$	0.97

Supplementary schemes:

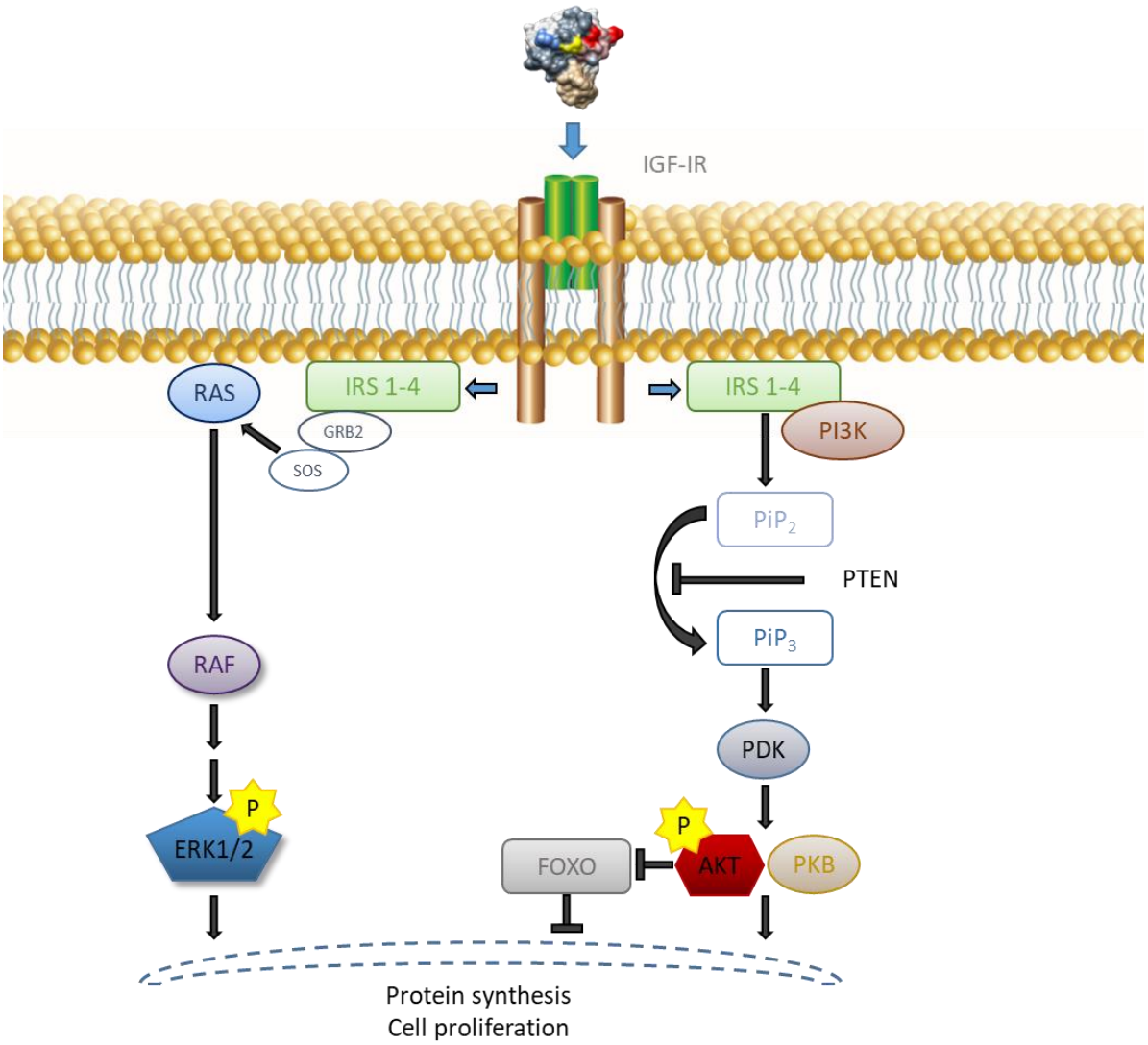

Supplementary scheme 1: Intracellular signaling of IGF-I. Binding to the IGF-IR activates both mitogen-activated protein kinase (MAPK) and phosphatidylinositol-3-kinase (PI3K) pathways responsible for cell proliferation, modulation of tissue differentiation, and protection from apoptosis.

Supplementary figures:

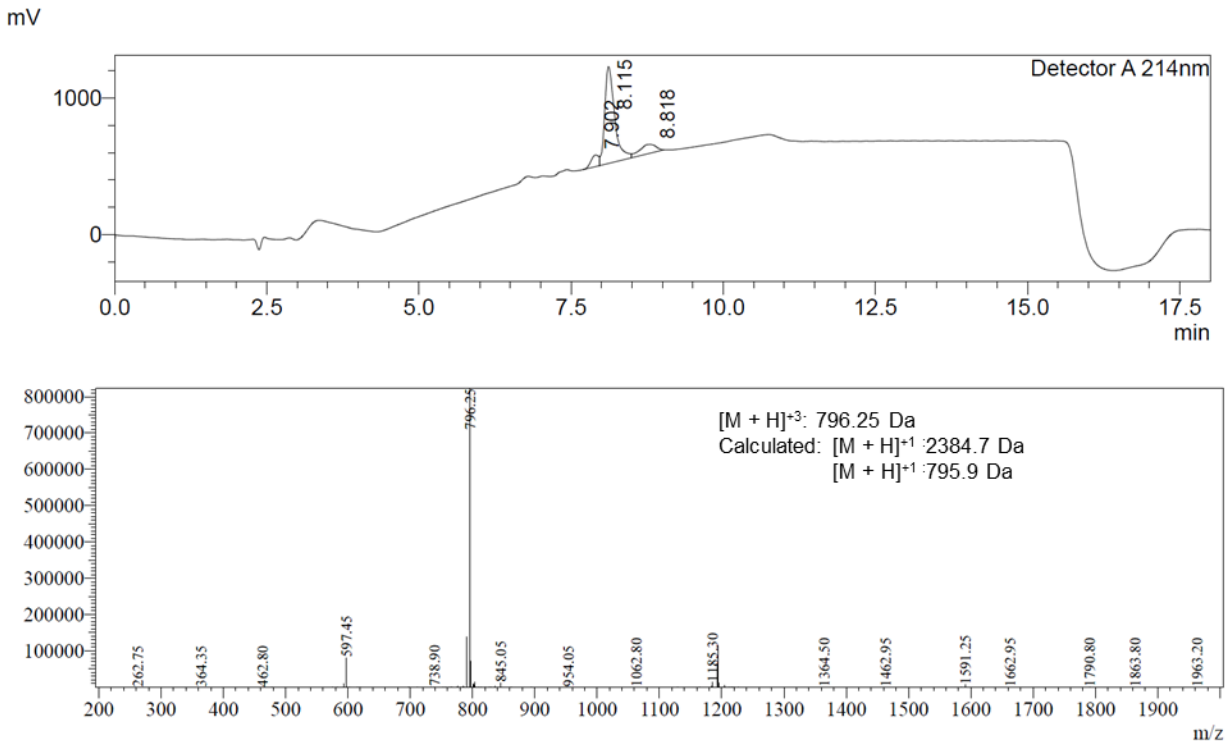

Supplementary figure 1: LC-MS analysis of the PSL for evaluation of peptide purity.

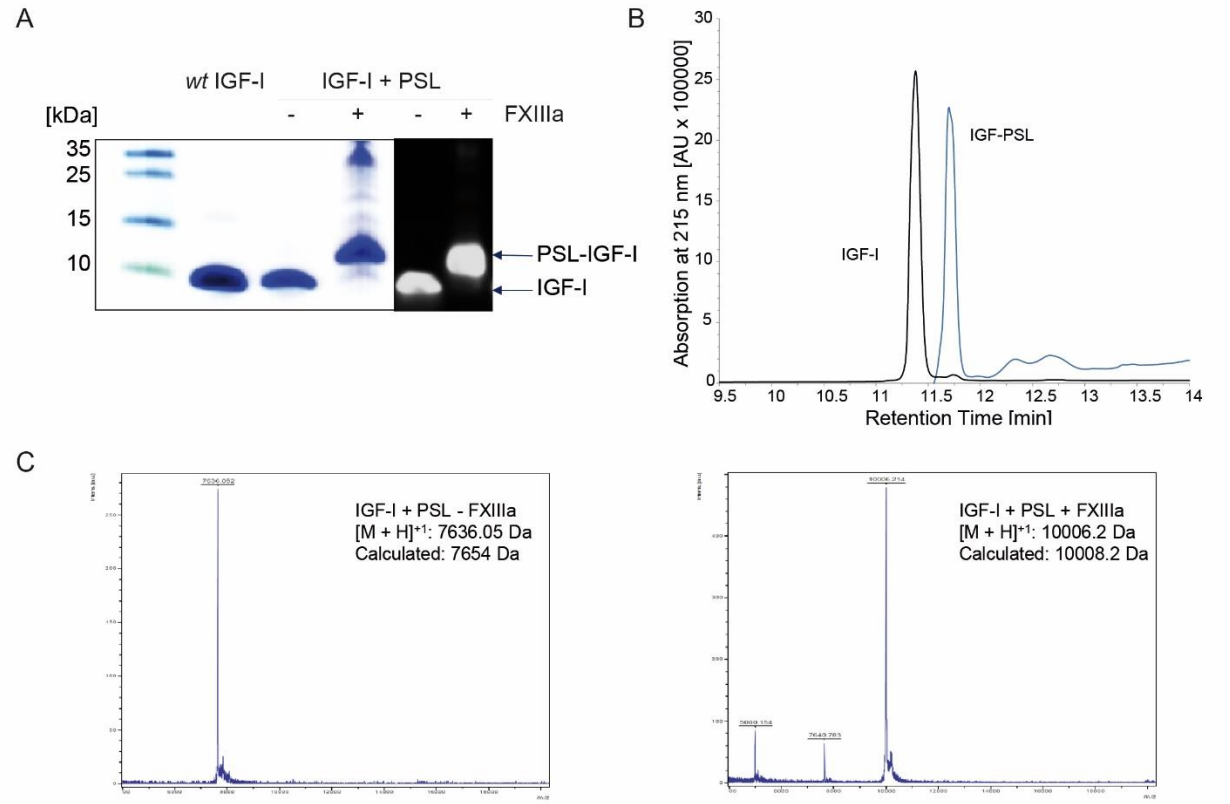

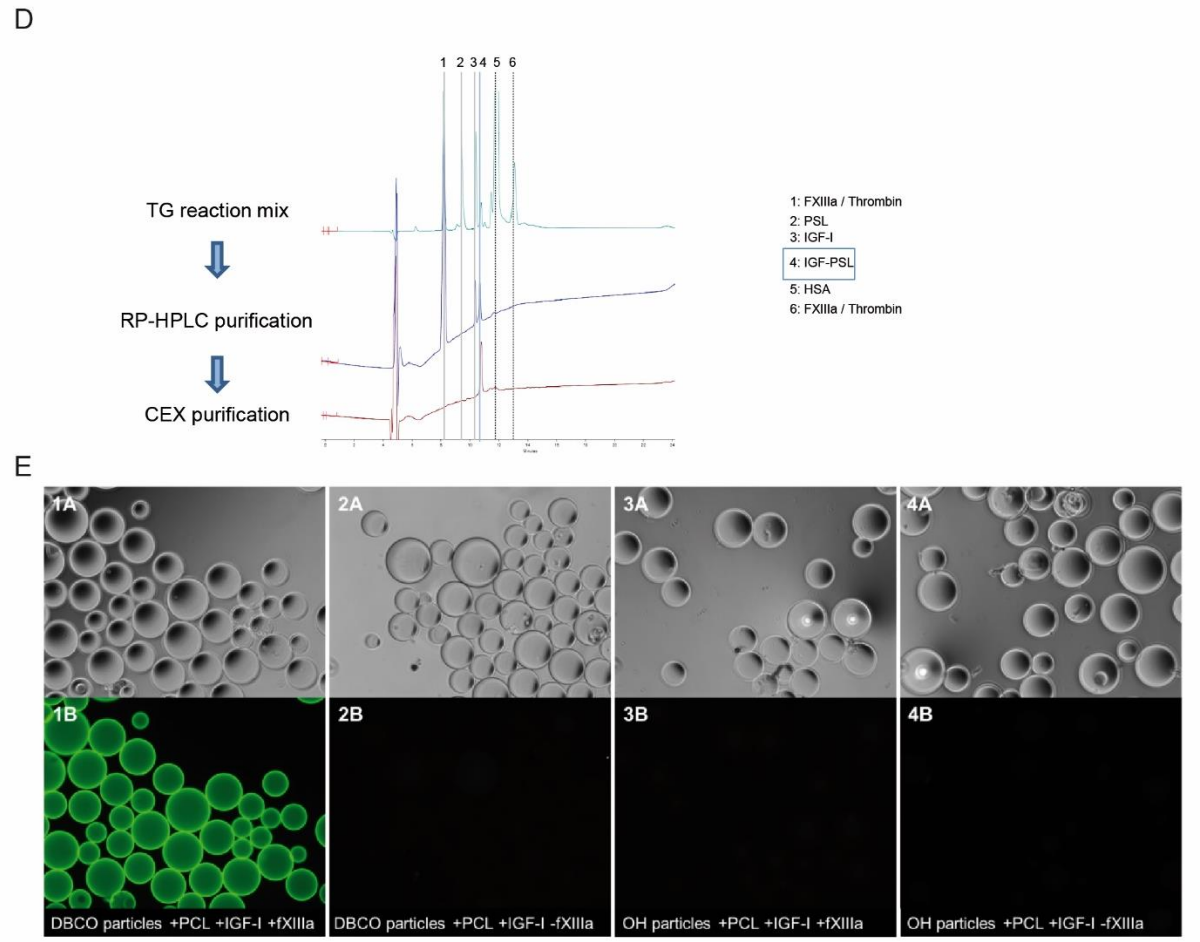

Supplementary figure 2: (A) IGF-I was crosslinked to the PSL by FXIIIa and analyzed by SDS-PAGE (lanes #1-3) and by immunoblotting using a monoclonal anti-IGF-I antibody (lanes #4, 5). The cross-linking reaction in presence of FXIIIa (lane #3, #5) is confirmed by a shift to a ~2 kDa higher molecular weight compared to the IGF-I reference (lane #1) and the reaction performed in absence of FXIIIa (lane #2, #4). (B) HPLC analysis of the transamidation reaction of IGF-I and the PSL catalyzed by FXIIIa (C) MALDI-MS analysis of IGF-I incubated with the PSL for 30 minutes in absence (left chromatogram) and presence (right chromatogram) of Factor XIIIa. Observed average mass of the FXIIIa unexposed IGF-I 7,636.05, observed average mass of the FXIIIa exposed IGF-I 10,006.2; calculated average mass of the IGF-PSL conjugate 10,008.2 Da. (D) Purification steps of the IGF-PSL. After RP-HPLC and cation exchange chromatography (CEX), the fractions were analyzed by analytical HPLC. (E) Fluorescence microscopy images of PSL and IGF-I decorated particles labeled with anti-IGF-I antibody and Alexa Fluor 488 secondary antibody conjugate. Agarose particles were modified with DBCO-amine (1, 2) or ethanolamine (3, 4) followed by coupling with PSL and IGF-I in presence (1, 3) and absence (2,4) of FXIIIa, respectively.

A

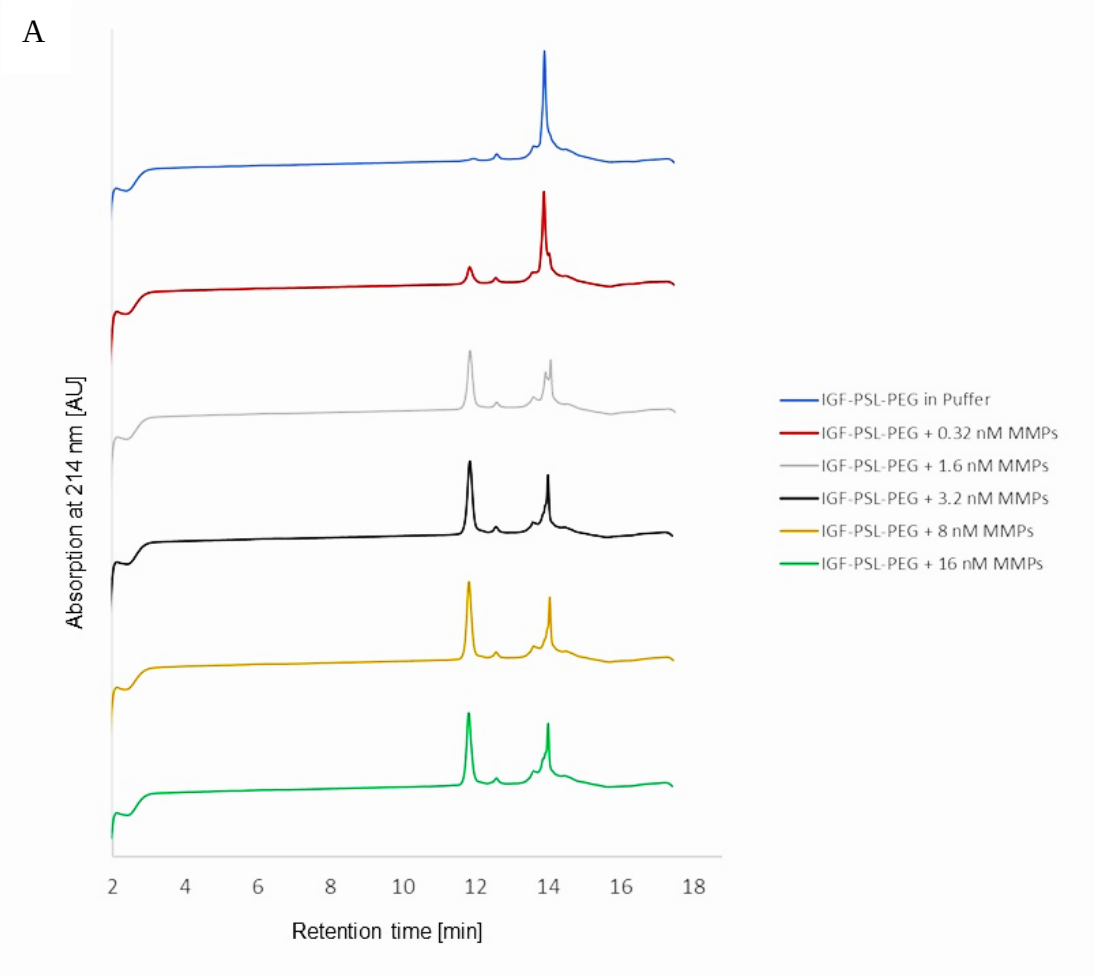
Absorption at 214 nm [AU]
2
4
6
8
10
12
14
16
18
Retention time [min]
IGF-PSL-PEG in Puffer
IGF-PSL-PEG + 0.32 nM MMPs
IGF-PSL-PEG + 1.6 nM MMPs
IGF-PSL-PEG + 3.2 nM MMPs
IGF-PSL-PEG + 8 nM MMPs
IGF-PSL-PEG + 16 nM MMPs

B

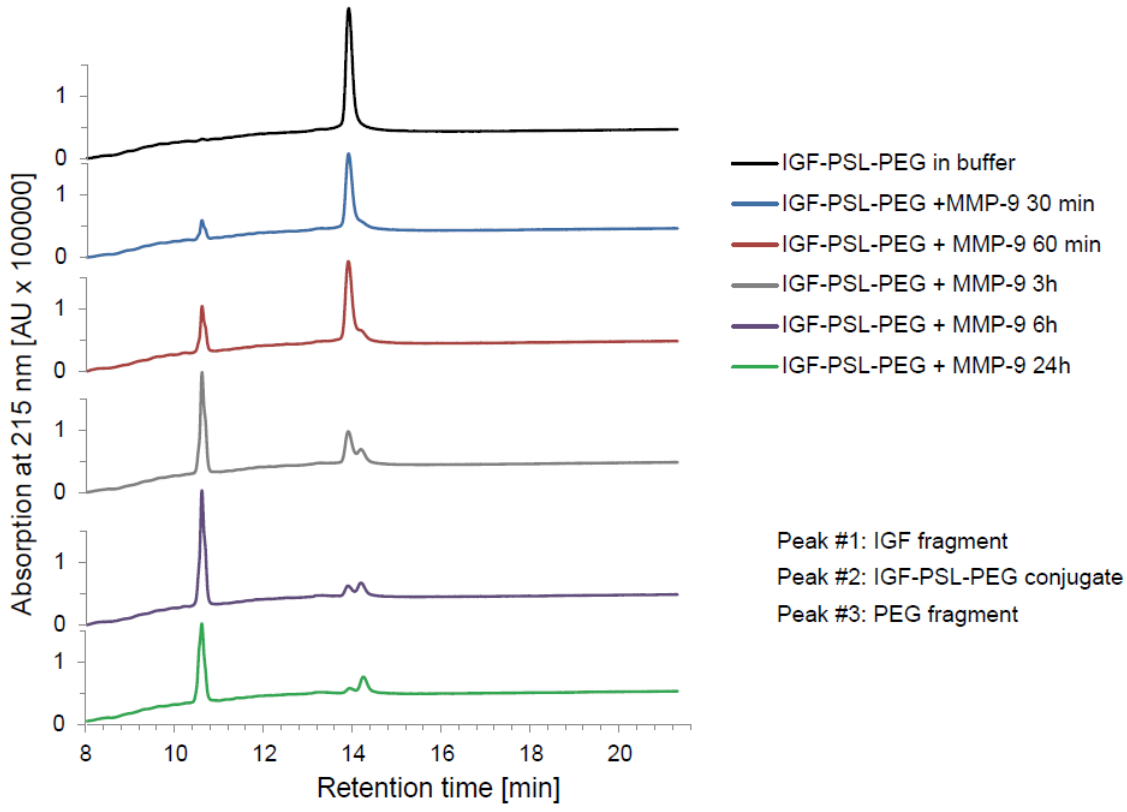
Absorption at 215 nm [AU x 100000]
1
0
8
10
12
14
16
18
20
Retention time [min]
IGF-PSL-PEG in buffer
IGF-PSL-PEG +MMP-9 30 min
IGF-PSL-PEG + MMP-9 60 min
IGF-PSL-PEG + MMP-9 3h
IGF-PSL-PEG + MMP-9 6h
IGF-PSL-PEG + MMP-9 24h
Peak #1: IGF fragment
Peak #2: IGF-PSL-PEG conjugate
Peak #3: PEG fragment

C

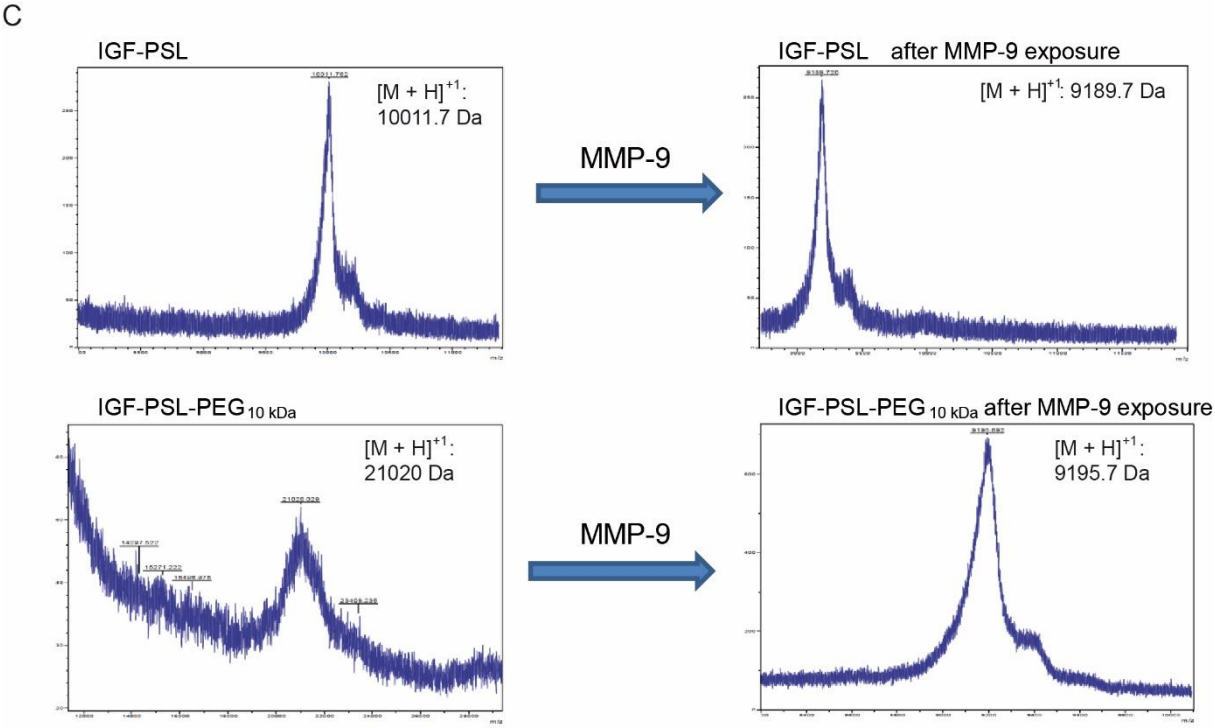

Supplementary Figure 3: (A) HPLC curves of IGF-PSL-PEG exposed to a mixture of different total concentrations of MMP-8, -9 and -13 for a period of 6 hours. (B) RP-HPLC analysis of time-dependent cleavage of IGF-PSL-PEG following exposure to MMP-9 for 30 min, 60 min, 3 h, 6 h, and 24 h, respectively, in comparison to MMP-unexposed control. (C) MALDI-MS analysis of IGF-PSL and IGF-PSL-PEG_{10kDa} after exposure to MMP-9 for 6 hours. (Obs. average mass of IGF-PSL = 10011.76 Da, calc. average mass = 10008.2 Da. Obs. average mass of IGF-PSL after MMP-exposure = 9189.72 Da, calc. average mass = 9189.14 Da. Obs. average mass of IGF-PSL-PEG_{10kDa} = 21020.03 Da, calc. average mass = 20021.7 Da. Obs. average mass of IGF-PSL-PEG_{10kDa} after MMP-exposure = 9195.59 Da, calc. average mass = 9189.14 Da).

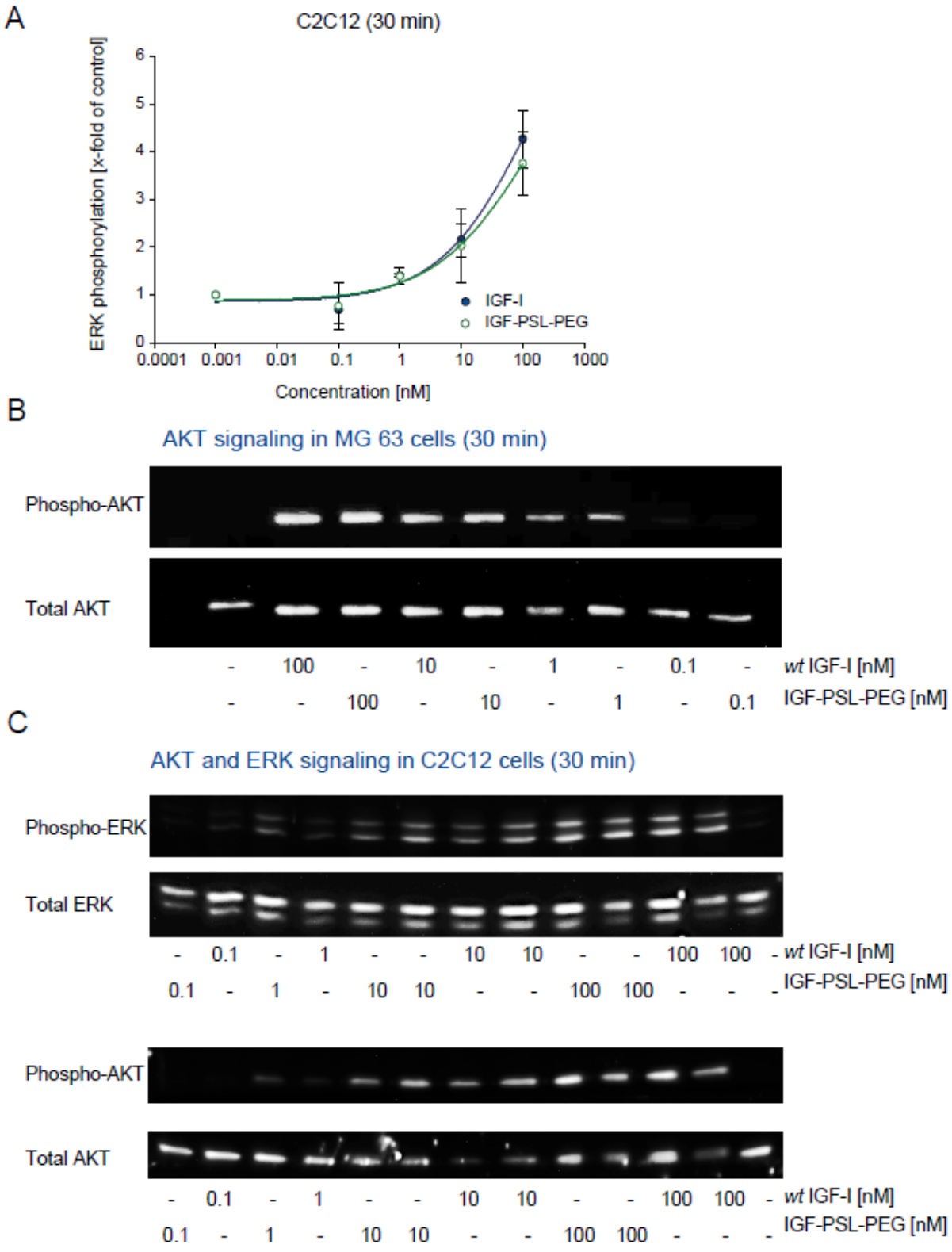
A
C2C12 (30 min)
ERK phosphorylation [x-fold of control]
Concentration [nM]
IGF-I
IGF-PSL-PEG
B
AKT signaling in MG 63 cells (30 min)
Phospho-AKT
Total AKT
wt IGF-I [nM]
IGF-PSL-PEG [nM]
C
AKT and ERK signaling in C2C12 cells (30 min)
Phospho-ERK
Total ERK
Phospho-AKT
Total AKT

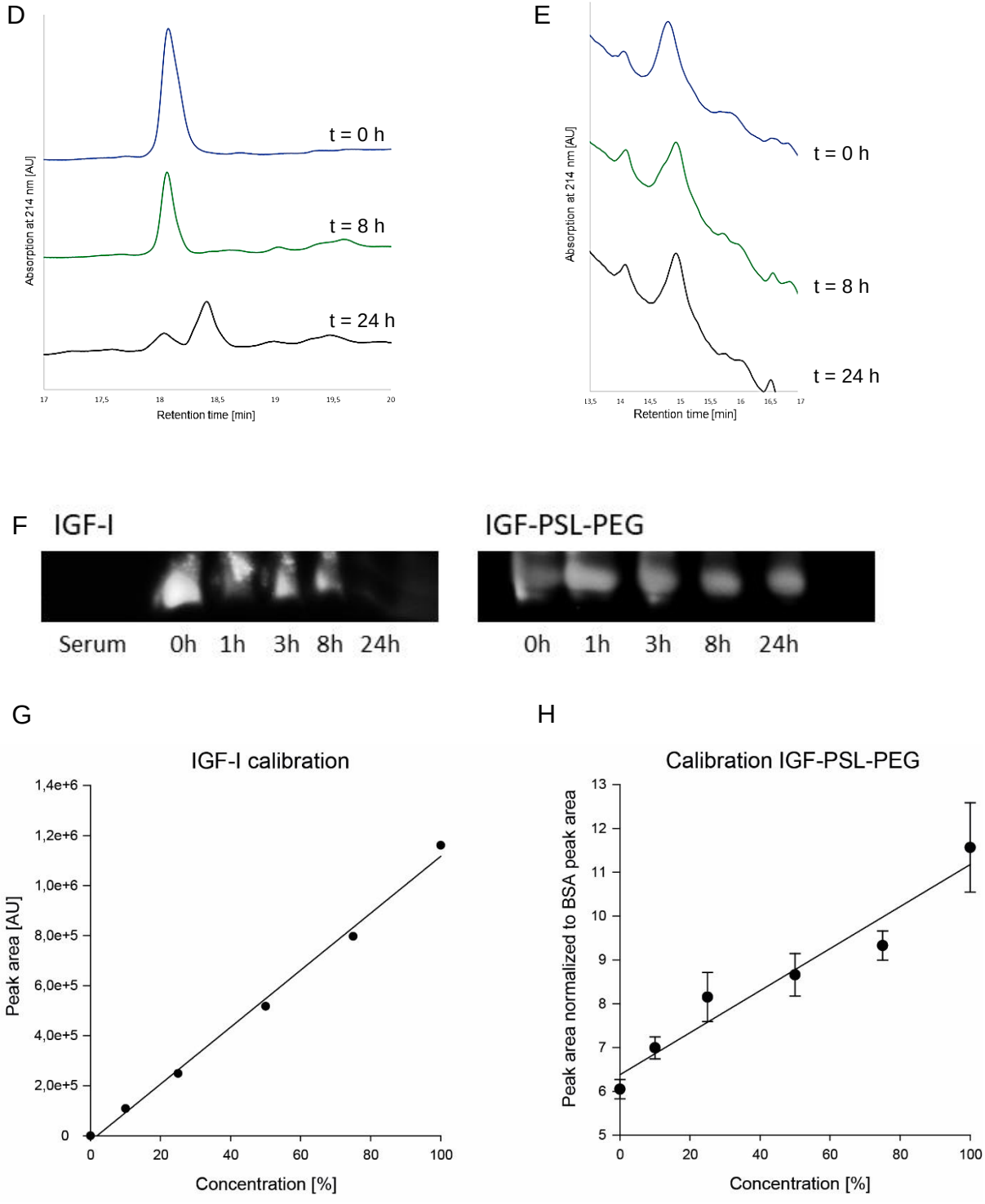

Supplementary figure 4: (A-C) Bioactivity of the IGF-PSL-PEG conjugate compared to *wt* IGF-I. (A) ERK phosphorylation of C2C12 cells normalized to total ERK expression. Cells were treated with different concentrations (ranging from 0.001 to 100 nM) of IGF-PSL-PEG or IGF-I for 30 min in serum-depleted medium and analyzed by Western blot analysis. (B) AKT phosphorylation in MG63 cells and (C) AKT and ERK phosphorylation in C2C12 cells after 30 minutes stimulation with increasing concentrations of *wt* IGF-I and IGF-PSL-PEG, respectively. (D-H) Degradation of IGF-I and IGF-PSL-PEG in serum. RP-HPLC curves of (D) IGF-I and (E) IGF-PSL-PEG after incubation for 0 h, 8 h and 24 h in 10% human serum at 37°C. (F) Western Blot of the serum samples taken after 0 h, 1 h, 3 h, 8 h,

and 24 h incubation and visualized with a IGF-I antibody. (G, H) Calibration curves for evaluation of the degree of degradation. Different concentrations of (G) IGF-I and (H) IGF-PSL-PEG were prepared in inactivated serum and immediately analyzed using RP-HPLC. The peak areas of the serum samples (Supp Figure 4 D, E and Figure 3 F) were referred to these calibration curves to calculate the remaining IGF-I or IGF-PSL-PEG concentration, respectively. The peak area of IGF-I as a function of IGF-I concentration follows: $f(x) = 11088x + 727$ ($r^2 = 0.9938$) and the peak area of IGF-PSL-PEG is related to the HSA peak as an internal standard. The ratio of IGF-PSL-PEG to HSA as a function of IGF-PSL-PEG concentration follows $f(x) = 0.048x + 6.3787$ ($r^2 = 0.9438$).

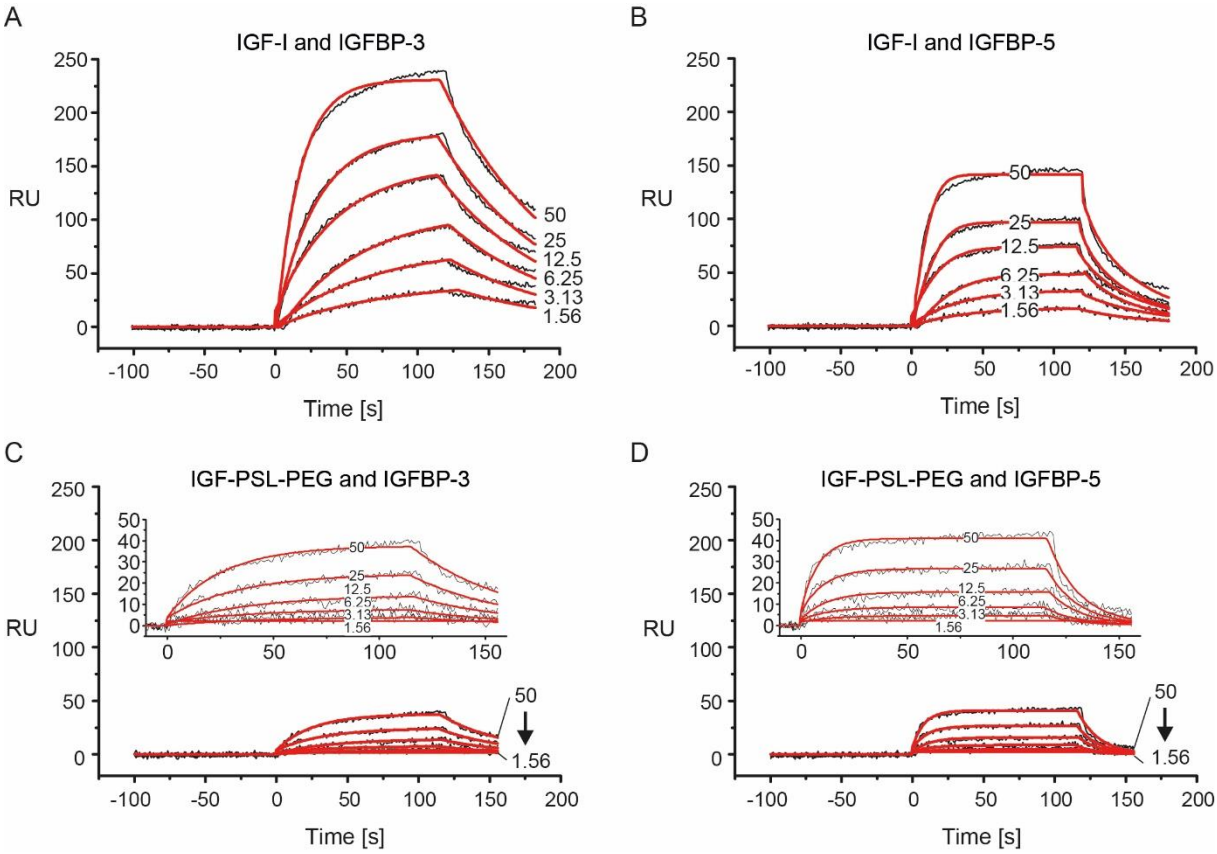

Supplementary figure 5: SPR interaction analysis of (A, B) wild-type IGF-I and (C, D) IGF-PSL-PEG with IGFBP-3 (A, C) and IGFBP-5 (B, D), respectively. IGFBPs were immobilized as ligands on the sensor surface via amine-coupling. Six analyte concentrations (IGF-I or IGF-PSL-PEG) ranging from 1.56 to 50 nM were perfused over the biosensor. Equilibrium binding constants (K_d) were calculated from association and dissociation rate constants employing the equation $K_d = k_{off}/k_{on}$. Black lines indicate raw interaction data, red lines represent fitted data.

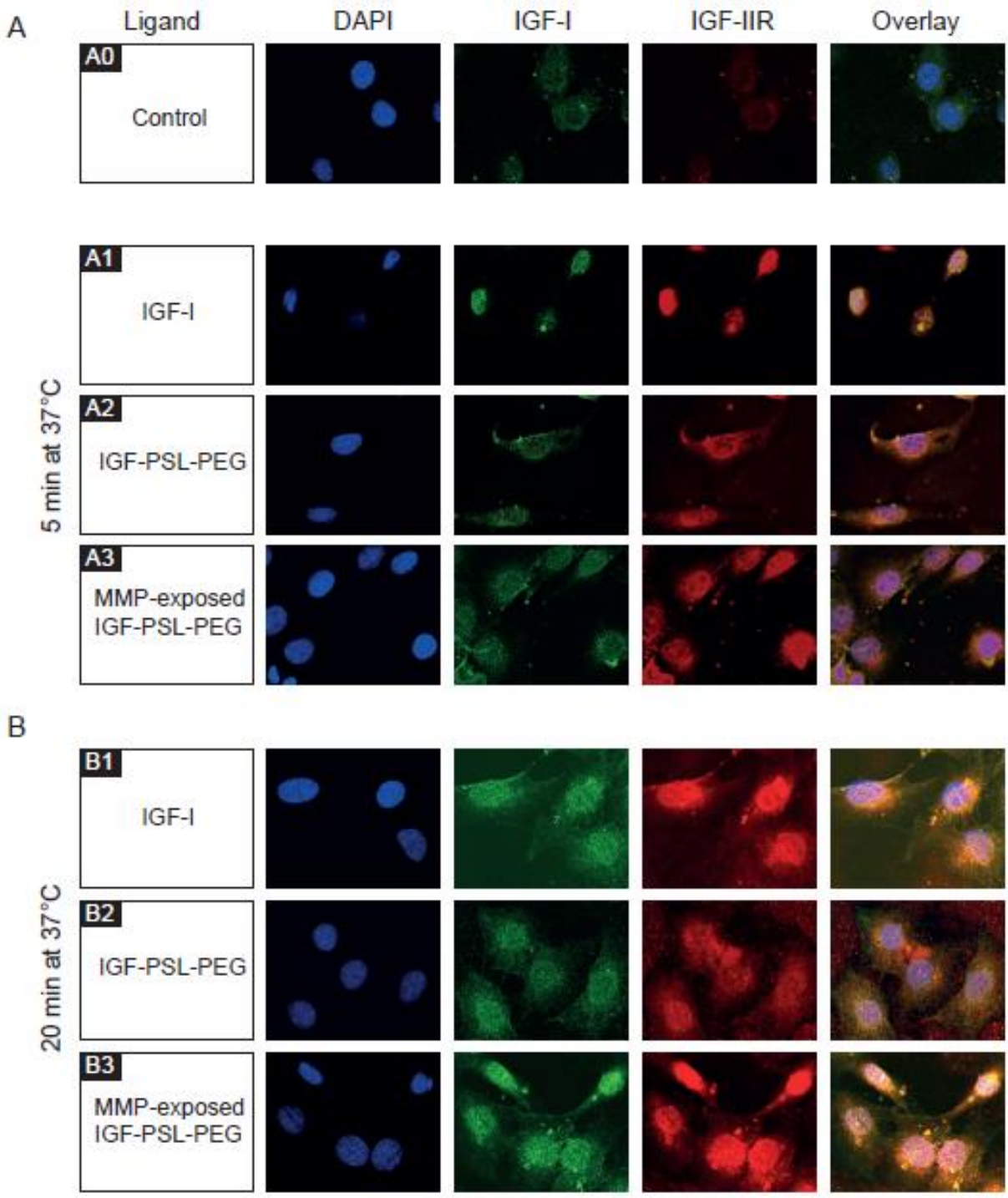
A
Ligand
DAPI
IGF-I
IGF-IIR
Overlay
A0
Control
A1
IGF-I
A2
IGF-PSL-PEG
A3
MMP-exposed IGF-PSL-PEG
5 min at 37°C
B
B1
IGF-I
B2
IGF-PSL-PEG
B3
MMP-exposed IGF-PSL-PEG
20 min at 37°C

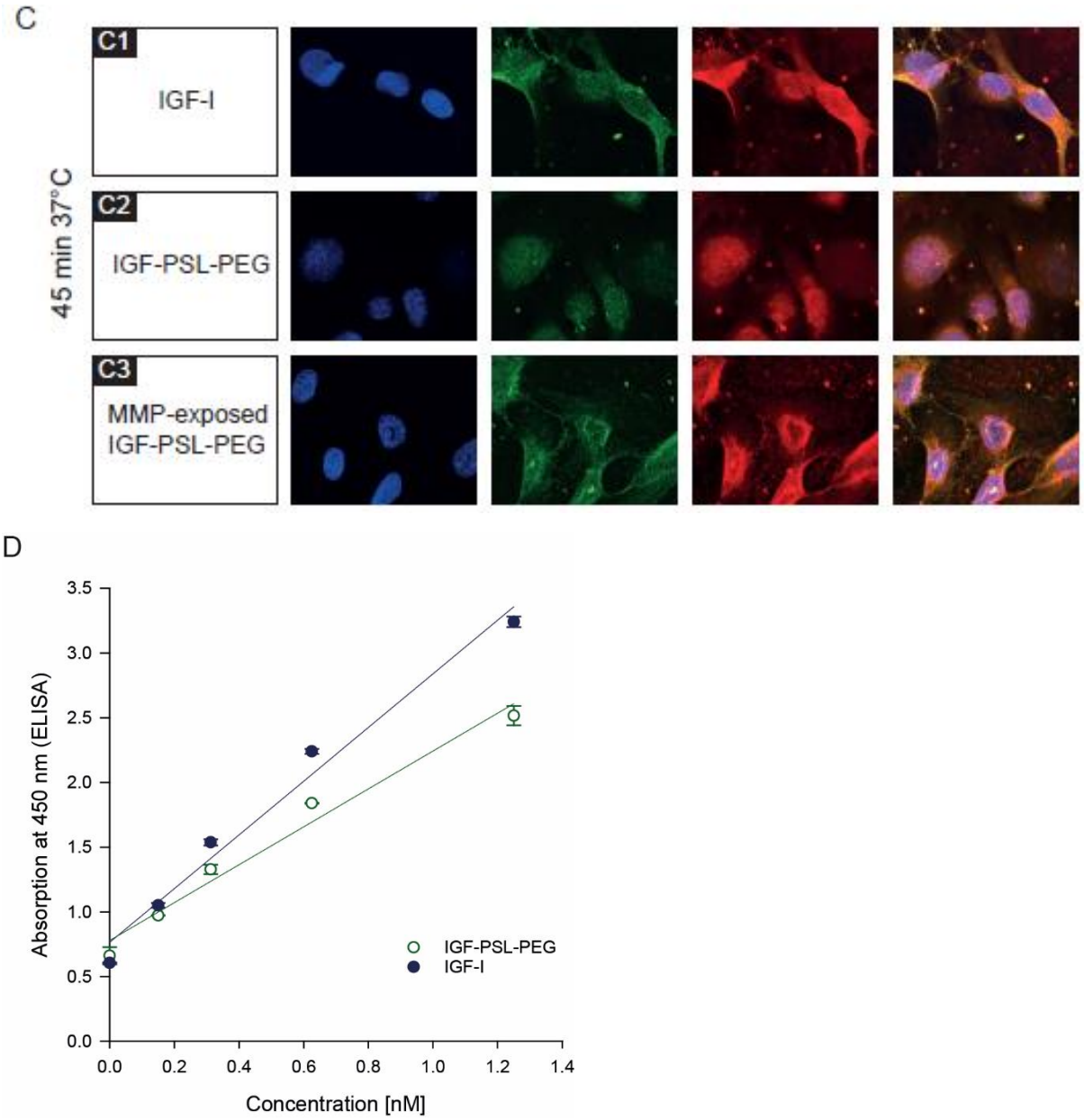

Supplementary figure 6: Time-dependent internalization of wt IGF-I, IGF-PSL-PEG and MMP-exposed IGF-PSL-PEG through the IGF-II/Mannose-6-phosphate receptor visualized by confocal microscopy. C2C12 were incubated with the IGF-I variant at 37°C for (A) 5, (B) 20 and (C) 45 minutes, respectively, and immediately stopped by washing with ice-cold PBS. Staining of fixed cells was performed with a monoclonal IGF-I antibody and AlexaFluor488-conjugated secondary antibody (green fluorescence), and with IGF-II/Mannose-6-phosphate-receptor and AlexaFluor633-conjugated secondary antibody (red fluorescence). Cell nuclei were counterstained with DAPI (blue color). Images were taken with a Leica AOBS SP2 confocal laser scanning microscope by acquisition of 10 z-slices. (D) Calibration curves used for the calculation of internalized amounts of IGF-I and IGF-PSL-PEG, respectively. As antibody binding is lower for the PEG-conjugate, the slope of the equation is lower with $f(x) = 1.4634x + 0.7793$ ($r^2 = 0.9755$) in contrast to IGF-I, following $f(x) = 2.0735x + 0.7655$ ($r^2 = 0.9798$).

References

[1] S.N.S. Alconcel, A.S. Baas, H.D. Maynard, FDA-approved poly(ethylene glycol)-protein conjugate drugs, Polymer Chemistry, 2 (2011) 1442-1448.
[2] I. Bjørnsdottir, O. Sternebring, W.A. Kappers, H. Selvig, H.T. Kornø, J.B. Kristensen, M.A. Bagger, Pharmacokinetics, tissue distribution and excretion of 40 kDa PEG and PEGylated rFVIII (N8-GP) in rats, European Journal of Pharmaceutical Sciences, 87 (2016) 58-68.
[3] K.D. Hinds, S.W. Kim, Effects of PEG conjugation on insulin properties, Advanced Drug Delivery Reviews, 54 (2002) 505-530.
[4] A. Kolate, D. Baradia, S. Patil, I. Vhora, G. Kore, A. Misra, PEG — A versatile conjugating ligand for drugs and drug delivery systems, Journal of Controlled Release, 192 (2014) 67-81.
[5] J.M. Harris, R.B. Chess, Effect of pegylation on pharmaceuticals, Nat Rev Drug Discov, 2 (2003) 214-221.
[6] V. Gaberc-Porekar, I. Zore, B. Podobnik, V. Menart, Obstacles and pitfalls in the PEGylation of therapeutic proteins, Current opinion in drug discovery & development, 11 (2008) 242-250.
[7] P. Bailon, A. Palleroni, C.A. Schaffer, C.L. Spence, W.-J. Fung, J.E. Porter, G.K. Ehrlich, W. Pan, Z.-X. Xu, M.W. Modi, A. Farid, W. Berthold, M. Graves, Rational Design of a Potent, Long-Lasting Form of Interferon: A 40 kDa Branched Polyethylene Glycol-Conjugated Interferon α-2a for the Treatment of Hepatitis C, Bioconjugate Chemistry, 12 (2001) 195-202.
[8] S. Foser, A. Schacher, K.A. Weyer, D. Brugger, E. Dietel, S. Marti, T. Schreitmüller, Isolation, structural characterization, and antiviral activity of positional isomers of monopegylated interferon α-2a (PEGASYS), Protein Expression and Purification, 30 (2003) 78-87.
[9] F.M. Veronese, Peptide and protein PEGylation: a review of problems and solutions, Biomaterials, 22 (2001) 405-417.
[10] H. Lee, T.G. Park, Preparation and Characterization of Mono-PEGylated Epidermal Growth Factor: Evaluation of in Vitro Biologic Activity, Pharmaceutical Research, 19 (2002) 845-851.
[11] T. Luehmann, G. Jones, M. Gutmann, J.-C. Rybak, J. Nickel, M. Rubini, L. Meinel, Bio-orthogonal Immobilization of Fibroblast Growth Factor 2 for Spatial Controlled Cell Proliferation, Acs Biomaterials-Science & Engineering, 1 (2015) 740-746.
[12] H. Cho, T. Daniel, Y.J. Buechler, D.C. Litzinger, Z. Maio, A.-M.H. Putnam, V.S. Kraynov, B.-C. Sim, S. Bussell, T. Javahishvili, S. Kaphle, G. Viramontes, M. Ong, S. Chu, B. GC, R. Lieu, N. Knudsen, P. Castiglioni, T.C. Norman, D.W. Axelrod, A.R. Hoffman, P.G. Schultz, R.D. DiMarchi, B.E. Kimmel, Optimized clinical performance of growth hormone with an expanded genetic code, Proceedings of the National Academy of Sciences, 108 (2011) 9060-9065.
[13] M.F. Debets, S.S. van Berkel, S. Schoffelen, F.P.J.T. Rutjes, J.C.M. van Hest, F.L. van Delft, Aza-dibenzocyclooctynes for fast and efficient enzyme PEGylation via copper-free (3+2) cycloaddition, Chemical Communications, 46 (2010) 97-99.
[14] A. Fontana, B. Spolaore, A. Mero, F.M. Veronese, Site-specific modification and PEGylation of pharmaceutical proteins mediated by transglutaminase, Advanced Drug Delivery Reviews, 60 (2008) 13-28.
[15] A.C. Braun, M. Gutmann, T. Lühmann, L. Meinel, Bioorthogonal strategies for site-directed decoration of biomaterials with therapeutic proteins, Journal of Controlled Release, 273 (2018) 68-85.
[16] M. Griffin, R. Casadio, C.M. Bergamini, Transglutaminases: nature's biological glues, Biochemical Journal, 368 (2002) 377-396.
[17] A. Mero, M. Schiavon, F.M. Veronese, G. Pasut, A new method to increase selectivity of transglutaminase mediated PEGylation of salmon calcitonin and human growth hormone, Journal of Controlled Release, 154 (2011) 27-34.
[18] H. Sato, Enzymatic procedure for site-specific pegylation of proteins, Advanced Drug Delivery Reviews, 54 (2002) 487-504.
[19] B. Spolaore, S. Raboni, A.A. Satwekar, A. Grigoletto, A. Mero, I.M. Montagner, A. Rosato, G. Pasut, A. Fontana, Site-Specific Transglutaminase-Mediated Conjugation of Interferon α-2b at Glutamine or Lysine Residues, Bioconjugate Chemistry, 27 (2016) 2695-2706.

[20] W. Steffen, F.C. Ko, J. Patel, V. Lyamichev, T.J. Albert, J. Benz, M.G. Rudolph, F. Bergmann, T. Streidl, P. Kratzsch, M. Boenitz-Dulat, T. Oelschlaegel, M. Schraeml, Discovery of a microbial transglutaminase enabling highly site-specific labeling of proteins, Journal of Biological Chemistry, 292 (2017) 15622-15635.
[21] H.F. Upchurch, E. Conway, M.K. Patterson, M.D. Maxwell, Localization of cellular transglutaminase on the extracellular matrix after wounding: Characteristics of the matrix bound enzyme, Journal of Cellular Physiology, 149 (1991) 375-382.
[22] J.C. Schense, J.A. Hubbell, Cross-linking exogenous bifunctional peptides into fibrin gels with factor XIIIa, Bioconjugate Chemistry, 10 (1999) 75-81.
[23] A. Sala, M. Ehrbar, D. Trentin, R.G. Schoenmakers, J. Voros, F.E. Weber, Enzyme Mediated Site-Specific Surface Modification, Langmuir, 26 (2010) 11127-11134.
[24] B.G.H. Schoser, D. Blottner, H.J. Stuerenburg, Matrix metalloproteinases in inflammatory myopathies: enhanced immunoreactivity near atrophic myofibers, Acta Neurologica Scandinavica, 105 (2002) 309-313.
[25] S. Kherif, C. Lafuma, M. Dehaupas, S. Lachkar, J.G. Fournier, M. Verdiere-Sahuque, M. Fardeau, H.S. Alameddine, Expression of matrix metalloproteinases 2 and 9 in regenerating skeletal muscle: A study in experimentally injured and mdx muscles, Developmental Biology, 205 (1999) 158-170.
[26] M. Nakamura, S.i. Miyamoto, H. Maeda, G. Ishii, T. Hasebe, T. Chiba, M. Asaka, A. Ochiai, Matrix metalloproteinase-7 degrades all insulin-like growth factor binding proteins and facilitates insulin-like growth factor bioavailability, Biochemical and Biophysical Research Communications, 333 (2005) 1011-1016.
[27] Y. Gong, J.-C. Leroux, M.A. Gauthier, Releasable Conjugation of Polymers to Proteins, Bioconjugate Chemistry, 26 (2015) 1172-1181.
[28] Y. Shechter, M. Mironchik, S. Rubinraut, H. Tsubery, K. Sasson, Y. Marcus, M. Fridkin, Reversible pegylation of insulin facilitates its prolonged action in vivo, European Journal of Pharmaceutics and Biopharmaceutics, 70 (2008) 19-28.
[29] H. Zhao, K. Yang, A. Martinez, A. Basu, R. Chintala, H.-C. Liu, A. Janjua, M. Wang, D. Filpula, Linear and Branched Bicin Linkers for Releasable PEGylation of Macromolecules: Controlled Release in Vivo and in Vitro from Mono- and Multi-PEGylated Proteins, Bioconjugate Chemistry, 17 (2006) 341-351.
[30] D. Filpula, H. Zhao, Releasable PEGylation of proteins with customized linkers, Advanced Drug Delivery Reviews, 60 (2008) 29-49.
[31] H. Tsubery, M. Mironchik, M. Fridkin, Y. Shechter, Prolonging the Action of Protein and Peptide Drugs by a Novel Approach of Reversible Polyethylene Glycol Modification, Journal of Biological Chemistry, 279 (2004) 38118-38124.
[32] A.J. Garman, S. Barret Kalindjian, The preparation and properties of novel reversible polymer-protein conjugates 2-ω-Methoxypolyethylene (5000) glycoxymethylene-3-methylmaleyl conjugates of plasminogen activators, FEBS Letters, 223 (1987) 361-365.
[33] S. Zalipsky, N. Mullah, C. Engbers, M.U. Hutchins, R. Kiwan, Thiolytically Cleavable Dithiobenzyl Urethane-Linked Polymer–Protein Conjugates as Macromolecular Prodrugs: Reversible PEGylation of Proteins, Bioconjugate Chemistry, 18 (2007) 1869-1878.
[34] L. Wang, L. Yuan, H. Wang, X. Liu, X. Li, H. Chen, New Strategy for Reversible Modulation of Protein Activity through Site-Specific Conjugation of Small Molecule and Polymer, Bioconjugate Chemistry, 25 (2014) 1252-1260.
[35] G. Pasut, F.M. Veronese, State of the art in PEGylation: The great versatility achieved after forty years of research, Journal of Controlled Release, 161 (2012) 461-472.
[36] R. Böttger, D. Knappe, R. Hoffmann, Readily adaptable release kinetics of prodrugs using protease-dependent reversible PEGylation, Journal of Controlled Release, 230 (2016) 88-94.
[37] F.I. Nollmann, T. Goldbach, N. Berthold, R. Hoffmann, Controlled Systemic Release of Therapeutic Peptides from PEGylated Prodrugs by Serum Proteases, Angewandte Chemie International Edition, 52 (2013) 7597-7599.
[38] J. Hardwicke, E.L. Ferguson, R. Moseley, P. Stephens, D.W. Thomas, R. Duncan, Dextrin–rhEGF conjugates as bioresponsive nanomedicines for wound repair, Journal of Controlled Release, 130 (2008) 275-283.

[39] E. Rinderknecht, R.E. Humbel, The amino acid sequence of human insulin-like growth factor I and its structural homology with proinsulin, J Biol Chem, 253 (1978) 2769-2776.
[40] D.R. Clemmons, Insulin-like growth factors - their binding proteins and growth regulation, in: E. Canalis (Ed.) Skeletal growth factors, Lippincott Williams & Wilkins, Philadelphia, 2000.
[41] G. Goldspink, S.D.R. Harridge, Growth factors and muscle ageing, Exp. Gerontol., 39 (2004) 1433-1438.
[42] T.N. Stitt, D. Drujan, B.A. Clarke, F. Panaro, Y. Timofeyva, W.O. Kline, M. Gonzalez, G.D. Yancopoulos, D.J. Glass, The IGF-1/PI3K/Akt pathway prevents expression of muscle atrophy-induced ubiquitin ligases by inhibiting FOXO transcription factors, Molecular cell, 14 (2004) 395-403.
[43] L. Meinel, O.E. Illi, J. Zapf, M. Malfanti, M.H. Peter, B. Gander, Stabilizing insulin-like growth factor-I in poly(d,l-lactide-co-glycolide) microspheres, J. Controlled Release, 70 (2001) 193-202.
[44] L. Meinel, E. Zoidis, J. Zapf, P. Hassa, M.O. Hottiger, J.A. Auer, R. Schneider, B. Gander, V. Luginbuehl, R. Bettschart-Wolfisberger, O.E. Illi, H.P. Merkle, R.B. von, Localized insulin-like growth factor I delivery to enhance new bone formation, Bone (San Diego, CA, U. S.), 33 (2003) 660-672.
[45] V. Luginbuehl, E. Wenk, A. Koch, B. Gander, H.P. Merkle, L. Meinel, Insulin-like Growth Factor I-Releasing Alginate-Tricalciumphosphate Composites for Bone Regeneration, Pharm. Res., 22 (2005) 940-950.
[46] L. Uebersax, H.P. Merkle, L. Meinel, Insulin-like growth factor I releasing silk fibroin scaffolds induce chondrogenic differentiation of human mesenchymal stem cells, J. Controlled Release, 127 (2008) 12-21.
[47] E. Wenk, A.J. Wandrey, H.P. Merkle, L. Meinel, Silk fibroin spheres as a platform for controlled drug delivery, J. Controlled Release, 132 (2008) 26-34.
[48] X. Wang, E. Wenk, X. Zhang, L. Meinel, G. Vunjak-Novakovic, D.L. Kaplan, Growth factor gradients via microsphere delivery in biopolymer scaffolds for osteochondral tissue engineering, J. Controlled Release, 134 (2009) 81-90.
[49] E. Wenk, A.J. Meinel, S. Wildy, H.P. Merkle, L. Meinel, Microporous silk fibroin scaffolds embedding PLGA microparticles for controlled growth factor delivery in tissue engineering, Biomaterials, 30 (2009) 2571-2581.
[50] O. Germershaus, I. Schultz, T. Luhmann, M. Beck-Broichsitter, P. Hogger, L. Meinel, Insulin-like growth factor-I aerosol formulations for pulmonary delivery, Eur. J. Pharm. Biopharm., 85 (2013) 61-68.
[51] V. Luginbuehl, E. Zoidis, L. Meinel, R.B. von, B. Gander, H.P. Merkle, Impact of IGF-I release kinetics on bone healing: A preliminary study in sheep, Eur. J. Pharm. Biopharm., 85 (2013) 99-106.
[52] F. Metzger, W. Sajid, S. Saenger, C. Staudenmaier, C. van der Poel, B. Sobottka, A. Schuler, M. Sawitzky, R. Poirier, D. Tuerck, E. Schick, A. Schaubmar, F. Hesse, K. Amrein, H. Loetscher, G.S. Lynch, A. Hoeflich, P. De Meyts, H.J. Schoenfeld, Separation of fast from slow anabolism by site-specific PEGylation of insulin-like growth factor I (IGF-I), J Biol Chem, 286 (2011) 19501-19510.
[53] M. Sivaramakrishnan, T.I. Croll, R. Gupta, D. Stupar, D.R. Van Lonkhuyzen, Z. Upton, G.K. Shooter, Lysine residues of IGF-I are substrates for transglutaminases and modulate downstream IGF-I signalling, Biochimica et Biophysica Acta (BBA) - Molecular Cell Research, 1833 (2013) 3176-3185.
[54] A.C. Braun, M. Gutmann, R. Ebert, F. Jakob, H. Gieseler, T. Lühmann, L. Meinel, Matrix Metalloproteinase Responsive Delivery of Myostatin Inhibitors, Pharmaceutical Research, (2016).
[55] D. Ahrens, A.E. Koch, R.M. Pope, M. Stein-Picarella, M.J. Niedbala, Expression of matrix metalloproteinase 9 (96-kd gelatinase B) in human rheumatoid arthritis, Arthritis & Rheumatism, 39 (1996) 1576-1587.
[56] I. Tchetverikov, L.S. Lohmander, N. Verzijl, T.W. Huizinga, J.M. TeKoppele, R. Hanemaaijer, J. DeGroot, MMP protein and activity levels in synovial fluid from patients with joint injury, inflammatory arthritis, and osteoarthritis, Annals of the rheumatic diseases, 64 (2005) 694-698.

[57] B.J. Heard, L. Martin, J.B. Rattner, C.B. Frank, D.A. Hart, R. Krawetz, Matrix metalloproteinase protein expression profiles cannot distinguish between normal and early osteoarthritic synovial fluid, BMC Musculoskeletal Disorders, 13 (2012) 126.
[58] H. Nagase, G.B. Fields, Human matrix metalloproteinase specificity studies using collagen sequence-based synthetic peptides, Biopolymers, 40 (1996) 399-416.
[59] I. Coin, M. Beyermann, M. Bienert, Solid-phase peptide synthesis: from standard procedures to the synthesis of difficult sequences, Nature Protocols, 2 (2007) 3247-3256.
[60] O. Germershaus, I. Schultz, T. Lühmann, M. Beck-Broichsitter, P. Högger, L. Meinel, Insulin-like growth factor-I aerosol formulations for pulmonary delivery, European Journal of Pharmaceutics and Biopharmaceutics, 85 (2013) 61-68.
[61] M.M. Kurfurst, Detection and molecular weight determination of polyethylene glycol-modified hirudin by staining after sodium dodecyl sulfate-polyacrylamide gel electrophoresis, Analytical biochemistry, 200 (1992) 244-248.
[62] S.J. Koussoroplis, S. Heywood, C. Uyttenhove, C. Barilly, J. Van Snick, R. Vanbever, Production, purification and biological characterization of mono-PEGylated anti-IL-17A antibody fragments, Int J Pharm, 454 (2013) 107-115.
[63] J.P. O'Connell, F. Willenbrock, A.J.P. Docherty, D. Eaton, G. Murphy, Analysis of the role of the COOH-terminal domain in the activation, proteolytic activity, and tissue inhibitor of metalloproteinase interactions of gelatinase B, Journal of Biological Chemistry, 269 (1994) 14967-14973.
[64] F. Wu, A. Braun, T. Lühmann, L. Meinel, Site-Specific Conjugated Insulin-like Growth Factor-I for Anabolic Therapy, ACS Biomaterials Science & Engineering, 4 (2018) 819-825.
[65] M.A. Cascieri, G.G. Chicchi, J. Applebaum, N.S. Hayes, B.G. Green, M.L. Bayne, Mutants of human insulin-like growth factor I with reduced affinity for the type 1 insulin-like growth factor receptor, Biochemistry, 27 (1988) 3229-3233.
[66] T. Sitar, G.M. Popowicz, I. Siwanowicz, R. Huber, T.A. Holak, Structural basis for the inhibition of insulin-like growth factors by insulin-like growth factor-binding proteins, Proceedings of the National Academy of Sciences, 103 (2006) 13028-13033.
[67] M.L. Bayne, J. Applebaum, D. Underwood, G.G. Chicchi, B.G. Green, N.S. Hayes, M.A. Cascieri, The C region of human insulin-like growth factor (IGF) I is required for high affinity binding to the type 1 IGF receptor, Journal of Biological Chemistry, 264 (1989) 11004-11008.
[68] M. Thiersch, M. Rimann, V. Panagiotopoulou, E. Öztürk, T. Biedermann, M. Textor, T.C. Lühmann, H. Hall, The angiogenic response to PLL-g-PEG-mediated HIF-1α plasmid DNA delivery in healthy and diabetic rats, Biomaterials, 34 (2013) 4173-4182.
[69] T. Lühmann, L. Meinel, Nanotransporters for drug delivery, Current Opinion in Biotechnology, 39 (2016) 35-40.
[70] M. Gutmann, A. Braun, J. Seibel, T. Lühmann, Bioorthogonal Modification of Cell Derived Matrices by Metabolic Glycoengineering, ACS Biomaterials Science & Engineering, (2018).
[71] D.Y.S. Chau, R.J. Collighan, E.A.M. Verderio, V.L. Addy, M. Griffin, The cellular response to transglutaminase-cross-linked collagen, Biomaterials, 26 (2005) 6518-6529.
[72] E.F. Pettersen, T.D. Goddard, C.C. Huang, G.S. Couch, D.M. Greenblatt, E.C. Meng, T.E. Ferrin, UCSF chimera - A visualization system for exploratory research and analysis, Journal of Computational Chemistry, 25 (2004) 1605-1612.
[73] M. Gutmann, E. Memmel, A.C. Braun, J. Seibel, L. Meinel, T. Lühmann, Biocompatible Azide–Alkyne “Click” Reactions for Surface Decoration of Glyco-Engineered Cells, ChemBioChem, 17 (2016) 866-875.
[74] J.C. Schense, J.A. Hubbell, Cross-linking exogenous bifunctional peptides into fibrin gels with factor XIIIa, Bioconjug Chem, 10 (1999) 75-81.
[75] M. Ehrbar, A. Metters, P. Zammaretti, J.A. Hubbell, A.H. Zisch, Endothelial cell proliferation and progenitor maturation by fibrin-bound VEGF variants with differential susceptibilities to local cellular activity, Journal of Controlled Release, 101 (2005) 93-109.
[76] K.M. Lorentz, L. Yang, P. Frey, J.A. Hubbell, Engineered insulin-like growth factor-1 for improved smooth muscle regeneration, Biomaterials, 33 (2012) 494-503.

[77] E. Vardar, H.M. Larsson, E.M. Engelhardt, K. Pinnagoda, P.S. Briquez, J.A. Hubbell, P. Frey, IGF-1-containing multi-layered collagen-fibrin hybrid scaffolds for bladder tissue engineering, Acta Biomaterialia, 41 (2016) 75-85.
[78] B.-H. Hu, P.B. Messersmith, Rational Design of Transglutaminase Substrate Peptides for Rapid Enzymatic Formation of Hydrogels, Journal of the American Chemical Society, 125 (2003) 14298-14299.
[79] J. Ritzer, T. Lühmann, C. Rode, M. Pein-Hackelbusch, I. Immohr, U. Schedler, T. Thiele, S. Stübinger, B.v. Rechenberg, J. Waser-Althaus, F. Schlottig, M. Merli, H. Dawe, M. Karpíšek, R. Wyrwa, M. Schnabelrauch, L. Meinel, Diagnosing peri-implant disease using the tongue as a 24/7 detector, Nature Communications, 8 (2017) 264.
[80] P. Koolwijk, A.M. Miltenburg, M.G. van Erck, M. Oudshoorn, M.J. Niedbala, F.C. Breedveld, V.W. van Hinsbergh, Activated gelatinase-B (MMP-9) and urokinase-type plasminogen activator in synovial fluids of patients with arthritis. Correlation with clinical and experimental variables of inflammation, The Journal of rheumatology, 22 (1995) 385-393.
[81] H. Nagase, R. Visse, G. Murphy, Structure and function of matrix metalloproteinases and TIMPs, Cardiovascular Research, 69 (2006) 562-573.
[82] G.J. Peppin, S.J. Weiss, Activation of the endogenous metalloproteinase, gelatinase, by triggered human neutrophils, Proceedings of the National Academy of Sciences of the United States of America, 83 (1986) 4322-4326.
[83] Z. Gu, M. Kaul, B. Yan, S.J. Kridel, J. Cui, A. Strongin, J.W. Smith, R.C. Liddington, S.A. Lipton, S-Nitrosylation of Matrix Metalloproteinases: Signaling Pathway to Neuronal Cell Death, Science, 297 (2002) 1186-1190.
[84] Y. Ogata, Y. Itoh, H. Nagase, Steps Involved in Activation of the Pro-matrix Metalloproteinase 9 (Progelatinase B)-Tissue Inhibitor of Metalloproteinases-1 Complex by 4-Aminophenylmercuric Acetate and Proteinases, Journal of Biological Chemistry, 270 (1995) 18506-18511.
[85] P.S. Burrage, K.S. Mix, C.E. Brinckerhoff, Matrix metalloproteinases: role in arthritis, Frontiers in bioscience : a journal and virtual library, 11 (2006) 529-543.
[86] Y. Yoshihara, H. Nakamura, K. Obata, H. Yamada, T. Hayakawa, K. Fujikawa, Y. Okada, Matrix metalloproteinases and tissue inhibitors of metalloproteinases in synovial fluids from patients with rheumatoid arthritis or osteoarthritis, Annals of the rheumatic diseases, 59 (2000) 455-461.
[87] I. Tchetverikov, L.R. Lard, J. DeGroot, N. Verzijl, J.M. TeKoppele, F.C. Breedveld, T.W. Huizinga, R. Hanemaaijer, Matrix metalloproteinases-3, -8, -9 as markers of disease activity and joint damage progression in early rheumatoid arthritis, Annals of the rheumatic diseases, 62 (2003) 1094-1099.
[88] L.S. Lohmander, H. Roos, L. Dahlberg, L.A. Hoerrner, M.W. Lark, Temporal patterns of stromelysin-1, tissue inhibitor, and proteoglycan fragments in human knee joint fluid after injury to the cruciate ligament or meniscus, Journal of orthopaedic research : official publication of the Orthopaedic Research Society, 12 (1994) 21-28.
[89] D.D. Dean, J. Martel-Pelletier, J.P. Pelletier, D.S. Howell, J.F. Woessner, Jr., Evidence for metalloproteinase and metalloproteinase inhibitor imbalance in human osteoarthritic cartilage, The Journal of clinical investigation, 84 (1989) 678-685.
[90] V.D. Nadarajah, M. van Putten, A. Chaouch, P. Garrood, V. Straub, H. Lochmueller, H.B. Ginjaar, A.M. Aartsma-Rus, G.J.B. van Ommen, J.T. den Dunnen, P.A.C. t Hoen, Serum matrix metalloproteinase-9 (MMP-9) as a biomarker for monitoring disease progression in Duchenne muscular dystrophy (DMD), Neuromuscular Disorders, 21 (2011) 569-578.
[91] K. Masuhara, T. Nakai, K. Yamaguchi, S. Yamasaki, Y. Sasaguri, Significant increases in serum and plasma concentrations of matrix metalloproteinases 3 and 9 in patients with rapidly destructive osteoarthritis of the hip, Arthritis and rheumatism, 46 (2002) 2625-2631.
[92] D.R. Clemmons, Role of insulin-like growth factor binding proteins in controlling IGF actions, Molecular and Cellular Endocrinology, 140 (1998) 19-24.
[93] J.I. Jones, D.R. Clemmons, Insulin-Like Growth Factors and Their Binding Proteins: Biological Actions*, Endocrine Reviews, 16 (1995) 3-34.

[94] M.S. Hede, E. Salimova, A. Piszczek, E. Perlas, N. Winn, T. Nastasi, N. Rosenthal, E-Peptides Control Bioavailability of IGF-1, PLOS ONE, 7 (2012) e51152.
[95] M. Sivaramakrishnan, A.S. Kashyap, B. Amrein, S. Saenger, S. Meier, C. Staudenmaier, Z. Upton, F. Metzger, PEGylation of lysine residues reduces the pro-migratory activity of IGF-I, Biochimica et Biophysica Acta (BBA) - General Subjects, 1830 (2013) 4734-4742.
[96] J. Beattie, K. Phillips, J.H. Shand, M. Szymanowska, D.J. Flint, G.J. Allan, Molecular interactions in the insulin-like growth factor (IGF) axis: a surface plasmon resonance (SPR) based biosensor study, Molecular and Cellular Biochemistry, 307 (2008) 221-236.
[97] F. Folli, S. Ghidella, L. Bonfanti, C.R. Kahn, A. Merighi, The early intracellular signaling pathway for the insulin/insulin-like growth factor receptor family in the mammalian central nervous system, Molecular neurobiology, 13 (1996) 155-183.
[98] S. Mitragotri, P.A. Burke, R. Langer, Overcoming the challenges in administering biopharmaceuticals: formulation and delivery strategies, Nat Rev Drug Discov, 13 (2014) 655-672.
[99] J. Giudice, L.S. Barcos, F.F. Guaimas, A. Penas-Steinhardt, L. Giordano, E.A. Jares-Erijman, F. Coluccio Leskow, Insulin and insulin like growth factor II endocytosis and signaling via insulin receptor B, Cell Communication and Signaling, 11 (2013) 18.
[100] R. Dobrowolski, E.M. De Robertis, Endocytic control of growth factor signalling: multivesicular bodies as signalling organelles, Nat Rev Mol Cell Biol, 13 (2012) 53-60.

Chapter 4: Predicting critical micelle concentration and micelle molecular weight of polysorbate 80 using compendial methods

Alexandra C. Braun[1], David Ilko[1], Benjamin Merget[1], Henning Gieseler[2], Oliver Germershaus[1], Ulrike Holzgrabe[1], Lorenz Meinel[1, §]

[1]Institute for Pharmacy and Food Chemistry, University of Wuerzburg, Am Hubland, DE-97074 Wuerzburg, Germany

[2]GILYOS GmbH, Friedrich-Bergius-Ring 15, DE-97076 Wuerzburg, Germany

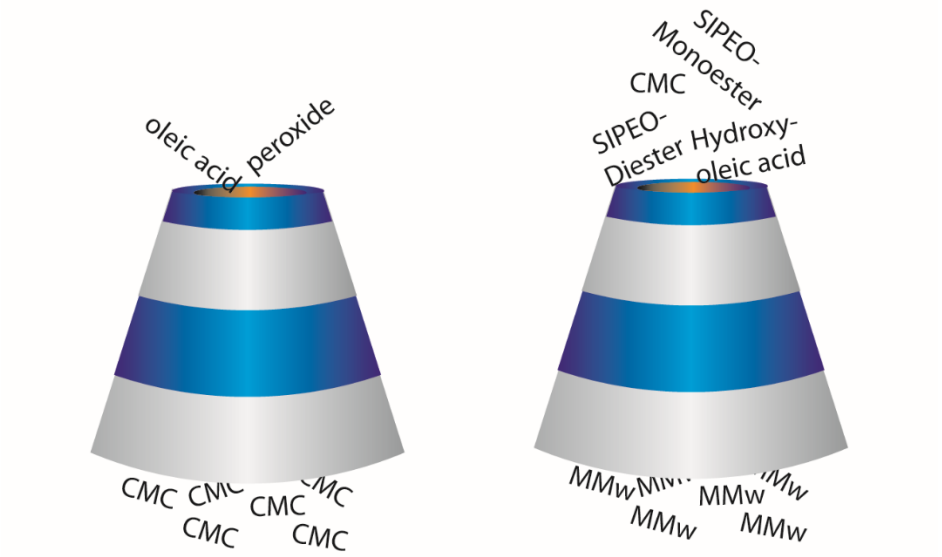

Cartoon for the prediction of the critical micelle concentration (left) and the micelle molecular weight (right). Input parameters are shown above the funnel. SIPEO = sorbitan- and isosorbide polyethoxylate fatty acid

This chapter was originally published in European Journal of Pharmaceutics and Biopharmaceutics vol. 94, pp. 559-68, 2015. DOI: 10.1016/j.ejpb.2014.12.015. With permission of Elsevier, license number: 4347540322073.

Abstract

This manuscript addresses the capability of compendial methods in controlling polysorbate 80 (PS80) functionality. Based on the analysis of sixteen batches, functionality related characteristics (FRC) including critical micelle concentration (CMC), cloud point, hydrophilic-lipophilic balance (HLB) value and micelle molecular weight were correlated to chemical composition including fatty acids before and after hydrolysis, content of non-esterified polyethylene glycols and sorbitan polyethoxylates, sorbitan- and isosorbide polyethoxylate fatty acid mono- and diesters, polyoxyethylene diesters, and peroxide values. Batches from some suppliers had a high variability in functionality related characteristic (FRC), questioning the ability of the current monograph in controlling these. Interestingly, the combined use of the input parameters oleic acid content and peroxide value – both of which being monographed methods – resulted in a model adequately predicting CMC. Confining the batches to those complying with specifications for peroxide value proved oleic acid content alone as being predictive for CMC. Similarly, a four parameter model based on chemical analyses alone was instrumental in predicting the molecular weight of PS80 micelles. Improved models based on analytical outcome from fingerprint analyses are also presented. A roadmap controlling PS80 batches with respect to FRC and based on chemical analyses alone is provided for the formulator.

Introduction

Polysorbate 80 (PS80) is a frequently used surfactant for biopharmaceutical product formulation. This non-ionic emulsifier is typically formulated at concentrations of 0.01 - 0.1% (v/v) for active pharmaceutical ingredient (API) stabilization, reduction of surface adsorption, or to avoid stress-induced aggregation (e.g., freezing, storage, transport, reconstitution of lyophilized products) [1-3]. Compendial grade PS80 is composed of polyoxyethylene sorbitan esters with fatty acids, at least 58% of which being specified as oleic acid along with myristic, palmitic, palmitoleic, stearic, linoleic, and α-linolenic acid esters, respectively [4, 5]. Critical PS80 material attributes were derived from a focus on its impact on API or excipient stability, as e.g. residual peroxides within PS80 batches may drive oxidation. However, PS80 attributes were to a lesser extent selected based on galenical considerations / functionality related characteristics (FRC), an aspect which is thoroughly addressed here within. The batch-to-batch variability e.g. in residual peroxides was linked to the supplier's manufacturing and purification processes, packaging, or storage [6]. Polysorbates are inherently prone to radical autoxidation, leading to hydrolysis [2, 7-9], and placing formulated proteins at risk of oxidative damage [10-12]. Apart from peroxides, variability is introduced by the type and amount of esterified and free fatty acids, unbound ethoxylates as well as the level of impurities [13-16]. Consequently, the United States Pharmacopeia (USP) and the European Pharmacopeia (Ph.Eur) specify the entire (free and esterified) fatty acid composition, the peroxide value as well as the acid, saponification, and hydroxyl value, respectively. In addition, ethylene oxide, dioxin and heavy metal content are specified [4, 5]. In more recent efforts, both pharmacopoeias allude to functionality related characteristics (FRCs; Ph.Eur. 5.15) or excipient performance (USP <1059>) in non-mandatory sections, detailing an approach for reliable excipient performance through additional specifications designed on top of compendial requirements. Several studies within the context of PS80 suggest a need for such additional specifications. For example, the stability of biologic formulations during processing or storage has been linked to the surface activity of polysorbates [17]. Other reports detailed the impact of polydispersed oxyethylenes on colloidal properties [18, 19]. However, neither surface activity nor colloidal properties are monographed at present. It is for these exemplary selected reports on PS80 that compliance with compendial specifications alone has been questioned before yielding stable formulation outcome [20, 21].

Consequently, we are addressing the need to set additional PS80 specification. We are also addressing the hypothesis, that monographed methods are sufficient in specifying PS80 batches for stable outcome with respect to FRC, when these are released based on adequate models. In order to identify possible input parameters for model building, PS80 batches were broadly characterized by numerous methods. For that, we correlated galenical functionality from sixteen PS80 batches (CMC, cloud point, hydrophilic-lipophilic balance (HLB) value and micelle molecular weight) with batch composition from thorough analytical studies (PS80 fatty acid composition before and after hydrolysis [22], unbound PEGs, sorbitan polyethoxylates, and mono-and diesters) as well as with peroxide value.

Experimental Details

Materials

Sixteen PS80 batches of 5 different qualities (qualities being different suppliers or different supplier grades being distributed from one supplier) were used for the study. The polysorbate samples were from Croda (East Yorkshire, UK), Kolb (Hedingen, Switzerland), Merck (Darmstadt, Germany) and NOF (Tokyo, Japan). The order of the supplier names does not necessarily coincide with the order of the codes used within the manuscript. Grade, supplier and date of manufacture from each sample were detailed (**Table 1**). All samples were stored at room temperature, under nitrogen and protected from light and the experiments were conducted after storage times as indicated. Sorbitan monooleate 80 (Span 80), methylene blue, paraffin oil were from Sigma-Aldrich (Taufkirchen, Germany). Type 2 water (ASTM D1193, ISO 3696) was used (Millipore, Billerica, MA). All other chemicals or solvents were of at least analytical or pharmaceutical grade and obtained from Sigma-Aldrich or VWR (Darmstadt, Germany).

Sample preparation

For the cloud point determination, the polysorbate 80 samples were dissolved at 3% (w/v) in freshly prepared 1M sodium chloride in water on a roller mixer to minimize foaming (SRT1, Sigma-Aldrich, Germany) until the solution was visibly clear and free from foam before further processing. Samples for surface tension measurement were dissolved in water.

Table 1: Overview of the PS80 batches.

Quality	Batch	Months of storage	Peroxide value at time of release*	Peroxide value after storage
A	1	26	0.6	8.2
A	2	18	1.3	8.2
A	3	21	0.2	9.2
A	4	21	0.5	16.5
B	1	17	0.4	21.2
B	2	20	0.0	19.7
B	3	31	0.6	16.1
C	1	27	1.0	4.8
C	2	27	1.0	3.7
C	3	16	0.0	4.4
D	1	10	0.1	4.9
D	2	20	0.1	4.4
D	3	18	0.8	2.9
E	1	6	0.2	11.6
E	2	18	1.3	3.9
E	3	14	1.7	8.7

* taken from CoA

Critical micelle concentration (CMC) by surface tension measurement

The CMC was determined by surface tension measurements using the Wilhelmy plate method with a Krüss K12 (Hamburg, Germany). Temperature was controlled at 20 ± 0.5 °C (Fryka, G.Heinemann, Schwäbisch-Gmünd, Germany) and experiments were conducted at atmospheric pressure. The surface tension of water was determined prior to measurements of the surfactant samples and to ensure agreement (± 5 mN/m) with the reference value of 72.75 mN/m [23]. Freshly prepared, serial dilutions of the surfactants each in about 75 - 80 mL of water were equilibrated at 20 ± 0.5 °C for at least 30 minutes and then stirred for 60 seconds [24], and again equilibrated for 5 minutes before measurement (n = 3). The surface tension was recorded from ten different dilutions per sample and the CMC was fitted from the intersection of the straight lines for the linear concentration-dependent section and the concentration-independent section using Krüss tensiometer software (version 5.05) [25-27].

Cloud point

The cloud point was turbidimetrically determined from a 3% (w/v) PS80 sample solution in 1 M sodium chloride, measured in a water bath at increasing temperature. Vials with 8 mL of the surfactant solution were placed in the water bath with heating at a rate of 1.2 °C/min from room temperature to 45 °C and then at a rate of 0.3 °C/min. until the cloud point,

controlled with a thermometer accuracy of 0.2 °C. The cloud point was visually assessed by phase separation. Furthermore, the cloud point was confirmed by microcalorimetry. For that, 3 mL of identically prepared samples as used for the turbidimetric method were heated at a rate of 0.5 K/min from 35 to 90 °C in the small volume sample vessel of a C80 calorimeter (Setaram, Caluire, France) and recorded against 3 mL of the identical solution without PS80 in the reference cell. Cells were equilibrated at 35 °C until heat flow between the cells was constant.

Hydrophilic-lipophilic balance (HLB) value

Determination of HLB values was performed using the "Blender-Centrifuge Method" [28], combining polysorbate 80 sample (HLB ~ 15), sorbitan oleate (Span 80; HLB ~ 4.3), paraffin (required HLB (RHLB) ~ 10.5 and water. In brief, stock emulsions of 25 mg emulsifier per gram emulsion were prepared by diluting the polysorbate sample with water and diluting Span 80 with the paraffin oil and mixing them in varying proportions, with stock A yielding a HLB of 12.33 and stock B yielding a HLB of 6.98, respectively. Stocks were homogenized for 2 minutes after addition of a small amount of methylene blue. A series of emulsions were prepared from stocks, bracketing the RHLB by weighing each stock emulsion into a 15 mL centrifuge tube to yield a total amount of 10 g emulsion. Tubes were shaken to ensure mixing, centrifuged at 4000 r.p.m. for 20 minutes and stored at room temperature. After 15 days, the heights of the aqueous phase were measured and the HLB value of the emulsion showing the least phase separation was recorded as the RHLB value, from which the PS80 HLB value was calculated.

Static light scattering

All static light scattering experiments were conducted at 23 °C using a CGS-3 MD Goniometer (ALV, Langen, Germany). The laser light source was a He-Ne laser operating at $\lambda = 632.8$ nm. All measurements were collected at scattering angles in the range of 30° - 150° using 8 separate detectors. Serial dilutions of the PS80 samples in the concentration range between 1 and 5 g/L were freshly prepared and filtered through a 0.22 µm PVDF syringe filter (Carl Roth, Karlsruhe, Germany) prior to use. The refractive index increment of the sample dilutions was measured using a SEC-3010 refractometer (WGE Dr. Bures, Dallgow-Doeberitz, Germany). The micelle molecular weight and the second virial coefficient were calculated by means of the multiangular Zimm-Plot using ALV-Fit & Plot software.

HPLC-CAD

Fatty acid composition and free fatty acid content were determined by high performance liquid chromatography with charged aerosol detection as described by Ilko et al. [22]. In brief, following hydrolysis with 1 M potassium hydroxide solution, the fatty acids were extracted with methyl-*tert.*-butylether (MTBE) modified from a previous protocol [29]. For the determination of free fatty acids, heptadecanoic acid was used as internal standard and mixed with the samples and MTBE followed by centrifugation and collection of the organic phase. Measurements were performed with a 1100 HPLC system (Agilent, Waldbronn, Germany) and a Kinetex C18 (100 x 3.0 mm, 2.6 µm particle size) analytical column (Phenomenex, Aschaffenburg, Germany). A gradient was applied (mobile phase A being 0.05 % formic acid in water, and mobile phase B being 0.05 % formic acid in acetonitrile) starting with 75 % mobile phase B for 5 minutes followed by a linear increase to 85 % within 10 minutes at a flow rate of 0.6 mL/min. Detection was performed with a Corona charged aerosol detector (Thermo Scientific, Idstein, Germany) using a gas inlet pressure (nitrogen) of 35 psi and settings set to no filter at an electric current range of 100 pA.

Fingerprint analyses

Fingerprinting was performed as described before with modification [30]. The separation was carried out on an LC1100 (Agilent) using a Kinetex C18 (100 x 3.0 mm, 2.6 µm particle size) analytical column. Mobile phase A consisted of 0.1% (v/v) formic acid in water and mobile phase B of 0.1% (v/v) formic acid and 5% water in acetonitrile. A gradient was used increasing the portion of mobile phase B from 10 to 100% within 12 min and holding this for further 12 min. The flow rate was 0.6 mL/min and the injection volume 10 µL. A CAD was used for detection with following settings: range: 100 pA, filter: “none”.

Peroxide value

Peroxide content was determined using a peroxide quantification kit (Pierce Quantitative Peroxide Assay Kit, Thermo Scientific, Rockford, USA). Samples were diluted with water to 2 % (w/v). 20 µL of the diluted samples were mixed with 200 µL of the reagent (250 µM ammonium ferrous(II) sulfate, 125 µM xylenol orange, 100 µM sorbitol in 25 mM sulfuric acid), incubated for 20 minutes at room temperature prior to reading at λ = 595 nm on a SPECTRAmax 250 automated microtiter plate reader (Molecular Devices, Sunnyvale,

USA). Hydrogen peroxide was used to prepare standard curves and peroxide levels in polysorbate 80 were obtained as peroxide equivalent to the hydrogen peroxide concentration.

Statistics

Comparisons were performed using one way ANOVA and normality was tested according to Shapiro-Wilk. *Post hoc* test was performed according to Tukey (pairwise comparison). The statistical software Minitab® 16 (Minitab, Coventry, UK) was used for analysis. Statistically significant results were concluded for $p < 0.05$ (the use of the term "significant" is exclusively used in a statistical way within the manuscript). Results are displayed as mean with standard deviation (SD) and measurements were in triplicate, unless otherwise noted. Linear models were derived, analyzed and plotted using the statistical framework R and associated packages.

Results

Critical micelle concentration, cloud point, and hydrophilic–lipophilic balance values

Sixteen PS80 samples from 4 suppliers (including two different qualities of one supplier, which are for simplicity categorized as if from two suppliers) were assigned A – E and numbers indicate the different batches from the respective supplier (e.g. E1 – E3 are three different batches from E). Structural formulas are provided for polysorbate 80 and relevant molecules referred to within this manuscript (**Figure 1**).

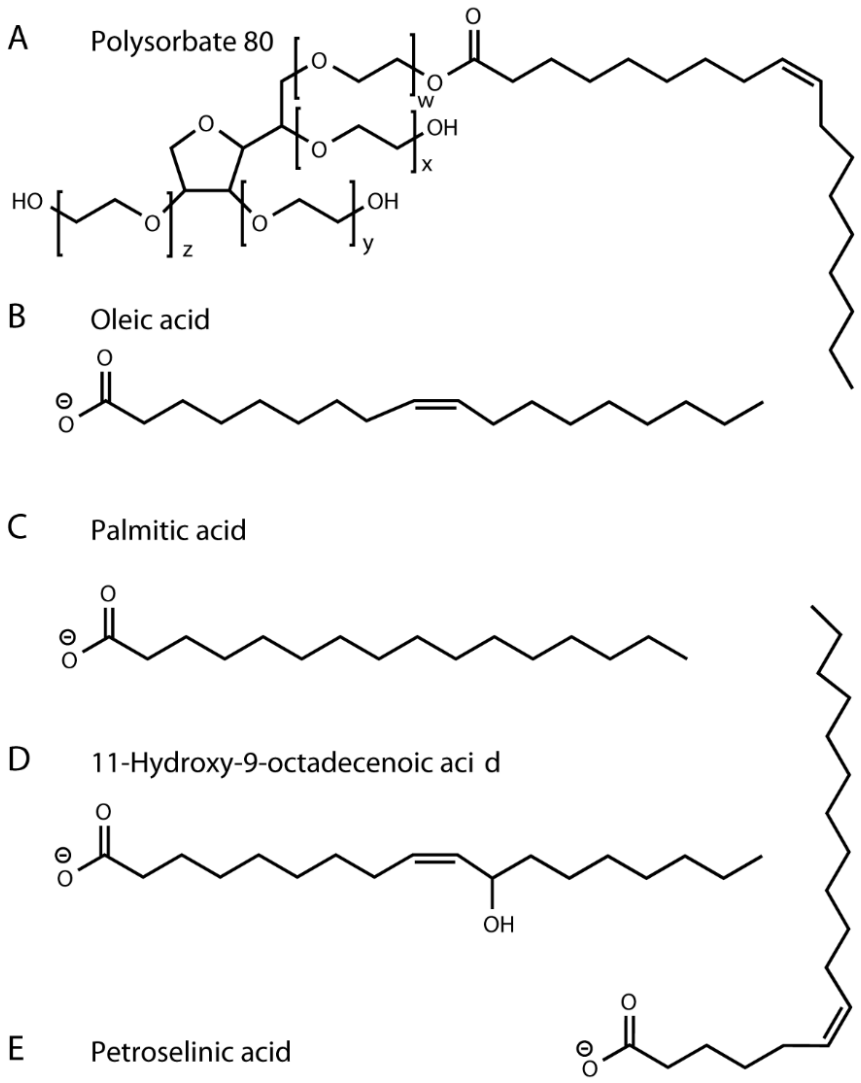

Figure 1: (A) Main structure of Polysorbate 80, (B) structure of oleic acid, (C) structure of palmitic acid, (D) structure of 11-hydroxy-9-octadecenoic acid, (E) structure of petroselinic acid.

The batches were sorted according to CMC outcome, covering a range from 13.4 ± 0.6 mg/L to 24.7 ± 1.4 mg/L (**Figure 2A**). Batches E1 – E3 clustered at a low CMC range and were significantly lower as compared to all other samples apart from A1. Batches B1 – B3 were significantly different as compared to batches E1 – E3, or A4. C3 was significantly higher as compared to C1 and C2 and D1 was significantly lower as compared to D2 and D3. Therefore, significant within-quality differences were observed for A, C, and D but not for B and E.

A similar distribution was observed for the results of the cloud point measurements (**Figure 2B**) covering a range from 56.0 ± 0.2 °C to 65.3 ± 0.4 °C with the majority of samples ranging from 59.8 °C to 61.4 °C. Quality E was significantly higher as compared to all other qualities other than sample A1. Quality A had a high variability ranging from 56.0 ± 0.2 °C to 64.3 ± 0.1 °C, whereas qualities B and C had a narrow distribution in the range of 60.7 ± 0.2 °C to 61.2 ± 0.2 °C and 60.4 ± 0.2 °C to 61.1 ± 0.1 °C, respectively. Within-batch variability was observed for qualities D and E (one batch being significantly different compared to the other two) and A (all batches differed significantly from each other) but no differences among samples as observed within B and C.

Cloud points determined by the turbidimetric method (**Figure 2B**) correlated strongly with cloud point assessment by calorimetric measurements

$$Tc_{turbidimetric}[°C] = 0.89 * Tc_{calorimetric}[°C] + 4.4$$

($r^2 = 0.95$; **Supplementary Figure 1A and B**) and were consistently found 2 °C above those measured by the turbidimetric method, likely due to pressure differences (turbidimetric method was performed under isobaric while the calorimetric method was performed under isochoric conditions, respectively).

HLB values scattered within 14.4 to 15.6 with the majority of the batches scattering within a range from 14.5 to 15.1 (n = 1; **Figure 2C**). Outcome from E suggested clustering of HLB values exceeding 15.0, in contrast to the other qualities which clustered below that threshold. A linear correlation following

$$CMC\ \left[\frac{mg}{L}\right] = -1.25 * Tc_{turbidimetric}\ [°C] + 95\ (r^2 = 0.79)$$

was observed between CMC and cloud point (**Figure 2D**).

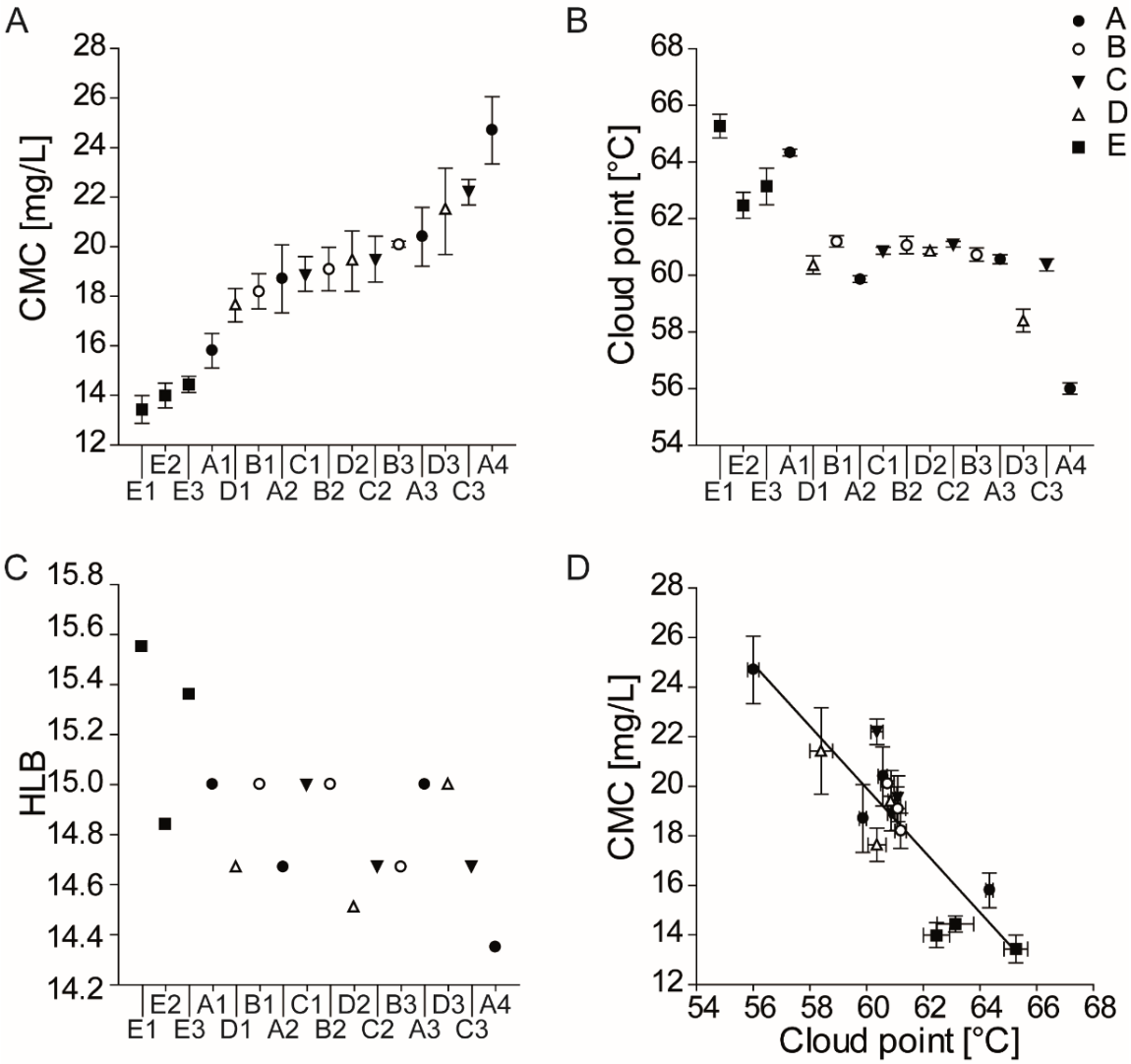

Figure 2: (A) Critical micelle concentration (CMC) [mg/L], and (B) cloud point [turbidimetric; °C] of the different batches. (C) Hydrophilic-lipophilic balance (HLB) of the different batches (n = 1). (D) Correlation of CMC and cloud point. Please note that axes do not start at zero.

We correlated HLB with CMC and cloud point for the reason that these physicochemical parameters reflect the amphiphilic structure of the surfactant and the variability in the hydrophilic or lipophilic moieties may impact both parameters [31-34]. Linear regression of CMC over HLB and cloud point over HLB demonstrated a poor correlation when fitted linearly (r^2 = 0.47; **Supplementary Figure 1C** and r^2 = 0.51; **Supplementary Figure 1D**), however, demonstrating a relationship among these parameters.

Impact of supplier/quality and storage on critical micelle concentration and peroxide value

The CMC of batches from A scattered widely (**Figure 3A**) in contrast to qualities B and more strongly E. The CMC of E was significantly lower as compared to all other qualities. Generally, no trend (increase or decrease) in CMC was recorded with storage time (**Figure 3B**). For example, E1 – E3 (covering storage of 6 to 18 months) were not significantly different in CMC whereas – in spite of identical storage times – batches A3 and A4 differed significantly.

Peroxide values of the polysorbate batches were determined at the same time when all experiments were conducted (and do not reflect values as provided from manufacturers at the time of release at which all batches complied with specifications of the monograph at ≤ 10 ppm according to the certificates of analyses [4]; **Figure 3C**; **Table 1**). 5 batches exceeded 10 ppm (**Figure 3C**). Generally, the peroxide values of the different batches covered a range from 2.9 to 21.2 ppm with storage times of 6 to 31 months. The highest peroxide values were observed for batches B1 – B3 (16.1 – 21.2 ppm) and A4 (16.5 ppm). Interestingly, no impact of storage time on peroxide value was detected (**Figure 3D**), with e.g. low-peroxide batches C1 and C2 being stored for 27 months in contrast to high-peroxide-batches B1 and B2 being stored within 17 to 20 months.

Peroxide value variability was strikingly different among suppliers, with C, and D, displaying low, A and E intermediate and B high variability, respectively (**Figure 3E**).

A correlation between oleic acid content and CMC was apparent (**Figure 3F**). However, 4 batches clearly deviated from the linearity and all these did not comply with the compendial specifications for peroxide value (≤ 10 ppm) and the relationship is further analyzed in more detail (*vide infra*). A potential trend of increasing peroxide value with elevated amount of polyethoxylate diesters may be postulated (**Supplementary Figure 3E**). At this point we concluded that oleic acid and peroxide value may be instrumental input parameters for model building of a predicted CMC.

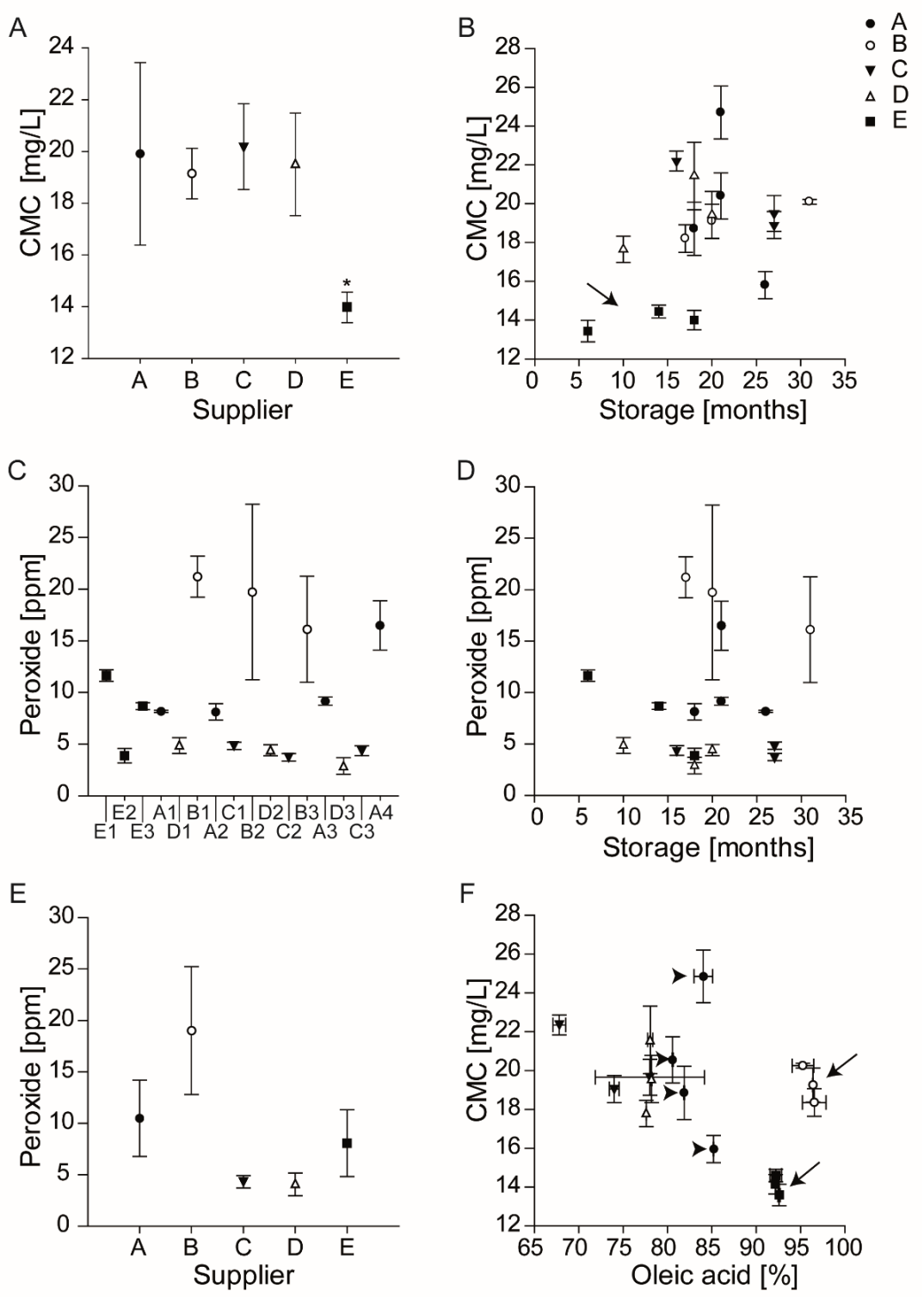

Figure 3: (A) Critical micelle concentration [mg/L] as a function of the supplier/quality. (B) CMC as a function of months of storage. (C) Peroxide value [ppm] of the different batches. (D) Peroxide value [ppm] as a function of months of storage. (E) Peroxide value [ppm] as a function of the supplier/quality. (F) Correlation of CMC with the content of oleic acid [%; after hydrolysis]. Arrows in (B) and (F) highlight the low outcome variability of batches E1 – E3 in spite of different storage times (B) or oleic acid content (F). Arrowheads in (F) indicate supplier A which in spite of a narrow distribution of oleic acid content displays large variability in CMC.

Impact of the PS80 chemical batch composition on CMC

Following hydrolysis, the fatty acid composition of all batches was analyzed by HPLC-CAD (**Table 2**). The monographs request oleic acid contents of at least 58 % upon hydrolysis [4]. The content of oleic acid complied with compendial specifications for all batches and ranged from 67.8 ± 0.7 % to 96.6 ± 1.3 % (**Figure 3F**), representing differences of up to 30% among batches. HPLC-CAD analyses were also conducted on non-hydrolyzed (i.e. crude) PS80 samples, referred to as "free acid" in this manuscript ([15, 22, 35], **Supplementary Figure 2A**). A general trend of increasing CMC with increasing free fatty acid content was observed (**Supplementary figure 2B**). Batches from B and E had a significantly lower free fatty acid content as compared to the other qualities, and variability was strikingly low for B, D, and E and in contrast to A and C (**Supplementary Figure 2C**). Storage did not impact the amount of free fatty acids (**Supplementary Figure 2D**).

Besides free fatty acid composition and fatty acid composition upon hydrolysis, the content of unesterified PEG/sorbitan polyethoxylates (peaks are reported together), sorbitan- and isosorbide polyethoxylate mono- and diesters, as well as polyoxyethylene diesters, was followed by "fingerprinting" analyses (**Supplementary Figure 3A – D).** Among qualities, some differences were observed especially in content of free PEGs and sorbitan polyethoxylates. For example, batches of E were low in terms of free PEGs and sorbitan polyethoxylates (**Supplementary Figure 3A).** Polyethoxylate-fatty acid diesters were found in batches of qualities A and B but only in selected batches of the other qualities (**Supplementary Figure 3D).** None of these parameters alone (unesterified PEG/sorbitan polyethoxylates, sorbitan-, isosorbide polyethoxylate mono- and diesters, polyoxyethylene diesters) correlated with CMC or peroxide value.

Table 2: Fatty acid composition of the PS80 batches after hydrolysis and liquid–liquid extraction (n=3).

Supplier/ quality	Batch	Petro-selinic acid [%]	Linoleic acid [%]	Palmi-toleic acid [%]	Stearic acid [%]	Palmitic acid [%]	Oleic acid [%]	Hydroxy oleic acid [%]
A	1	0.82	6.58	0.76	1.24	5.40	85.22	0.00
A	2	1.20	9.59	0.52	1.40	5.38	81.92	0.00
A	3	1.00	10.13	0.79	1.65	5.83	80.61	0.00
A	4*	1.20	6.80	0.60	1.62	5.74	84.08	0.00
B	1	0.00	0.00	0.00	0.38	0.82	96.58	2.24
B	2	0.00	0.00	0.00	0.48	1.01	96.44	2.08
B	3	0.00	0.00	0.00	0.35	0.67	95.29	3.69
C	1	1.03	9.44	0.64	2.72	12.16	74.05	0.00
C	2	0.87	7.10	0.49	2.94	10.56	78.04	0.00
C	3*	2.65	10.74	0.66	3.55	14.58	67.84	0.00
D	1	0.28	11.34	0.00	2.04	8.25	77.65	0.45
D	2*	0.33	11.55	0.00	1.86	7.52	78.24	0.50
D	3	0.25	11.79	0.00	2.01	7.38	78.09	0.54
E	1*	1.16	1.06	0.00	2.66	2.53	92.62	0.00
E	2	1.03	0.00	0.00	3.08	2.99	92.21	0.70
E	3	0.96	0.00	0.00	2.80	2.41	92.25	1.60
Specification Ph.Eur (8th Edition)		Not specified	≤ 18.0%	≤ 8.0%	≤ 6.0%	≤ 16.0%	≥ 58%	Not specified
Specification USP 37 NF 32								

* Data were previously reported [22] and are repeated.

Impact of supplier, critical micelle concentration, or fatty acid composition on micelle molecular weight (MM_w)

MM_w was characterized for selected batches (**Figure 4A**), covering a range from 111.2 to 126.8 kDa (n = 1) and the highest MM_w was observed for batches C1 and B2. Substantial differences for MM_w were observed within all qualities apart from supplier/quality E. MM_w was correlated with oleic acid content (**Figure 4B)**. In spite of a low variability in the oleic acid composition within qualities, substantial differences in MM_w were found other than for E. In summary, oleic acid content alone is not adequately predicting MM_w outcome (**Figure 4B**). However, the pattern of variability as identified by the CMC (**Figure 3A**) was also reflected by the MM_w (**Supplementary Figure 4A and B**). The static light scattering experiments with which the MM_w was determined were also used to calculate the second

virial coefficient (B_2) of the batches (**Supplementary Figure 4C**) and no correlation was found to any of the parameters mentioned above (data not shown).

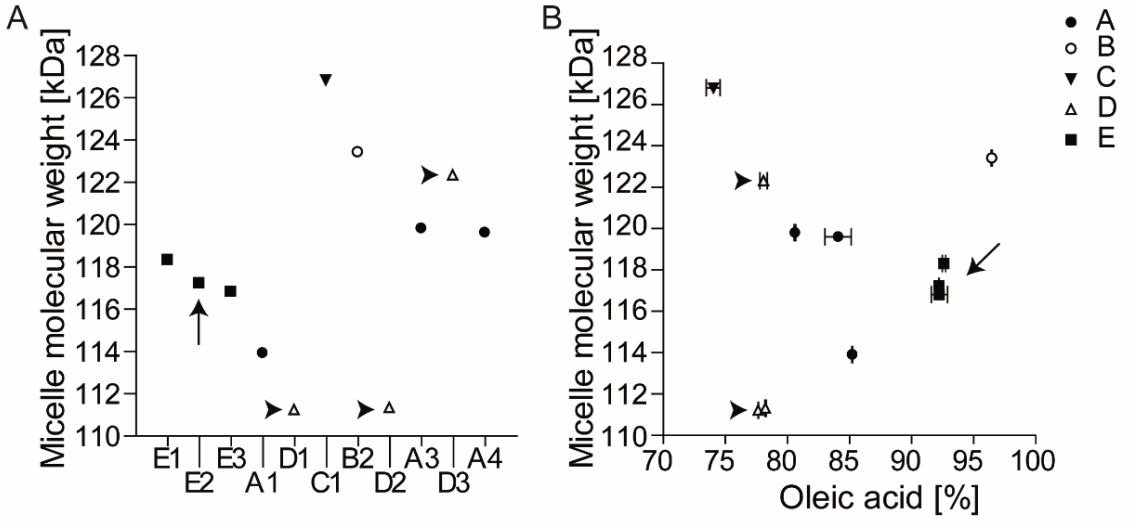

Figure 4: (A) Micelle molecular weight [kDa] as a function of different batches. (B) Correlation of micelle molecular weight with oleic acid content [%; after hydrolysis]. Arrows highlight the low outcome variability in (A) within quality E and for the correlation of micelle molecular weight with (B) oleic acids, respectively. Arrowheads (A and B) indicate supplier D which in spite of a narrow distribution of unsaturated fatty acid content displayed large variability in micelle molecular weight.

Model building for the prediction of CMC and MM_w by the input parameters fatty acids, fingerprint data and peroxide value

Our general inability to reliably predict CMC and MM_w as galenical parameters for PS80 performance by individual values (*vide supra*) prompted us to combine all input parameters for model building (**Figure 5; Table 3**). On the basis of outcome from all batches, a valuable prognostic model was built for CMC by use of oleic acid content and peroxide value (**Figure 5A**). Both of these input parameters are specified in the compendial monographs. These results demonstrated that once both parameters were used in combination, a prediction of CMC is possible. They also demonstrated that independent use of these parameters - as currently done- did not necessarily control CMC. A second model using data obtained from all batches proved valuable deploying the amount of polyoxyethylene diesters as additional input parameter (**Figure 5B**), thus refining the model based on peroxide value and oleic acid content alone (**Figure 5A**). Complicated models using more than four factors are not presented here due to their complexity likely rendering them useless in daily practice but are reported (**Supplementary figure 5A**).

Table 3: Glossary (Input or output parameters for models are highlighted in bold)

Parameter	Method of measurement	Impact on a model
Critical micelle concentration (CMC, [mg/L])	Surface tension measurement	Output parameter for models 1 - 3 (**Figure 5A - C**); Input parameter for model 4 (**Figure 5D**)
Cloud point [°C]	Turbidimetric / calorimetric measurement	[d]
Hydrophilic-lipophilic balance (HLB)	Stability evaluation on emulsion series	[e]
Micelle molecular weight (MM_W; [kDa])	Static light scattering	Output parameter for model 4 (**Figure 5D**)
Second virial coefficient (B_2,[mol*L/g^2])	Static light scattering	[e]
Peroxide value [ppm]	FOX Assay (colourimetric)	Input parameter for models 1 and 2 (**Figure 5A - B**)
Oleic acid content [%]	Fatty acid composition determined after hydrolysis (according to monograph) using HPLC-CAD [22]	Input parameter for models 1 – 3 (**Figure 5A - C**)
Hydroxy-oleic acid [%][a]		Input parameter for model 4 (**Figure 5D**)
Palmitic acid content [%]		[c]
Stearic acid content [%]		[c]
Palmitoleic acid content [%]		[c]
Linoleic acid content [%]		[c]
Petroselinic acid content [%][b]		**-**
Free fatty acids [%]	HPLC-CAD analysis on crude (non-esterified) material	[c]
Free PEGs and sorbitan-polyethoxylates [%]	Fingerprint analyses using HPLC-CAD [30]	[c]
Sorbitan- and isosorbide-polyethoxylate monoesters [%]		Input parameter for model 4 (**Figure 5D**)
Sorbitan- and isosorbide-polyethoxylate diesters [%]		Input parameter for model 4 (**Figure 5D**)
Diester-polyethoxylates [%]		Input parameter for model 2 (**Figure 5B**)

[a] Oxidation product of Oleic acid (**Figure 1D**);
[b] Double bond positional isomer to oleic acid (**Figure 1E**)
[c] Had no significant impact on model (**Supplementary Figure 5**)
[d] Was not used as an output parameter due to the correlation with CMC.
[e] Could not be predicted by a model based on the input parameters addressed here within.

In a second set of model building for the prediction of CMC, we restricted the analysis to batches which complied with the release specifications of the pharmacopeias for peroxide values. Thereby, we excluded data from batches E1, B1 – B3 and A4 due to the peroxide values exceeding 10 ppm (as specified by the monographs). Interestingly, the 10 ppm value specification for peroxide content was sufficient to allow building of a valuable model with a single input parameter - oleic acid content – yielding a precise prediction of CMC (**Figure 5C**).

In more detail, the first model (**Figure 5A**) was

$$CMC\ [mg/L] = \ 48.2 - 0.4 * c(oleic\ acid[\%]) + 0.5 * c(peroxides\ [ppm])$$

(n = 16; r^2 = 0.66; F = 12.4; model built with data from all batches; these and the following factors were rounded). In this model, all parameters were significant ($p < 0.01$).

The second model was built from the same batches/samples and included 3 parameters as of

$$CMC\ [mg/L] = 52.1 + 0.8 * c(polyoxyethylene\ diesters\ [\%]) - 0.4 * c(oleic\ acid\ [\%]) + 0.3 * c(peroxides\ [ppm])$$

(n = 16; r^2 = 0.74; F = 11.3; **Figure 5B**).

By involving polyoxyethylene diester content as additional parameter, the correlation resulted in increased accuracy (r^2 = 0.74 as compared to r^2 = 0.66) with comparable F value, indicating that the additional parameter and the associated increase in r^2 did not negatively impact the F value, as the evidence that the extended model did not result in overfitting (F = 11.3 compared to F = 12.4 for the first model with 2 parameters). The level of significance for polyoxyethylene diester content ($p < 0.1$) was lower as compared to the two parameters, peroxide value and oleic acid content ($p < 0.05$).

For model building using readouts from batches complying with compendial specifications for the peroxide value (≤ 10 ppm), a (surprisingly) simple model was adequate as of

$$CMC\ [mg/L] = 44.6 - 0.3 * c(oleic\ acid\ [\%])$$

(n = 11; r^2 = 0.77; F = 29.6; **Figure 5C**).

Oleic acid was a highly significant input parameter for the model ($p < 0.001$). Therefore, the specification by the monograph for the peroxide value at 10 ppm was sufficient to render the model independent of peroxide content (**Supplementary figure 5B**).

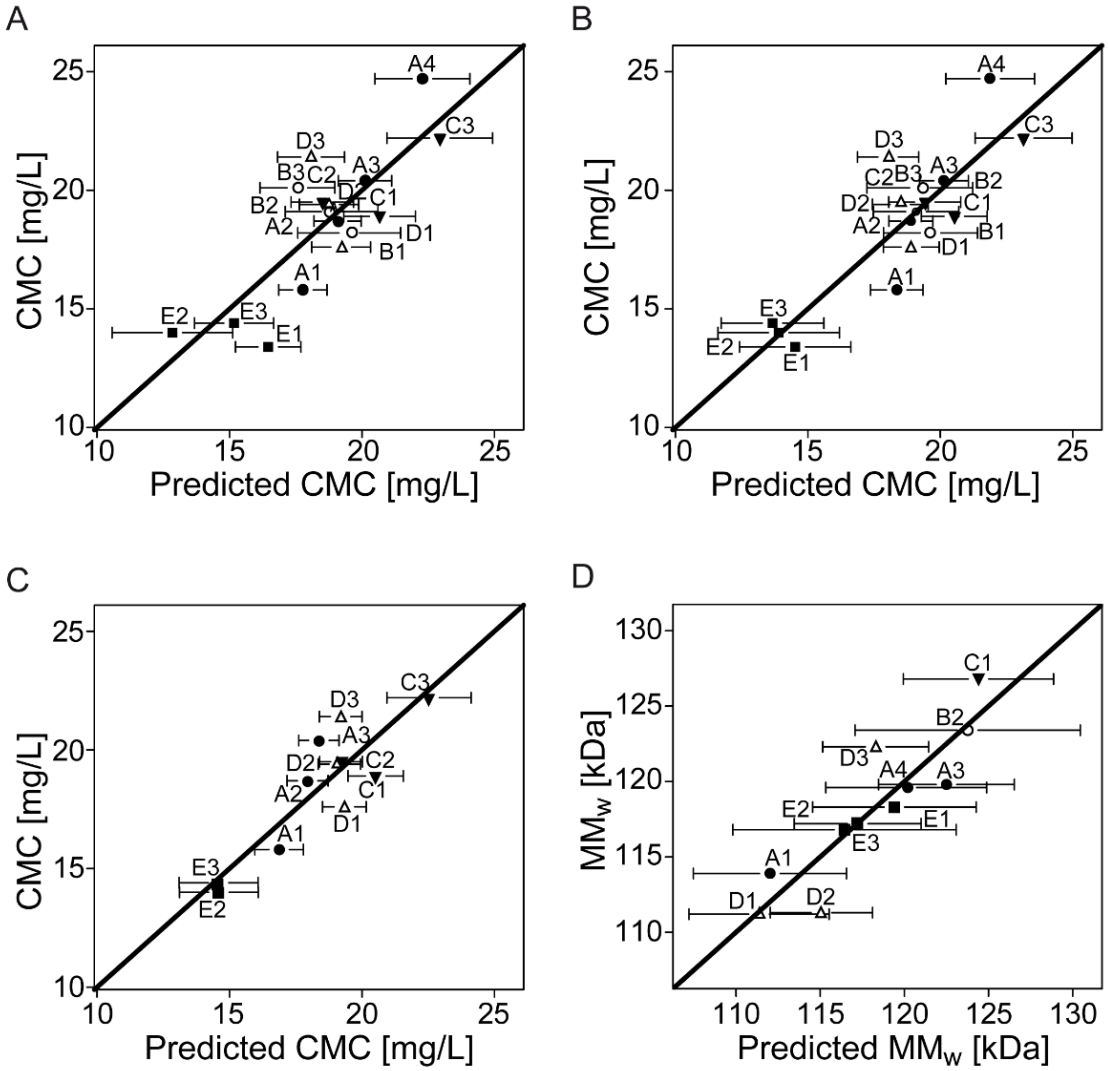

Figure 5: (A) Measured CMC [mg/L] versus predicted CMC [mg/L] including 90% confidence intervals calculated by oleic acid content and peroxide value for the complete data set from all batches (r^2 = 0.66) and (B) with oleic acid content, peroxide value and amount of polyoxyethylene diesters for the complete data set from all batches (r^2 = 0.74) and (C) with oleic acid content alone for reduced data (excluding batches not complying with compendial specifications for peroxide value; r^2 = 0.77). (D) Measured MM_w [kDa] versus predicted MM_w [kDa] calculated by CMC, hydroxy-oleic acid content, amount of sorbitan- and isosorbide-polyethoxylate monoesters and sorbitan- and isosorbide-polyethoxylate diesters (r^2 = 0.80). Please note that axes do not start at zero.

The CMC as measured input parameter also proved suitable for the prediction of the molecular micelle weight of PS80. For the prediction of MM_w, building of a valuable prognostic model required 4 parameters (**Figure 5D**). By using the experimental CMC in combination with hydroxy-oleic acid content, amount of sorbitan- and isosorbide-polyethoxylate monoesters and sorbitan- and isosorbide-polyethoxylate diesters,

MM_w was predicted by

$$MM_w\ [kDa] = 91.4 + 1.4 * CMC\left[\frac{mg}{L}\right] - 0.7 * c(Monoester\ [\%]) + 1.7 * c(Diester\ [\%]) + 5.4 * c(hydroxy - oleic\ acid\ [\%])$$

(n = 11; r^2 = 0.80; F = 5.9; **Figure 5D**). In this model, all parameters were significant ($p < 0.05$). Again, even more complicated models were not reported in detail here but are provided (**Supplementary figure 5C**).

Discussion

Striking physical, geometrical and chemical differences were observed among batches (in spite of complying with specifications), with some qualities (e.g. E) demonstrating significantly lower variability in outcome than others (e.g. **Figure 3A**). The supplier variability in CMC was neither a function of storage time nor predicted by one chemical parameter in isolation such as free fatty acid content (**Supplementary Figure 2**). As a result, one may conclude that a careful selection of the supplier is perhaps the most important parameter impacting the quality of PS80 containing formulations, and presumably at least as important as storage conditions or storage time at the supplier or the end user. The demonstrated homogeneity in chemical and physical properties e.g. observed for E suggested that refined manufacturing and purification processes lead to controlled physicochemical properties and overall low variability among all parameters tested. However, a pharmaceutical manufacturer likely resists to rely on the supplier alone; instead one requires reliable and standardized methods to internally control/predict PS80 quality. The challenge in the previous sentence is the term "standardized methods". For example, batches of quality A – demonstrating significant variability in chemical and physicochemical features – can be adequately controlled if additional release specifications are set on outcome from cloud point or CMC measurements, respectively. However, neither CMC, nor cloud point, nor static light scattering are compendial methods (Ph.Eur; light scattering is mentioned in method <851> of the United States Pharmacopeia (USP) [5]). It is easier for the manufacturer and supplier alike if specifications are set on methods known by the pharmacopeias. We studied the possibility to use compendial methods for the control over the CMC (with CMC serving as the surrogate to address functionality related characteristics (FRC) as it correlated with other physical parameters including cloud point (**Figure 2D**), HLB (**Supplementary figure 1C**) but not readily detectable to MM_w (**Supplementary Figure 4A**).

Surprisingly simple models were built, allowing easy implementation in manufacturers' and suppliers' laboratories. One of the models suggested, that if the peroxide value does not exceed 10 ppm (the specified threshold in the monographs), oleic acid content alone is sufficient and appropriate in predicting CMC outcome (**Figure 5C**). Hence, for those batches matching peroxide value specifications, precise determination of oleic acid content correlates with sufficient prediction of the CMC. An illustration is provided to demonstrate the potential use of the models outlined here within. For example, batches E2 and C3 complied with compendial specifications regarding the peroxide value (3.9 versus 4.4 ppm, respectively; **Table 1**). Consequently, the model described as of $CMC\ [mg/L] = 44.6 - 0.3 * c(oleic\ acid\ [\%])$ (**Figure 5C**) would be selected for the prediction of the CMC and resulted in 17 mg/L and 24.5 mg/L for E2 and C3, respectively, with a difference of 7.5 mg/L among batches. Experimental data indicated a mean CMC of 14 mg/L and 22 mg/L for E2 and C3, respectively (**Figure 2A**), hence a difference of 8 mg/L. The intercept with the ordinate as of 44.6 mg/L indicated, that extrapolation of the model outside the design space assessed here within might be misleading whereas prediction within the range used for model building was robust (67.8–96.6%, **Table 2**). Possibly, the model can be extended to the specification limit of 58% provided by the current monograph but more data are required to substantiate this extrapolation. This also corroborated the excellent compendial choice of 10 ppm for the peroxide value, not only from the perspective of oxidative stress on API/excipients, but also from a galenical perspective. Another conclusion is that the oleic acid content was linked to the respective CMC by a factor of 0.3. Therefore, batches complying with compendial specifications (range as of 58% to perhaps practically less than 98% leading to a difference as of maximally 40%) have predicted differences in CMC up to 12 mg/L (and accepting the extrapolation of the model to 58% as outlined above). The model built on outcome from all batches (including those with peroxide values ≥ 10 ppm), required the peroxide value as input parameter along with oleic acid content (**Figure 5A**). Therefore, we conclude that CMC (as a surrogate for FRCs) can indeed be adequately predicted by current compendial methods. We also conclude, that once peroxide values comply with compendial specifications (≤ 10 ppm), oleic acid content alone (for which a compendial method is described) is sufficient to control FRCs of polysorbate 80 with respect to micelle related processes / CMC.

In each model, oleic acid concentration in batches was negatively correlated with CMC. Thermodynamic considerations may help to approach the fundamentals of this observation.

To assess the effectiveness of a surfactant, the free enthalpy balance between two processes may be discussed (i) of micelle formation and (ii) the migration of surfactant molecules from the bulk into interfaces [31-34]. One potential model is that during the process of micelle formation, the polar head groups of the surfactant remain in the polar environment of the aqueous environment (changes before and after micelle formation are negligible), whereas the hydrophobic chains get in close contact with each other (driving the change). Therefore, the change in Gibb's free enthalpy – as a result of micelle formation – is mainly from the new hydrophobic environment and due to the arrangement of the hydrophobic tails within the spherical micelles. A possible entropy change due to arrangement of these tails within the micelles is ignored in this consideration as is any effect of changes of solvent molecule arrangements as a result of micelle formation. The adsorption at the interface/surface follows similar considerations as for micelles, but the hydrophobic element of the surfactant in the interface is between two phases and not within a micelle. Therefore, the packaging of the hydrophobic tail is different (like staked palisades) and likely more arranged as compared to the spherical micelles. The higher the degree of order the lower is the respective Gibb's free enthalpy. In addition, the difference of the free enthalpies of the micelle formation process and the adsorption at the interfaces, respectively, directly correlates to the logarithm of the quotient of the CMC and C_{20} [36]. C_{20} is the concentration of the surfactant yielding a reduction of the surface tension by 20 mJ/m² starting off the pure solvent (C_{20}; << CMC for polysorbate 80). C_{20} – a measure for the efficiency of a surfactant – is presumably less impacted by structural changes as a result of oleic acid content differences among batches, as C_{20} relevant events are at concentrations by far lower than the CMC (but typically in the area in which the maximal surface excess Γ_{max} has already been reached in all experiments). To this point we assume, that enthalpic terms can be neglected (as suggested before [2]), that C_{20} as a characteristic for surfactant efficiency is equivalent among batches and, that entropy changes to the surrounding solvent molecules can be ignored. Based on these assumptions, one may speculate that the impact of "kinked" oleic acid (**Figure 1**) on the molecular order can be higher in the more ordered interface as compared to the less ordered micelles. In other words, the potential of the "kinked" structure to more effectively induce disorder in the relatively more ordered surface of the interface as compared to the (generally less ordered) micelle would explain a difference in entropy among batches with high *versus* low oleic acid content and as detailed (**Table 2**). Under these assumptions (*vide supra*), the indirect correlation of oleic acid content and CMC would be partially explained. Obviously, the

assumptions above reflect the simplicity of this explanation and the lack of required experiments to substantiate our explanation. With peroxide value being a parameter impacting many possible events within polysorbate 80 batches, we refrain from linking this to basic considerations based on the data set reported here within and leave this observation at an empirical level. Previous attempts have linked autoxidation to degradation products (generation of short chain ethoxylates), and linking the surface activity of these impurities / degradation products to differences in CMC [37].

The model was further refined by integrating the next parameter, the amount of polyethylene glycol diesters (**Supplementary Figure 5**). The more complex model corroborated the negative correlation for oleic acid with CMC and positive correlation of peroxide value with CMC while in addition suggesting a positive correlation for polyethylene glycol diesters. Manufacturers are also confirmed by these models in their strong effort to control peroxide values until use, as the strong impact of this input parameter was again demonstrated in this multifactorial model. Lastly, a model was postulated for the prediction of the micelle molecular weight (MM_w). The correlation of MM_w with CMC alone was weak, with the model indicating that higher CMC may result in an increase in MM_w (**Supplementary Figures 5C** and **4A**). Notably, this model indirectly confirmed the predictive value of peroxide value and oleic acid content for the CMC. Similarly, the model suggested that fatty acid monoesters correlate negatively, while fatty acid diesters and hydroxy-oleic acid correlated positively.

Conclusion

Our data demonstrated that PS80 batches in spite of complying with compendial specifications demonstrated high variability in physical characteristics, as described by CMC, cloud point, HLB, and micelle molecular weight, respectively. The pharmaceutical manufacturer should translate this insight in that complying with compendial specifications alone may not necessarily yield reliable galenical outcome in instances in which a high reproducibility e.g. of CMC is desired. Homogenous outcome among batches is key in controlling PS80 quality, as demonstrated. Surprisingly, functionality related characteristics (FRC) – as demonstrated for CMC as a surrogate for micellar processes – were excellently predicted by oleic acid content alone, when the analysis was restricted to batches complying with compendial specifications for the peroxide values (≤ 10 ppm). Another conclusion from our data is that compendial specifications are elegantly set for peroxide value and oleic acid

content and no changes in the current specifications are needed based on the data reported here within.

Acknowledgments

We thank Stefanie Munzert and Prof. Dr. Dirk Kurth (Chair of Chemical Technology of Materials Synthesis, University of Wuerzburg) for their help with static light scattering measurements and data analyses. This research was supported by the Bavarian Research Foundation (BFS; Program Formosa) and SFB630. None of the authors stated a conflict of interests.

Supplementary information

Supplementary figures:

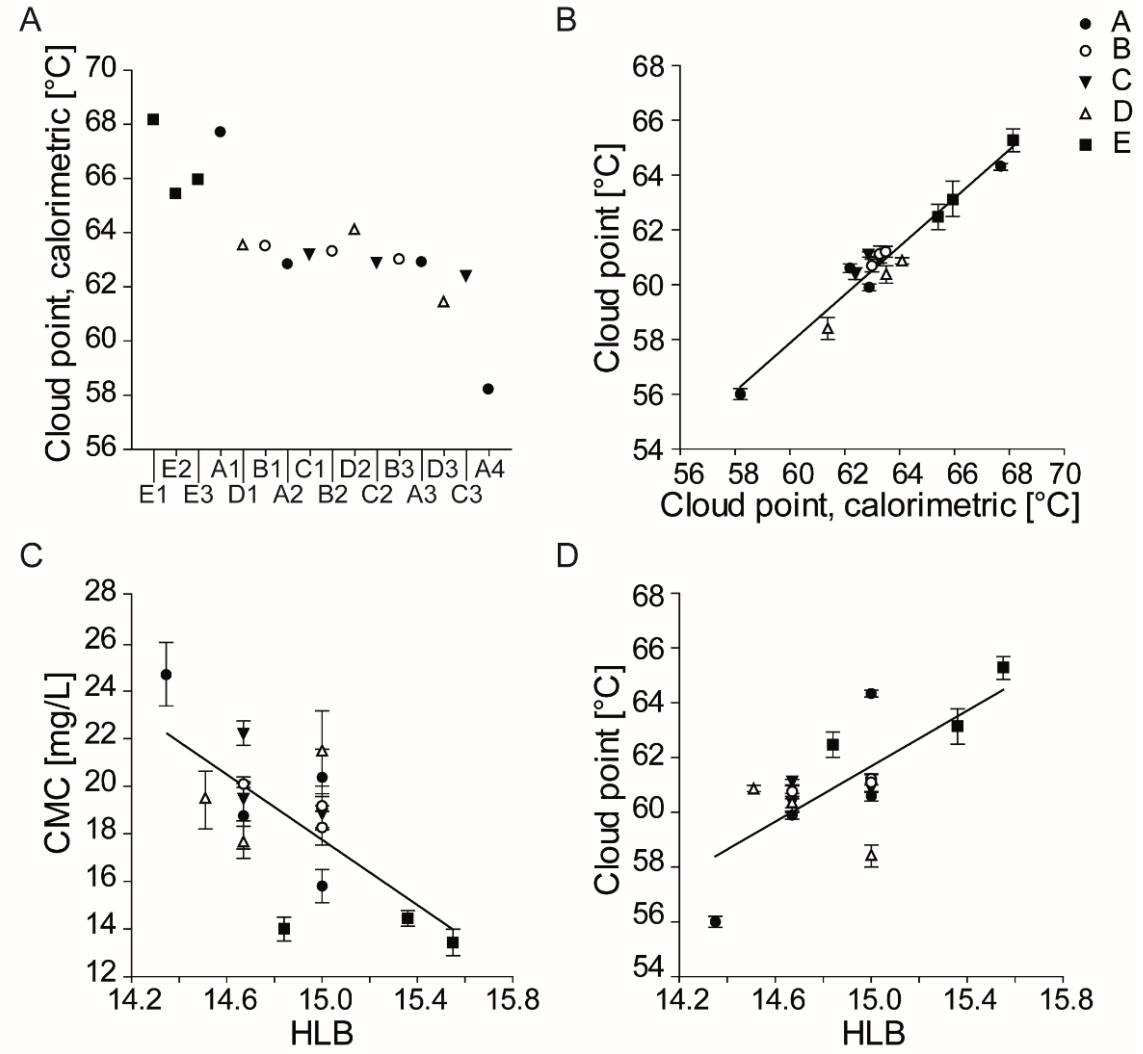

Supplementary figure 1: (A) Cloud point [calorimetric; °C] as a function of different batches. (B) Correlation of cloud point measured by the turbidimetric method [°C] and cloud point determined by calorimetric measurement [°C]. (C) Correlation of CMC and HLB. (D) Correlation of cloud point [turbidimetric; °C] and HLB.

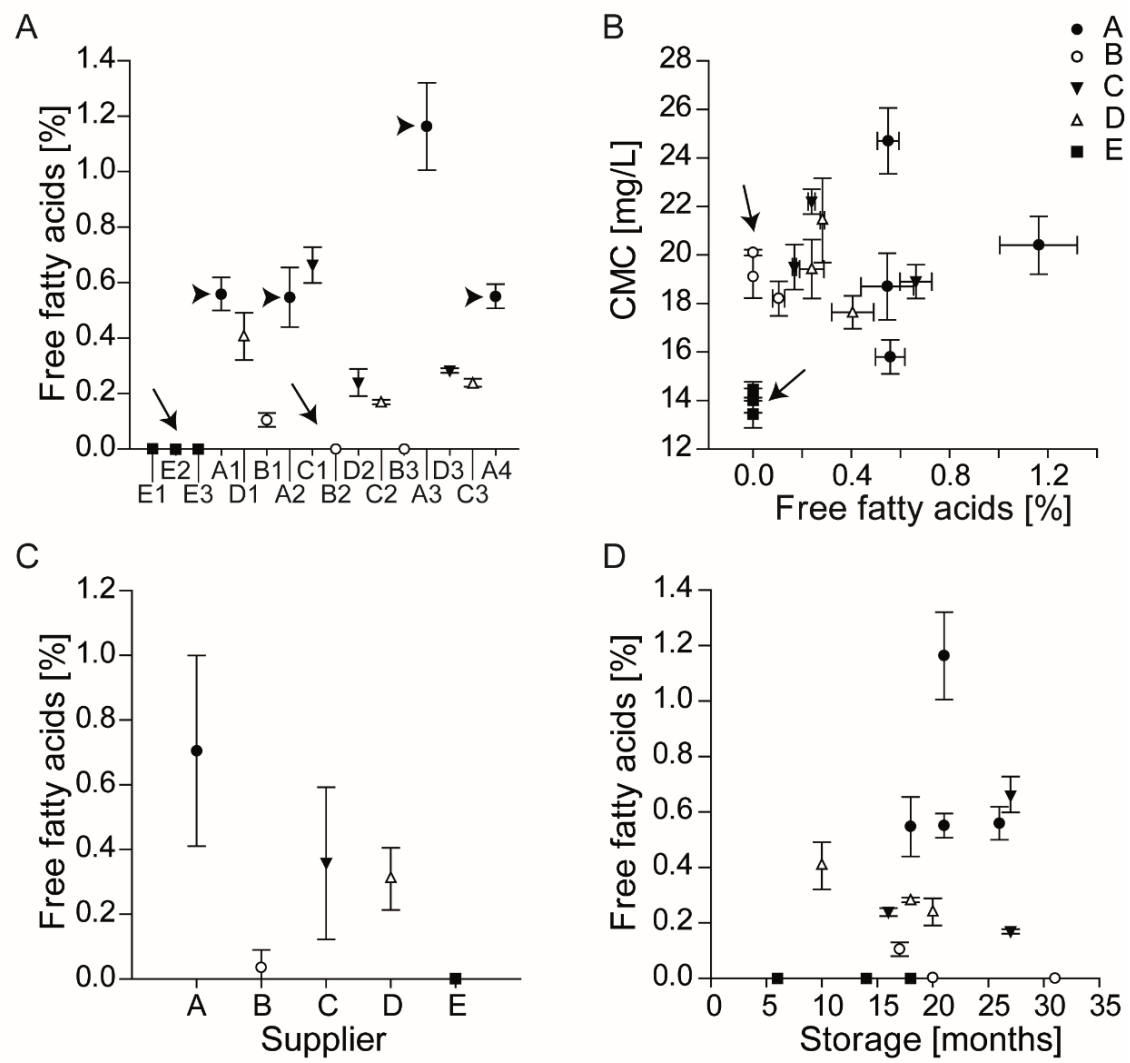

Supplementary figure 2: (A) Free fatty acid content [%; no hydrolysis] as a function of batches. (B) Correlation of CMC [mg/L] with free fatty acid content [%; no hydrolysis]. (C) Fatty acid content [%] as a function of supplier or (D) storage [months]. Arrows indicate batches with low, arrowheads batches with high variability.

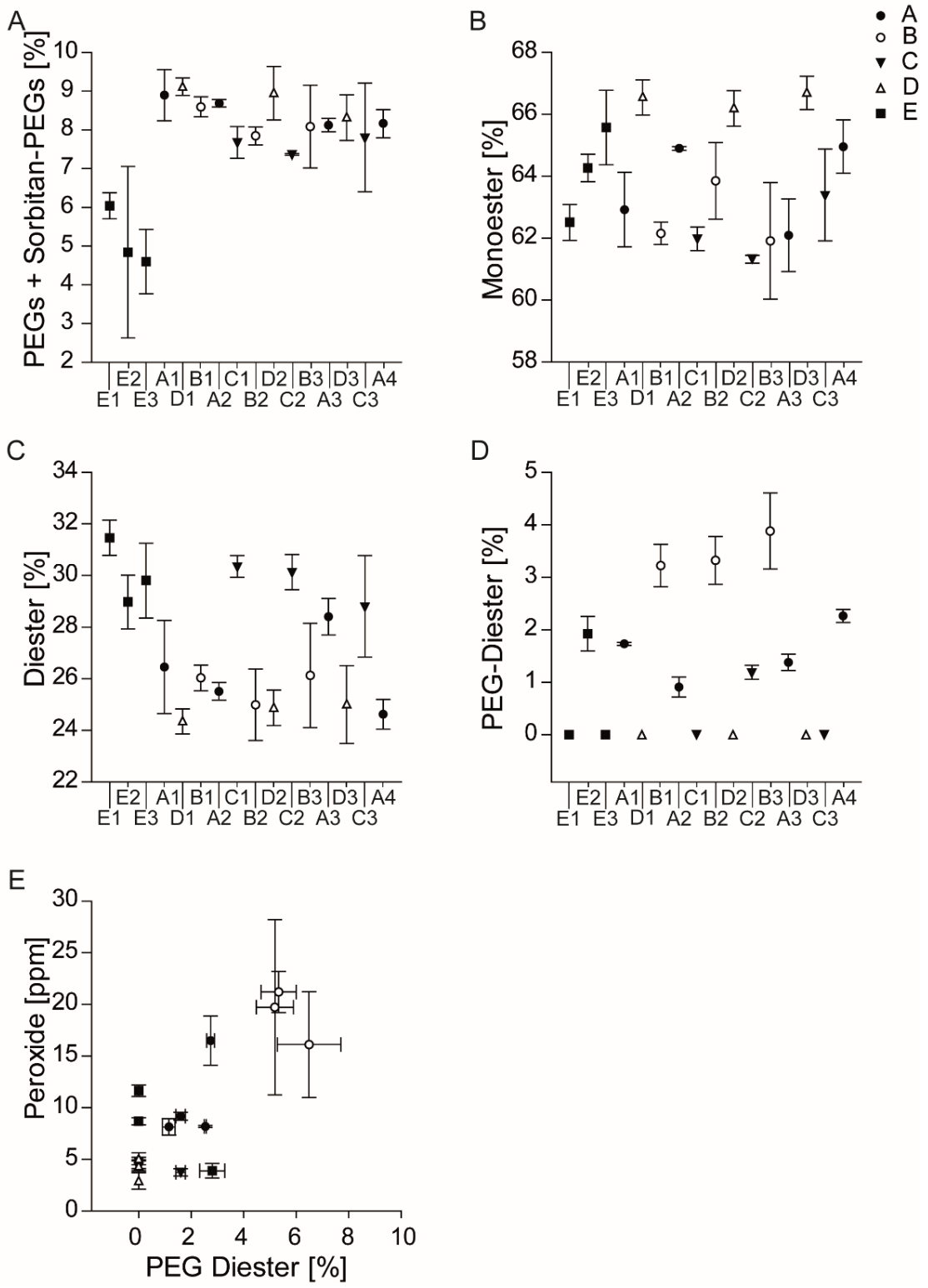

Supplementary figure 3: (A) Content of non-esterified polyethylene glycols and sorbitan polyethoxylates [%]; and (B) sorbitan- and isosorbide-polyethoxylate monoesters [%]; and (C) sorbitan- and isosorbide-polyethoxylate diesters [%]; and (D) diester-polyethoxylates [%] of the different batches. (E) Correlation of diester-polyethoxylates [%] and peroxides [ppm].

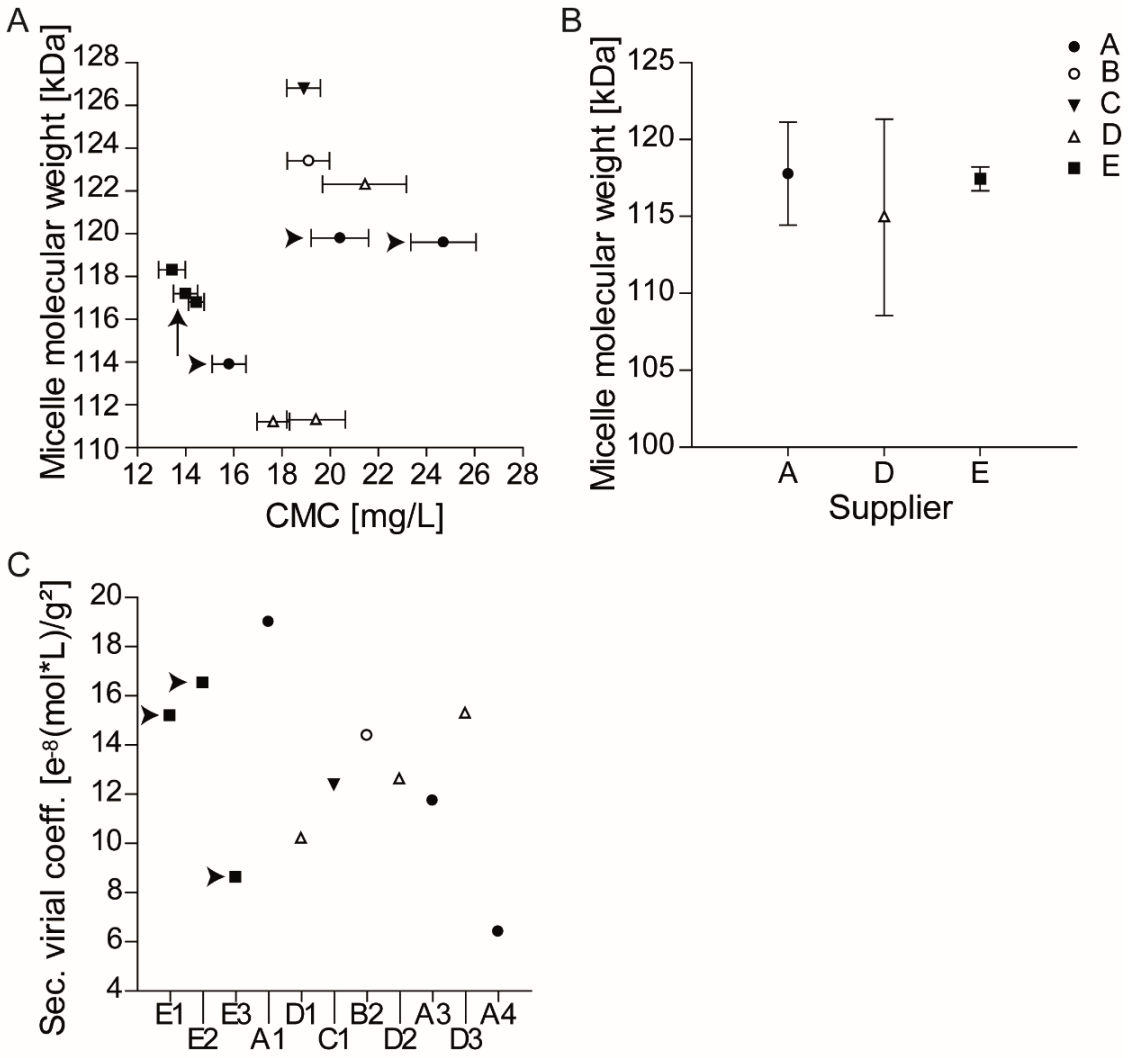

Supplementary figure 4: (A) Correlation of micelle molecular weight [kDa] and CMC [mg/L]. (B) Micelle molecular weight [kDa] as a function of supplier. (C) Second virial coefficient $[e^{-8}\,(mol*L)/g^2]$ as a function of different batches (n = 1). Arrows indicate batches with low, arrowheads batches with high variability.

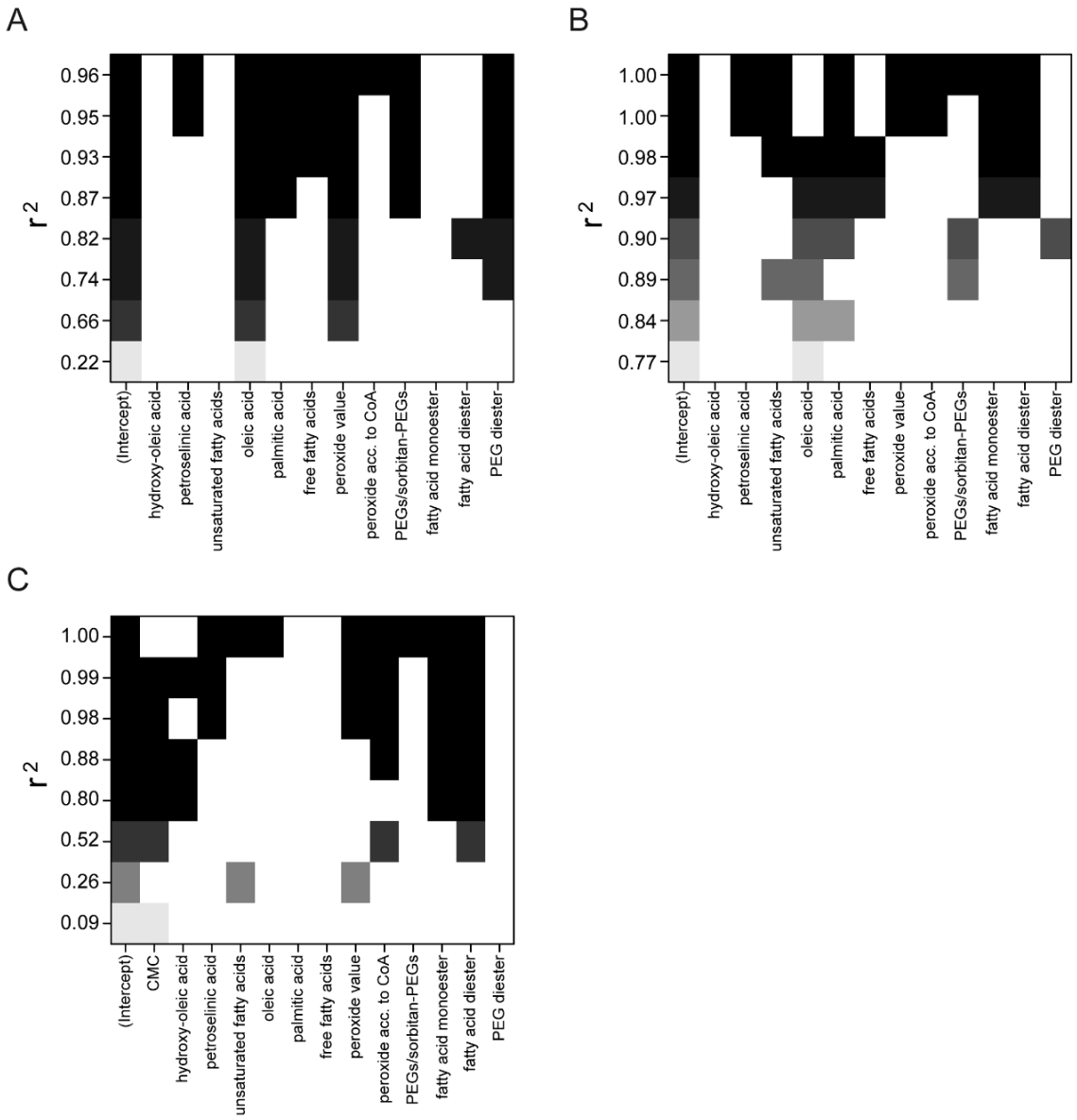

Supplementary figure 5: (A) Parameter selection for model building with calculated r^2 as a function of considered parameters for (A) CMC prediction for the complete data set from all batches and (B) from the data set excluding batches not complying with compendial specifications for peroxide value, and (C) for MM_w prediction based on the complete data set from all batches. For example, using oleic acid content alone in panel (A) yielded an r^2 of 0.22, using the peroxide value in addition increased r^2 to 0.66, including PEG diesters on top resulted in a model with a r^2 of 0.74, etc. Thereby, the reader can see the impact of the various outcomes reported here within on model building. For each output parameter, the best possible model was identified (**Figure 5)**.

References

[1] B.S. Chang, B.S. Kendrick, J.F. Carpenter, Surface-induced denaturation of proteins during freezing and its inhibition by surfactants, Journal of Pharmaceutical Sciences, 85 (1996) 1325-1330.
[2] B.A. Kerwin, Polysorbates 20 and 80 used in the formulation of protein biotherapeutics: Structure and degradation pathways, Journal of Pharmaceutical Sciences, 97 (2008) 2924-2935.
[3] T.M. Göppert, R.H. Müller, Polysorbate-stabilized solid lipid nanoparticles as colloidal carriers for intravenous targeting of drugs to the brain: Comparison of plasma protein adsorption patterns, Journal of Drug Targeting, 13 (2005) 179-187.
[4] Polysorbate 80 Monograph, in: European Pharmacopoeia, European Directorate for the Quality of Medicines & HealthCare (EDQM), Strasbourg, France, 2014.
[5] Polysorbate 80 Monograph, in: United States Pharmacopoeia, The United States Pharmacopeial Convention, Rockville, MD, USA, 2014.
[6] S.R. Singh, J. Zhang, C. O'Dell, M.-C. Hsieh, J. Goldstein, J. Liu, A. Srivastava, Effect of Polysorbate 80 Quality on Photostability of a Monoclonal Antibody, Aaps Pharmscitech, 13 (2012) 422-430.
[7] M. Donbrow, E. Azaz, A. Pillersdorf, Autoxidation of polysorbates, Journal of Pharmaceutical Sciences, 67 (1978) 1676-1681.
[8] R.S.K. Kishore, A. Pappenberger, I.B. Dauphin, A. Ross, B. Buergi, A. Staempfli, H.-C. Mahler, Degradation of Polysorbates 20 and 80: Studies on Thermal Autoxidation and Hydrolysis, Journal of Pharmaceutical Sciences, 100 (2011) 721-731.
[9] J. Yao, D.K. Dokuru, M. Noestheden, S.S. Park, B.A. Kerwin, J. Jona, D. Ostovic, D.L. Reid, A Quantitative Kinetic Study of Polysorbate Autoxidation: The Role of Unsaturated Fatty Acid Ester Substituents, Pharmaceut Res, 26 (2009) 2303-2313.
[10] E. Ha, W. Wang, Y.J. Wang, Peroxide formation in polysorbate 80 and protein stability, Journal of Pharmaceutical Sciences, 91 (2002) 2252-2264.
[11] W. Wang, Y.J. Wang, D.Q. Wang, Dual effects of Tween 80 on protein stability, International Journal of Pharmaceutics, 347 (2008) 31-38.
[12] V.M. Knepp, J.L. Whatley, A. Muchnik, T.S. Calderwood, Identification of antioxidants for prevention of peroxide-mediated oxidation of recombinant human ciliary neurotrophic factor and recombinant human nerve growth factor, PDA journal of pharmaceutical science and technology / PDA, 50 (1996) 163-171.
[13] S. Frison-Norrie, P. Sporns, Investigating the molecular heterogeneity of polysorbate emulsifiers by MALDI-TOF MS, J Agr Food Chem, 49 (2001) 3335-3340.
[14] M. Verbrugghe, E. Cocquyt, P. Saveyn, P. Sabatino, D. Sinnaeve, J.C. Martins, P. Van der Meeren, Quantification of hydrophilic ethoxylates in polysorbate surfactants using diffusion H-1 NMR spectroscopy, J Pharmaceut Biomed, 51 (2010) 583-589.
[15] A. Christiansen, T. Backensfeld, S. Kuehn, W. Weitschies, Stability of the non-ionic surfactant polysorbate 80 investigated by HPLC-MS and charged aerosol detector, Pharmazie, 66 (2011) 666-671.
[16] R.S.K. Kishore, S. Kiese, S. Fischer, A. Pappenberger, U. Grauschopf, H.-C. Mahler, The Degradation of Polysorbates 20 and 80 and its Potential Impact on the Stability of Biotherapeutics, Pharmaceut Res, 28 (2011) 1194-1210.
[17] H.L. Kim, A. McAuley, J. McGuire, Protein Effects on Surfactant Adsorption Suggest the Dominant Mode of Surfactant-Mediated Stabilization of Protein, J. Pharm. Sci., 103 (2014) 1337-1345.
[18] T. Chakraborty, S. Ghosh, S.P. Moulik, Micellization and related behavior of binary and ternary surfactant mixtures in aqueous medium: Cetyl pyridinium chloride (CPC), cetyl trimethyl ammonium bromide (CTAB), and polyoxyethylene (10) cetyl ether (Brij-56) derived system, Journal of Physical Chemistry B, 109 (2005) 14813-14823.
[19] M. Donbrow, R. Hamburger, E. Azaz, A. Pillersdorf, Development of acidity in nonionic surfactants - formic and acetic-acid, Analyst, 103 (1978) 400-402.

[20] H. Kristensen, Functionality-Related Characteristics of Excipients, Pharmaceutical Technology, 31 (2007) 134 - 138.
[21] N.A. Armstrong, Functionality related tests for excipients, Int. J. Pharm., 155 (1997) 1-5.
[22] D. Ilko, A. Braun, O. Germershaus, L. Meinel, U. Holzgrabe, Fatty acid composition analysis in polysorbate 80 with high performance liquid chromatography coupled to charged aerosol detection, European Journal of Pharmaceutics and Biopharmaceutics, 94 (2015) 569-574.
[23] N.B. Vargaftik, B.N. Volkov, L.D. Voljak, International tables of the surface-tension of water, Journal of Physical and Chemical Reference Data, 12 (1983) 817-820.
[24] E. Mohajeri, G.D. Noudeh, Effect of Temperature on the Critical Micelle Concentration and Micellization Thermodynamic of Nonionic Surfactants: Polyoxyethylene Sorbitan Fatty Acid Esters, E-Journal of Chemistry, 9 (2012) 2268-2274.
[25] K.L. Mittal, Determination of CMC of polysorbate 20 in aqueous-solution by surface-tension method, Journal of Pharmaceutical Sciences, 61 (1972) 1334-&.
[26] L.S.C. Wan, P.F.S. Lee, CMC of Polysorbates, Journal of Pharmaceutical Sciences, 63 (1974) 136-137.
[27] A. Patist, S.S. Bhagwat, K.W. Penfield, P. Aikens, D.O. Shah, On the measurement of critical micelle concentrations of pure and technical-grade nonionic surfactants, Journal of Surfactants and Detergents, 3 (2000) 53-58.
[28] J.E. Robbers, V.N. Bhatia, Technique for rapid determination of HLB and Required-HLB values, Journal of Pharmaceutical Sciences, 50 (1961) 708-709.
[29] V. Matyash, G. Liebisch, T.V. Kurzchalia, A. Shevchenko, D. Schwudke, Lipid extraction by methyl-tert-butyl ether for high-throughput lipidomics, Journal of Lipid Research, 49 (2008) 1137-1146.
[30] E. Hvattum, W.L. Yip, D. Grace, K. Dyrstad, Characterization of polysorbate 80 with liquid chromatography mass spectrometry and nuclear magnetic resonance spectroscopy: Specific determination of oxidation products of thermally oxidized polysorbate 80, J. Pharm. Biomed. Anal., 62 (2012) 7-16.
[31] N.T. Southall, K.A. Dill, A.D.J. Haymet, A View of the Hydrophobic Effect, J. Phys. Chem. B, 106 (2002) 521-533.
[32] M. Dahanayake, A.W. Cohen, M.J. Rosen, Relationship of structure to properties of surfactants. 13. Surface and thermodynamic properties of some oxyethylenated sulfates and sulfonates, J. Phys. Chem., 90 (1986) 2413-2418.
[33] P. Atkins, P. de Julio, Physical Chemistry, Oxford University Press, Oxford, 2010.
[34] P.C. Hiemenz, Principles of colloid and surface chemistry, Marcel Dekker Inc., New York, 1986, pp. 127, 133, 147.
[35] F.O. Ayorinde, S.V. Gelain, J.H. Johnson, Jr., L.W. Wan, Analysis of some commercial polysorbate formulations using matrix-assisted laser desorption/ionization time-of-flight mass spectrometry, Rapid Commun. Mass Spectrom., 14 (2000) 2116-2124.
[36] M.J. Rosen, Solubilization by solutions of surfactants: micelle related catalysis, In: *Surfactants and Interfacial Phenomena*, 1989, John Wiley Sons, Inc.; New York, 170–206.
[37] A. Patist, S.S. Bhagwat, K.W. Penfield, P. Aikens, D.O. Shah, On the measurement of critical micelle concentrations of pure and technical-grade nonionic surfactants, J. Surfactants Deterg., 3 (2000) 53-58.

Conclusion and outlook

The rapidly increasing prevalence of sarcopenia calls for efficient and widely applicable therapy to protect affected patients from frailty, risk of the loss of independence, impaired quality of life, and increased mortality [1]. The underlying pathophysiological conditions are attributed to lower tissue concentrations of anabolic growth factors including insulin-like growth factor I (IGF-I), and/or upregulated inhibitory cytokines including myostatin – a strong repressor of muscle differentiation and inductor of skeletal muscle atrophy [2-5]. For this reason, several possibilities of therapeutic intervention were developed, predominantly using the potent growth factor IGF-I [6]. Due to its versatility and anabolic functions in various tissues, the benefit of IGF-I treatment is indicated in many different musculoskeletal diseases, such as muscle atrophy, growth failure, cartilage lesions, fracture repair, osteoporosis or arthritis [7]. Other therapeutic approaches focused on anti-catabolic treatment, e.g. by targeting the ActRIIB receptor, using the endogenous inhibitor follistatin or scavenger antibodies against myostatin [8-10]. However, the translation of the therapeutic potential of these therapeutic molecules into clinical settings is impeded by the pharmacokinetic (PK) shortcomings and substantial safety issues associated with strong side effects in various tissues [6]. This thesis describes novel delivery strategies for the anabolic growth factor IGF-I and a peptide inhibitor of myostatin addressing these limitations in order to compensate the imbalance of catabolic and anabolic stimuli in dystrophic muscles and to provide a safe and efficient therapy. Strategies include development of depot delivery systems using bioorthogonal conjugation to improve the pharmacokinetic features of IGF-I and a targeted release of the therapeutics from the conjugates, thereby improving the benefit-risk profile of these potent therapeutics.

Although several strategies were presented to adequately address PK issues, including biotechnological modifications such as PEGylation [11], microparticle conjugation or functionalization of implants [12-15], reproducible and efficient therapeutic outcome is frequently challenged by the heterogeneity of these conjugates. This work addresses two heterogeneity issues of current pharmaceuticals: (i) unspecific coupling strategies applied for production of protein conjugates jeopardizing the biological performance of APIs, and (ii) the heterogenous composition of formulation components impacting the performance of the biotherapeutic in the formulated product. Ever since the recall of batches of PEGylated proteins due to deviations in bioactivity and the withdrawal of first-generation antibody-drug

conjugates (ADC) owing to the ineffectiveness and safety concerns, problems of unspecific conjugation became obvious [16, 17]. Novel site-directed coupling strategies for therapeutic proteins were summarized and critically evaluated in this work. Benefits and limitations of each chemical and enzymatic conjugation strategy were outlined and guidance for selection of the suitable strategy for certain applications, e.g. polymer attachment, intermolecular protein conjugation, generation of ADCs or biomaterial immobilization was provided. Based on this comprehensive compilation of recent methods, general rules have been derived regarding applicability of strategies to a certain protein or use. For example, the exceptionally fast reaction kinetics of copper(I)-catalyzed azide-alkyne cycloaddition (CuAAC) comes at a price. Among other restrictions, protein PEGylation is impaired by complexation of copper ions, aggregation of proteins with free thiol groups is facilitated, and sensitive proteins or living organisms suffer from cytotoxicity due to formation of reactive oxygen species (ROS) [18-21]. Cu(I)-induced ROS formation was associated with DNA strand breaks, oxidative processes, and the cleavage and cross-linking of amino acids in proteins [19, 22]. Regarding ROS sources, not only copper exposure during conjugation, but also the formulation composition should be taken into consideration. As detailed in the last part of this work, contaminating oxidants may derive from various sources, including formulation excipients such as polysorbate 80 (PS80). Residual peroxides found in certain PS80 batches were reported to cause oxidative degradation and covalent aggregation of proteins during processing and storage [23-25]. These chemical and conformational instabilities possibly result in loss of biologic activity of the therapeutic protein. All in all, these chapters intend to raise awareness of the different aspects, which should be taken into account when designing delivery systems for biological drugs to preserve their integrity and bioactivity over long storage periods for a successful therapy.

Despite the PK improvements of several sustained release systems recently proposed for IGF-I and myostatin inhibitors, the entire therapeutic potential was not fully exploited due to pharmacodynamic impairments [26]. Principal reasons for this reduced therapeutic efficacy comprise insufficient targeting to diseased tissues and limited biologic activity owing to masking of essential ligand binding sites of the conjugated protein [16, 27, 28]. These considerations were translated into innovative delivery systems, locally releasing the active biomolecules in response to a stimulus at the site of need. Two advanced strategies were developed (i) a DDS with immobilized myostatin inhibitor (MI) based on microparticles for local administration and (ii) soluble polymer-IGF-I conjugates for

systemic administration. In the first study, biocompatible agarose particles served as carriers for immobilization of the MI with inter-positioned protease-sensitive linker (PSL). Among the different coupling strategies tested – CuAAC, strain-promoted azide-alkyne cycloaddition (SPAAC) and transglutaminase(TG)-catalyzed crosslinking – SPAAC and TG-mediated conjugation proved more advantageous compared to CuAAC, as copper species triggered MI aggregation as reflected in reduced bioactivity. Immobilization of MI on the particle surface translated into a constitutively active delivery device able to bind and inactivate elevated myostatin levels in atrophic muscles. In addition, integration of the PSL enables this system to optimally respond to inflammatory conditions by massive release of MI for silencing myostatin in adjacent muscles as well. As inflammation typically preludes the onset of myositis flares, localized matrix metalloproteinase (MMP) upregulation was used as a surrogate marker driving MI release from the particles in order to build up clinically relevant MI concentration gradients within tissues of need [29, 30]. The delivery device effectively responded to elevated MMP levels by sustained release of bioactive MI within 24 hours exposition to the index protease, thereby complying with the kinetics of MMP-9 and myostatin upregulation during myositis [31, 32]. The *in vitro* data confirmed bioactivity of cleaved MI following MMP-triggered release by antagonizing myostatin-mediated catabolic effects. However, *in vivo* studies in relevant animal systems have to be performed to assess the benefit resulting from bioresponsive MI release, but the promising *in vitro* data encourage us to follow up on the strategy of bioresponsive MI delivery. Novel approaches for tissue repair and regeneration could be based on biomaterials – either using biodegradable implants or exploiting endogenous extracellular matrix (ECM) for local immobilization and disease-driven release of the MI. Ongoing research focuses on *in situ* MI immobilization on ECM for capturing locally upregulated myostatin to prevent its negative actions on tissue regeneration.

For IGF-I, the development was extended to novel systemic delivery systems using reversible PEGylation as a biomimetic strategy. Therefore, a proteolytically cleavable linker was placed between IGF-I and the PEG polymer for targeted IGF-I release from the conjugate upon cleavage at the disease site, thus exerting its anabolic role in a strictly confined manner. Such targeted IGF-I delivery deploying bioresponsive linkers represents an attractive strategy, since inflammatory diseases are usually associated with upregulated protease activity [29]. Conjugation of IGF-I to the PSL and subsequent modification with the 30 kDa-PEG was realized using dual enzymatic and chemical conjugation strategies. As

IGF-I has an inherent TG substrate domain, which is not required for its biologic functions, I took advantage of this natural reactivity by deploying TG-catalyzed transamidation for connection to the PSL [33]. The subsequent site-specific attachment of the PEG using SPAAC resulted in homogenous IGF-I conjugates. Previous studies showed, that systemically administered IGF-PEG conjugates were able to improve half-life and to reduce the hypoglycemia risk of the growth factor *in vivo* [11]. On the other hand, these conjugates did not show the full suite of biologic actions due to the delicate control of IGF-I activity *in vivo* [26]. The *in vitro* results confirm, that the IGF-PSL-PEG conjugate shows impaired insulin-like binding protein (IGFBP) interactions, submaximal proliferative cellular responses and altered endocytosis pattern compared to the native growth factor. On the basis of this complexity of IGF-I's actions, I selected the bioresponsive strategy of transient PEGylation to avoid the PD restrictions of permanent PEGylation. The IGF-PSL-PEG conjugate was able to improve serum stability of IGF-I, but upon exposure to MMPs the growth factor was readily liberated from the PEGylated conjugate. Following release, the full pharmacologic profile of IGF-I was restored with unaffected bioactivity compared to wild-type IGF-I. This work showed the feasibility of the controlled release strategy for reduction of dosage frequency combined with temporal and spatial activation of the growth factor to deliver its full anabolic potential. In the future, these innovative IGF-I delivery systems will have to be tested in conclusive animal models to reliably predict features such as PK properties, release profile following MMP upregulation and therapeutic efficacy.

Innovative approaches should focus on the conjunction of the anti-catabolic stimulus through the MI – to counteract the inhibiting effect of myostatin on myogenesis – with the anabolic activity of IGF-I. This synergistic activity has great potential to rebalance the homeostasis of muscle loss and regeneration [34]. The intended design using integrated cleavable linkers enables simultaneous bioresponsive delivery of both factors. This massive release of both anti-catabolic and anabolic drugs upon entering diseased tissue has great potential to overcome current challenges of sarcopenia therapy, such as the lack of targeting, rapidly depleted local concentrations and substantial safety issues associated with the side effects of systemic growth factor therapy [7]. A variety of design concepts arise from this strategy for development of innovative co-delivery systems. For a local therapy, biomaterials such as biodegradable scaffolds, extracellular matrix (ECM) components or silk fibroin could prove beneficial to serve as carriers for the therapeutics [35-37]. Soluble conjugates could be prepared based on biocompatible polymers or dendrimers for improved PK [38, 39], and

modifications with targeting moieties – such as folate or antibodies – or with cell-penetrating peptides (CPPs) add additional functionalities to the drug delivery system, including targeting specific cell types or the ability to reach intracellular targets [40, 41]. Innovative approaches also feature "carrier-free" systems by connecting the therapeutics in series like pearls in a necklace. This concept can also be realized using block designs with different PSLs for the MI and IGF-I, respectively, in an effort to bioresponsively release first the MI, followed by IGF-I, etc.

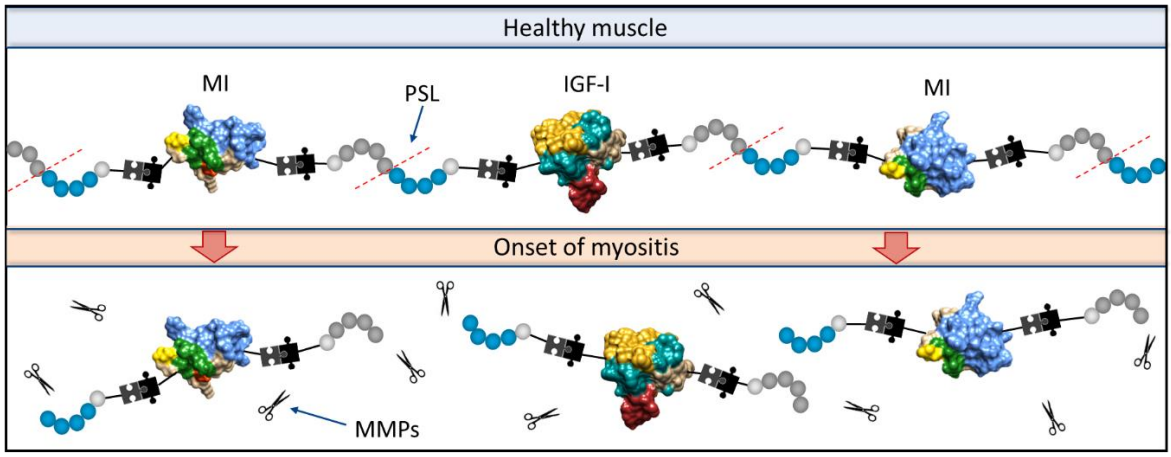

Figure 1: Scheme of the "Necklace" drug delivery system.

These ideas illustrate the numerous possibilities, which can be readily implemented by this modular system. The versatility and potential for transfer to other therapeutic proteins allow the design of advanced delivery systems with multiple options for individual adaptation. In case disease progression is associated with upregulation of a certain protease (or a certain stimulus such as changes in pH, redox potential or hydrogen peroxide levels [42-44]), optimized linkers can be designed, which are effectively cleaved at the site of need. Bioresponsive release profiles can be easily adapted by exchanging the PSL (aiming e.g. at more sustained delivery profiles or higher sensitivity to the protease/stimulus [45]) or the PK features can be modified by selecting the carrier, e.g. a linear or branched PEG with certain molar weight [46].

The ultimate goal of these concepts is gaining better control over drug action and, thereby laying the first stone for a personalized medicine strategy. For instance, on the basis of expression patterns of enzymes associated with pathogenesis of a particular disease, patients can be stratified for optimum therapeutic benefit. The vision exits, that one day the appropriate therapy for an individual person can be systematically selected and the outcome

can be reliably predicted based on valid surrogate markers in serum or tissue and/or characteristics of the disease. This evidence-based approach enables tailored treatment to individual patients, contrasting current trial-and-error approaches of standard therapy. Evaluation of the pharmacodynamics in affected tissue (e.g. assessment of the cleavage rate) could be realized by integration of a mass tag into the PEG moiety. After cleavage and concomitant release of the mass tag, quantification in urine or blood allows the estimation of released protein levels at the disease site. Thereby, the therapeutic outcome can be predicted and allows early intervention in case of insufficient response of the patient. Together with the prediction of the formulation performance of excipients for stabilization and prevention of the bioactivity of the therapeutic – as presented for PS80 through analysis of the chemical composition – a well-defined therapeutic agent can be applied to the patient.

References

[1] R. Roubenoff, V.A. Hughes, Sarcopenia: Current concepts, Journals of Gerontology Series a-Biological Sciences and Medical Sciences, 55 (2000) M716-M724.
[2] D.D. Bikle, C. Tahimic, W. Chang, Y. Wang, A. Philippou, E.R. Barton, Role of IGF-I signaling in muscle bone interactions, Bone, 80 (2015) 79-88.
[3] M.A. Egerman, D.J. Glass, Signaling pathways controlling skeletal muscle mass, Critical Reviews in Biochemistry and Molecular Biology, 49 (2014) 59-68.
[4] S. Cohen, J.A. Nathan, A.L. Goldberg, Muscle wasting in disease: molecular mechanisms and promising therapies, Nature Reviews Drug Discovery, 14 (2015) 58-74.
[5] A.U. Trendelenburg, A. Meyer, D. Rohner, J. Boyle, S. Hatakeyama, D.J. Glass, Myostatin reduces Akt/TORC1/p70S6K signaling, inhibiting myoblast differentiation and myotube size, American Journal of Physiology-Cell Physiology, 296 (2009) C1258-C1270.
[6] A.L. Rosenbloom, Mecasermin (recombinant human insulin-like growth factor I), Advances in Therapy, 26 (2009) 40.
[7] Y.-H. Song, J.L. Song, P. Delafontaine, M.P. Godard, The therapeutic potential of IGF-I in skeletal muscle repair, Trends in endocrinology and metabolism: TEM, 24 (2013) 310-319.
[8] E. Lach-Trifilieff, G.C. Minetti, K. Sheppard, C. Ibebunjo, J.N. Feige, S. Hartmann, S. Brachat, H. Rivet, C. Koelbing, F. Morvan, S. Hatakeyama, D.J. Glass, An Antibody Blocking Activin Type II Receptors Induces Strong Skeletal Muscle Hypertrophy and Protects from Atrophy, Molecular and Cellular Biology, 34 (2014) 606-618.
[9] H. Gilson, O. Schakman, S. Kalista, P. Lause, K. Tsuchida, J.-P. Thissen, Follistatin induces muscle hypertrophy through satellite cell proliferation and inhibition of both myostatin and activin, American Journal of Physiology-Endocrinology and Metabolism, 297 (2009) E157-E164.
[10] E. Latres, J. Pangilinan, L. Miloscio, R. Bauerlein, E. Na, T.B. Potocky, Y. Huang, M. Eckersdorff, A. Rafique, J. Mastaitis, C. Lin, A.J. Murphy, G.D. Yancopoulos, J. Gromada, T. Stitt, Myostatin blockade with a fully human monoclonal antibody induces muscle hypertrophy and reverses muscle atrophy in young and aged mice, Skeletal Muscle, 5 (2015).
[11] F. Metzger, W. Sajid, S. Saenger, C. Staudenmaier, C. van der Poel, B. Sobottka, A. Schuler, M. Sawitzky, R. Poirier, D. Tuerck, E. Schick, A. Schaubmar, F. Hesse, K. Amrein, H. Loetscher, G.S. Lynch, A. Hoeflich, P. De Meyts, H.J. Schoenfeld, Separation of fast from slow anabolism by site-specific PEGylation of insulin-like growth factor I (IGF-I), J Biol Chem, 286 (2011) 19501-19510.
[12] X.M. Lam, E.T. Duenas, A.L. Daugherty, N. Levin, J.L. Cleland, Sustained release of recombinant human insulin-like growth factor-I for treatment of diabetes, Journal of Controlled Release, 67 (2000) 281-292.
[13] I. Schultz, J. Wurzel, L. Meinel, Drug delivery of Insulin-like growth factor I, European Journal of Pharmaceutics and Biopharmaceutics, 97, Part B (2015) 329-337.
[14] L. Meinel, O.E. Illi, J. Zapf, M. Malfanti, H. Peter Merkle, B. Gander, Stabilizing insulin-like growth factor-I in poly(d,l-lactide-co-glycolide) microspheres, Journal of Controlled Release, 70 (2001) 193-202.
[15] K.M. Lorentz, L. Yang, P. Frey, J.A. Hubbell, Engineered insulin-like growth factor-1 for improved smooth muscle regeneration, Biomaterials, 33 (2012) 494-503.
[16] V. Gaberc-Porekar, I. Zore, B. Podobnik, V. Menart, Obstacles and pitfalls in the PEGylation of therapeutic proteins, Current opinion in drug discovery & development, 11 (2008) 242-250.
[17] A.D. Ricart, Antibody-Drug Conjugates of Calicheamicin Derivative: Gemtuzumab Ozogamicin and Inotuzumab Ozogamicin, Clinical Cancer Research, 17 (2011) 6417-6427.
[18] V. Hong, S.I. Presolski, C. Ma, M.G. Finn, Analysis and Optimization of Copper-Catalyzed Azide–Alkyne Cycloaddition for Bioconjugation, Angewandte Chemie International Edition, 48 (2009) 9879-9883.
[19] M. Gutmann, E. Memmel, A.C. Braun, J. Seibel, L. Meinel, T. Lühmann, Biocompatible Azide–Alkyne “Click” Reactions for Surface Decoration of Glyco-Engineered Cells, ChemBioChem, 17 (2016) 866-875.

[20] G.J. Brewer, Risks of Copper and Iron Toxicity during Aging in Humans, Chemical Research in Toxicology, 23 (2010) 319-326.
[21] G. Tabbì, S.C. Fry, R.P. Bonomo, ESR Study of the Non-Enzymic Scission of Xyloglucan by an Ascorbate–H2O2–Copper System: The Involvement of the Hydroxyl Radical and the Degradation of Ascorbate, Journal of Inorganic Biochemistry, 84 (2001) 179-187.
[22] P. Kay, J.R. Wagner, H. Gagnon, R. Day, K. Klarskov, Modification of Peptide and Protein Cysteine Thiol Groups by Conjugation with a Degradation Product of Ascorbate, Chemical Research in Toxicology, 26 (2013) 1333-1339.
[23] E. Ha, W. Wang, Y.J. Wang, Peroxide formation in polysorbate 80 and protein stability, Journal of Pharmaceutical Sciences, 91 (2002) 2252-2264.
[24] W. Wang, Y.J. Wang, D.Q. Wang, Dual effects of Tween 80 on protein stability, International Journal of Pharmaceutics, 347 (2008) 31-38.
[25] V.M. Knepp, J.L. Whatley, A. Muchnik, T.S. Calderwood, Identification of antioxidants for prevention of peroxide-mediated oxidation of recombinant human ciliary neurotrophic factor and recombinant human nerve growth factor, PDA journal of pharmaceutical science and technology / PDA, 50 (1996) 163-171.
[26] M. Sivaramakrishnan, A.S. Kashyap, B. Amrein, S. Saenger, S. Meier, C. Staudenmaier, Z. Upton, F. Metzger, PEGylation of lysine residues reduces the pro-migratory activity of IGF-I, Biochimica et Biophysica Acta (BBA) - General Subjects, 1830 (2013) 4734-4742.
[27] J.M. Harris, R.B. Chess, Effect of pegylation on pharmaceuticals, Nat Rev Drug Discov, 2 (2003) 214-221.
[28] S. Foser, A. Schacher, K.A. Weyer, D. Brugger, E. Dietel, S. Marti, T. Schreitmüller, Isolation, structural characterization, and antiviral activity of positional isomers of monopegylated interferon α-2a (PEGASYS), Protein Expression and Purification, 30 (2003) 78-87.
[29] B.G.H. Schoser, D. Blottner, H.J. Stuerenburg, Matrix metalloproteinases in inflammatory myopathies: enhanced immunoreactivity near atrophic myofibers, Acta Neurologica Scandinavica, 105 (2002) 309-313.
[30] K. Fukushima, A. Nakamura, H. Ueda, K. Yuasa, K. Yoshida, S.i. Takeda, S.-i. Ikeda, Activation and localization of matrix metalloproteinase-2 and-9 in the skeletal muscle of the muscular dystrophy dog (CXMDJ), Bmc Musculoskeletal Disorders, 8 (2007).
[31] S. Kherif, C. Lafuma, M. Dehaupas, S. Lachkar, J.G. Fournier, M. Verdiere-Sahuque, M. Fardeau, H.S. Alameddine, Expression of matrix metalloproteinases 2 and 9 in regenerating skeletal muscle: A study in experimentally injured and mdx muscles, Developmental Biology, 205 (1999) 158-170.
[32] S. McCroskery, M. Thomas, L. Platt, A. Hennebry, T. Nishimura, L. McLeay, M. Sharma, R. Kambadur, Improved muscle healing through enhanced regeneration and reduced fibrosis in myostatin-null mice, Journal of Cell Science, 118 (2005) 3531-3541.
[33] M. Sivaramakrishnan, T.I. Croll, R. Gupta, D. Stupar, D.R. Van Lonkhuyzen, Z. Upton, G.K. Shooter, Lysine residues of IGF-I are substrates for transglutaminases and modulate downstream IGF-I signalling, Biochimica et Biophysica Acta (BBA) - Molecular Cell Research, 1833 (2013) 3176-3185.
[34] N. Bursac, M. Juhas, T.A. Rando, Synergizing Engineering and Biology to Treat and Model Skeletal Muscle Injury and Disease, in: M.L. Yarmush (Ed.) Annual Review of Biomedical Engineering, Vol 17, 2015, pp. 217-242.
[35] R. Duncan, H.C. Cable, J.B. Lloyd, P. Rejmanová, J. Kopeček, Polymers Containing Enzymatically Degradable Bonds, 7. Design of Oligopeptide Side-Chains in Poly[N-(2-hydroxypropyl)methacrylamide] Copolymers to Promote Efficient Degradation by Lysosomal Enzymes, Die Makromolekulare Chemie, 184 (1983) 1997-2008.
[36] M. Gutmann, A. Braun, J. Seibel, T. Lühmann, Bioorthogonal Modification of Cell Derived Matrices by Metabolic Glycoengineering, ACS Biomaterials Science & Engineering, (2018).
[37] H. Zhao, E. Heusler, G. Jones, L. Li, V. Werner, O. Germershaus, J. Ritzer, T. Luehmann, L. Meinel, Decoration of silk fibroin by click chemistry for biomedical application, Journal of Structural Biology, 186 (2014) 420-430.

[38] E. Lallana, F. Fernandez-Trillo, A. Sousa-Herves, R. Riguera, E. Fernandez-Megia, Click Chemistry with Polymers, Dendrimers, and Hydrogels for Drug Delivery, Pharmaceutical Research, 29 (2012) 902-921.
[39] Z. Yu, L.Y. Ho, Z. Wang, Q. Lin, Discovery of New Photoactivatable Diaryltetrazoles for Photoclick Chemistry via 'Scaffold Hopping', Bioorganic & Medicinal Chemistry Letters, 21 (2011) 5033-5036.
[40] D.J. Lee, E. Kessel, T. Lehto, X. Liu, N. Yoshinaga, K. Padari, Y.C. Chen, S. Kempter, S. Uchida, J.O. Radler, M. Pooga, M.T. Sheu, K. Kataoka, E. Wagner, Systemic Delivery of Folate-PEG siRNA Lipopolyplexes with Enhanced Intracellular Stability for *In Vivo* Gene Silencing in Leukemia, Bioconjugate Chemistry, 28 (2017) 2393-2409.
[41] V.P. Torchilin, R. Rammohan, V. Weissig, T.S. Levchenko, TAT Peptide on the Surface of Liposomes Affords their Efficient Intracellular Delivery even at Low Temperature and in the Presence of Metabolic Inhibitors, Proceedings of the National Academy of Sciences, 98 (2001) 8786-8791.
[42] T. Lühmann, L. Meinel, Nanotransporters for drug delivery, Current Opinion in Biotechnology, 39 (2016) 35-40.
[43] K.Y. Choi, M. Swierczewska, S. Lee, X. Chen, Protease-Activated Drug Development, Theranostics, 2 (2012) 156-178.
[44] L. Ducry, B. Stump, Antibody-Drug Conjugates: Linking Cytotoxic Payloads to Monoclonal Antibodies, Bioconjugate Chemistry, 21 (2010) 5-13.
[45] H. Nagase, G.B. Fields, Human matrix metalloproteinase specificity studies using collagen sequence-based synthetic peptides, Biopolymers, 40 (1996) 399-416.
[46] P. Bailon, A. Palleroni, C.A. Schaffer, C.L. Spence, W.-J. Fung, J.E. Porter, G.K. Ehrlich, W. Pan, Z.-X. Xu, M.W. Modi, A. Farid, W. Berthold, M. Graves, Rational Design of a Potent, Long-Lasting Form of Interferon: A 40 kDa Branched Polyethylene Glycol-Conjugated Interferon α-2a for the Treatment of Hepatitis C, Bioconjugate Chemistry, 12 (2001) 195-202.

Abbreviations

ACN	Acetonitrile
ActRIIB	Activin receptor IIB
ADC	Antibody drug conjugate
AKT	Protein kinase B
α_2PI	α-2 plasmin inhibitor
ANOVA	Analysis of variance
API	Active pharmaceutical ingredient
au	Arbitrary units
BCA	Bicinchoninic acid
BSA	Bovine serum albumin
CAD	Charged aerosol detection
CBD	Collagen-binding domain
CBT	Cyanobenzothiazole
CEX	Cation exchange chromatography
CMC	Critical micelle concentration
CPP	Cell-penetrating peptide
CSR	Click sulfonamide reaction
CuAAC	Copper(I)-catalyzed azide-alkyne cycloaddition
DAPI	4´,6-diamidine-2-phenylindol
DAR	Drug-antibody ratio
DBCO	Dibenzocyclooctyne
DDS	Drug delivery system
DIBAC	Dibenzoazacyclooctyne
DM	Differentiation medium
DMD	Duchenne muscular dystrophy
DMEM	Dulbecco’s modified Eagle’s medium
DMSO	Dimethyl sulfoxide
DTT	Dithiothreitol
ECM	Extracellular matrix
EDC	1-Ethyl-3-(3dimethylaminopropyl) carbodiimide
EDTA	Ethylenediaminetetraacetic acid
EGF	Epidermal growth factor
eGFP	Enhanced green fluorescent protein
ELISA	Enzyme-linked immunosorbent assay
ERK	Extracellular Signal-Regulated Kinase
ESI-MS	Electrospray ionization mass spectrometry
FBS	Fetal bovine serum
FDA	Food and Drug Administration
FGE	Formylglyine-converting enzyme
FGF	Fibroblast growth factor
FPLC	Fast protein liquid chromatography

FRC	Functionality related characteristic
GDF-8	Growth differentiation factor 8
hGH	Human growth hormone
HLB	Hydrophilic-lipophilic balance
HPLC	High performance liquid chromatography
IC_{50}	Half maximal inhibitory concentration
IGF-I	Insulin-like growth factor I
IGFBP	Insulin-like growth factor binding protein
IL-1β	Interleukin 1β
K_d	Dissociation constant
LC-MS	Liquid chromatography - mass spectrometry
MALDI-MS	Matrix-assisted laser desorption ionization mass spectrometry
MAPK	Mitogen-Activated Protein Kinase
MEM	Minimal essential medium Eagle
MI	Myostatin inhibitor
MMP	Matrix metalloproteinase
MM_w	Micelle molecular weight
MSTN	Myostatin
mTG	Microbial transglutaminase
MyHC	Myosin heavy chain
NEA	Nonessential amino acids
NF-κB	Nuclear factor-kappa B
NHS	N-hydroxysuccinimide
PBS	Phosphate buffered saline
PCL	Protease cleavable linker
PSL	Protease sensitive linker
PD	Pharmacodynamic
PEG	Polyethylene glycol
Pen/Strep	Penicillin and streptomycin
Ph.Eur.	European Pharmacopeia
PK	Pharmacokinetic
PMMA	Poly(methyl methacrylate)
PS80	Polysorbate 80
RHLB	Required hydrophilic-lipophilic balance
RLU	Relative light unit
ROS	Reactive oxygen species
RP-HPLC	Reversed-phase high performance liquid chromatography
RT-PCR	Real time polymerase chain reaction
SBE	SMAD binding element
SC	Satellite cell
SD	Standard deviation
SDS-PAGE	Sodium dodecyl sulfate polyacrylamide gel electrophoresis
SF	Silk fibroin

SLS	Static light scattering
SPAAC	Strain-promoted azide-alkyne cycloaddition
SPANC	Strain-promoted alkyne-nitrone cycloaddition
Span 80	Sorbitan monooleate
SPPS	Solid phase peptide synthesis
SPR	Surface plasmon resonance
TBS	Tris buffered saline
TBTA	Tris((1-benzyl-4-triazolyl)methyl)amine
TCEP	Tris(2-carboxyethyl)phosphine
TFA	Trifluoracetic acid
TG	Transglutaminase
TGF–β	Transforming growth factor beta
THPTA	Tris(3-hydroxypropyltriazolylmethyl)amine
TIMP	Tissue inhibitor of metalloproteinases
TNFα	Tumor necrosis factor α
uAA	Unnatural amino acid
UPLC	Ultra performance liquid chromatography
USP	United States Pharmacopeia
VEGF	Vascular endothelial growth factor
WST-1	Water soluble tetrazolium

Curriculum vitae

PUBLICATIONS

Journal articles

Braun AC, Gutmann M, Mueller TD, Lühmann T, Meinel L (2018). "Bioresponsive release of insulin-like growth factor-I from its PEGylated conjugate." J Control Release, 279: 17-28.

Gutmann M, Braun A, Seibel J, Lühmann T (2018). "Bioorthogonal modification of cell derived matrices by metabolic glycoengineering." ACS Biomater Sci Eng., 4(4): 1300-1306.

Wu F, Braun A, Lühmann T, Meinel L (2018). "Site-specific conjugated insulin-like growth factor-I for anabolic therapy." ACS Biomater Sci Eng., 4(3): 819-825.

Braun AC, Gutmann M, Lühmann T, Meinel L (2018). "Bioorthogonal strategies for site-directed decoration of biomaterials with therapeutic proteins." J Control Release. 273: 68-85.

Braun AC, Gutmann M, Ebert E, Jakob F, Gieseler H, Lühmann T, Meinel L (2016). „Matrix metalloproteinase responsive delivery of Myostatin inhibitors," Pharmaceutical Research 34(1):58-72.

Gutmann M, Memmel E, Braun A, Seibel J, Meinel L, Lühmann T (2016). „Biocompatible azide alkyne 'click' reactions for surface decoration of glyco-engineered cells," ChemBioChem 17(9):866-75.

Braun AC, Ilko D, Merget B, Gieseler H, Germershaus O, Holzgrabe U, Meinel L (2015). „Predicting critical micelle concentration and micelle molecular weight of polysorbate 80 using compendial methods," Eur J Pharm Biopharm, 94: 559-568.

Ilko D, Braun A, Germershaus O, Meinel L, Holzgrabe U (2015). „Fatty acid composition analysis in polysorbate 80 with high performance liquid chromatography coupled to charged aerosol detection," Eur J Pharm Biopharm, 94: 569-574.

Oral and poster presentations

Braun A et al. (2016) Site-directed conjugation and bioresponsive delivery of IGF-I, Chemical symposium, Würzburg, Germany.

Braun A et al. (2016) Muscle wasting diseases: Bioresponsive co-delivery of anti-catabolic and anabolic proteins. Controlled Release Society, Seattle, WA.

Braun A. et al. (2015) Site-directed immobilization and bioresponsive release of anti-catabolic agents for muscle regeneration. DPhG annual meeting, Düsseldorf, Germany.

Braun A. (2015) Site-directed immobilization and controlled release of anabolic and anticatabolic agents for muscle regeneration. Joint Symposium at Hoshi University, Tokyo, Japan.

Braun A et al. (2014) Site-directed modification of Myostatin inhibitors for muscle regeneration. DPhG annual meeting, Frankfurt, Germany.

Braun A et al. (2014) Synthesis and characterization of ‚clickable' Myostatin-Inhibitors. Controlled Release Society – German Local Chapter Meeting, Kiel, Germany.

Acknowledgments

I would like to sincerely thank Prof. Dr. Dr. Lorenz Meinel for choosing this fascinating topic of bioresponsive drug delivery systems, for the possibility to get access to a plentitude of scientific methods and for his helpful advice and constructive feedback. Thank you for your professional scientific input and the freedom to design the project according to my own ideas.

Prof. Dr. Franz Jakob, Orthopedic Center for Musculoskeletal Research, is gratefully acknowledged for the initiation of this interesting project, the coordination of the 'FORMOsA' research network, the great collaboration with his group and the interesting conversations. Furthermore, I would like to express my gratitude to PD Dr. Henning Gieseler, GILYOS GmbH, for his constant support and the possibility to use the freeze drying equipment during my whole work. Additionally, I want to acknowledge the financial support of the Bavarian Research Foundation (BFS) in the frame of Grant No. AZ-1044-12 (FORMOsA).

Prof. Dr. Petra Högger from the Chair for Clinical Pharmacy and Prof. Dr. Utz Fischer from the Chair of Biochemistry are gratefully acknowledged for co-refereeing this thesis.

My gratitude is also directed to PD Dr. Tessa Lühmann for always offering me her expertise and time. Many thanks to Prof. Dr. Ulrike Holzgrabe, Prof. Dr. Oliver Germershaus and Dr. David Ilko for their contributions to Chapter IV and the great cooperation. I thank Prof. Dr. Thomas Mueller for his support concerning SPR experiments, PD Dr. Regina Ebert and Dr. Juliane Pochhammer for assistance with the Luciferase Assay, Stephanie Lamer for the NanoLC-MS/MS measurements and Dr. Werner Schmitz for the ESI-MS measurements. Furthermore, I want to acknowledge the essential help of Dr. Stefanie Munzert regarding SLS measurements and Dr. Benjamin Merget for his support concerning multivariance analysis and mathematical modelling.

I am truly grateful for the support and friendship of my PhD colleagues and I want to thank the whole team at the Chair for Drug Formulation and Delivery for the good time we spent together in Würzburg. Special thanks to Valerie Spieler and Dr. Gabriel Jones for the great atmosphere in our office. Especially Cecilia Amstalden, Dr. Isabel Schultz, Dr. Eva Heusler, Katharina Dodt, Marco Saedtler, Cornelius Hermann and Dr. Johannes Wiest are kindly

acknowledged for many scientific and personal discussions. Above all, my deepest gratitude applies to Marcus Gutmann for the extremely valuable help regarding biochemical and cell-based methods, the exchange of ideas, the inspiring discussions and his friendship.

Finally, I want to express my gratitude to my parents, my sister Patricia, my brother Daniel, my boyfriend Patrick and my close friends for their immeasurable support, encouragement and appreciation.

Documentation of authorship

This section contains a list of the individual contribution for each author to the publications reprinted in this thesis. Unpublished manuscripts are handled, accordingly.

P1	**Braun A C, Gutmann M, Lühmann T, Meinel L** (2018) Bioorthogonal strategies for site-directed decoration of biomaterials with therapeutic proteins. Journal of Controlled Release **273**: 68-85. DOI: 10.1016/j.jconrel.2018.01.018.				
Author		**1**	**2**	**3**	**4**
Manuscript planning		x		x	x
Manuscript writing		x			x
Design of the graphics		x	x		
Correction of manuscript		x	x	x	x
Supervision of Alexandra Braun					x

P2	**Braun A C, Gutmann M, Ebert R, Jakob F, Gieseler H, Lühmann T, Meinel L** (2017) Matrix metalloproteinase responsive delivery of myostatin inhibitors. Pharmaceutical Research **34**(1): 58-72. DOI: 10.1007/s11095-016-2038-6.							
Author		**1**	**2**	**3**	**4**	**5**	**6**	**7**
Synthesis, chemical modification, and molecular weight of the myostatin inhibitors		x						
Bioconjugation of the different MI variants		x						
Luciferase-based reporter gene assay		x		x				
C2C12 differentiation and immunostaining		x	x					
Western Blot of differentiated C2C12 cells		x						
RT-PCR (Quantitative real-time PCR of differentiation markers)			x					
Cleavage experiments of the protease cleavable linkers		x						
Decoration of 3D Carboxy-poly(methyl methacrylate) particles and exposure to MMPs		x						
Flow cytometry		x	x					
Decoration of NHS activated agarose particles and exposure to MMPs		x						
Statistics		x						
Study design/concept development		x			x	x	x	x
Data analysis and interpretation		x	x					x
Manuscript planning		x					x	x
Manuscript writing		x						x
Correction of manuscript		x	x	x	x	x	x	x
Supervision of Alexandra Braun								x

P3	**Braun A C, Gutmann M, Mueller T D, Lühmann T, Meinel L** (2017) Bioresponsive release of insulin-like growth factor-I from its PEGylated conjugate. Journal of Controlled Release **279**: 17-28. DOI: 10.1016/j.jconrel.2018.04.009.					
Author		**1**	**2**	**3**	**4**	**5**
Synthesis and purification of the $\alpha_2PI_{1\text{-}8}$-PSL		x				
Conjugation of IGF-I to the PSL in presence of activated transglutaminase		x				
Site-specific PEGylation with DBCO-PEG_{30kDA}		x				
High performance liquid chromatography		x				
SDS-PAGE and Western Blot for IGF-I variants		x				
Trypsin digestion and mass spectrometric characterization		x	x			
Exposure of PSL and IGF-PSL-PEG to MMPs		x				
Cell proliferation assay (WST-1)		x				
Cell signaling and Western immunoblotting		x				
Serum stability		x				
Surface Plasmon Resonance				x		
IGF-II receptor-mediated internalization of IGF-I and IGF-PSL-PEG		x	x			
Statistical analysis		x				
Study design/concept development		x			x	x
Data analysis and interpretation		x	x	x	x	x
Manuscript planning		x				x
Manuscript writing		x				
Correction of manuscript			x	x	x	x
Supervision of Alexandra Braun						x

P4	**Braun A C, Ilko D, Merget B, Gieseler H, Germershaus O, Holzgrabe U, Meinel L** (2015) Predicting critical micelle concentration and micelle molecular weight of polysorbate 80 using compendial methods. European Journal of Pharmaceutics and Biopharmaceutics **94**: 559-68. DOI: 10.1016/j.ejpb.2014.12.015.							
Author		**1**	**2**	**3**	**4**	**5**	**6**	**7**
Sample preparation		x						
Critical micelle concentration (CMC) by surface tension measurement		x						
Cloud point		x				x		
Hydrophilic–lipophilic balance (HLB) value		x						
Static light scattering		x						
HPLC-CAD			x					
Fingerprint analyses			x					
Peroxide value		x						
Calculation of models using descriptors				x				
Statistics		x						
Study design/concept development		x				x	x	x
Data analysis and interpretation		x	x	x	x	x	x	x
Manuscript planning		x						x
Manuscript writing		x						x
Correction of manuscript		x	x	x	x	x	x	x
Supervision of Alexandra Braun								x

Erklärung zu den Eigenanteilen des Doktoranden sowie der weiteren Doktoranden als Koautoren an Publikationen und Zweitpublikationsrechten bei einer kumulativen Dissertation.

Für alle in dieser kumulativen Dissertation verwendeten Manuskripte liegen die notwendigen Genehmigungen der Verlage (‚reprint permission') für die Zweitpublikation vor, außer das betreffende Kapitel ist noch gar nicht publiziert. Dieser Umstand wird einerseits durch die genaue Angabe der Literaturstelle der Erstpublikation auf der ersten Seite des betreffenden Kapitels deutlich gemacht oder die bisherige Nichtveröffentlichung durch den Vermerk „unpublished" oder „nicht veröffentlicht" gekennzeichnet.

Die Mitautoren der in dieser kumulativen Dissertation verwendeten Manuskripte sind sowohl über die Nutzung als auch über die oben angegebenen Eigenanteile informiert und stimmen dem zu.

Die Anteile der Mitautoren an den Publikationen sind in den vorausgehenden Tabellen aufgeführt.

Prof. Dr. Dr. Lorenz Meinel	Unterschrift
Alexandra Braun	Unterschrift